C6-673/33

07

Volume II
Technical Summary Report

Study of Structural Bending Adaptive Control Techniques for Large Launch Vehicles

Contract No. NAS8-20056

Prepared for George C. Marshall Space Flight Center

Huntsville, Alabama 35812

March 16, 1966

AUTONETICS
A DIVISION OF NORTH AMERICAN AVIATION, INC.

DATA SYSTEMS DIVISION
Department 345-4
P.O. Box 4171
3370 Miraloma Avenue
Anaheim, California 92803

TABLE OF CONTENTS

LIST OF FIGURES

LIST OF FIGURES (cont'd)

LIST OF FIGURES (cont'd)

LIST OF FIGURES (cont'd)

LIST OF FIGURES (cont'd)

LIST OF FIGURES (cont'd)

LIST OF TABLES

SECTION 1.0

SUMMARY

This final report presents the results of the Study of Structural Bending Adaptive Control Techniques for Large Launch Vehicles performed under NASA Contract NAS8-20056. The system studied utilizes the principles of spectral identification to identify the vehicle dynamics and uses the identified parameters of the vehicle to compute the required control compensation for proper system performance and stability. Computations are performed digitally, and the functions of identification/compensation are performed continuously during vehicle operation. The study is devoted primarily to the problem of decoupling the elastic modes and the rigid mode of a large booster of the Saturn class. A secondary portion of the study was devoted to investigating the problems associated with active bending control using a single force point for control (main nozzles).

This report summarizes the overall study objectives, describes the basic spectral identification system and presents study results. In addition, an appendix section is included which shows the pertinent equations of motion, vehicle data, a brief description of control using digital computers, and additional study results.

The study results include the stability and trajectory analyses as well as the modifications to the basic spectral identification which were necessary to satisfy the system requirements. The stability analyses results are presented in the form of gain-phase plots and were performed for three flight cases--8 sec, 78 sec and 157 sec after launch. Satisfactory stability has been achieved for all cases with the complete spectral identification system operative.

The trajectory results cover the complete first stage and show the dynamic behavior of the identification system and the ability of the vehicle to follow the trajectory in the presence of atmospheric disturbances and instrument noise. The trajectories are pitch plane digital simulations from 0 sec to 157 sec with the digital compensation and frequency identification

system functionally mechanized in the study as they would be in a digital control computer. The results indicate the capability of the system to provide stable control of a vehicle with wide margins of uncertainty in the vehicle dynamic and flexibility coefficients.

1.1 INTRODUCTION

The effective size of a boost vehicle designed for a space mission is measured by the usable payload pounds that can be placed in orbit. The major positive contributor to payload pounds is the weight and efficiency of the rocket propellant. The major negative contributor to payload pounds is the weight of the structure required to hold the propellant, engines and payload together. The best boost vehicle design thus minimizes the structural weight. Minimum structure results in increased vehicle flexibility (i.e., ability for the vehicle to bend). Increased flexibility has an adverse effect upon the performance of the attitude control system.

The purpose of the attitude control system is to measure the direction of vehicle travel and to maintain the direction desired by the guidance system in a manner that will not destroy the vehicle. A boost vehicle is similar to a long rod which bends in two ways when forces are placed upon it. The first is a steady state bend equivalent to the sag in a rod when it is supported horizontally at both ends. The second way is an oscillatory bend which would be exhibited by the rod if a weight were to be dropped on it while horizontally supported. This oscillatory bending will tend to die out by itself unless it is being continually forced and excited. The control system in maintaining proper heading is continually applying forces to the vehicle. The control system must be designed so that in continually applying forces to the vehicle it does not also continually excite the bending in a manner to increase bending deflections and ultimately destroy the vehicle. The attitude of the vehicle is measured by an instrument rigidly attached to the vehicle structure. The sensor measures not only the vehicle attitude but also the local vehicle bending at the sensor location. The attitude control forces computed from the sensor output are thus partially determined by the bending magnitude at the sensor. Factors depending upon the relative bending direction between the sensor locations and the attitude control force point, plus computational delays in computing the attitude control force magnitude from the sensor output determine whether the applied force will tend to increase or decrease any bending that may exist. The effects of computational delays are directly dependent upon the oscillatory frequency of the bending.

A normal control system for a flexible vehicle will not allow high frequencies to pass through to the force point, thus eliminating the reinforcing of high frequency oscillatory bending modes. Computational delays will be so designed that the low frequency oscillatory bending modes are suppressed by the control forces rather than reinforced. With very large and very flexible vehicles the normal control system design cannot be achieved. With very flexible vehicles the bending oscillatory frequencies become low enough that even the higher modes cannot be filtered out without detrimental effects upon the attitude control. With large vehicles it is impossible to predetermine the bending oscillatory frequency to the accuracy required to adjust the computational delays in a manner to achieve guaranteed stable control.

A method of obtaining stable control under these adverse bending conditions would be to accurately measure the bending frequencies during flight and place notch filters in the control system at these frequencies so that just the bending frequencies are inhibited from contributing to the attitude control force. Even with perfect identification of the bending frequencies and notch filters tuned to these frequencies the vehicle will still bend as it is excited by forces other than the attitude control forces. Since this is the case, the sensor output will in general contain signals representative of the oscillatory bending even with perfect control system notch filtering. If the power spectral density of the sensor output is measured there would be expected peaks at the bending frequencies. It is the measurement of these peaks and the determination of the frequencies which are used in flight to determine the bending frequencies and tune the notch filters.

This report shows the results of an investigation where the Spectral Identification Adaptive Control System was applied to a realistic large launch vehicle in a complete closed loop trajectory simulation with bending frequencies changing and initial frequency uncertainties. The vehicle was subjected to realistic winds and gust inputs. Appendix 6.1 gives a detailed development of the spectral filter amplitude response plus a discussion of the major parameters that affected the development of identification system as used in the study.

Appendix 6.2 contains a brief description of digital control systems and analysis techniques applied in the study of the digital control system. This section should be of particular interest to those unfamiliar with digital control systems.

Appendix 6.3 is a vehicle description including the equations of motion plus a list of vehicle data for all 24 flight cases. The vehicle used is Model Vehicle No. 2 (see Figure 1) which was developed by NASA to represent any large flexible space vehicle (similar or larger than the Saturn V) but not intended to represent any specific vehicle.

SECTION 2.0

STUDY OBJECTIVES AND GROUND RULES

The objectives of the study were to:

1. Design a spectral identification system to achieve minimum coupling between bending modes and short period.
2. Provide basic system stability.
3. Achieve a practical mechanization of the final system.
4. Demonstrate the Spectral Identification Adaptive Control System in a complete closed loop time varying trajectory simulation, including adaptive features working with vehicle bending frequency changes in combination with realistic wind and gust inputs.

The study ground rules were:

1. The study is based on Model Vehicle II data received from George Marshall Space Flight Center, Huntsville, Alabama.
2. The study is restricted to the pitch phase.
3. The study is restricted to the first stage.
4. Slosh dynamics are included in stability analyses.
5. The dynamics include the short period mode, three flexible modes, engine compliance, sensors, actuator and fuel slosh.
6. It is assumed that the bending frequencies are not restricted to a prescribed frequency band, but a total bandwidth is defined which includes all bending modes of interest.

SECTION 3.0

DETAILED DISCUSSION

3.1 SPECTRAL IDENTIFICATION ADAPTIVE CONTROL SYSTEM

The Spectral Identification Adaptive Control System includes a conventional short period control system where the attitude command is summed in the proper ratio with the output of an attitude gyro and attitude rate gyro. This composite error signal is filtered by a short period compensator and then filtered by three notch filters which eliminate the 1st, 2nd and 3rd bending mode components from the error signal. The output of the final notch filter is used as a command to the deflection of the main thrust nozzles. In order that the notch filters remove the bending they must be tuned to the bending frequencies. The bending frequencies are initially uncertain due to uncertainties in the vehicle dynamics and change during the trajectory as propellant is expended. In order to insure that the notch filters are tuned to the bending frequencies the bending frequencies are identified during the flight.

3.1.1 FREQUENCY IDENTIFICATION SYSTEM

The bending frequency is identified by placing 24 spectral filters tuned to 24 frequencies over the expected frequency band of the first three bending modes. The frequencies of these filters are given in Table 1. n is an integer associated with each filter, m_n the number of .01 second sampling periods in 1/2 period of the tuned frequency and ω_n the tuned frequency in radians per second. The output of each spectral filter is an approximate measurement of the energy in the input signal at the spectral filters' tuned frequency. The input signal to the spectral filters used in this study is derived by subtracting the output of two rate gyros, one mounted in the instrument compartment and the other in the interstage region between the first and second stage. In a previous study a single rate gyro was used as the spectral filter input sensor with adequate system performance. In the selection of the spectral filter input sensor care must be exercised to insure that an effective null point on any bending mode to be identified does not exist at any time during the flight.

n	m_n	ω_n rad/sec
1	22	14.28
2	24	13.09
3	26	12.083
4	28	11.22
5	30	10.472
6	32	9.81
7	36	8.73
8	40	7.85
9	44	7.14
10	48	6.54
11	54	5.82
12	60	5.24
13	66	4.76
14	74	4.25
15	82	3.83
16	92	3.41
17	100	3.14
18	112	2.8
19	124	2.53
20	138	2.28
21	154	2.04
22	170	1.85
23	188	1.67
24	208	1.51

Table I. Spectral Filter Tuned Frequencies

The operation and analysis of a spectral filter is thoroughly explained in Appendix 6.1. A spectral filter output, A, is determined by the solution of the equations

$$S_i = -\int_{t_o}^{t_o + ip} (-1)^i \, E_{in}(t) \, dt \tag{1}$$

$$C_i = -\int_{t_o}^{t_o + ip/2} (-1)^i \, E_{in}(t) \, dt + \int_{t_o + ip/2}^{t_o + ip} (-1)^i \, E_{in}(t) \, dt \tag{2}$$

$$U_i = S_i + S_{i-1} \tag{3}$$

$$V_i = C_i + C_{i-1} \tag{4}$$

$$S = \frac{1}{p\ell} \sum_{i=1}^{\ell} U_i \tag{5}$$

$$C = \frac{1}{p\ell} \sum_{i=1}^{\ell} V_i \tag{6}$$

$$A = S^2 + C^2 \tag{7}$$

Descriptively the solution of these equations is: S_i is the integral over 1/2 period (p) of a square wave kernal times the spectral input signal with the kernal phased to change from -1 to +1 at t_o. C_i is the integral of the square wave kernal times the spectral input signal with the kernal phased to change from +1 to -1 at $t_o + p/2$. The kernal used in determining C_i is in quadrature with the kernal used in determining S_i. U_i being the sum of S_i and S_{i-1} is thus the integral of the kernal times the spectral input signal with the integration period a complete period of the spectral filter tuned frequency. A value of U_i is computed for each half period time point however. V_i is equivalent to U_i except computed using the quadrature kernal. S is the sum of ℓ past values of U_i times a normalizing constant which removes the normal decrease in an integrator output with increase in input frequency. C is equivalent to S except computations are made using V_i instead of U_i. The total spectral filter output is then computed by taking the sum of the squares of S and C. Figure 2 is the output amplitude of a spectral filter as the input frequency is varied. The amplitude is plotted versus normalized frequency, r, computed by dividing the input frequency by the tuned frequency. The spectral filter response is dependent upon the phase relationship between the input frequency and the square wave. Figure 2 shows two curves, one drawn with a continuous line and the other with a dashed line. These two curves represent the extremes in spectral filter gain as the input signal phase changes. The integration period was 5 periods (i.e., $\ell = 9$).

Since there are 24 spectral filters there are 24 values of A computed which will be distinguished from each other by the subscript n (i.e., A_n) corresponding to the entries in Table 1. Because the spectral filter output amplitudes should be greatest when the spectral filter tuned frequency is near a bending frequency amplitude, peaks in the A_n array are used to determine the bending frequencies. The following step by step procedure is used in determining the bending frequencies.

1. All values of A_n smaller than a set of resolution values are set equal to zero. This is done to eliminate the identification of any peaks if the total bending activity is very low. Under the conditions when bending activity is low and resolution levels are not present, frequency identification will be based mostly upon system noise. This can allow the notch filters to become detuned enough to produce unstable bending. The bending activity immediately picks up and proper identification is made before the vehicle loads are exceeded; however, the total bending activity is greater than when the resolution levels are set.

2. The three largest peaks are determined from the complete A_n array. A value of A_n is a peak only if $A_n > A_{n-1}$ and $A_n > A_{n-2}$ and $A_n > A_{n+1}$ and $A_n > A_{n+2}$, i.e., A_n is a peak only if it is larger than two values of A on each side of A_n. In general the amplitude of the peak associated with the first bending mode is larger than the peak associated with the second mode which is in turn larger than the peak associated with the third mode. It is not uncommon to have several spectral filter amplitudes in the vicinity of the first mode frequency be larger than any other of the spectral filter amplitudes. If A_n were to be compared with only a single spectral filter output on each side of itself there would be at times a situation where A_{n+1} was less than A_n and A_{n+2} in the neighborhood of the first bending mode. In this case typically A_{n+2} would be identified as a peak along with A_n and the peak at A_{n+2} would be larger than either the second or third bending mode peaks. The frequencies associated with A_n and A_{n+2} would both be identified and thus two notch filters would be placed in the vicinity of the first bending mode. This is eliminated when two values of A on each side of the peak value are required to determine a bending mode. Since two filters are required on each side of the peak filter to determine a peak, the two filters on each end of the array (i.e., A_1, A_2 and A_{23}, A_{24}) constitute a special case. Filters A_1 and A_{24} are never candidates for a peak while a peak at A_2 exists if $A_2 > A_1$ and $A_2 > A_3$ and $A_2 > A_4$ and a peak exists at A_{23} if $A_{23} > A_{24}$ and $A_{23} > A_{22}$ and $A_{23} > A_{21}$. If more than three peaks are identified **only** the three largest peaks are considered legitimate. With three peaks identified the peaks are arranged in ascending orders of n and tentatively associated with the 3^{rd}, 2^{nd} and 1^{st} bending modes, respectively.

3. If less than three peaks are identified special processing must be performed to determine with which bending modes the peaks are associated. The values of n for each mode, that were determined the last time an identification was made on that mode, are compared with the present values of n. The present identified peaks are then associated with the bending mode which in the past identification had the nearest n value to the present n value.

4. At this time 0, 1, 2 or 3 peaks have been identified and tentatively, in each case, associated with a bending mode. A further test is made to determine if the identification is acceptable. It is known that for a real vehicle, except at the time of staging, the bending frequencies change in a more or less continuous manner. For this reason for each mode the present identified n value is compared with the previous n value associated with that filter. If the difference between the present and past n values is greater than 7 the presently identified peak is rejected as being unacceptable.

5. A further test is made so that the change between the present value of n and the past value of n is limited to be no greater than 3.

6. The vehicle bending mode frequencies are more or less harmonically related to each other within a tolerance band. This relationship is used to keep the mode identifications separated within the tolerance band. The ratio of ω_n at the second bending mode and ω_n at the first bending mode is compared with a fixed constant such that if the ratio is less than the constant, the second mode identification is rejected. A second test is made between the first and third mode with the third mode identification being rejected when the test fails.

7. At this time a frequency is computed for each identified mode from the formula

$$\omega_{F_I} = \frac{A_{n-1}\,\omega_{n-1} + A_n\,\omega_n + A_{n+1}\,\omega_{n+1}}{A_{n-1} + A_n + A_{n+1}} \tag{8}$$

8. ω_{F_I} for each mode is filtered to remove high frequency noise on the identified frequency by the formula

$$\omega_{T_{I_n}} = .5\,\omega_{F_{I_n}} + .5\,\omega_{T_{I_{n-1}}} \,. \tag{9}$$

ω_{T_I} is then used as the frequency to tune the notch filters.

The complete process is a rather complicated procedure though much has been done to reduce the computer speed requirements. At a .01 second sampling rate the integrations of equations 1 and 2 are performed using a rectangular integration algorithm. Also at .01 seconds testing is made to determine if the time to +ip/2 or t_o + ip has arrived (i.e., the upper integration limits). If the upper limit integration time has not arrived this is the only computation for each spectral filter that is done at the .01 sampling rate. When the upper limit integration time t_o + ip/2 on the first integral in Equation (2) arrives, a change in sign of the kernal is made. When the upper limit integration time t_o + ip arrives for any spectral filter the computations of U_i and V_i are made and S_i and C_i for that spectral filter reset to zero. At a sampling rate of .411 seconds the rest of the computations and testing to determine ω_T is made and notch transfer functions changed.

Special considerations are required when the identifiers are started at launch. All past values of U_i, V_i, S_i and C_i are set equal to zero. The ω_T frequencies are initialized to the expected launch bending frequencies. A time long enough so that the first 10 spectral filters can compute their first values of C_i and S_i (.48 seconds) must elapse before any identification of a new frequency is attempted and then only the third mode frequency. A time long enough for the first 15 spectral filters to obtain a complete C_i and S_i computation (.82 seconds) elapses before the third and second bending modes are allowed to be identified and total of 2.08 seconds elapses before all three modes are identified. In that initially the summations of U_i and V_i do not contain a total of 9 (the value of ℓ used in the system) terms, the normalizing constant for computing S and C is adjusted for each spectral filter.

Figure 3 shows the frequency identification performance for an ideal signal input of the form

$$F(t) = B_1 \sin \omega_1 t + B_2 \sin \omega_2 t + B_3 \sin \omega_3 t$$

where $B_1 = B_2 = B_3$ and the frequencies (ω_1, ω_2 and ω_3) change linearly with time as shown by the solid lines in Figure 3. Of major system importance is the initial response of the identification system from its initial setting to the actual bending frequency. The response time constant of the initial identification is dependent upon the actual frequency being identified plus the relative amplitudes of the three bending modes. Because of the relative wave lengths the third mode should be identified before the second mode which in turn should be identified before the first mode. This is dependent upon the relative bending amplitudes of each mode since the identification is based upon relative amplitude measurements. More rapid identification can be expected of a mode having a larger relative amplitude.

Figure 4 shows the time history of the identified frequencies in an actual trajectory run for the time period from 10 to 50 seconds. The trajectory was pitch plane with no wind disturbances. The expected bending frequency was initially set 25% below the known open loop bending frequency to determine the starting characteristics. The solid lines represent the known open loop bending frequencies. The closed loop bending frequencies are not known but should be close to the open loop frequencies. Poor identification on the third mode is due to the third mode being fairly unexcited.

A study of the required computer speed and size to perform the identification and control computations was not made during the study, however, making rough estimates based on previous studies and computer sizing experience indicates a computer memory size of 2000 words with a 5 μs add time and a 16 bit word length. This estimate should be verified by a computer sizing study. The physical size of a flight computer of this capacity and speed would be smaller than 1/2 cu ft.

A more complete description of the identification system is given in Appendix 6.1.

3.1.2 CONTROL SYSTEM STABILITY ANALYSIS

The basic vehicle pitch control system is shown in Figure 5. The system feedback is composed of attitude position and attitude rate. This signal is fed through a short period compensation and 3 notch filters tuned to the 1^{st}, 2^{nd} and 3^{rd} bending mode frequencies. A discussion of digital control systems and notch filter design is given in Appendix 6.2. Several basic control system designs were made as the study progressed. These designs followed each other in a natural progression as additional insight into the total system was obtained with each individual control system studied.

The problem of designing a best compensation configuration for Model Vehicle II (Appendix 6.3) which is compatible with frequency identification adaptive loop and the uncertainty factors associated with the vehicle data requires a series of tradeoffs which depend directly or indirectly on the system considerations listed below.

1. The level of uncertainty associated with the vehicle data, especially bending mode frequencies, mode slopes and mode shapes.
2. The typical variation of all of the vehicle parameters with trajectory time.
3. The required trajectory following capability, i.e., the required short period control frequency.
4. Vehicle structural load considerations.
5. The speed and accuracy of the frequency identification system.
6. The digital computer speed and resolution required for system mechanization.

A major influence in achieving good stability design is the placement of the poles which are required to generate the notch zeros. In the first configuration these poles were used to obtain a significant gain margin on the third bending mode. This was done because: 1) third mode identification was expected to be poorest because of sampling, 2) the instrument locations chosen cause third mode instabilities, 3) with the third mode gain stabilized higher bending modes which were not included in the stability analysis should also be gain stabilized and offer no problems. Table II gives the control system parameters for what will be called Compensation Configuration #1. In mechanizing the control system the notch filters are dc gain normalized, while the short period filter is not. Figures 6, 7 and 8 show the open loop gain phase of the system at 8, 78 and 157 seconds, respectively, with the notch zeros perfectly tuned to the open loop bending frequencies. With the perfectly tuned notches the 1st bending mode is phase stable with 120° of phase margin at t=8 sec which degenerates to only 20° of phase margin at 157 sec. The second and third modes are always gain stable with about 9 db on both of them at 8 sec and improving to 15 db on the second mode at 157 sec and 52 db on the third mode at 157 sec. The short period frequency is lower than desired, starting at about .5 rad and remaining at this value until late in flight where it moves to about .6 radians. The main cause of the low short period frequency is the poles which must be mechanized with the notch zeros. In order that these poles themselves do not go unstable they must have a damping much greater than the notch zero damping. At a lower frequency such as the short period the overall effect of the notch (including both its poles and zeros) is to produce phase lag. This reduces the short period frequency that can be maintained with an approximate 6 db short period high frequency gain margin.

Sampling rate	.1 sec
Rate Gain	2.5 sec
Short Period	
Zero	.6 rad/sec (Z- .9417)
Pole	2.4 rad/sec (Z- .7848)
1^{st} Mode Notch	
Zero damping	.025
Zero frequency	ω_{T_1} *
Pole damping	.5
Pole Frequency	2.5 rad/sec (Z- .8622 $\pm$ j .191)
2^{nd} Mode Notch	
Zero damping	.05
Zero frequency	ω_{T_2} *
Pole damping	.7
Pole frequency	3.0 rad/sec (Z- .792 $\pm$ j .175)
3^{rd} Mode Notch	
Zero damping	.05
Zero frequency	ω_{T_3} *
Pole damping	.7
Pole frequency	6.5 rad/sec (z- .559 $\pm$ j .3036)
Loop Gain	
0 sec to 112 sec	1.406
112 sec to 144 sec	.887
144 sec to 157 sec	.445

*Identified frequency

Table II. Compensation Configuration #1

In Compensation Configuration #1 the most critical point is the low phase margin on the first bending mode at 157 seconds. It is not possible to identify the exact bending frequency, plus it is not the open loop but the closed loop bending frequency which is being identified. Figure 9 is a gain phase of the 157 sec case using Compensation Configuration #1 with the notch zero tuned 2% high, i.e., at a frequency 1.02 times the open loop frequency. This plot shows an unstable first bending mode, in fact the phase margin point has moved left by approximately 40° indicating from the original 20° phase margin that the first mode identification at 157 sec will have to be within 1% at the high side. Narrow tolerance bands are more acceptable on the high side rather than the low side because the natural tendency of the bending modes is to increase in frequency during the trajectory. The identification system has a number of lags built into it so that it normally will identify a frequency which is lower than the frequency occurring.

A much more important question must be answered in determining the absolute stability of the configuration in conjunction with the frequency identification system. If the identification system is operating perfectly it will identify the closed loop bending frequency and move the notch zero to this frequency. In moving the notch zero the control system is changed, which in turn changes the closed loop bending frequency. At some place a null point will exist where the notch zero frequency and the closed loop bending frequency are identical. The stability question that then arises is "Is the system stable when operating at this null point?" If the answer to this question is no, the configuration is unacceptable. Figure 8 is a plot of the notch filter frequency ω_o versus the closed loop bending frequency $\omega_\square$ for the first bending mode of the 157 sec case using Compensation Configuration #1. This curve is divided into two parts, one part representing a stable first bending mode for the notch zero at the indicated frequency and the other part an unstable first bending mode for the notch zero at the indicated frequency. Also on the plot is a line representing the locus of all possible null points (i.e., $\omega_o = \omega_\square$). On this particular plot the null point is on the unstable part of the curve. Thus Compensation Configuration #1 is an unacceptable control system. The other flight cases and bending modes were checked in the same manner. The other modes and flight cases do not result in instability even when the notch zeros are detuned by 10%. If this unacceptable effect is to be eliminated, a change in control system values must be made. The control system parameters which would be expected to have the greatest effect upon the first mode stability are the first mode notch filter parameters. If a control system parameter such as the notch zero damping were changed, then the curve of Figure 10 would move to a new position, where possibly the null point would be on the stable portion of the curve. Figure 11 shows two curves, one is the notch filter frequency at which the boundary between the stable and unstable region occurs versus the notch zero damping. The other curve is the frequency of the null point versus the notch zero damping. The curve shows that for dampings of .0185 or less the null point will be in a stable region. Figure 10 is a gain phase of the 157 sec case with the notch zero tuned to 2.942 radians/sec which is the frequency at which the null point occurs. The gain phase shows the first mode is unstable verifying Figure 10 and Figure 11 at .025 damping. Figure 11 shows that with zero damping the null point is in a stable region. Figure 12 is a gain phase of the system with zero damping and the notch tuned to the null frequency of 2.889 radians/sec. With zero damping on the notch zero the marginally stable point occurs when the notch is tuned to 2.922 radians/sec. This is shown by the gain phase at Figure 14.

A second parameter which should have significant influence upon the first bending mode stability is the frequency of the first bending mode notch pole. Figure 15 shows the null point and the boundary between stable and unstable region for values of the first mode notch pole frequency. The null point enters a stable region as the first mode notch pole frequency is raised. A gain phase of the system with the first mode notch pole frequency raised to 3.5 rad/sec and the notch zero tuned to the null frequency is shown in Figure 16. The gain phase confirms the stable operation indicated by Figure 15. Figure 17 shows the gain phase of the same system except the first bending mode zero is set at the marginally stable point of 2.9912 radians/sec. The gain phase plot shows marginal stability.

This analysis indicates a better system from the standpoint of first mode stability would be achieved if the first mode notch pole frequency were made 3.5 rad/sec and the notch zero damping set at zero. Figure 18 is a gain phase of this system with the notch zero perfectly tuned to the open loop bending frequency. A point of primary interest is still the accuracy of identification required. Figure 19 and 20 are gain phase plots of the same system with the notch zero frequency tuned 3% low and 3% high. The 3% low case is stable but the 3% high case is unstable thus, the first mode must still be identified better than 3% on the high side.

If the design of the original system were made such that a greater phase margin were maintained on the first mode during the entire trajectory the effects of the unstable null point could be avoided. This was done in designing Compensation Configuration #2. The control system parameters associated with this configuration are given in Table III. In this configuration all of the notch pole frequencies have been raised and the short period lead-lag further separated. Figure 21, 22 and 23 are gain phase plots of this system with the zeros perfectly tuned for the three flight cases at t=8,

Sampling Rate	.1 sec
Rate Gain	2.0 sec
Short Period	
Zero	.4 rad/sec
Pole	2.8 rad/sec
1st Mode Notch	
Zero damping	.025
Zero frequency	ω_{T_1}*
Pole damping	.5
Pole frequency	3.625 rad/sec
2nd Mode Notch	
Zero damping	.025
Zero frequency	ω_{T_2}*
Pole damping	.7
Pole frequency	3.625 rad/sec
3rd Mode Notch	
Zero damping	.025
Zero frequency	ω_{T_3}*
Pole damping	.7
Pole frequency	5.0 rad/sec
Loop Gain	
0 to 112 sec	2.
112 sec to 144 sec	1.25
144 sec to 157 sec	.64

*Identified frequency

Table III. Compensation Configuration #2

78, 157 sec, respectively. As would be expected by increasing the notch pole frequencies and spreading the lead-lag, there is a reduction of the gain margin at the 2nd and 3rd bending modes. This is most significant at the 8 second flight case where the margins are the narrowest. The first mode phase margin at 157 sec has been increased to almost 80^{o} in comparison with the 20^{o} for Compensation Configuration #1. This configuration allows a 5% error in frequency identification on all modes except the first bending mode at 157 sec flight case where better than 3% error is allowable. Figure 24 through 41 show the gain phase for the 8, 78, and 157 second flight cases with the notch zeros tuned 5% high and 5% low for each mode except the 1st mode at 157 sec where only a 3% error is shown. All cases show a fair stability boundary still remains with the identification errors indicated except for the 2nd mode tuned low at the 8 sec flight case and the 3rd mode tuned low at the 8 sec and 78 sec flight cases. Compensation Configuration #2 still has a relatively low short period frequency, about .46 radians/sec during the major portion of the flight.

In the general control system configuration of Figure 5 the system design variables which can be changed in order to improve the short period frequency are:

1. rate instrument location
2. rate gain
3. short period lead-lag compensation
4. notch zero damping
5. notch pole frequency
6. notch pole damping

The desired effect upon the gain phase in increasing the short period frequency is to obtain more lead phase shift at those frequencies near the short period high frequency crossover of Compensation

Configuration #2 (i.e., near 1 radian/sec). Viewing the six types of design variables listed above to determine how they can be used to increase the short period frequency and how such changes affect overall stability results in:

1. Rate Instrument Location - A change in the rate instrument location will, in general, have no direct effect upon the short period frequency, but indirectly any additional lead at the short period frequency will cause a loss of gain margin at the higher frequencies. A change in the rate instrument location may increase the higher frequency gain margins especially at the bending modes, however, the rate instrument locations chosen for Compensation Configuration #1 and #2 were made on the basis of obtaining the most high frequency gain margin obtainable from acceptable instrument locations. Thus, a change in the rate instrument location to any other allowable location should have a harmful effect upon increasing the short period frequency.
2. Rate Gain - Increasing the rate gain will increase the short period frequency, however, it will also decrease the third bending mode gain margin.
3. Short Period Lead-Lag Compensation - Increasing the lead at the short period high frequency crossover frequency can be accomplished by means of the lead lag compensation at the expense of decreasing the high frequency gain margins. The lead-lag in Compensation Configurations #1 and #2 have been adjusted to obtain a near optimum short period frequency with the other control system design variables held fixed. Thus, little or no gain in short period frequency can be expected by just adjusting the lead-lag compensation.

4. Notch Zero Damping - Increasing the damping on the notch zeros will produce more phase lead at the short period, however a much more rapid reduction in gain margin at the 2nd and 3rd bending modes will occur.
5. Notch Pole Frequency - Increasing the notch pole frequency will reduce the amount of lag phase shift at the short period frequency, which is effectively adding lead. It will also reduce the higher frequency gain margins.
6. Notch Pole Damping - Decreasing the notch pole damping will reduce the lag phase shift at the short period frequency. It will cause some increase in gain margin above and below the notch pole frequency but will cause a large reduction in gain margin at the notch pole frequency by causing a bulge in the gain phase curve at this frequency.

Each design variable (except for rate instrument location) can be used to increase the short period frequency at the expense of a degradation in stability at some other frequency. A tradeoff was made between these parameters to obtain a near maximum short period frequency with the maximum allowable degradation in high frequency stability margins. The max q - 78 sec flight case was used as the major design point because an increase in short period frequency is desired to reduce trajectory following errors produced by wind disturbances and thus aerodynamic loads on the vehicle. These loads are most effective at max q. Table IV gives the control system parameters arrived at for the 78 sec flight case to obtain the maximum short period frequency. Figure 42 is a gain phase of this system which will be called Compensation Configuration #3. The short period frequency has been increased to .7 rad/sec when operating with 6 db of high frequency gain margin. The second and third mode are both only about 4 db below the operating gain and slightly phase stable. The first bending mode is in approximately the same location as it was in Compensation Configuration #2.

Sampling Rate	.1 sec
Rate Gain	3.0 sec
Short Period	
Zero	1.0 rad/sec
Pole	2.4 rad/sec
1st Mode Notch	
Zero Damping	.02
Zero frequency	ω_{T_1} *
Pole damping	.55
Pole frequency	4.5
2nd Mode Notch	
Zero damping	.025
Zero frequency	ω_{T_2} *
Pole damping	.55
Pole frequency	4.5
3rd Mode Notch	
Zero damping	.02
Zero frequency	ω_{T_3}
Pole damping	.7
Pole frequency	5.0
Loop Gain	1.23

*Identified Frequency

Table IV. Compensation Configuration #3 at 78 sec

This Compensation Configuration cannot be applied directly to other flight cases as a result of its being so highly optimized to the 78 sec flight case. Figure 43 and 44 are gain phase plots of this system applied directly to the 8 and 157 sec flight cases, respectively. In Figure 43 the 2^{nd} and 3^{rd} bending modes extend well into the area desired as a short period operating point. In Figure 44 the short period operating region is cut into by a frequency between the 1^{st} and 2^{nd} bending modes. This is caused by the two notch filter poles at 4.5 rad/sec and .55 damping. In order to maintain the configuration at 78 seconds and improve the operation at other flight cases the notch poles can be moved along with the notch zeros. In order to make such a system coincide with the 78 sec flight case the first mode notch pole frequency would be 1.95 ω_{T_1}, the second mode notch pole frequency .804 ω_{T_2}, and the third mode notch pole frequency .55 ω_{T_3}. Figure 45 and 46 are gain phase plots of the 8 and 157 sec flight cases with the notch pole frequencies determined in this manner. Only a slight improvement has been made at the 8 sec case by allowing the notch pole frequencies to change with the notch zero frequencies, about 2.5 db at the second bending mode. A much greater improvement is made at the 157 sec flight case. The normal short period operating region is cleared of all high frequency loci. By operating with a loop gain of .5 a short period frequency above .7 radians/sec is obtained with 6 db of high frequency short period gain margin. The first bending mode is phase stabilized by 125° and the second mode by 50°. By allowing the notch poles to vary along with the notch zeros an entirely new picture is created with respect to the adaptive stability. Before this system could be considered acceptable, study would have to be made to determine if an identification null can be achieved with an unstable system (i.e., an operating point similar to that shown in Figure 10.

Fourth Bending Mode

The basic vehicle data suggests that the fourth bending mode will have little influence upon the system operation or stability except possibly at 149 seconds when its mass drops to a minimum of 1600 K_g - sec^2/m. A gain phase of this flight case using Compensation Configuration #2 including the fourth bending mode is shown in Figure 47. It is evident from the plot that the fourth bending mode has a significant residue, however, the open loop gain at the fourth mode frequency can be reduced by 12 db using a simple lag at 5 radians. The fourth bending mode therefore does not present a significant vehicle stability problem.

Stability with Fuel Slosh

The fuel slosh modes have a much greater influence upon system stability and in turn will influence the identification performance of the spectral system. The majority of the stability and trajectory analysis did not include fuel slosh because of the significant increase in computations required with slosh included with the resultant increase in cost and time to perform the analysis. A stability analysis was made using Compensation Configuration #2 for the 8, 78 and 157 sec flight case with fuel slosh and baffles included. The gain phase curves generated in the analysis are given in Figure 48, 49 and 50. These figures should be compared with the no slosh case shown in Figure 21, 22 and 23, respectively. In comparing the 8 sec case (Figure 48 and 21) where the major alteration is in the first bending mode which has either been raised in frequency or been replaced by a slosh mode. In either case the mode with slosh is much greater in magnitude with a reduced phase margin. If this in actuality represents a slosh mode the effect upon the spectral identification system is questionable since the input sensor to the spectral identification system contains only bending and no direct slosh measurements. At the 78 sec flight case (Figure 49 and 22) the first bending mode and significant slosh mode are both easily recognizable. The amplitude of the first bending mode is reduced and the slosh mode much more significant than the first mode. At the 157 sec flight case (Figure 50 and 23) the slosh has not greatly effected the first bending mode, however, the slosh mode itself, though reduced in magnitude from the other flight cases, has cut significantly into the short period stability boundaries.

The 8 sec flight case using Compensation Configuration #2 was run with fuel slosh and no baffles. A gain phase of this system is given in Figure 51. The third slosh mode is phase stable with only about 5^{o} of phase margin and the first slosh mode now shows a significant effect upon the gain phase.

It is evident from these plots that fuel slosh does definitely effect the system stability. Its effect upon the spectral identification system and thus the bending stability must be determined by simulation because the sensor used as an input to the spectral identifiers measures only bending and thus slosh excitation in the system could only effect the bending frequency identification by its influence on bending.

3.1.3 WORST CASE ANALYSIS

NASA working papers concerning bending parameter variations due to variations in Vehicle EI characteristics for the Saturn V were analyzed to obtain an estimate of worst case bending parameter variations for Model Vehicle II.

The data analyzed was of bending mass, frequency, slope and deflections for variations in vehicle stiffness of ± 50% at each interstage and ± 10% overall for the max q flight case. The bending parameter variations required for Model Vehicle II and the basic control system studied are the bending frequencies, mass, and slopes at the instrument unit and the 1:2 interstage region for the first three bending modes.

In obtaining the worst case data the following procedure was followed:

1. For each of the four variations in vehicle stiffness the incremental change from nominal of each bending parameter required was generated.
2. Table V was generated to show the effect of each stiffness variation on each bending parameter required (i.e., whether the tendency is to increase, decrease or is negligible).
3. Analyzing Table V shows that a maximum positive variation in all three bending frequencies is obtained if

   Interstage 1:2 stiffness is +50%
   Interstage 2:3 stiffness is +50%
   Interstage 3:4 stiffness is +50%
   Overall stiffness is -10%

A maximum negative variation in all three bending frequencies is obtained if

Interstage 1:2 stiffness is -50%
Interstage 2:3 stiffness is -50%
Interstage 3:4 stiffness is -50%
Overall stiffness is +10%

A maximum decrease in m_2, $Y_1'(IU)$, and $Y_2'(IU)$ and ${Y_3}'_{(1:2IS)}$ and a maximum increase in m_1, $Y_3'(IU)$, ${Y_1}'(1:2IS)$ and ${Y_2}'(1:2IS)$ is obtained if

Interstage 1:2 stiffness is +50%
Interstage 2:3 stiffness is -50%
Interstage 3:4 stiffness is -50%
Overall stiffness is -10%

A maximum increase in m_2, $Y_1'(IU)$, $Y_2'(IU)$ and ${Y_3}'_{(1:2IS)}$ and a maximum decrease in m_1, $Y_3'(IU)$, ${Y_1}'_{(1:2IS)}$ and ${Y_2}'_{(1:2IS)}$ is obtained if

	+50% at IS 1:2	-50% at IS 1:2	+50% at IS 2:3	-50% at IS 2:3	+50% at IS 3:4	-50% at IS 3:4	+10% overall	-10% overall
ω_1	+	-	+	-	+	-	-	+
ω_2	+	-	+	-	+	-	-	+
ω_3	+	-	+	-	+	-	-	+
m_1	+	-	-	+	-	+	0	0
m_2	-	+	+	-	+	-	0	0
m_3	+	-	-	+	+	-	0	0
$Y'_1(IU)$	-	+	+	-	+	-	0	0
$Y'_2(IU)$	-	+	+	-	+	-	0	0
$Y'_3(IU)$	+	-	-	+	-	+	0	0
$Y'_1(1:2IS)$	+	-	-	+	-	+	0	0
$Y'_2(1:2IS)$	+	-	0	0	-	+	-	0
$Y'_3(1:2IS)$	-	+	+	-	+	-	0	0

Table V. Stiffness Influence on Bending Parameters

Interstage 1:2 stiffness is -50%

Interstage 2:3 stiffness is +50%

Interstage 3:4 stiffness is +50%

Overall stiffness is +10%

A maximum increase in m_3 is obtained if

Interstage 1:2 stiffness is +50%

Interstage 2:3 stiffness is -50%

Interstage 3:4 stiffness is +50%

and a maximum decrease in m_3 is obtained if

Interstage 1:2 stiffness is -50%

Interstage 2:3 stiffness is +50%

Interstage 3:4 stiffness is -50%

These 6 variations in vehicle stiffness are then defined to be the worst case configurations 1 through 6, respectively.

4. For each of the six cases a total incremental variation in each bending parameter was obtained by adding the incremental changes for each appropriate stiffness variation. For the bending frequencies and masses these were converted to a percentage of the nominal in order to apply them to Model Vehicle II. Since the bending deflections are normalized to be 1 at the nozzle for both vehicles and since a percentage variation of a parameter which goes through zero is nebulous the slope incremental variations were transferred directly to Model Vehicle II. Although these variations are computed for the max q flight case (the only case for which data is available) they were assumed appropriate for all flight times. Table VI gives the variations as a percent for frequency and mass and as a magnitude for the slopes which were applied to Model Vehicle II in the worst case bending analysis. This data,

	WORST CASE CONFIGURATION					
	1	2	3	4	5	6
ω_1	+12.3%	-19.4%	-0.2%	-6.8%	+2.4%	-10.2%
ω_2	+11.0%	-13.4%	+0.9%	-3.2%	+5.1%	- 7.2%
ω_3	+ 7.0%	- 9.8%	+3.4%	-6.2%	+0.4%	- 3.0%
m_1	- 7.8%	+40.6%	+53.3%	-20.4%	+4.9%	+27.9%
m_2	- 5.3%	+12.8%	-32.2%	+40.7%	-15.0%	+23.7%
m_3	+10.3%	- 9.8%	+ 6.9%	- 6.0%	+15.1%	-14.7%
Y'_1(IU)	.0084	-.0338	-.0677	.0423	-.0208	-.0046
Y'_2(IU)	.0141	-.0237	-.0797	.0701	.0111	-.0207
Y'_3(IU)	-.02388	.01366	.04259	-.05281	-.00847	-.00175
$Y'_{1(1:2IS)}$	-.0055	-.0041	.0124	-.0220	-.0015	-.0081
$Y'_{2(1:2IS)}$	.0039	-.0305	.0102	-.0368	-.0039	-.0100
$Y'_{3(1:2IS)}$	.01391	.00502	.00983	.02858	.01012	.00863

Table VI. Incremental Variations in Bending Parameters for Model Vehicle II for 6 Worst Case Vehicle Configurations plus variations on the aerodynamic and dynamic data for Model Vehicle II, were utilized to investigate the effect on the system stability when the off-nominal vehicle parameters are utilized in conjunction with the control and adaptive system parameters designed using nominal vehicle parameters.

The six worst case configurations defined by Table VI plus worst case variations in the center of gravity (-.5 meters), center of pressure (+3.02 meters), C_{z_α} (+6%) and forward loop gain (-10%) were used to determine their effect upon systems stability. Figure 52 through 69 are gain phase plots for these six worst case configurations for 8, 78 and 157 sec flight case using Compensation Configuration #2.

All worst case configurations remained stable except for the 8 and 78 sec flight case using worst case configuration #2. In the worst case configuration #2 at 8 and 78 sec the second bending mode is unstable plus the third bending mode by about 1/2 db at the 8 sec case. In order to stabilize this case a lag phase shift of 40° at the 2nd bending mode and 5° at the third bending mode are required. This can be obtained by the addition of a lag lead network to the short period compensation and/or decreasing the damping on the first and second mode notch poles.

The most important point in this analysis is that neither the short period nor the first bending mode become unstable. Short period gain margins were reduced significantly in some case but absolute short period stability was always maintained.

3.1.4 LOAD RELIEF

The main purpose of the load relief system design was to demonstrate the operation of the spectral identification system. The principal features of the designed load relief system are:

a. The system features a conventional normal acceleration loop, including second order digital compensation in the N_z loop.

b. The load relief system becomes operative when the normal acceleration at the output of the N_z loop filter exceeds a threshold level.

c. When the N_z loop is operative, the ordinary short period and bending compensation is unchanged but the N_z loop (in the control computer) includes the option of using a different rate gain and a (constant factor) gain adjust on the system programmed forward loop gain.

Figure 70 is a gain-phase plot of Compensation Configuration #2 with the N_z loop closed. The N_z compensation is second order, and includes (frequency characteristics) a pole at .3 rad/sec, a zero at 1 rad/sec and a second pole at 3 rad/sec. Equation (10) is the Z form of the N_z compensator.

$$DN_z(Z) = \left.\frac{(Z-.90469)(Z+1)}{(Z-.97044)(Z-.73742)}\right|_{\text{gain normalized}} \qquad (10)$$

The N_z loop gain (actual) is +.368, the rate gain and system loop gain are respectively 3 and 1.1 when the N_z loop is operative. The N_z loop threshold used for the trajectory runs is 0.1 m/sec^2, monitored at the output of the DC gain normalized N_z loop filter. In the flight computer the N_z signal from the accelerometer (mounted at 46.54 m) would be processed through the N_z filter from lift-off, and the output of the filter tested at each control cycle time.

When this signal exceeds the threshold specified, a different control equation, including the N_z term, the new rate gain and the N_z loop gain adjust would be processed by the control computer. When the N_z signal from the N_z filter goes below the threshold, the normal system control equation would again be processed. This system results in a 37.7% reduction in peak loads due to wind disturbance. Additional load relief can be accomplished by increasing the short period frequency of the basic attitude control system as was done in Compensation Configuration #3. The increase in short period frequency of the attitude control loop will allow for higher load relief system gains and bandwidth.

The primary objective of establishing the adaptive system performance with load relief was achieved using this system.

3.1.5 TRAJECTORY SIMULATIONS

A great number of trajectory simulations were made which represents a huge bulk of material, a single trajectory run being represented by up to 70 time function plots. In order to extract the significant points from the trajectory simulations a double sifting of the data was performed. First the most significant trajectory runs were selected and secondly, from these runs only the plots of the most significant vehicle parameters are included

Compensation Configuration #1

Figure 71-1 through 71-8 is a partial trajectory covering the time period from t = 10 sec to t = 90 sec using Compensation Configuration #1. There is no wind and the spectral identifier is initialized 25% below the actual open loop bending frequencies. At this initial setting all three bending modes are unstable as shown by the gain-phase of Figure 72 which is at t = 8 sec with 25% detuning on all three bending modes. Figure 71-1 shows that after 8 sec of trajectory time the bending frequencies have been identified within 5% of the open loop frequencies which the stability analysis shows is a stable system. During the time that unstable operation existed the bending did not diverge or become excited enough to significantly disturb the gyro output (Figure 71-2), the rate gyro output (Figure 71-4), the delta rate gyro output (Figure 71-5) or the nozzle deflection (Figure 71-6). In Figure 71-1 from 66 to 80 sec all three identified bending frequencies remain constant. This is because the identification system found no legitimate peaks in that the bending amplitude was low enough to be below the resolution level set on the identifiers. Other parameters from this run are the nozzle rate and angle of attack. Another trajectory run was made for the time period t = 90 to t = 157 sec for this same system but is not included in this report. The stability analysis indicated that a 157 sec the first bending mode would be unstable if the adaptive spectral identification loop was at null. The system did not go unstable however, because lags in the identification system caused the first mode to be identified low at 157 sec.

Figure 73-1 through 73-8 is the same system as Figure 71-1 through 71-8 except for an α_{ω} input. The wind was not initiated until 24 sec and thus the first portion of the runs of Figures 71 and 73 are identical. Trajectory following was similar until the max q region indicated by Figures 71-2 and 73-2. The trajectory following became worse with the additions of winds as would be expected. The bending activity between the two runs is similar until 78 sec where a rapid change in the α_ω profile occurs which significantly increases the bending excitation as indicated by the differential rate gyro output (Figure 73-5-*). The second and third bending mode becomes poorly identified at times. This is caused primarily by wind energy being high at frequencies other than the bending frequencies. This run and other runs indicate that even though one or more bending modes are poorly identified at times, the proper identification will be regained before significant bending deflections are generated from a resultant unstable mode. This is because either the energy source producing the extraneous energy disappears or because the bending builds up just great enough to be larger than the extraneous energy source and thus identified. The wind profile used for this run was not the standard worst case wind profile used in the rest of the trajectory runs, but, in general, a worse wind than the worst case wind profile. Loads on the vehicle have increased significantly because of the wind profile which can be seen by comparing the nozzle deflections (Figures 71-6 and 73-6) and the angle of attack (Figures 71-8 and 73-8). These loads can be reduced by the addition of a load relief system and by increasing the vehicle response through more optimum control compensation.

The worst case wind profile is shown in Figure 74. This profile includes a peak gust at 72 seconds. In order to determine the effects of initially having the spectral identifiers tuned 25% high a gain-phase using Compensation Configuration #1 for the 8 sec flight case was generated and is shown in Figure 75. Figure 76 is a partial trajectory for the time period t = 10 to t = 90 seconds using Compensation Configuration #1 with the worst case MSFC winds and the notch filters initially detuned 25% high. For the first 52 seconds until the α_ω profile starts, this figure can be directly compared with Figure 71 where the notch zeros were initially detuned 25% low. Comparing the differential rate gyro outputs at an expanded scale showed that the second and third bending modes are much more excited with the notch zeros initially detuned low. At 72 seconds the bending excitation increases significantly due to the wind gust. The wind gust has a dual effect. It directly excites the bending to cause large deflections but it also detunes the identifiers, destabilizing the system and further increasing the bending excitation as indicated by Figure 76-1. When the gust is passed the spectral identifiers rapidly re-identify the bending and return to a stable configuration.

Compensation Configuration #2

Figures 77 and 78 are gain phase plots showing the effects of detuning the notch zeros 25% high and low. When tuned 25% high as shown in Figure 77, all modes are stable. When tuned 25% low as shown in Figure 78, the first and third modes are unstable. A trajectory response equivalent to Figure 76, but using Compensation Configuration #2, is shown in Figure 79. The response with Compensation Configuration #1 (Figure 76) and with Compensation Configuration #2 are very similar until the gust is applied at 72 seconds. With Compensation Configuration #2 the second bending mode is much more excited. With Compensation Configuration #2 the loading indicated by nozzle deflections and angle of attack is comparable with Compensation Configuration #1 indicating the requirement for increasing response and for a load relief system.

A complete trajectory, i.e., t = 10 to t = 157 sec, using Compensation Configuration #2 is shown in Figure 80. Trajectories were always started at t = 10 seconds rather than at t = 0 sec because with a digital simulation there is no excitation to the problem until pitchover occurs. In Figure 80 the load relief system is operative but does not cross the threshold and switch until after 60 sec. Comparing Figures 79-1 and 80-1 it can be seen that the identification is more rapid and better when the notch zeros are initially detuned low. This is caused by the first and third bending modes being initially unstable when the notch zeros are tuned low. With unstable bending modes the oscillatory bending deflection increases more rapidly and is thus more easily identified. With the spectral identification adaptive control system is is generally the case if the bending is well stabilized and thus excited very little, the spectral system will show poor identification because the bending enery is low. If, on the other hand, the bending energy is high due to poor bending stability, the bending frequencies are well identified by the spectral system. It is, in fact, this operation that guarantees stability if the basic control system is properly designed because the more unstable the bending becomes and thus more excited, the more accurate the identification becomes and thus, the better assurance of a resultant stable configuration. When the load relief system is initially turned on at 60 sec the identification becomes disturbed because of a large transient seen on the differential rate gyro signal (Figure 80-4). Identification accuracy returns to normal after the transient is passed and remains good throughout the rest of the load relief system operation until another transient is produced when it is switched out. The loads are most easily seen by the nozzle side force caused by the nozzle deflection (Figure 80-6) and are considerably reduced with the load relief system as compared with Figure 79-6. The load relief system results in a load reduction of 37.7%. A further load reduction would result if the short period response was increased by the use of Compensation Configuration #3.

Of basic conern is the effect of random noise on the identification system. The major source of random noise is random wind gusts. A worst case random wind gust profile was added to the MSFC worst case wind profile to generate a random input source for the simulation. These random wind gusts were generated by filtering the output of a random number generator to obtain known wind frequency characteristics. A peak gust velocity of 120 meters/sec was assumed. The total α_ω profile is shown in Figure 81. Figure 82 is a trajectory response with the α_ω profile of Figure 81 using Compensation Configuration #2 with the load relief operative. The frequency identification deviation during the high disturbance time (t = 50 to 90 sec) is less with gust energy present as can be seen by comparing Figures 80-1 and 82-1. In the vicinity of 112 sec there is a period when the second and third mode filters do not identify

(Figure 82-1). Figure 83 is a spectrograph of the spectral filter output amplitudes taken during this period of time. The spectral identification system first chooses the three largest peaks occurring at n values of 11, 15 and 20. These three peaks are associated with the three bending modes in the manner 20 with the first, 15 with the second and 11 with the third. A test of the ratios insuring the separation of the bending frequencies then rejects the peaks at 11 and 15. The peak at 15 is not caused by the bending but by the gust energy. The peak at 11 is caused by the second bending mode and thus should not be associated with the third mode. If the peak at 15 would have first been rejected as being too close to the first mode and then the three largest remaining peaks selected which occur at 20, 11 and 5, proper identification would have been made. It is evident that while no really bad tuning occurs due to the processing technique, more information is present in the filter outputs than is utilized. This is a good example to illustrate the identification accuracy vs. information processing sophistication tradeoff. In this case, very little would be gained by the additional processing since good dynamic stability is maintained without the additional processing. Normal identification of all three modes resumes near 120 sec in Figure 82-1.

As would be expected the addition of random gusts increases the bending activity but the spectral identification system maintains a stable control system thereby maintaining acceptable operation. In actuality, the identification is improved with the random gust input.

Instrument Noise

Another major source of random noise is generated by the control sensors. Wideband noise was added to each instrument. Peak instrument noise values used were $\pm$ 5 degrees on the attitude gyro, $\pm$ .25 deg/sec on the rate gyro and $\pm$ 1.1 deg/sec on the differential rate gyro. All of these values are much greater than would be ordinarily expected on a well functioning sensor. Figure is a trajectory response with these values of sensor noise. It is identical to the trajector of Figure 82 except for the addition of the instrument noise. The instrument noise further improves the frequency identification and does not significantly affect the trajectory following. The bending is more excited due to the increased activity of the nozzles caused by the sensor noise.

Fuel Slosh

In order to simplify the vehicle dynamics with slosh included and the resultant cost of simulating the vehicle, the conglomerate characteristics of the three slosh modes were approximated by a single slosh mode. The approximation was made by comparing the open loop gain phase of the vehicle with three slosh modes to that of the vehicle with one slosh mode. The best approximation occurred when the unmodified third slosh mode was used. An open loop gain phase of this system is shown in Figure 85. The slosh peak with only one mode is reduced by about 5 db from that with three modes. Since the mode is close to the 0° phase line this results in only about a 2 db change in the closed loop system. The general shape of the gain phase curve is the same for either 1 or 3 slosh modes. A trajectory run with the single slosh mode was made and is shown in Figure 86. A comparison of this trajectory with Figure 79 shows that the addition of the slosh mode increases the bending activity especially of the first mode, however, there is no tendency shown for the spectral identifier to identify the slosh frequency. There is a shift in the identified first bending mode frequency which can be attributed in part to a real shift in the bending frequency with the change in the vehicle dynamics and partly to poorer identification which is indicated by higher bending activity.

Figure 87 is a spectrograph of the spectral filter output amplitudes. A slosh peak is recognizable around the integer value 17. The identification system does not, however, interpret this as a legitimate peak because in each case there are not two integer points on each side of the peak which have amplitudes lower than the peak value.

With a more highly active slosh mode it would be expected that the slosh mode would be identified at times. If a notch were placed at the slosh frequency the system configuration would dictate whether the bending and/or slosh mode were to go unstable. If the system were to be designed so that the slosh mode remained stable whether the notch were placed at its frequency or not, then the displaced notch from the bending mode would cause the bending to become unstable, thus more excited and in turn, be re-identified. One would thus expect the vehicle to operate with the bending activity larger than the slosh activity as measured by the delta rate gyro signal so that the bending frequency would be identified.

3.2 ACTIVE CONTROL

The term active control is used to describe a control system designed for a flexible vehicle which goes beyond the normal system which is generally designed to control the vehicle in spite of bending. An active bending control system is one which controls the bending as well as vehicle attitude. To obtain a system which will control bending a sensor to measure bending is required. The obvious sensor to use is the differential rate gyro which as previously described has only bending signals on its output. The differential rate gyro output must then be processed and summed with the normal attitude control error to form the total nozzle command signal. This processing of the differential rate gyro signal in a linear system amounts to a compensation network. To obtain a system which is tolerant of changes in vehicle dynamics and flexibility parameters the compensation on the differential rate gyro output will have to be changed during flight by some adaptive control sensor. With these adaptive control loops removed the active control system open loop block diagram is represented by Figure 88. Before an adaptive system can be designed to generate the G-function the desired characteristics of this function must be determined. The total open loop transfer function of β_c/β_c can be expressed in partial fraction form. The partial fraction expression will contain two terms for each bending open loop root, one term having the complex conjugate root and residue of the other term. Defining a function γ to be the sum of one of the bending partial fraction terms for each bending mode then for three bending modes

$$\gamma = \frac{E_1 + j F_1}{Z + a_1 + j b_1} + \frac{E_2 + j F_2}{Z + a_2 + j b_2} + \frac{E_3 + j F_3}{Z + a_3 + j b_3} \tag{11}$$

For each of the vehicle transfer functions of Figure 86 an expression similar to γ can be defined, i.e., a function ϵ being the sum of one bending partial fraction term for each mode for $\phi_I + K_{\dot{\phi}} \dot{\phi}_{I_1}/\beta_c$ and ρ being the sum of one bending partial fraction term for each mode for $\dot{\phi}_{I_1} - \dot{\phi}_{I_2}/\beta_c$ yielding

$$\epsilon = \frac{A_1 + j B_1}{Z + a_1 + j b_1} + \frac{A_2 + j B_2}{Z + a_2 + j b_2} + \frac{A_3 + j B_3}{Z + a_3 + j b_3} \tag{12}$$

and

$$\rho = \frac{C_1 + j D_1}{Z + a_1 + j b_1} + \frac{C_2 + j D_2}{Z + a_2 + j b_2} + \frac{C_3 + j D_3}{Z + a_3 + j b_3} . \tag{13}$$

The function γ must then be the select partial fraction terms from $\epsilon + G(Z)\rho$. Thus, the γ function residues are

$$E_1 + j F_1 = A_1 + jB_1 + G(-a_1 - jb_1)(C_1 + jD_1) \tag{14}$$

$$E_2 + j F_2 = A_2 + jB_2 + G(-a_2 - jb_2)(C_2 + jD_2) \tag{15}$$

$$E_3 + j F_3 = A_3 + jB_3 + G(-a_3 - jb_3)(C_3 + jD_3) \tag{16}$$

Separating the real and imaginary portion of these equations produces a set of six equations. For each flight case with a fixed rate gain the values of A, B, C, and D are known for the nominal vehicle. If the values of E and F can be determined from the desired bending response then these six equations can be solved to determine six design variable coefficients in the G function in terms of the remaining design variable in the G function, assuming the existence of more than 6 design variables. For example, if we define a G function to be of the form:

$$G(Z) = \frac{\alpha_3 Z^3 + \alpha_2 Z^2 + \alpha_1 Z + \alpha_0}{Z^3 + \nu_2 Z^2 + \nu_1 Z + \nu_0} \tag{17}$$

then each of the equations (14), (15), and (16) are of the form

$$(C_i + jD_i) \{ [\alpha_3 (3a_i b_i^2 - a_i^3) + \alpha_2 (a_i^2 - b_i^2) - \alpha_1 a_i + \alpha_0]$$

$$+ j [\alpha_3 (b_i^3 - 3b_i a_i^2) + \alpha_2 \cdot 2a_i b_i - \alpha_1 b_1]\} = [(E_i - A_i) + j(F_i - B_i)] \{[(3a_i b_i^2 - a_i^3)$$

$$+ \nu_2 (a_i^2 - b_i^2) - \nu_i a_i + \nu_0] + j [(b_i^3 - 3b_i a_i^2) + \nu_2 \cdot 2a_i b_i - \nu_1 b_i]\} \tag{18}$$

where $i = 1, 2, 3$

Equation (18) can be separated into its real and imaginary parts producing a set of six equations. In these six equations there are seven unknowns (i.e., α_3, α_2, α_1, α_0, ν_2, ν_1 and ν_0). Six of these unknowns can be solved for in terms of the remaining unknown. If the remaining unknown is chosen to be α_3 then these six equations in matrix notation can be expressed as:

$$MX = V \tag{19}$$

where M is a 6 x 6 matrix and X and V are both 6-vectors. From equation (18)

$$M_{11} = C_1 (a_1^2 - b_1^2) - 2 a_1 b_1 D_1 \tag{20}$$

$$M_{12} = - a_1 C_1 + b_1 D_1 \tag{21}$$

$$M_{13} = C_1 \tag{22}$$

$$M_{14} = (A_1 - E_1)(a_1^2 - b_1^2) + 2(F_1 - B_1) a_1 b_1 \tag{23}$$

$$M_{15} = (E_1 - A_1)\ a_1 - b_1\ (F_1 - B_1) \tag{24}$$

$$M_{16} = A_1 - E_1 \tag{25}$$

$$M_{21} = C_2\ (a_2{}^2 - b_2{}^2) - 2\ a_2 b_2 D_2 \tag{26}$$

$$M_{22} = -a_2 C_2 + b_2 D_2 \tag{27}$$

$$M_{23} = C_2 \tag{28}$$

$$M_{24} = (A_2 - E_2)(a_2{}^2 - b_2{}^2) + 2\ a_2 b_2 (F_2 - B_2) \tag{29}$$

$$M_{25} = (E_2 - A_2)\ a_2 - b_2\ (F_2 - B_2) \tag{30}$$

$$M_{26} = A_2 - E_2 \tag{31}$$

$$M_{31} = C_3\ (a_3{}^2 - b_3{}^2) - 2\ a_3 b_3 D_3 \tag{32}$$

$$M_{32} = -a_3\ C_3 + b_3\ D_3 \tag{33}$$

$$M_{33} = C_3 \tag{34}$$

$$M_{34} = (A_3 - E_3)(a_3{}^2 - b_3{}^2) + 2\ a_3 b_3\ (F_3 - B_3) \tag{35}$$

$$M_{35} = (E_3 - A_3)\ a_3 - b_3\ (F_3 - B_3) \tag{36}$$

$$M_{36} = A_3 - E_3 \tag{37}$$

$$M_{41} = D_1\ (a_1{}^2 - b_1{}^2) + 2\ a_1 b_1 C_1 \tag{38}$$

$$M_{42} = -a_1 D_1 - b_1 C_1 \tag{39}$$

$$M_{43} = D_1 \tag{40}$$

$$M_{44} = (B_1 - F_1)(a_1{}^2 - b_1{}^2) + 2\, a_1 b_1\, (A_1 - E_1) \tag{41}$$

$$M_{45} = a_1\, (F_1 - B_1) + b_1\, (E_1 - A_1) \tag{42}$$

$$M_{46} = B_1 - F_1 \tag{43}$$

$$M_{51} = D_2\, (a_2{}^2 - b_2{}^2) + 2\, a_2 b_2 C_2 \tag{44}$$

$$M_{52} = -\, a_2 D_2 - b_2 C_2 \tag{45}$$

$$M_{53} = D_2 \tag{46}$$

$$M_{54} = (B_2 - F_2)(a_2{}^2 - b_2{}^2) + 2\, a_2 b_2\, (A_2 - E_2) \tag{47}$$

$$M_{55} = a_2\, (F_2 - B_2) + b_2\, (E_2 - A_2) \tag{48}$$

$$M_{56} = B_2 - F_2 \tag{49}$$

$$M_{61} = D_3\, (a_3{}^2 - b_3{}^2) + 2\, a_3 b_3 C_3 \tag{50}$$

$$M_{62} = -a_3 D_3 - b_3 C_3 \tag{51}$$

$$M_{63} = D_3 \tag{52}$$

$$M_{64} = (B_3 - F_3)(a_3{}^2 - b_3{}^2) + 2\, a_3 b_3\, (A_3 - E_3) \tag{53}$$

$$M_{65} = a_3\, (F_3 - B_3) + b_3\, (E_3 - A_3) \tag{54}$$

$$M_{66} = B_3 - F_3 \tag{55}$$

$$X_1 = \alpha_2 \tag{56}$$

$$X_2 = \alpha_1 \tag{57}$$

$$X_3 = \alpha_0 \tag{58}$$

$$X_4 = \nu_2 \tag{59}$$

$$X_5 = \nu_1 \tag{60}$$

$$X_6 = \nu_0 \tag{61}$$

$$V_1 = (E_1-A_1-\alpha_3C_1)(3a_1b_1^{\,2}-a_1^{\,3})-(F_1-B_1-\alpha_3D_1)(b_1^{\,3}-3b_1a_1^{\,2}) \tag{62}$$

$$V_2 = (E_2-A_2-\alpha_3C_2)(3a_2b_2^{\,2}-a_2^{\,3})-(F_2-B_2-\alpha_3D_2)(b_2^{\,3}-3b_2a_2^{\,2}) \tag{63}$$

$$V_3 = (E_3-A_3-\alpha_3C_3)(3a_3b_3^{\,2}-a_3^{\,3})-(F_3-B_3-\alpha_3D_3)(b_3^{\,3}-3b_3a_3^{\,2}) \tag{64}$$

$$V_4 = (F_1-B_1-\alpha_3D_1)(3a_1b_1^{\,2}-a_1^{\,3})+(E_1-A_1-\alpha_3C_1)(b_1^{\,3}-3b_1a_1^{\,2}) \tag{65}$$

$$V_5 = (F_2-B_2-\alpha_3D_2)(3a_2b_2^{\,2}-a_2^{\,3})+(E_2-A_2-\alpha_3C_2)(b_2^{\,3}-3b_2a_2^{\,2}) \tag{66}$$

$$V_6 = (F_3-B_3-\alpha_3D_3)(3a_3b_3^{\,2}-a_3^{\,3})+(E_3-A_3\alpha_3C_3)(b_3^{\,3}-3b_3a_3^{\,2}) \tag{67}$$

A possible desirable set of values for the open loop bending residues is zero. Under this condition the control system has no effect at all on the bending, thus producing a complete decoupling between attitude control and vehicle bending. This represents more decoupling than could be provided by placing the instruments on a theoretical though non-existent bending mode for all three modes, in that under this condition bending coupling would still exist through the aerodynamics and thrust forces.

These equations were solved for the 78 sec nominal flight case with the result:

$$\alpha_2 = -\ .32990995-2.3695892\ \alpha_3 \tag{68}$$

$$\alpha_1 = .49906993+2.1397287\ \alpha_3 \tag{69}$$

$$\alpha_0 = -\ .27268560-.6943850\ \alpha_3 \tag{70}$$

$$\nu_2 = -\ 2.48679068+.6887001\ \alpha_3 \tag{71}$$

$$\nu_1 = 2.45025842-.6612812\ \alpha_3 \tag{72}$$

$$\nu_0 = -1.28655078+.3283598\ \alpha_3 \tag{73}$$

A gain phase for this system with $\alpha_3 = 7.5$ is shown in Figure 89 It can be seen that all effects of bending on the gain phase have been removed. With no short period compensation it is possible to operate above 1 rad with a $\pm$ 12 db gain margin and 45° of phase margin. This can be compared with the gain phase of the system with no bending compensation, Figure 90 and with perfect instruments, that is the bending slopes for all three modes zero at the instrument locations, in Figure 91.

A root locus and time response were made of this system. The root locus is shown in Figure 92. The open loop poles and zeros show that the natural system bending zeros have been drawn in to exactly cancel the bending poles.

Figure 93 is a time response of the system with the vehicle dynamics fixed at 78 seconds. It is a yaw simulation with worst case winds. Figures 93-1 and 93-3 shows that the bending, especially the first mode, is still excited and very lowly damped. The nozzle deflection, Figure 93-4, shows no bending component at all which is further indicated by no bending observed on the nozzle rate, Figure 93-5.

The bending being generated is from the α_ω input. This leads one to two new areas of investigation. The first is to determine if a compensation on the delta rate gyro output can be designed to zero the closed loop residues of both the transfer functions η/α_ω and η/ϕ_c simultaneously. The second design direction is to cause the bending frequency open loop gain-phase value to be such that upon closing the loop the feedback will degenerate the bending independent of its excitation source. In both studies a great deal of effort will have to be applied to reducing the sensitivity of the closed loop response to variations in vehicle parameters. This system is very sensitive to bending mode slope values. In general one would expect unstable performance at other flight cases and for an off nominal vehicle. It is, however, possible to extend the technique of determining the G function to several flight cases. In doing this the order (i.e., the number of independent coefficients in the G function) is increased by six for each added flight case. It may be possible that a reasonable sized G function could be determined which would provide acceptable vehicle performance for all of the flight for nominal and off nominal vehicles. The actual search for such a function was felt to be beyond the scope of this study, however, considerations were given to how one might intelligently approach such a search. It can be noted from Equations (14), (15), and (16) that the G function of the single flight case example is uniquely determined by the equation

$$G(-a_i - jb_i) = \frac{E_i + j\,F_i - A_i - j\,B_i}{C_i + j\,D_i} \; ; \; i = 1,\, 2,\, 3. \tag{74}$$

In the example given all E_i's and F_i's were set equal to zero where in reality a region of values of the E_i's and F_i's are acceptable. If values of zero for the E_i's and F_i's are assumed the midpoint of the acceptable region then it will be noted that for each flight case the values of a_i and b_i vary and using Equation (74) with $E_i = 0$ and $F_i = 0$ a set of values of $a_i + j\,b_i$ with their desired value of $G(-a_i - j\,b_i)$ can be determined for a large number of nominal and off nominal flight cases. The desired G function good for all flight cases can then be produced using normal curve fitting procedures whereby a function is obtained which maps a set of numbers (i.e., the $a_i + j\, b_i$'s) into an associated set (i.e., the desired values of $G(-a_i - j\, b_i)$). In curve fitting the function order is in general specified, thus, the problem becomes one of determining the lowest order G function which will give acceptable performance over all nominal and off nominal flight conditions. Acceptable performance can be determined by running the gain phase curves for all the flight cases using the G functions determined from the curve fit.

Adaptive Generation of the G Function

The existence of a G function for a particular flight case which can completely remove all bending excitation from the nozzle command signal without disturbing the short period gain phase implies the possibility of utilizing an adaptive system to reduce the sensitivity of the basic system to parameter uncertainties and changes. The adaptive system must operate to remove all the bending from the system. Assume the total error signal ($\phi_I + K_{\dot\phi}\, \dot\phi_I$) before bending is removed to be composed of a dc term plus decaying sine waves at frequencies other than bending plus three sinusoidal bending terms. A single bending term can be derived off of the delta rate gyro signal by bandpass filtering and is assumed to be of the form $A_1 \sin \omega_1 t$. Differentiating this signal produces $A_1\, \omega_1 \cos \omega_1 t$. The first bending mode signal on the system error is assumed to be $B_1 \sin (\omega_1 t + \phi_1)$ which equals $B_1 \cos \phi_1 \sin \omega_1 t + B_1 \sin \phi_1 \cos \omega_1 t$ by trig identities. If the filtered delta rate gyro signal is multiplied by K_1 and its derivative by K_2 and both these signals subtracted from the error signal to form the β_c signal then the first bending mode signal on the error signal becomes

$$(B_1 \cos \phi_1 - A_1 K_1) \sin \omega_1 t + (B_1 \sin \phi_1 - A_1 K_2\, \omega_1) \cos \omega_1 t \tag{75}$$

The dc average of the total β_c signal times the filtered delta rate gyro output is

$$A_1 \frac{(B_1 \cos \phi_1 - A_1 K_1)}{2} \tag{76}$$

and the dc average of the total β_c signal times the derivative of the filtered delta rate gyro output is

$$\frac{A_1 \omega_1 (B_1 \sin \phi_1 - A_1 K_2 \omega_1)}{2} \tag{77}$$

If an adaptive loop is closed to generate K_1 by integrating (76) and K_2 by integrating (77) then K_1 becomes the solution of

$$\dot{K}_1 = \frac{A_1 (B_1 \cos \phi_1 - A_1 K_1)}{2} \tag{78}$$

and K_2 the solution of

$$\dot{K}_2 = \frac{A_1 \omega_1 (B_1 \sin \phi_1 - A_1 K_2 \omega_1)}{2} \tag{79}$$

The adaptive loop produces a steady state value of K_1 equal to

$$\frac{B_1 \cos \phi_1}{A_1}$$

and a steady state value of K_2 equal to $\frac{B_1 \sin \phi_1}{A_1 \omega_1}$.

Substituting this into Equation (75) reduces the first bending mode signal on β_c to zero.

In order to study the characteristics of the adaptive bending suppression system a simple open loop test was generated. Figure 94 is a block diagram of the adaptive system with test inputs. The test inputs are equivalent to having a single sinusoidal bending signal on both the system error and the delta rate gyro outputs. Provisions are made to vary the amplitude and phase relationships of both inputs along with system gains. Figure 95 shows the β_c response of the system for system parameters of

ω = 2 rad

ϕ = 45°

a = .1

b = .9

c = $\sqrt{2}$

D = 1

G_R = 10

T = .1 sec sampling rate

The system shows very rapid response in eliminating the bending sine wave on the system error input. Without the suppression system β_c would be a 2 radian sinusoidal with peak amplitude of $\sqrt{2}$. It is interesting to note that within 1 period 95.7% of the bending signal has been removed from the error signal which is equivalent to 27.5 db attenuation at the bending frequency, and the attenuation is even greater as time progresses. Figure 96 and 97 are the time response of the adaptive gains G_{ap} and G_{ar}, respectively. A difficulty exists with the system in that it is highly sensitive to input amplitude on ρ, the delta rate gyro input. Figure 98 is the β_c response where the ρ amplitude is doubled (i.e., D = 2). It is difficult to determine the amount of 2 radian signals in β_c, however, an intolerable amount of 1 radian (half the bending frequency) and 4 radians (twice the bending frequency) exists. Figure 99 is the β_c response with the amplitude on the delta rate gyro signal halved from that of Figure 95. In this case the rejection response is greatly slowed though there is no apparent generation of harmonics.

The reason for high amplitude sensitivity to the delta rate gyto input can be shown analytically by referring to Figure 100 which is a simplified diagram of half of Figure 94.

From the diagram $\dot{G}$ is obtained by putting the signal $\rho(\epsilon - G\rho)$ through a low pass filter. If it is assumed that $\rho = D \sin \omega t$, $\epsilon = c \sin (\omega t + \phi)$ and that the low pass filter will pass only dc then

$$\dot{G} = \text{dc portion of } [DC \sin \omega t \sin (\omega t + \phi) - DG^2 \sin^2 \omega t] \tag{80}$$

Using trig identities this becomes

$$\dot{G} = \text{dc portion of } [(DC \cos \phi - D^2 G) \sin^2 \omega t + DC \sin \phi \sin \omega t \cos \omega t] \tag{81}$$

which by double angle formulas is

$$\dot{G} = \text{dc portion of } [(DC \cos \phi - D^2 G)(\tfrac{1}{2} - \tfrac{1}{2} \cos 2 \omega t) + \frac{DC \sin \phi}{2} \sin 2 \omega t] \tag{82}$$

which is

$$\dot{G} = \frac{1}{2} (DC \cos \phi - D^2 G) \tag{83}$$

The Laplace transform of G is then

$$G(s) = \frac{\frac{1}{2} DC \cos \phi}{S + \frac{D^2}{2}} . \tag{84}$$

Thus, in the simplified case the adaptive loop has a pole at $D^2/2$ where D is the input amplitude of the delta rate gyro signal. In the real system the dynamics of sampling plus the non-ideal characteristics of the low pass filter and the system nonlinearities changes the response characteristics from that of a simple lag, however, it does not negate the sensitivity of the response to the square of the input amplitude of the delta rate gyro signal. The input amplitude on ϵ should have no affect upon the system response which is demonstrated by Figure 101 and 102 for values of $c = 8\sqrt{2}$ and $\frac{1}{8}\sqrt{2}$, respectively.

In order to remove the amplitude sensitivity of the ρ input a method of adaptively modifying the input amplitude must be used. Two methods of doing this were tried. In the first a low pass filter was placed on the square of the ρ input signal. The square root of 2 times the filter output was assumed to be the peak input amplitude as shown in Figure 103. This produced a fair measurement of D, however, with acceptable values of lag time constant "a" a large harmonic ($\sin 2\,\omega t$) component was on D causing a resultant large harmonic on β_c. The measured amplitude was used by dividing the input signal ρ by the amplitude to produce the input signal for the adaptive bending suppression system.

A second amplitude measuring system which produces much better results is a peak detection system which can best be described by the logic flow diagram of Figure 104.

In this mechanization A will be similar to D if ρ is sine wave with time varying amplitude. The peak detection system maintains A at the last peak magnitude of the $|\rho|$ unless the instantaneous value of $|\rho|$ is larger than A. Under this condition A is made equal to $|\rho|$.

Figure 105 is the response of Figure 103 with the ρ input modified to be $\frac{D \sin \omega t}{A}$ where A was determined by the logic of Figure 104. Values used for this run are $\omega = 2$, $\phi = 45$; $G_R = 7$, $T = .1$, $a = .4$ and $b = .6$. The response was found to be independent of both D and C. Using a pure sine wave on the ρ input the bending is rejected in almost one cycle time indicating excellent potential as a bending suppression system.

In an actual mechanization bandpass filtering will be required to remove the bending signal as a pure sine wave from both the delta rate gyro signal and from the β_c signal plus additional bandpass filters to maintain the desired phase relationships within the circuit.

Figure 106 shows the finalized version of the adaptive bending suppression system for removing one bending mode. The bandpass filtering on the $\Delta\dot{\phi}$ signal and the β_c signal is required to separate the bending signal as a sine wave from the conglomerate signal in each case. In order to maintain the proper phase relationship between the signals being multiplied for the gain determination, additional bandpass filtering must be inserted between the summation point into the error signal and the multiplication.

Each of the two adaptive loops (one required to remove the in-phase and the other the quadrature bending components from the error signal) can be thought of as a suppressed carrier ac modulated servo system with $\Delta\dot{\phi}$ derived bending signal acting as the ac reference. Figure 107 is one of these loops redrawn with this assumed representation. The bandpass in the $\Delta\dot{\phi}$ line has been represented as a phase shift network only. The system treats the amplitude of the bending signal on β_c as an error signal. The bandpass filter on the β_c output acts as a lag-lead to the bending amplitude on its input. The multiplication at the bandpass output acts as a demodulator. The bandpass is mechanized as a W-plane derived filter of the form

$$\frac{\zeta_n\ (\omega^2 + 2\ \zeta_n\ \omega + 1)}{\zeta_d\ (\omega^2 + 2\ \zeta_d\ \omega + 1)} \left[\frac{Z^2 - \dfrac{2\ (1 - \omega^2)}{\omega^2 + 2\ \zeta_n\ \omega + 1}\ Z + \dfrac{(1 - \omega^2)^2 + 4\ \omega^2\ (1 - \zeta_n{}^2)}{(\omega^2 + 2\ \zeta_n\ \omega + 1)^2}}{Z^2 - \dfrac{2\ (1 - \omega^2)}{\omega^2 + 2\ \zeta_d\ \omega + 1}\ Z + \dfrac{(1 - \omega^2)^2 + 4\ \omega^2\ (1 - \zeta_d{}^2)}{(\omega^2 + 2\ \zeta_d\ \omega + 1)^2}} \right] \tag{85}$$

where $\omega = \tan \dfrac{\omega_T\ T}{2}$. The filter has an approximate gain of one at the tuned frequency. The adaptive loop appears as a closed loop system operating on the bending amplitude. This closed loop system has an open loop transfer function of approximately

$$b\Delta T\ \frac{(1 - e^{-\zeta_d\ \omega_T T})}{(1 - e^{-\zeta_n\ \omega_T T})}\ \frac{Z^2\ (Z - e^{-\zeta_n\ \omega_T T})}{(Z-1)(Z-C)(Z - e^{-\zeta_d\ \omega_T T})} \tag{86}$$

producing an open loop pole zero plot as shown in Figure 108.

In order to simplify the analysis two circuits of the type shown in Figure 106 were mechanized for two bending modes. The time response runs indicate that there is more lag in the servo system than is indicated in the open loop pole-zero plot of Figure 107. It appears as if the additional lag is larger than a full sampling period transportation lag (i.e., Z^{-1}).

Preliminary time response analysis indicates the best performance is achieved with C = 0, that is no filtering on the product term to isolate only the dc component. Using a single transportation lag, root locus analysis indicates that a very large loop gain (e.g., 100) is required to produce a system with unity damping and thus no overshoot. Simulating this high of a loop gain produces instability. The instability may be caused by inadequate approximations in generating the equivalent circuit of Figure 107 or more likely with the high gains the nonlinearities in the actual circuit producing high frequency harmonics which are amplified to produce instability in these nonlinear modes.

A set of parameters for the system was chosen by using a time response program consisting of two circuits of the type shown in Figure 106. The $\Delta\dot{\phi}$ input was simulated with

$$\dot{\phi} = \sin 2.3t + \sin 5t \quad . \tag{87}$$

and the $\phi + K_{\dot{\phi}}\dot{\phi}$ input with

$$\phi + K_{\dot{\phi}}\dot{\phi} = \sin (2.3t + .5) + \sin (5t + .2) \tag{88}$$

where the two sine waves represent two bending frequencies at 2.3 and 5 radians per second. It was assumed that the bending frequencies were exactly identified for the purposes of placing the bandpass filters. The circuits for each bending mode were mechanized with identical parameters except for the bandpass tuned frequency.

Because of the harmonic content of the β_c output it was difficult to assess the quality of the operation for minor changes in circuit parameters. The circuit parameters arrived at using this analytic approach are hopefully near optimum under the constraints of the circuit configuration of Figure 106.

Referring to the nomenclature of Figure 106 the arrived at parameters are:

$$a = 4 \tag{89}$$

$$b = 4 \tag{90}$$

$$c = 0 \tag{91}$$

The bandpass filters on the $\Delta\dot{\phi}$ input had a numerator damping of .5 and a denominator damping of .025. All other bandpass filters had numerator dampings of .3 and denominator damping of .05. A sampling rate of .1 sec was used.

Figure 109 is the time response of various test points within the circuit using parameter values described above. Figure 109-1 is the total β_c output which with perfect operation under the test conditions of no short period signal should go to zero. Without the suppression system the β_c output will have a peak amplitude of 2. Better response than that shown is achieved when a more highly tuned bandpass is placed on the $\Delta\dot{\phi}$ input signal. In that the bending frequencies will not be identified exactly a certain amount of bandwidth is required of the bandpass filters. A denominator damping factor of .025 was selected in that this damping factor showed wide enough bandwidth when used for the notch filters in the standard spectral configuration.

Figure 109-2 through 109-11 are the time response for various points throughout the circuits of both bending modes as defined by the letters e, s, u, m and j on Figure 106. The adaptive gains s and u both appear to be somewhat underdamped. The open loop approximate transfer function indicates that larger damping can be achieved by increasing the adaptive loop gains. The unity amplitude sine waves are in the initial transients fairly poor, however, become quite clean in the steady state. Changes in the circuitry configuration may improve this however. If the derivative (or quadrature) signal derived from the $\Delta\dot{\phi}$ input was found by first taking the derivative then filtering and amplitude adjusting this transient operation should improve at the expense of an additional gain adjuster. The total adaptive operation might be improved if square waves rather than sine waves were generated in the adaptive loop, but sine waves were used for the subtraction from the main error signal.

A digital differentiation mechanized as $1-Z^{-1}$ does not have 90° phase shift characteristics at all frequencies having less than 90° phase shift at higher frequencies. The effect of less than 90° phase shift is to produce intercoupling between the in-phase and quadrature cancellation networks for that mode. Since the third mode is the highest bending frequency this intercoupling would be most significant on the third mode. A digital differentiator which has 90^{o} phase shift at all frequencies is mechanized by

$$\frac{(1-Z^{-1})}{(1+Z^{-1})} \cdot \tag{92}$$

This differentiator causes modulation at half the sampling frequency due to the pole at Z = -1. This modulation would make the peak detector operate in a manner to always generate an output having amplitude one but frequencies of half the sampling frequency. A differentiator mechanized as

$$1 - \frac{Z^{-1}}{\cos \omega T} \tag{93}$$

will always have 90^{o} phase shift at the frequency ω. This places the zero outside the unit circle however, it has the desired phase characteristics without the modulation at half the sampling frequency.

A large amount of harmonic noise is being produced by the bending suppression system. A great deal of this noise appears to be generated by forming the differential signal after adjusting the peak amplitude to one.

Better operation may be achieved if the in-phase and quadrature bending component signal is derived from the delta rate gyro signal by the circuit of Figure 110.

SECTION 4.0

CONCLUSIONS

The Spectral Identification Adaptive Control System has been demonstrated to be capable of controlling a realistic flexible vehicle of the Saturn V class with dynamic and flexibility parameter uncertainties. When operating in conjunction with a properly designed control system, stable performance is guaranteed. The more excited a bending mode becomes due to temporary instability the more accurately it will be identified and thus the greater assurance of obtaining a stabilizing control system. The system has been studied with up to 25% initial uncertainty and has performed well enough to assure that stable operation will be achieved with larger initial uncertainties.

The system maintains its performance in the presence of a realistic environment of winds and instrument noise. It will maintain stable control during the operation of a conventional load relief system.

The Spectral Identification Adaptive Control System must be designed around the vehicle it is to control. Obviously the frequencies at which the spectral filters are set must be over the total range of possible bending frequencies. The control system must be designed to give adequate short period response plus insure that at no time the condition can exist where a notch filter placed at an identified frequency can cause the vehicle to have an unstable mode at that frequency.

Little effort was placed on the design or improvement of the identification system itself. Both improvements in identification accuracy and reduction in the system complexity can be obtained if this becomes a requirement on some future vehicle. The possibility of the identification of the short period frequency should be no problem because in a system when this is a possibility, adjustments to the spectral filter processing could probably be made to reject such identification as a possible bending mode.

Loads were high in the trajectory runs shown, however, a reduction in these loads could be made by increasing the short period response and improving the load relief system. The short period response can be increased by using Compensation Configuration #3.

The study of the active control system did not proceed to the point of evaluation with a trajectory simulation. It was shown for one flight case, however, that with a single force point control it is possible to completely decouple the bending and attitude control with the possible extension to generating a control system which will provide artificial damping to the bending while maintaining adequate attitude control. This design is highly dependent upon vehicle parameter variations, however, the study indicates it may be possible to either design a fixed control system capable of controlling a band of off nominal vehicles or to obtain an adaptive system which will rapidly compute the desired control system.

SECTION 5.0

RECOMMENDATIONS FOR FURTHER STUDY

It has been demonstrated that the spectral system is capable of controlling a realistic boost vehicle over its entire trajectory. There are several areas which are worthy of further investigation in the spectral system, which are:

1. For a realistic vehicle determine the required identification accuracy and quantitatively determine system performance versus identification accuracy.
2. There are several changes in the identification system which could improve the identification accuracy. The major change would be to remove the integration from the identifiers by assuming the spectral input signal is an integrator output. This should increase the accuracy of identification at the higher bending modes. The second major change is a modification of the formula $\frac{\Sigma A\omega}{\Sigma A}$ which is used to determine the frequency from the measured spectral amplitudes. The formula is modified by adding pre-computed weighting constants to the ω's.
3. Combine Item 1 and 2 to determine the least complex identification system capable of obtaining the required accuracy. This step is necessary to reduce the required computer size.
4. Each bending mode of a flexible vehicle operates in two ways. The first is a high frequency oscillation which is removed by the spectral identification system with its notch filters. The second is a low frequency "steady state" bend which does not present a stability problem in itself but is the contribution to bending coupling into the short period. This is the reason that the short period frequency is difficult to increase in a very flexible vehicle. Consideration should be given toward implementing a differential

rate gyro, a differential gyro or a strain gage sensor to measure this "steady state" bend and feed it into the control system in a manner to reduce the "steady state" bending. If this is done the vehicle could be operated at a higher short period frequency, which will result in better trajectory following and lower loads.

5. The study of the active control system shows that the potential to control the bending and the attitude of the vehicle using the single nozzle force point exists. By using a differential rate gyro and assuming constant dynamics, any desirable control on the bending can be obtained with a minimum compensation requirement. An adaptive system can possibly be generated which can control the bending compensation. Extending the study of either the adaptive system or the determination of a fixed compensation giving the desired control throughout the trajectory for nominal and off nominal vehicle conditions would appear a worthwhile endeavor.

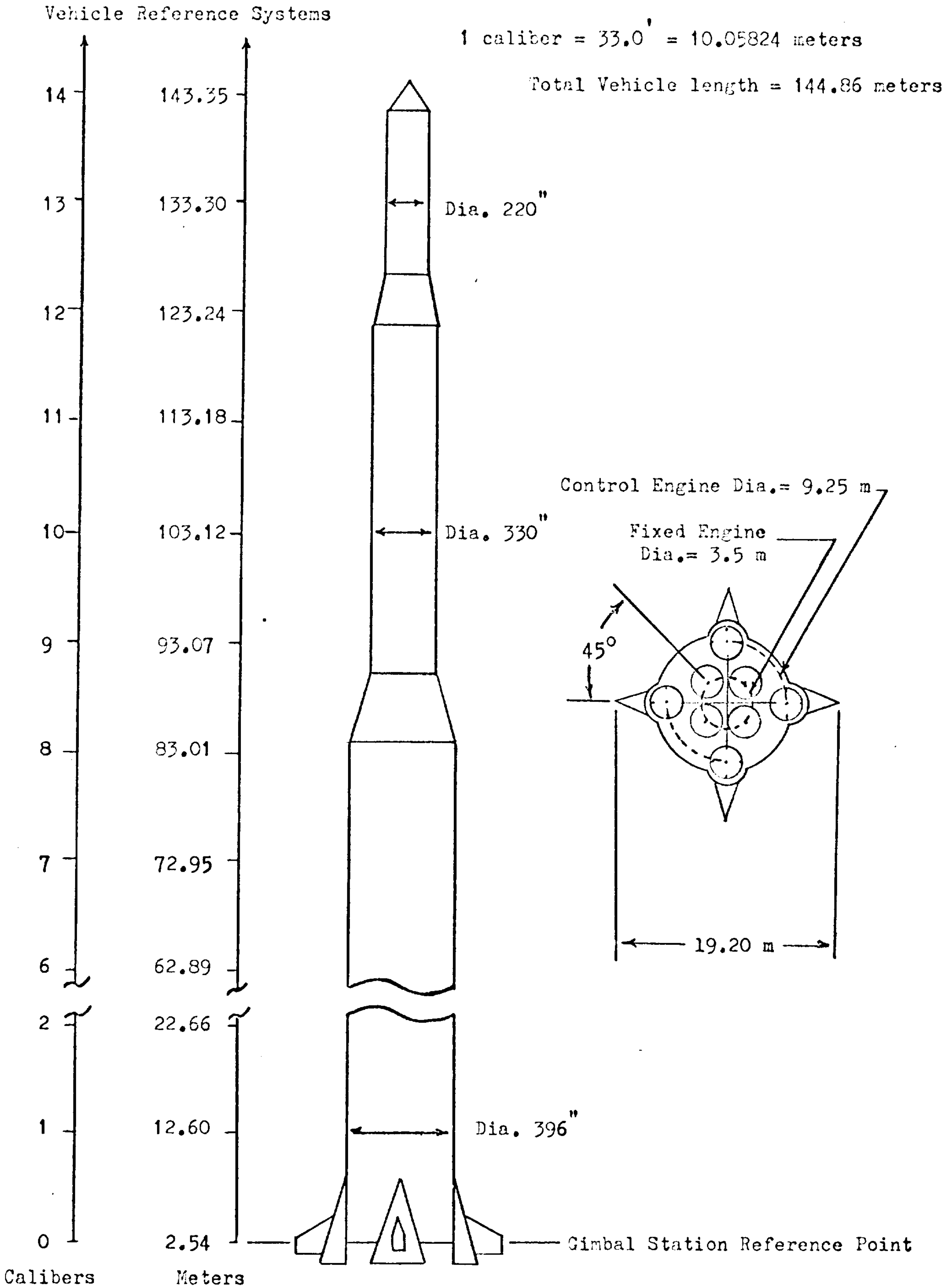

Figure 1. Model Vehicle No. 2

FIGURE 2 SPECTRAL FILTER FREQUENCY RESPONSE

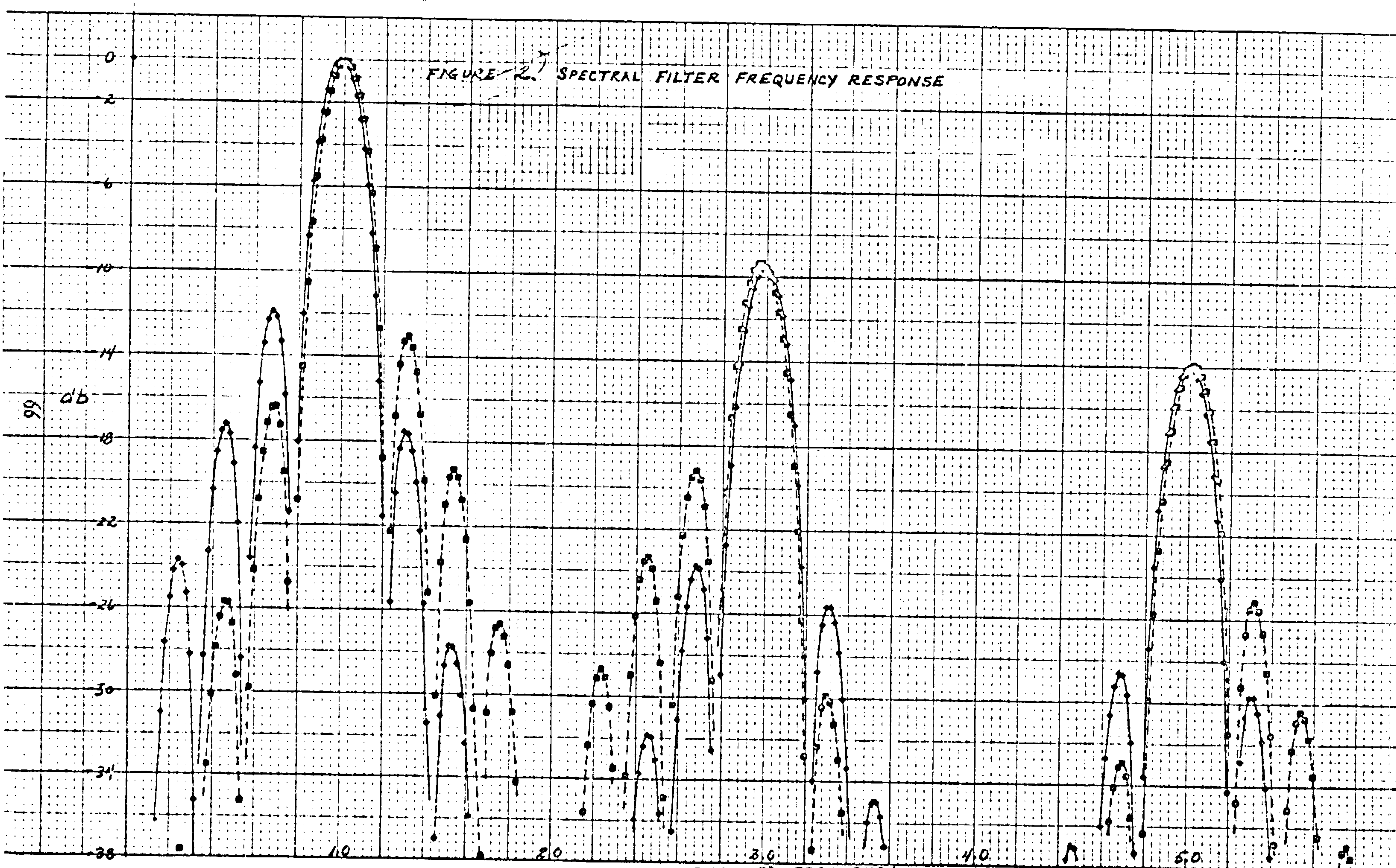

Filters initially detuned by 20%

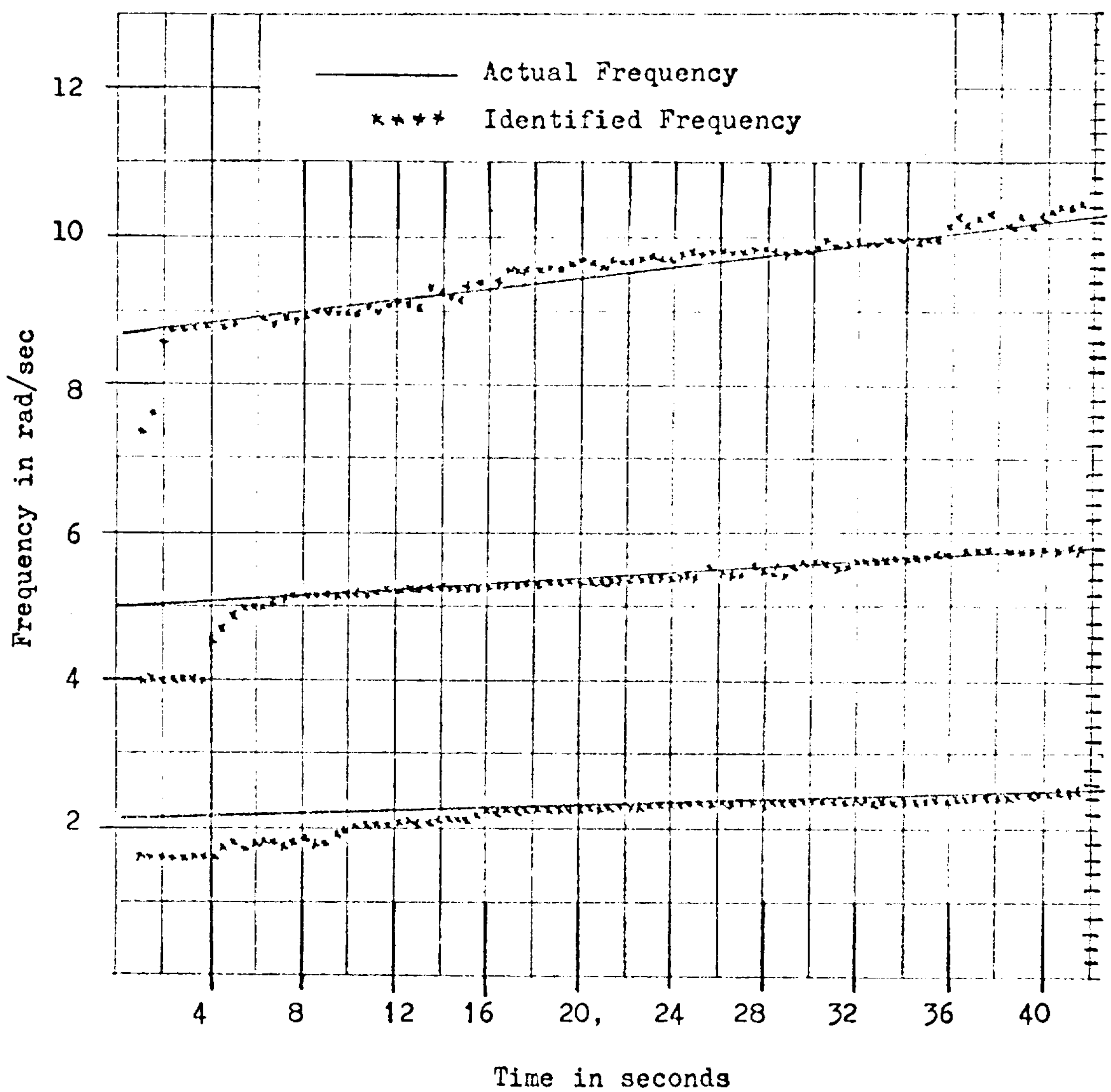

Figure 3. Spectral Identification System Performance - Ideal Signal Input

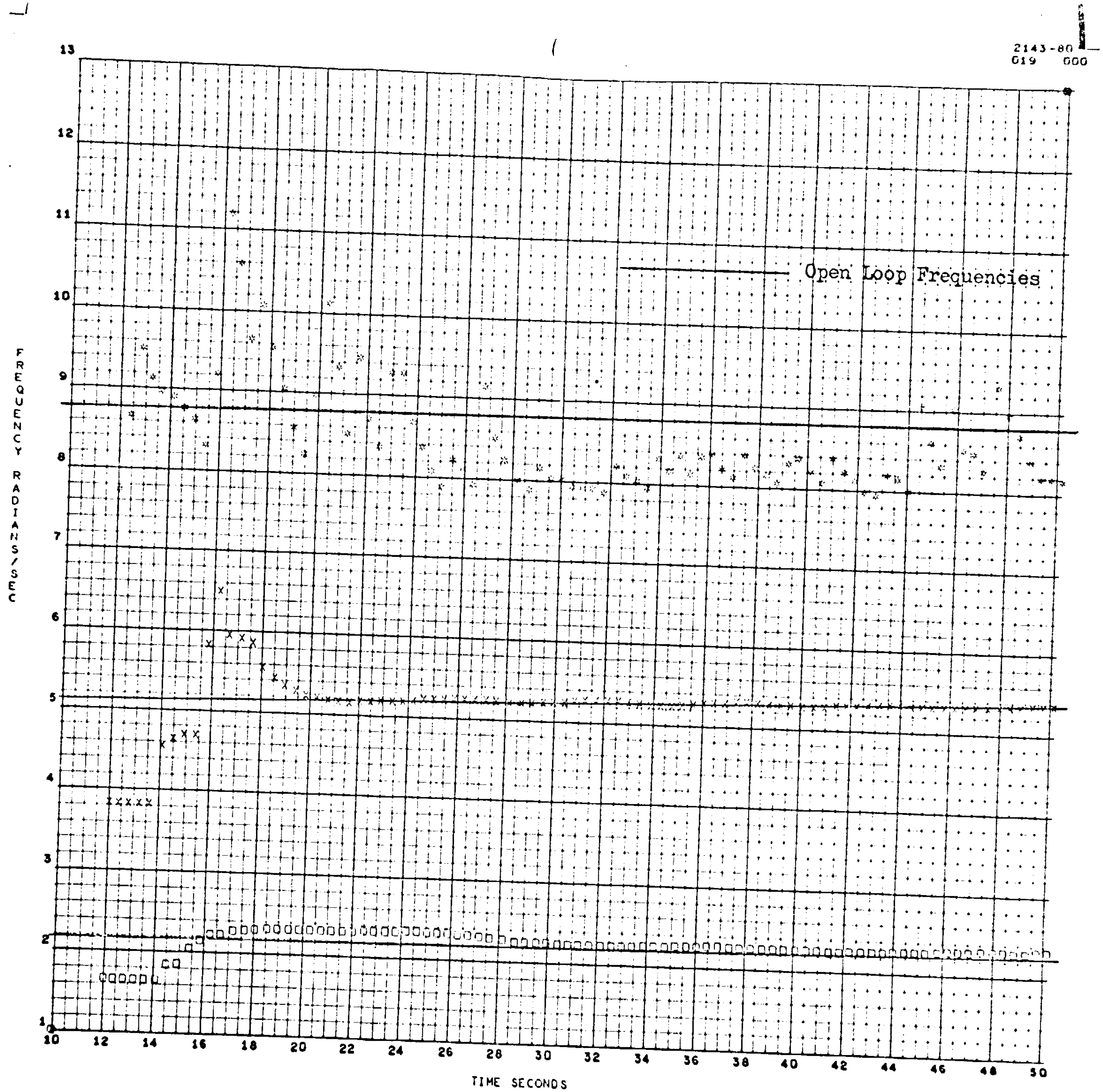

Figure 4. Frequency Identification During a Trajectory Run

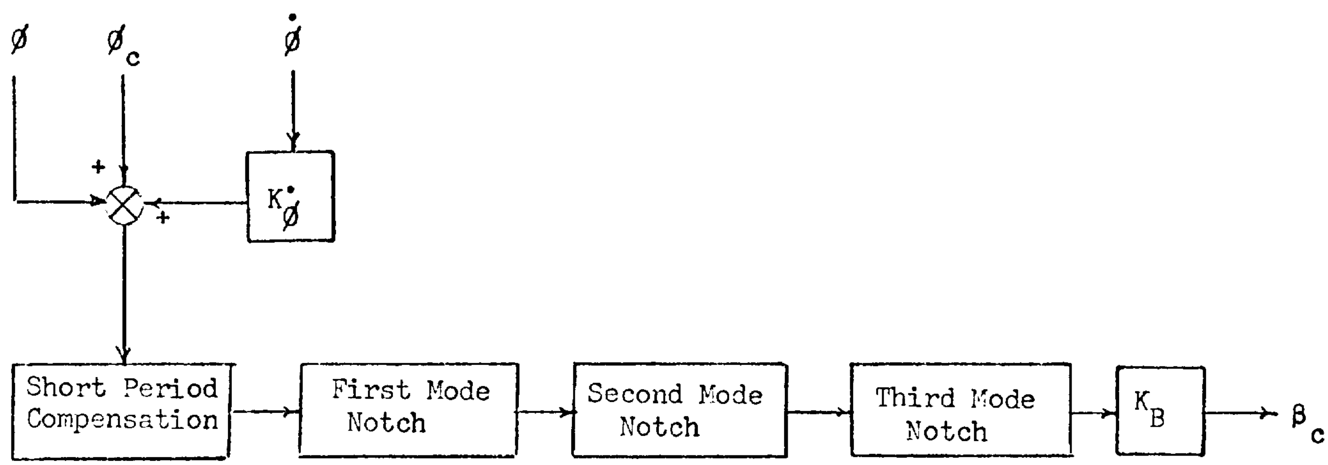

Figure 5. Basic Vehicle Control System

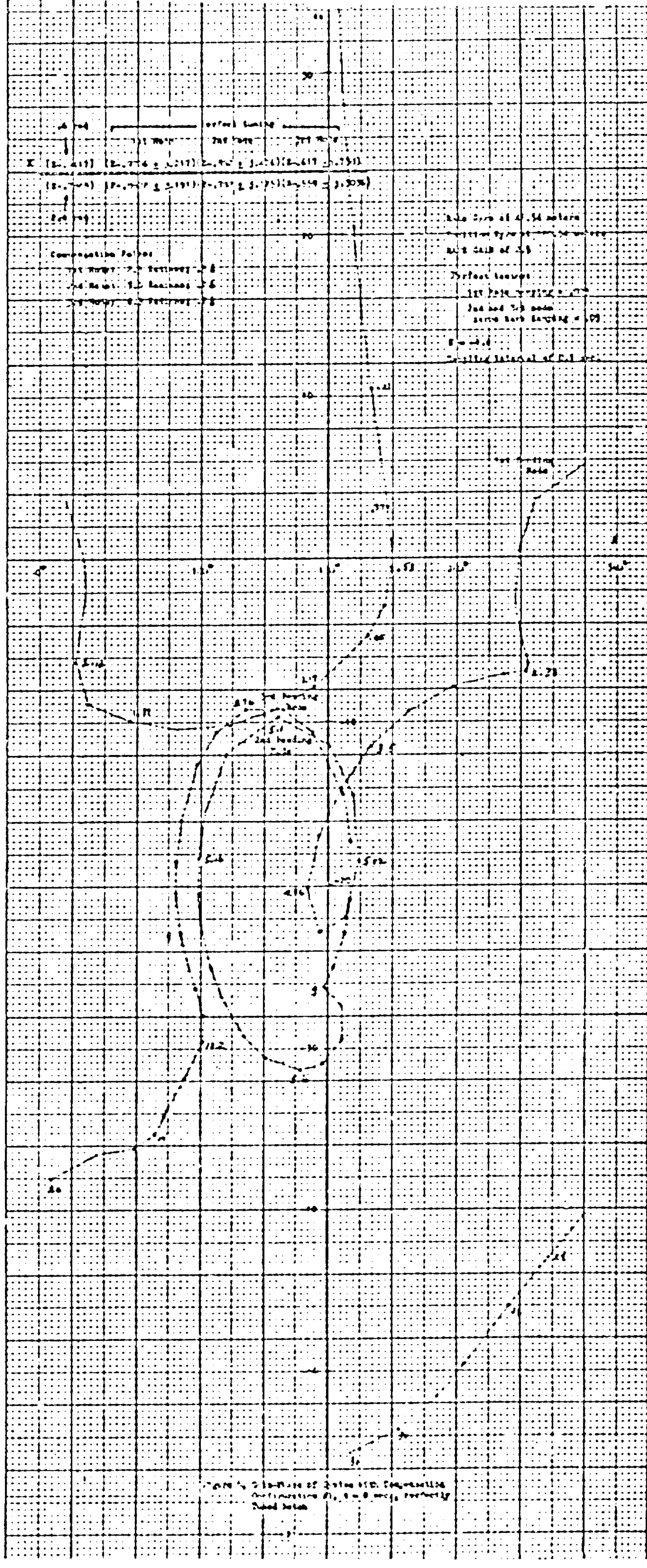

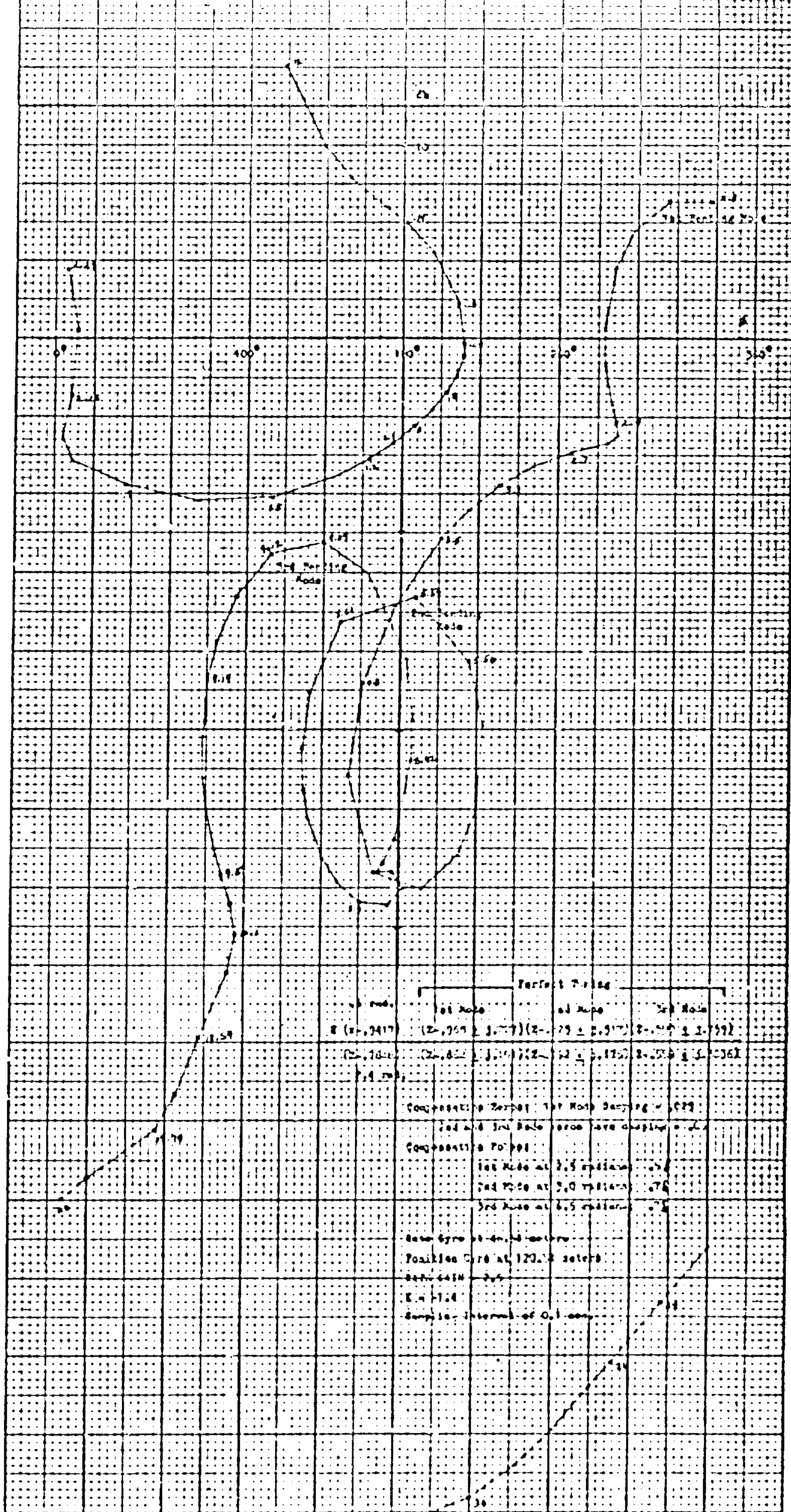

Figure 7. Gain-Phase of System with Compensation Configuration /I = 73 ... Perfectly Tuned Notch

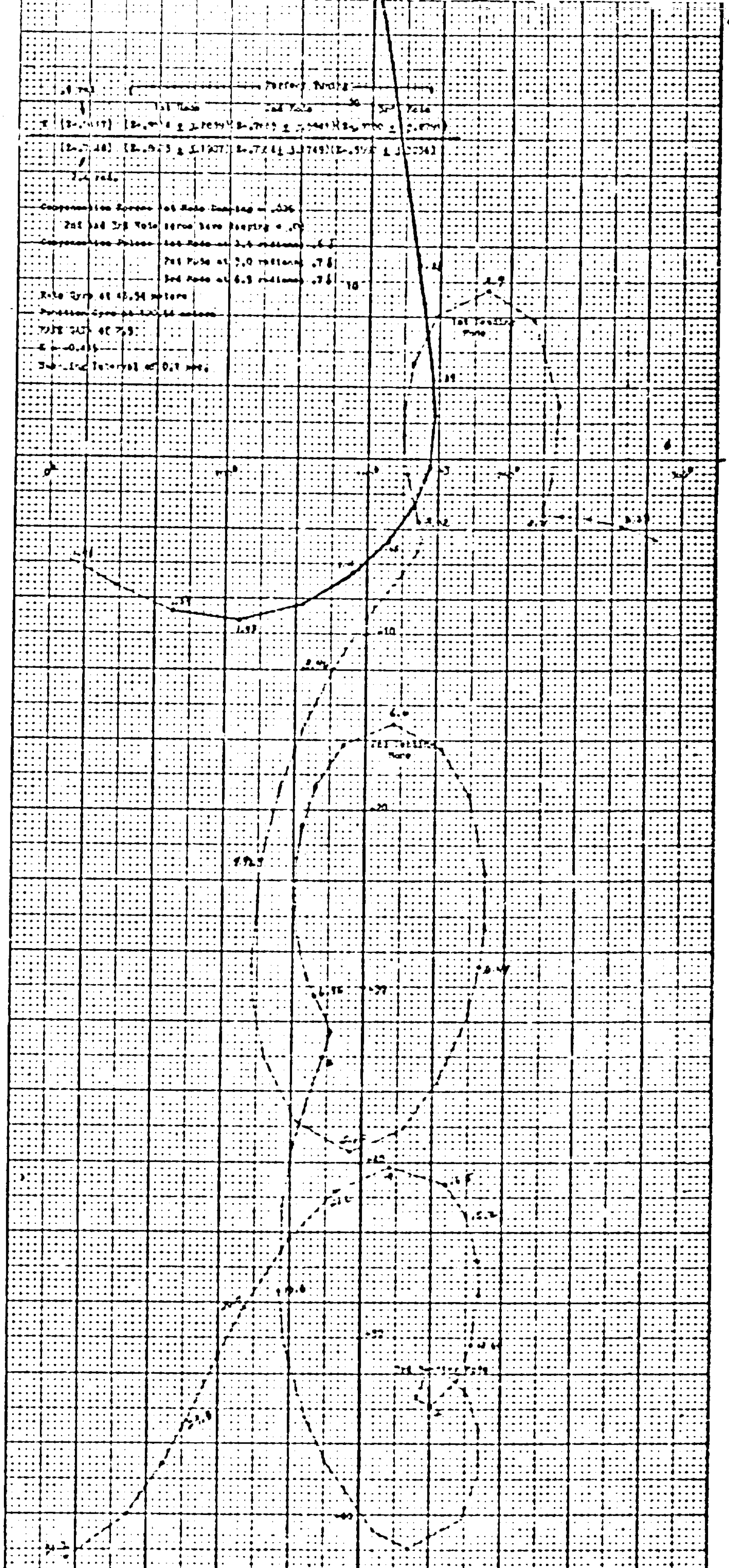

Figure [illegible]. Gain-Phase of System with [illegible] Configuration [illegible], t = 33[illegible] sec., Perfectly Tuned [illegible]

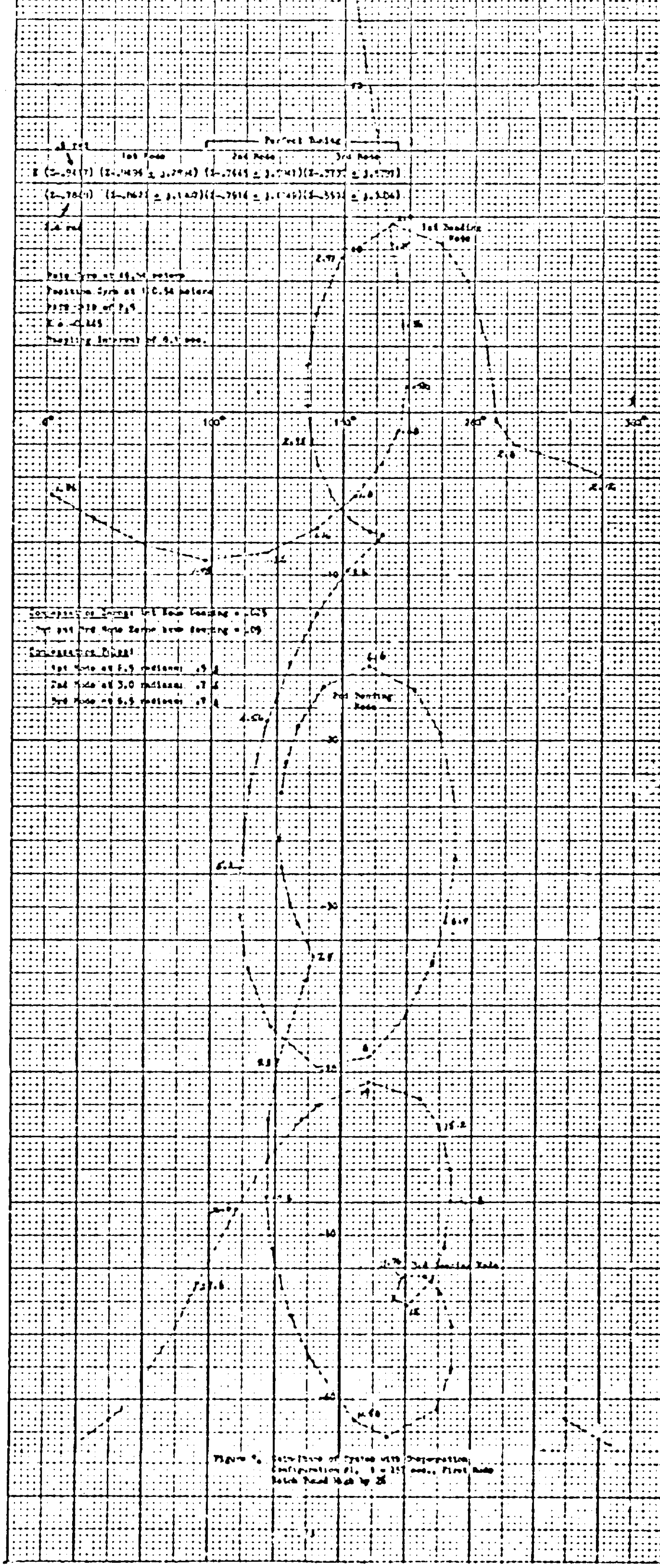
0°
100°
200°
300°

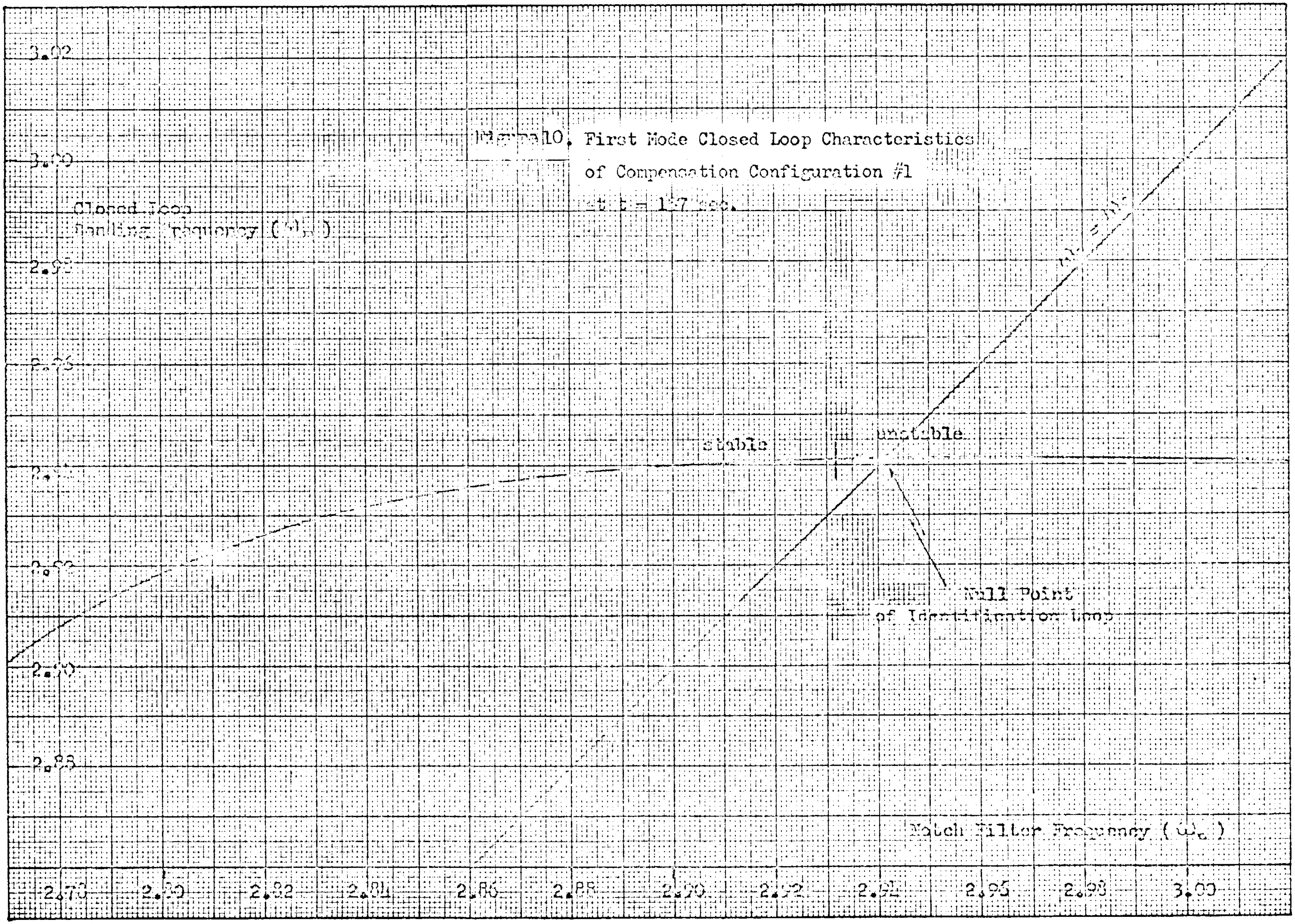

Figure 10. First Mode Closed Loop Characteristics of Compensation Configuration #1 at t = 1[illegible]7 sec.

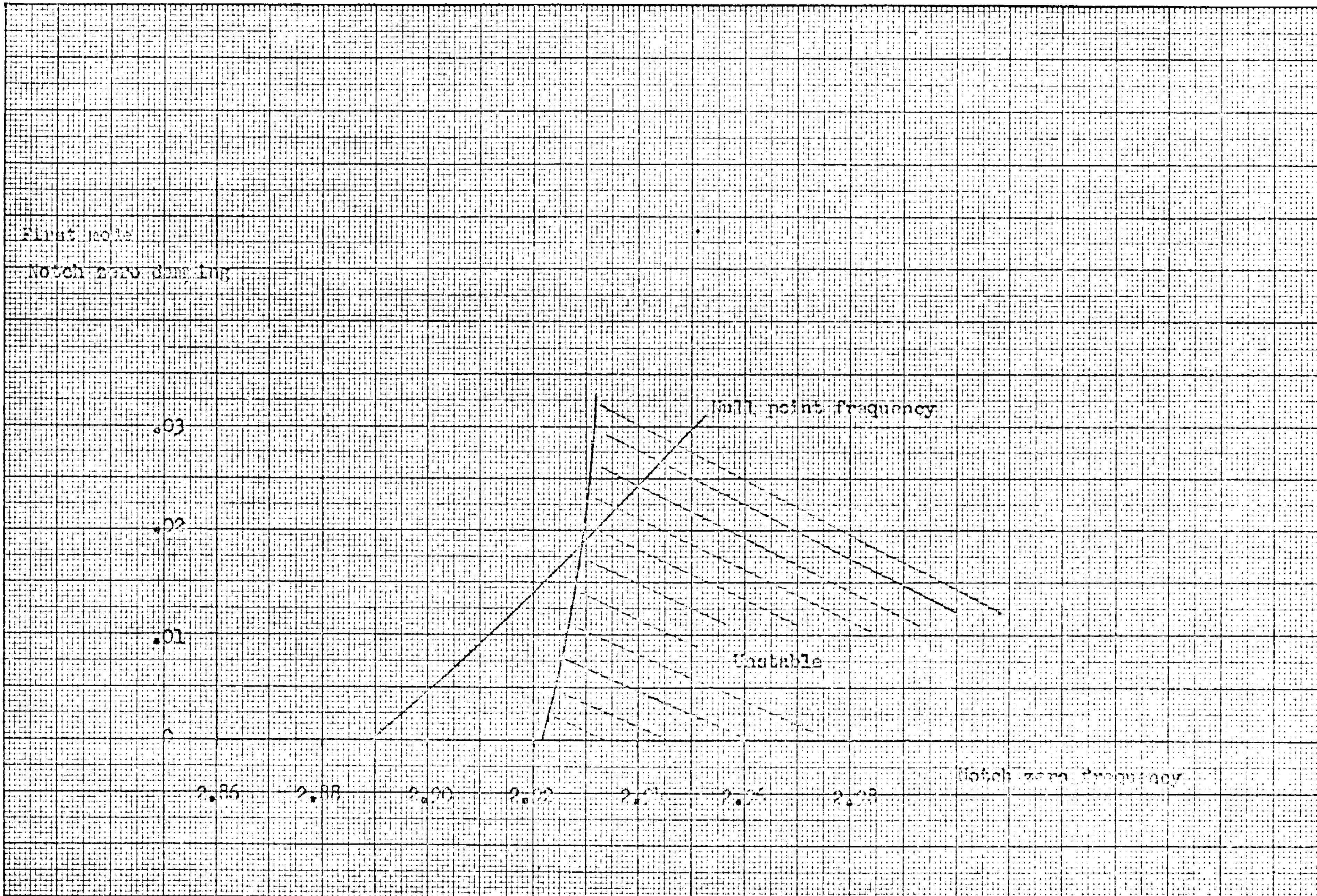

Figure 11. Compensation Configuration #1 with Variable First Mode (Zero) Damping

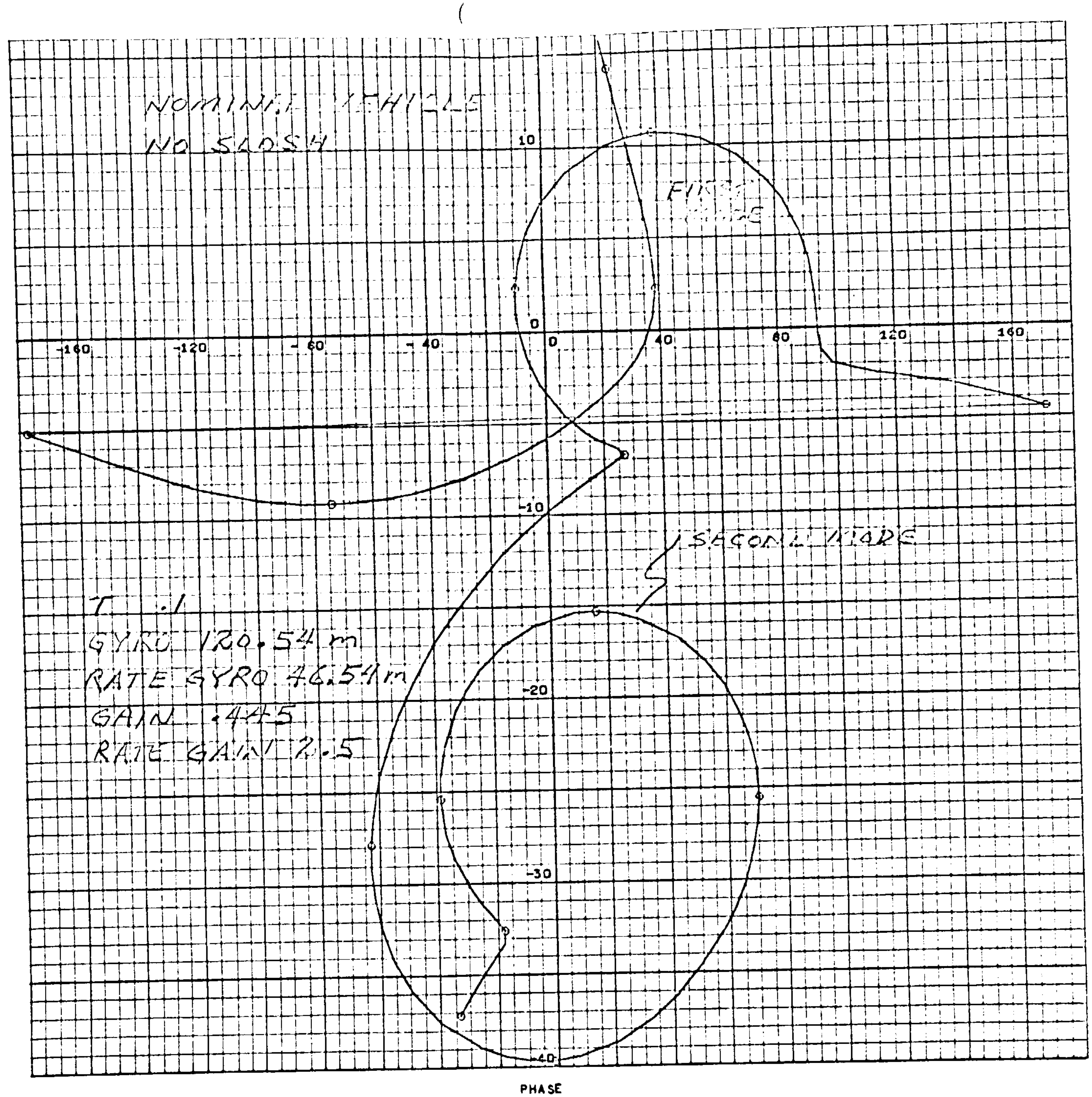

Figure 12. Gain-Phase t = 157 sec, Compensation Configuration #1 with First Mode Zero Tuned to the Null Point

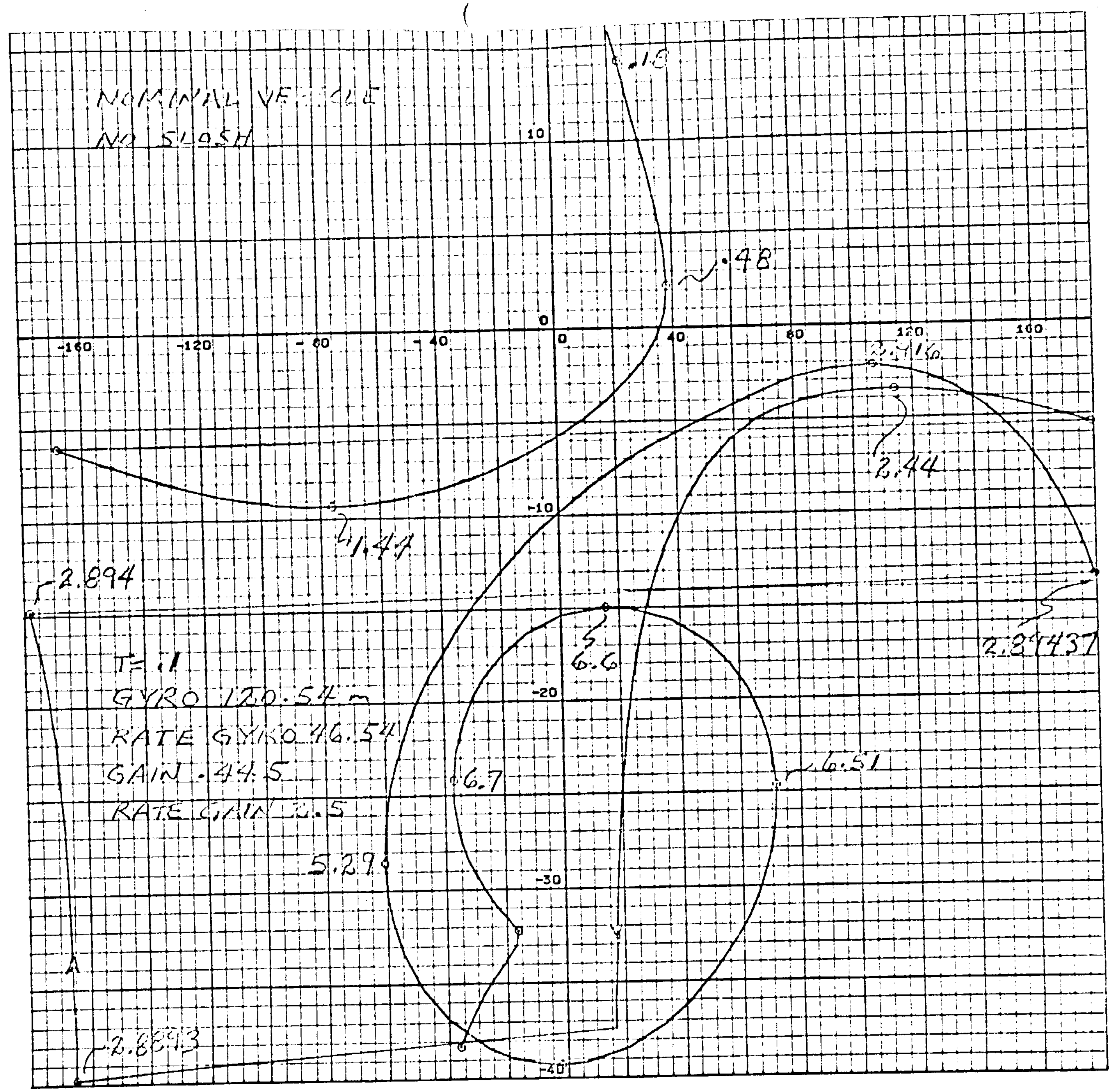

Figure 13. Gain-Phase t = 157 sec., Compensation Configuration #1 Except First Mode Zero Damping is Zero, Notch Frequency is at Identification Loop Null

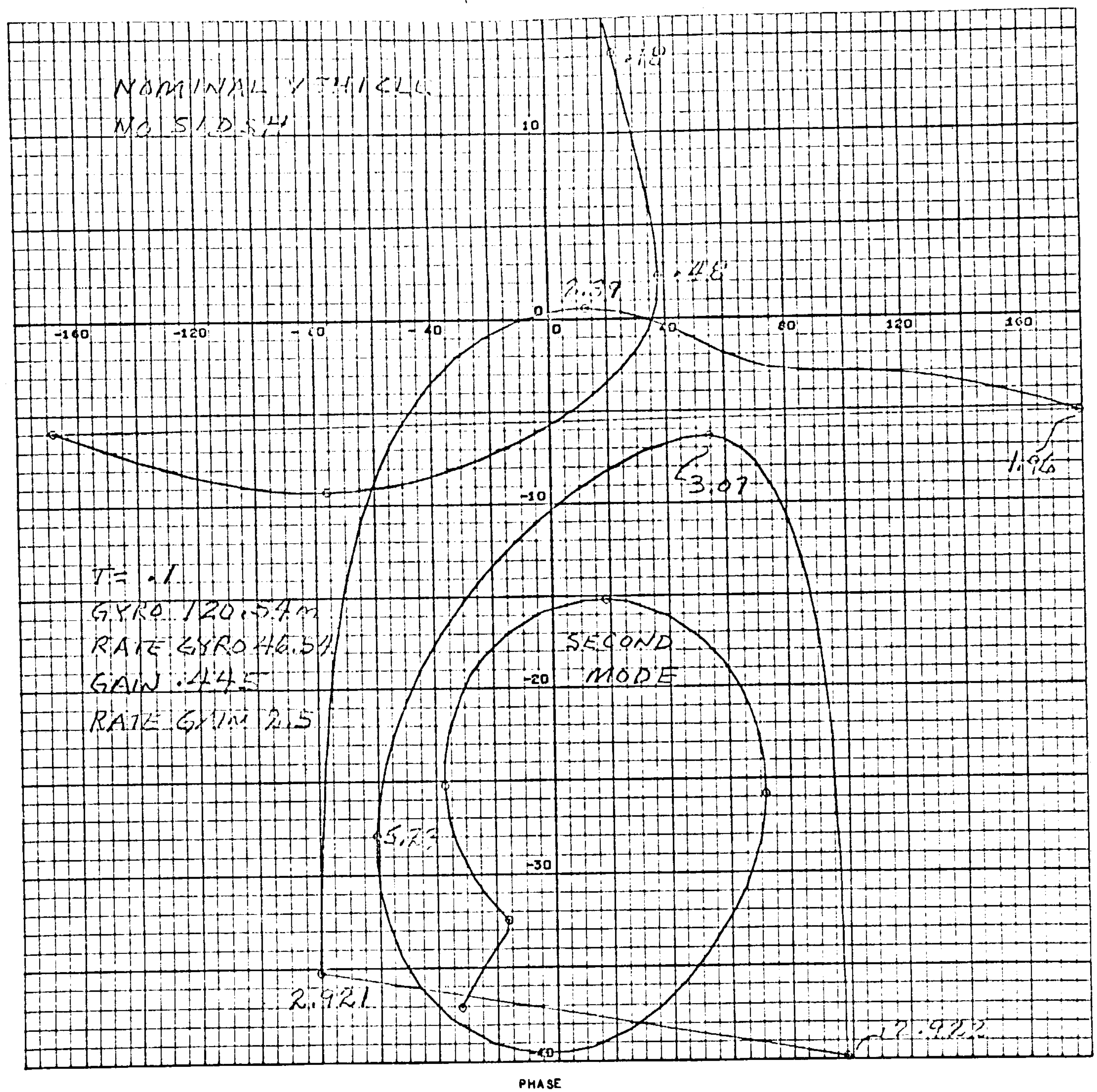

Figure 14. Gain-Phase t = 157 sec., Compensation Configuration #1 Except First Mode Zero Damping is Zero, Notch Frequency at Marginally Stable Value

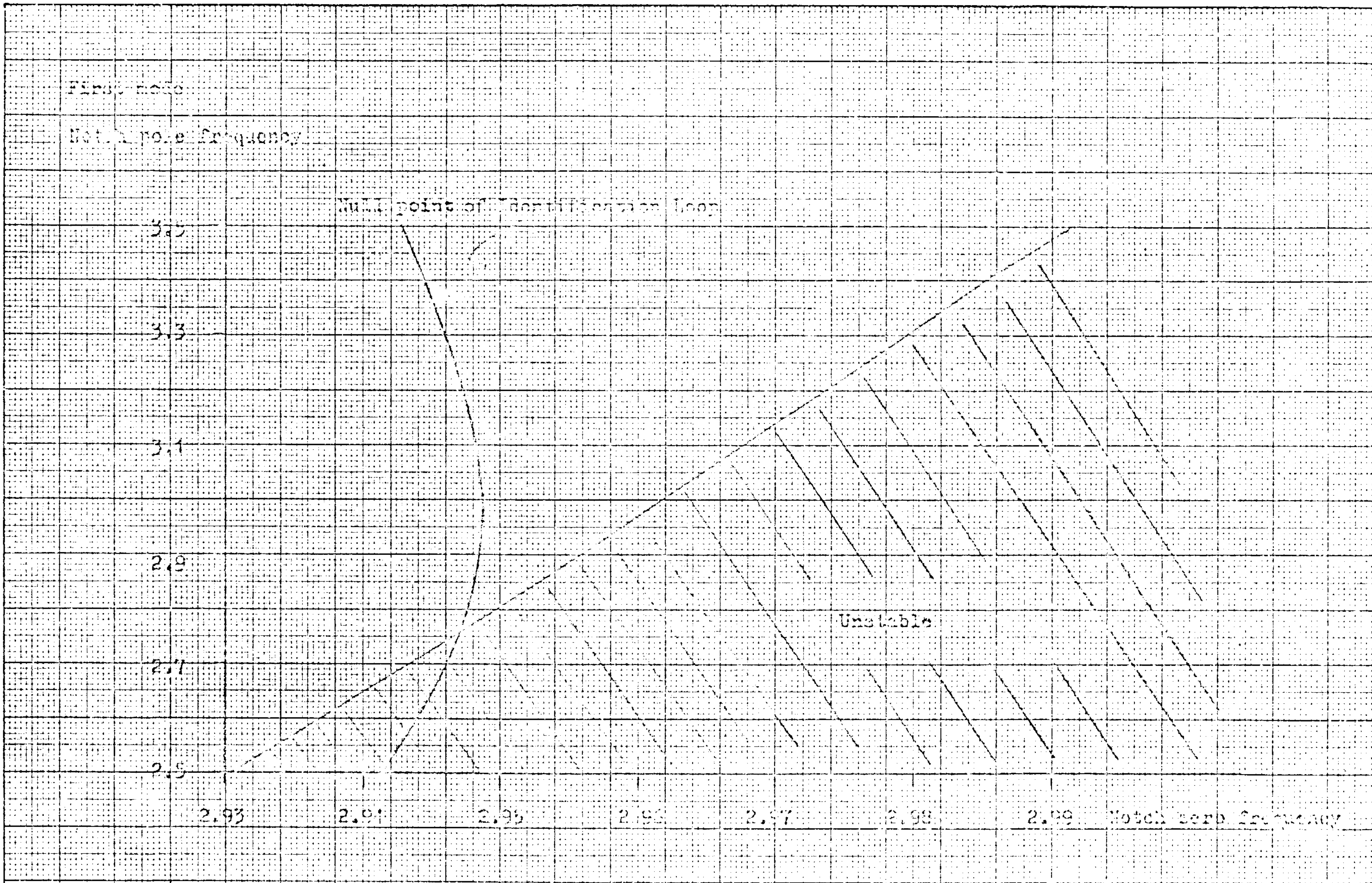

Figure 15. Compensation Configuration #2, t = 157 sec., with Variable First Mode Notch Pole Frequency

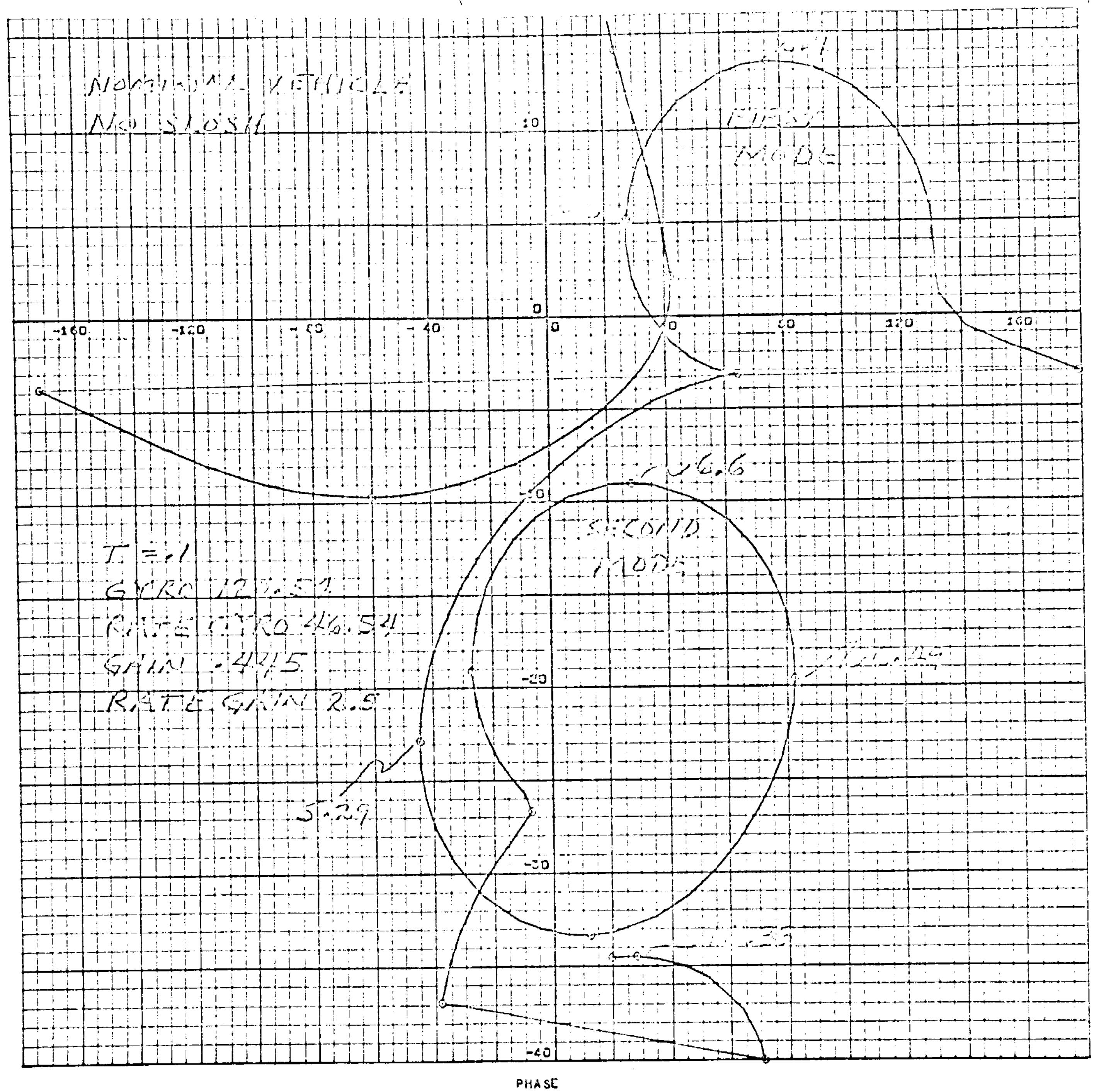

Figure 16. Gain-Phase t = 157 sec., Compensation Configuration #1, Except First Mode Notch Pole Frequency is 3.5 rad/sec, First Mode Zero is at the Null

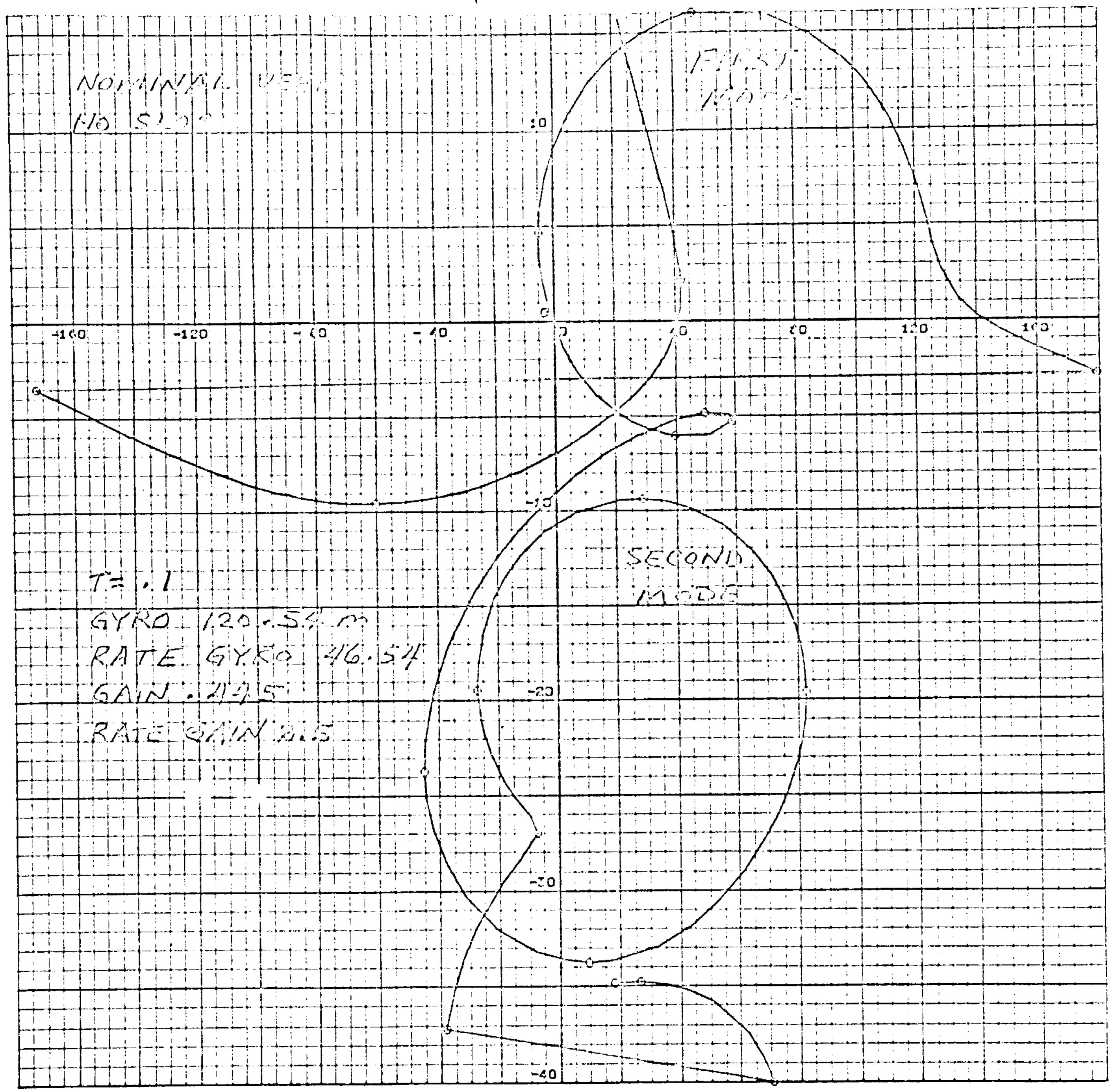

Figure 17. Gain-Phase t = 157 sec., Compensation Configuration #1 Except First Mode Notch Pole Frequency is 3.5 rad/sec First Mode Zero Frequency is at a Marginally Stable Value

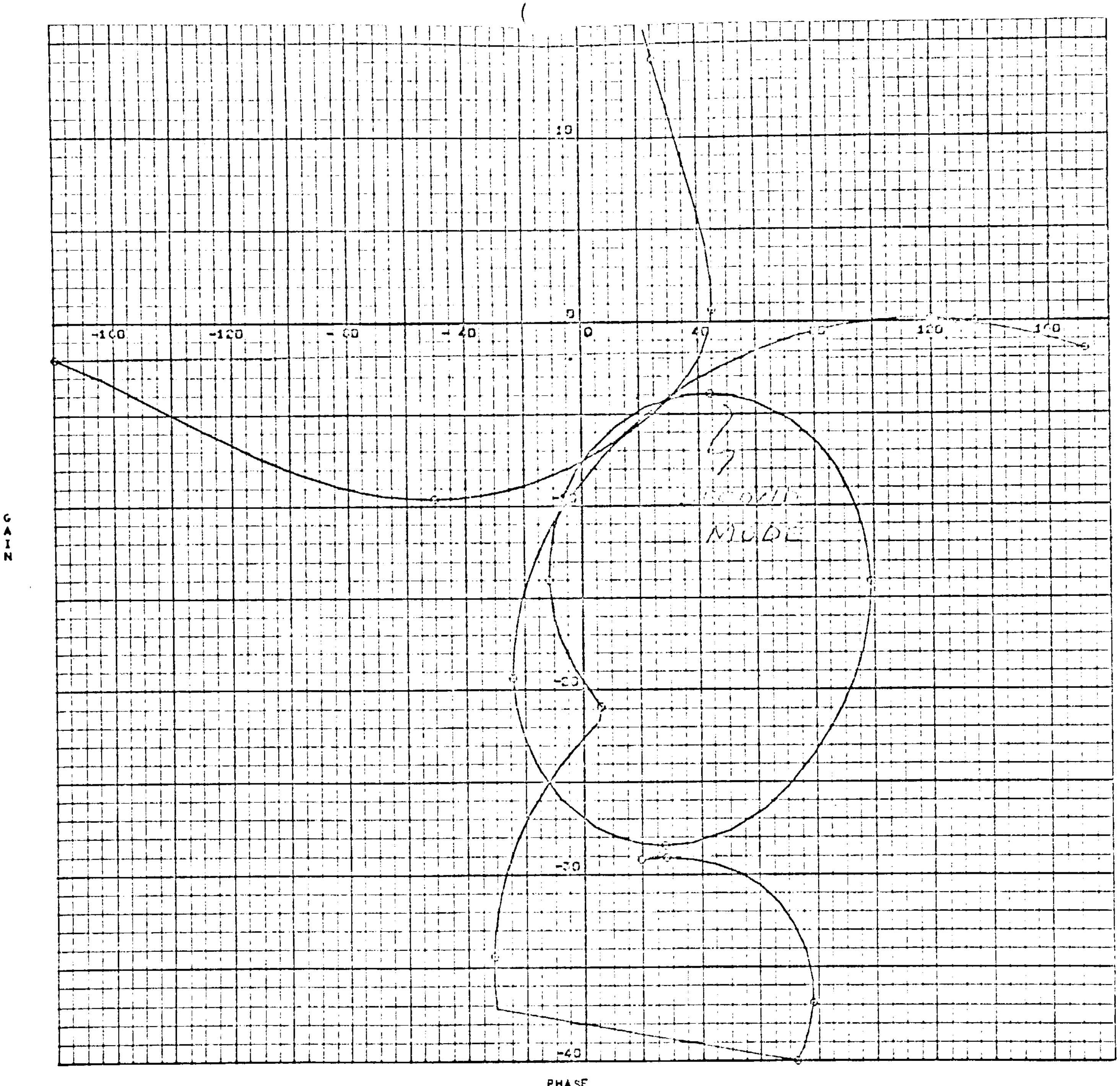

Figure 18. Gain-Phase t = 157 sec., Compensation Configuration #1 with First Mode Notch Pole Frequency at 3.5 rad/sec, Notch Zero Damping at Zero, Zero Perfectly Tuned

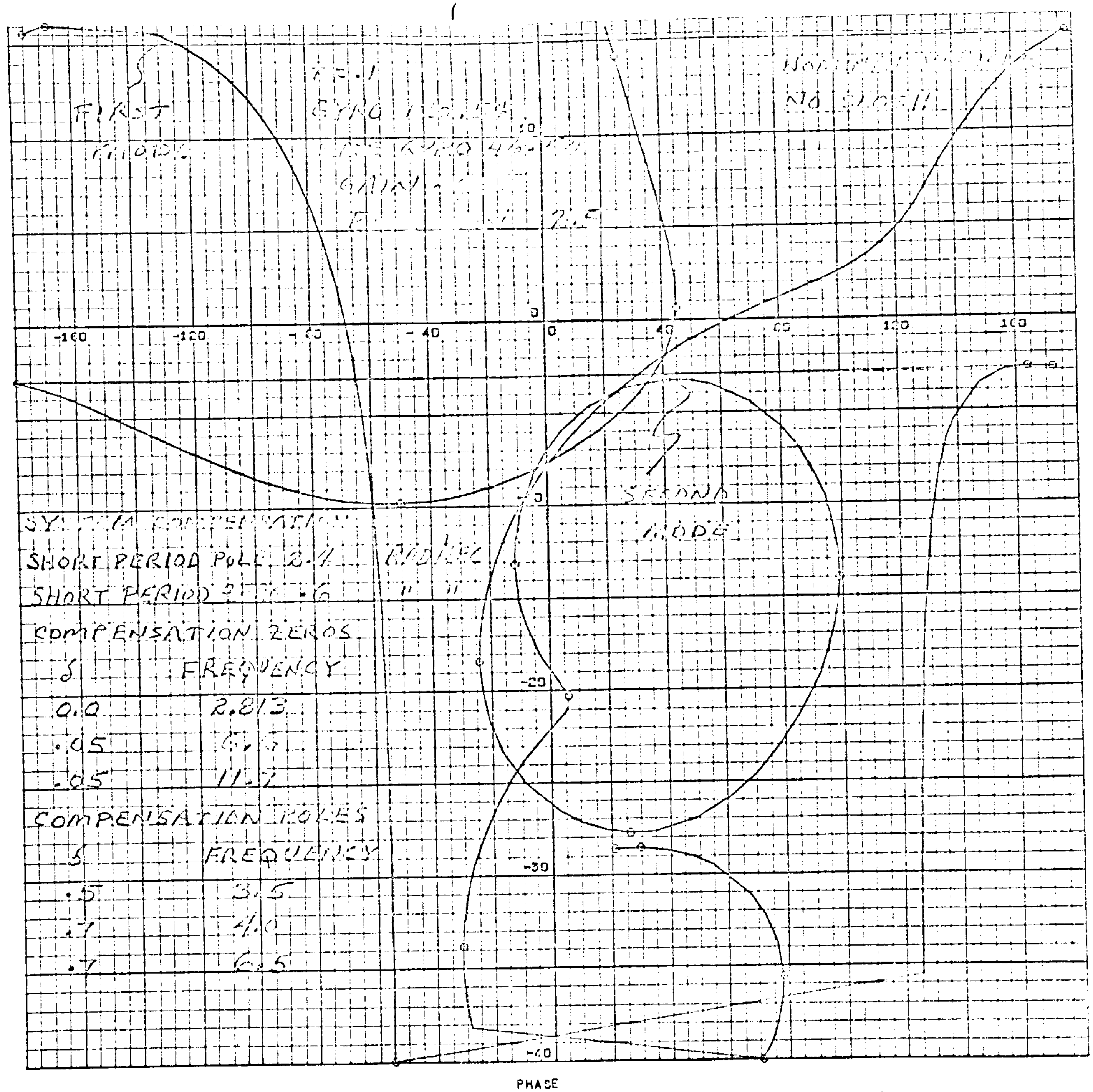

Figure 19. Gain-Phase t = 157 sec., Compensation Configuration #1 with First Mode Notch Pole Frequency at 3.5 rad/sec, Notch Zero Damping at Zero, Zero 3% Low

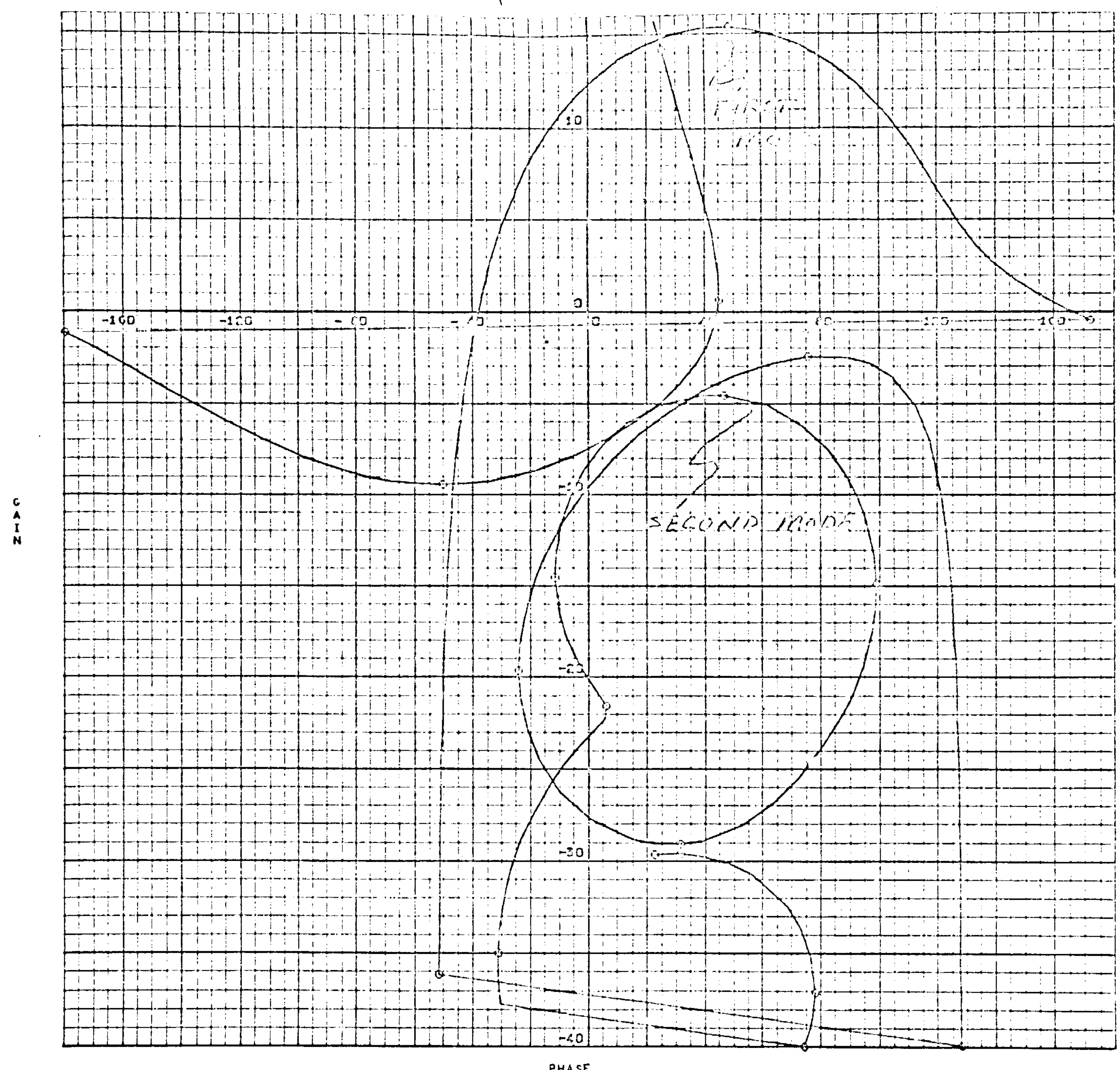

Figure 20. Gain-Phase $t = 157$ sec., Compensation Configuration #1 with First Mode Notch Pole Frequency at 3.5 rad/sec, Notch Zero Damping at Zero. Zero 3% High

Figure 21. Gain-Phase $t = 8$ sec, Compensation Configuration #2
Notch Zeros Nominal

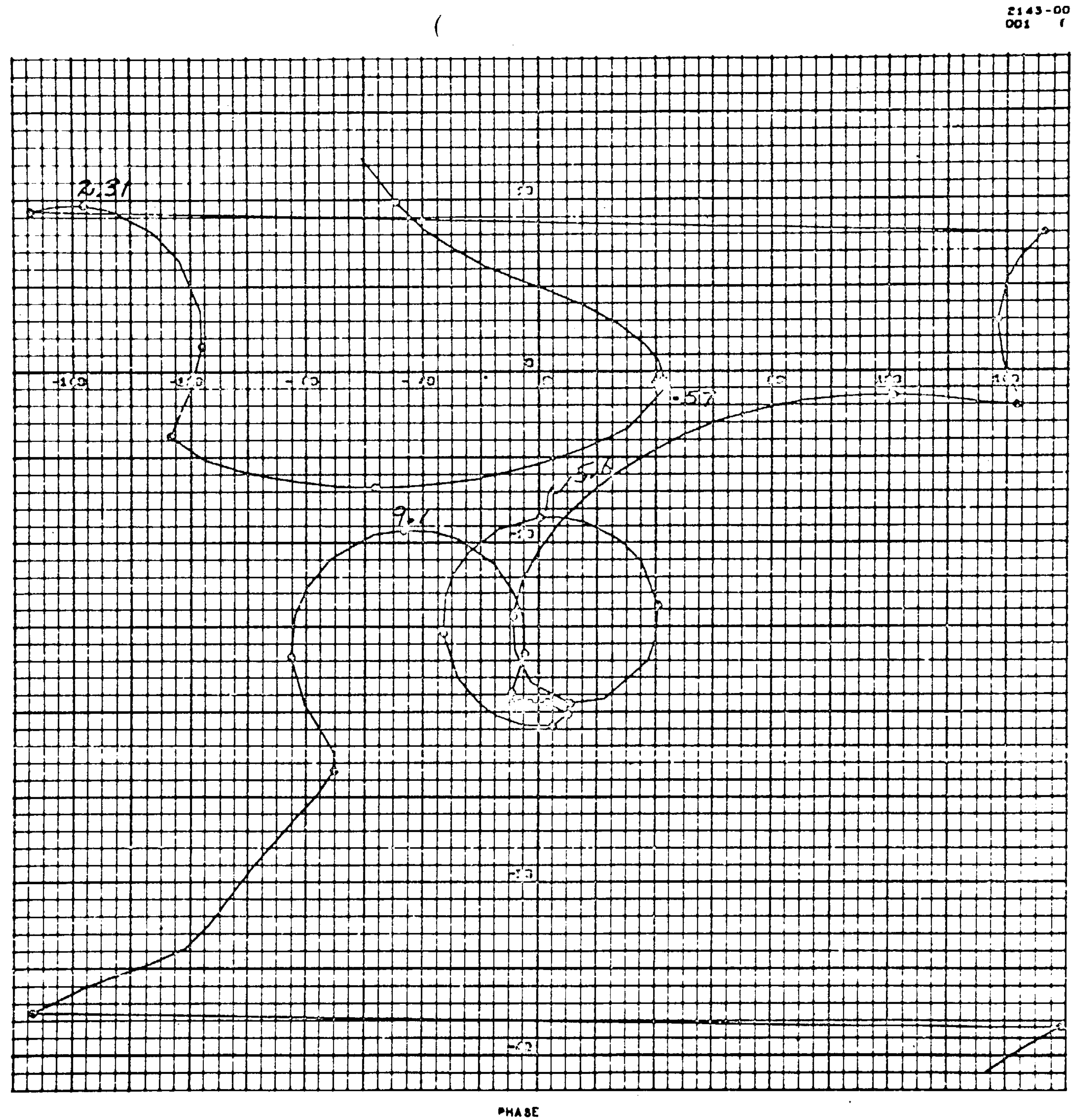

Figure 22. Gain-Phase t = 78 sec, Compensation Configuration #2

Notch Zeros Nominal

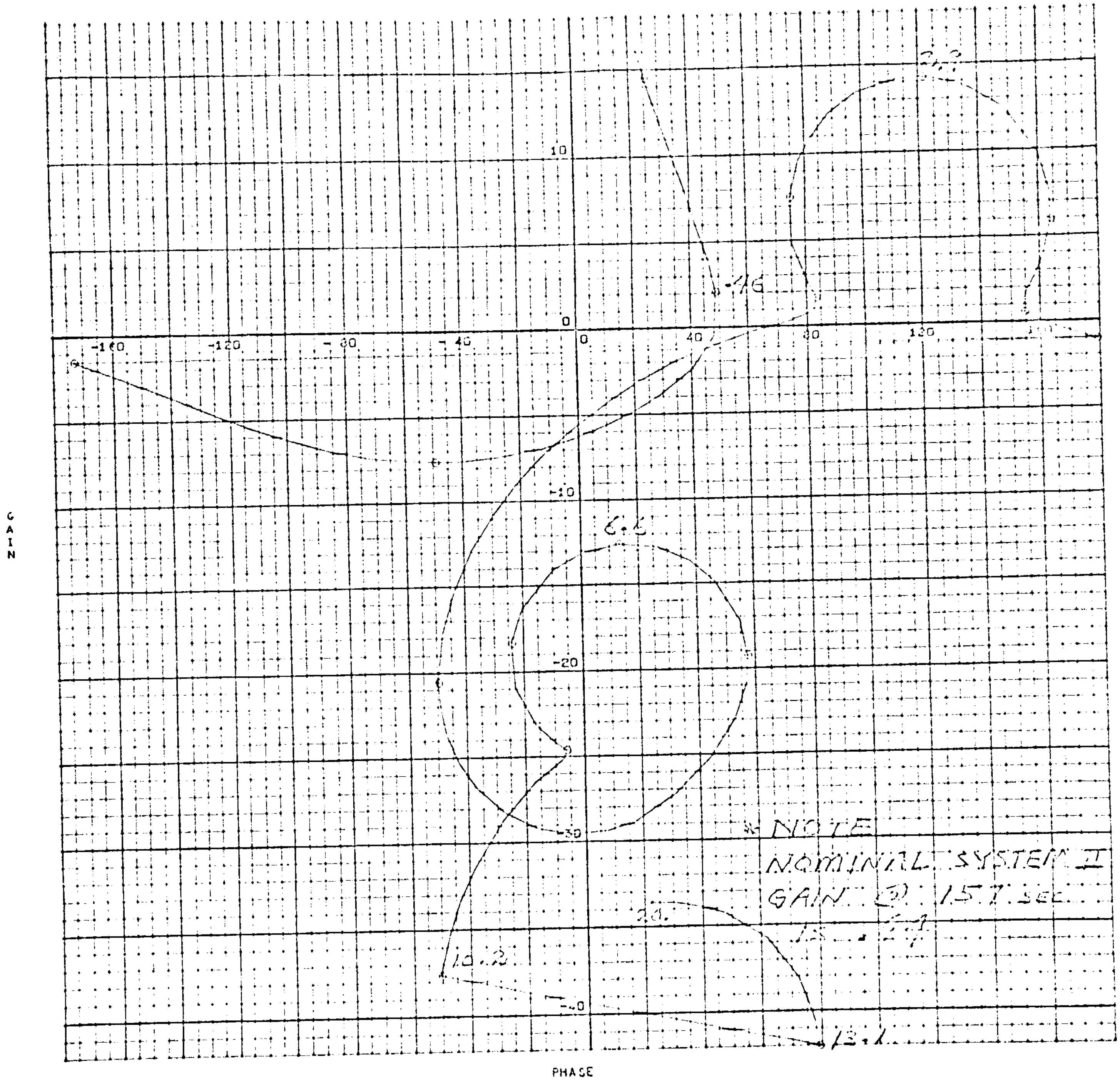

Figure 22. Gain-Phase t = 157 sec, Compensation Configuration #2

Notch Zeros Nominal

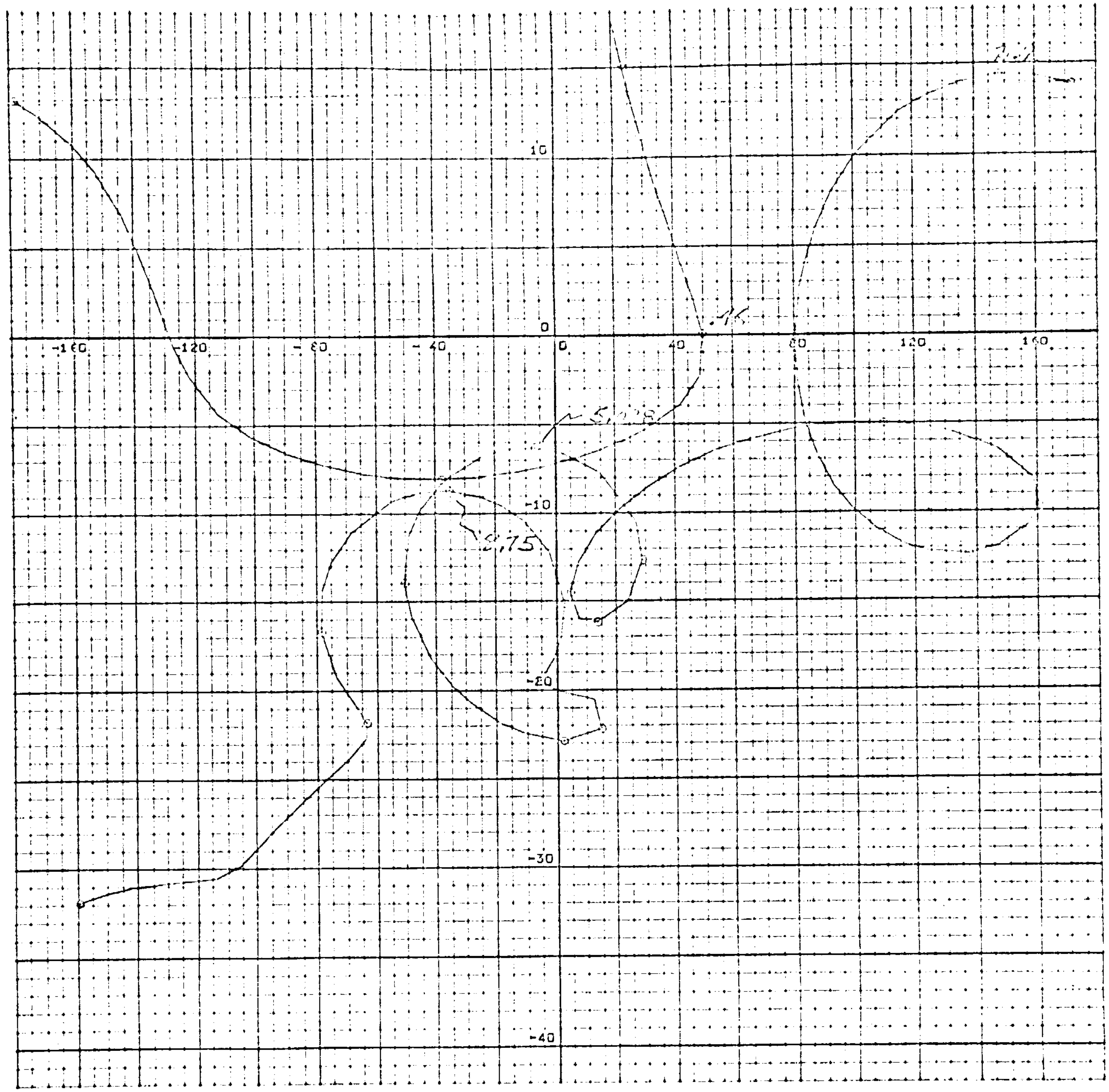

Figure 24. Gain-Phase t = 8 sec, Compensation Configuration #2

1st Mode Zero 5 % High

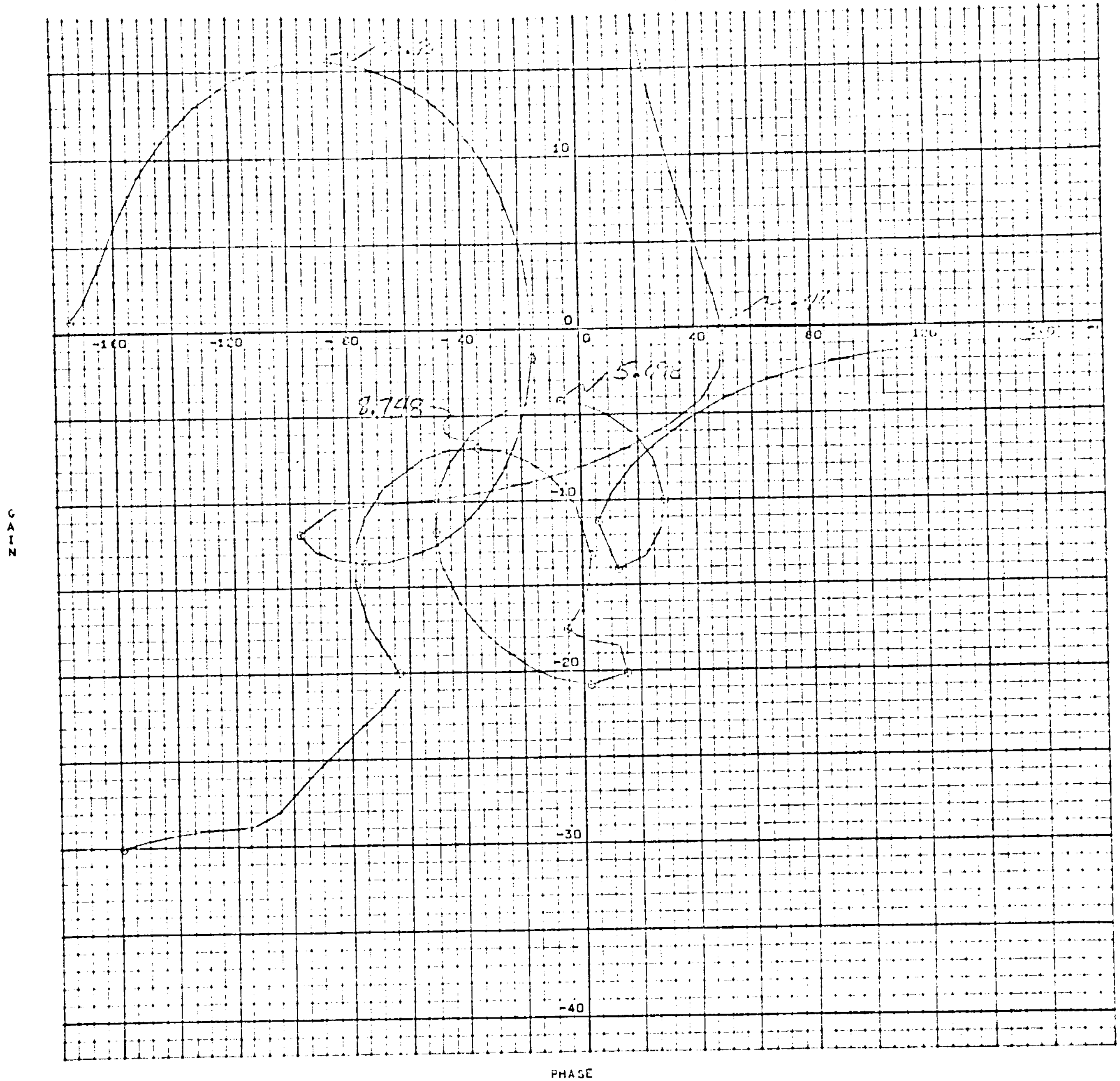

Figure 25. Gain-Phase t = 8 sec, Compensation Configuration #2

1st Mode Zero 5 % Low

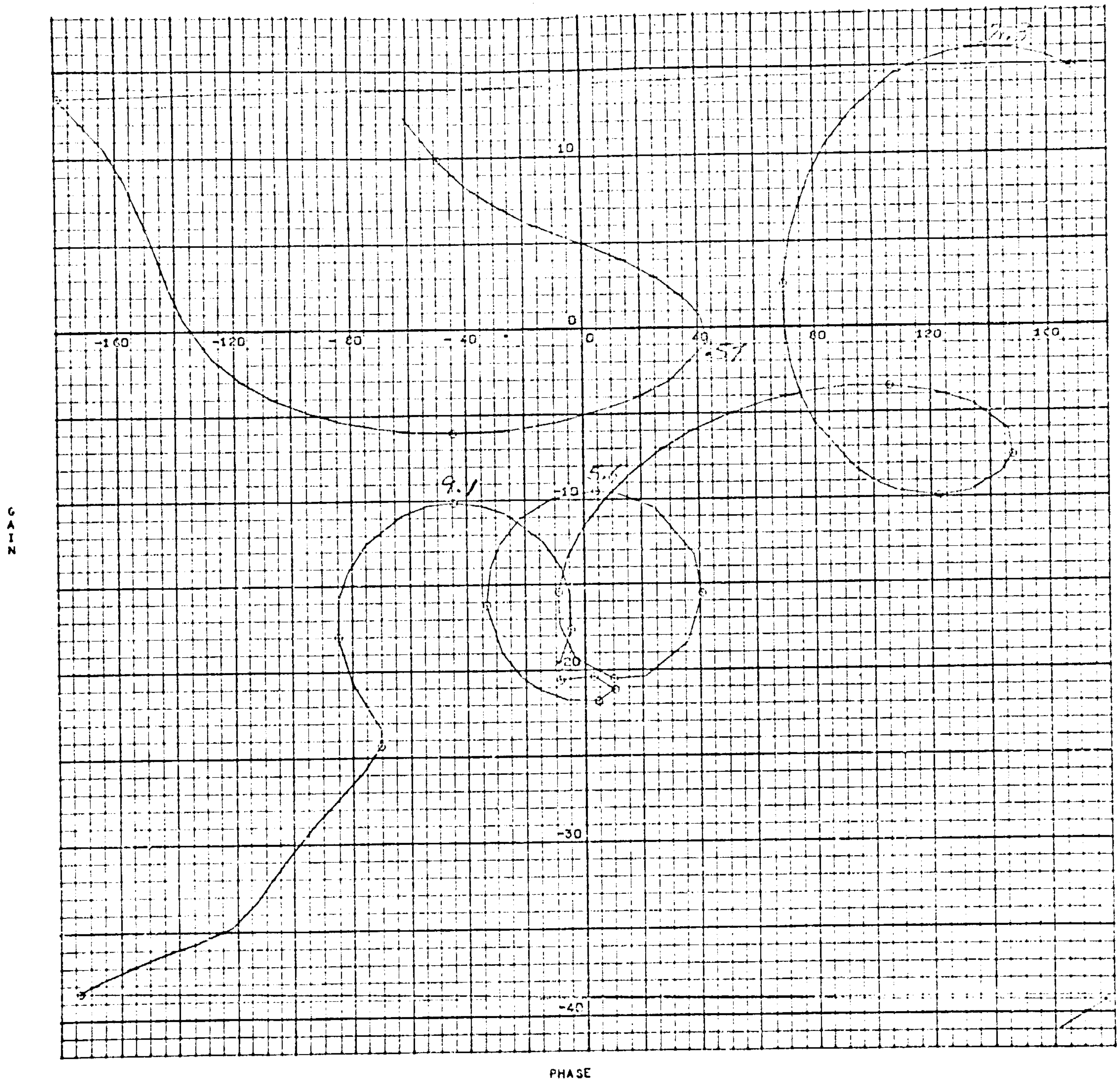

Figure 26. Gain-Phase t = 78 sec, Compensation Configuration #2
1st Mode Zero 5 % High

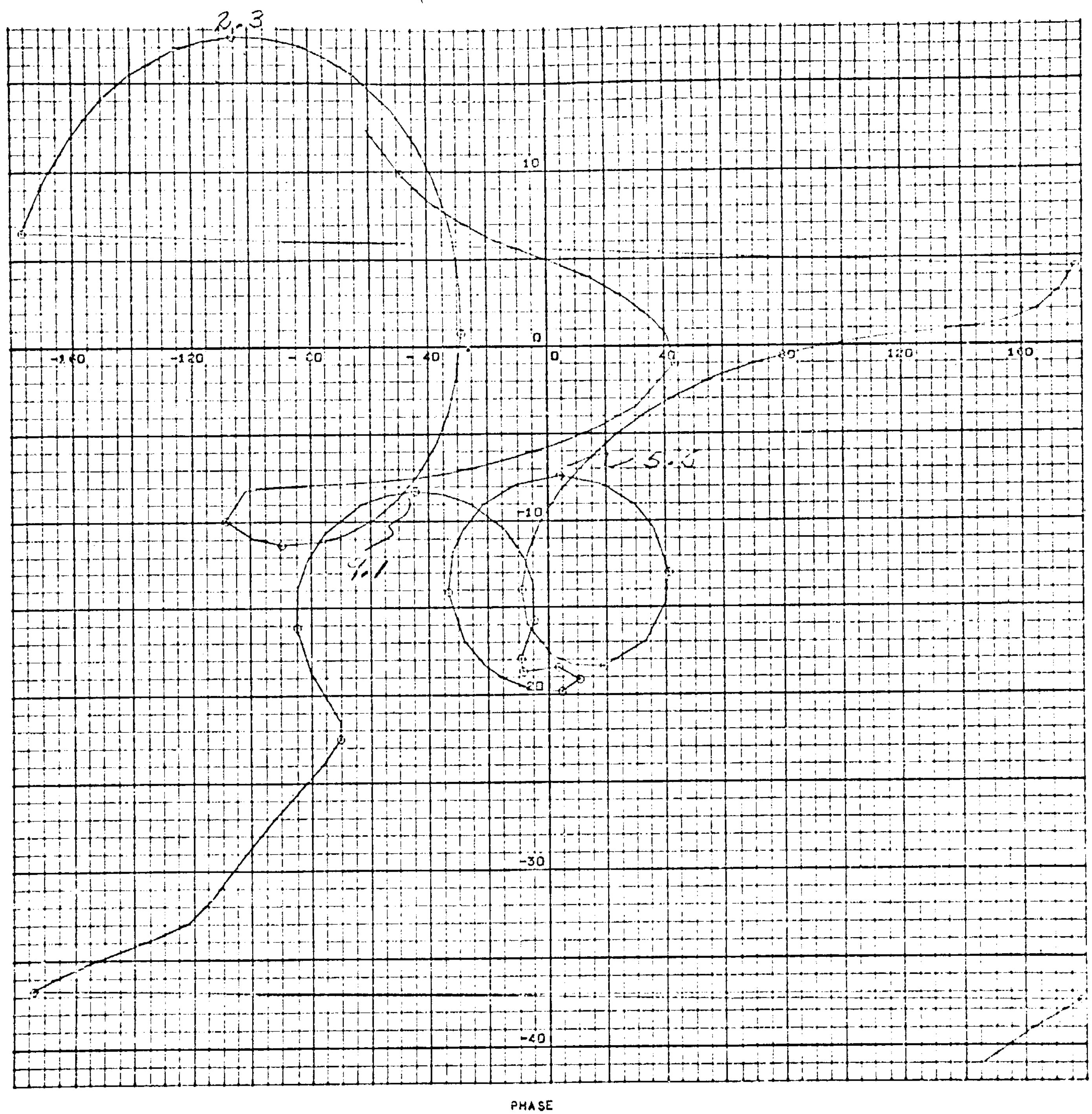

Figure 27. Gain-Phase t = 78 sec, Compensation Configuration #2
1st Mode Zero 5 % Low

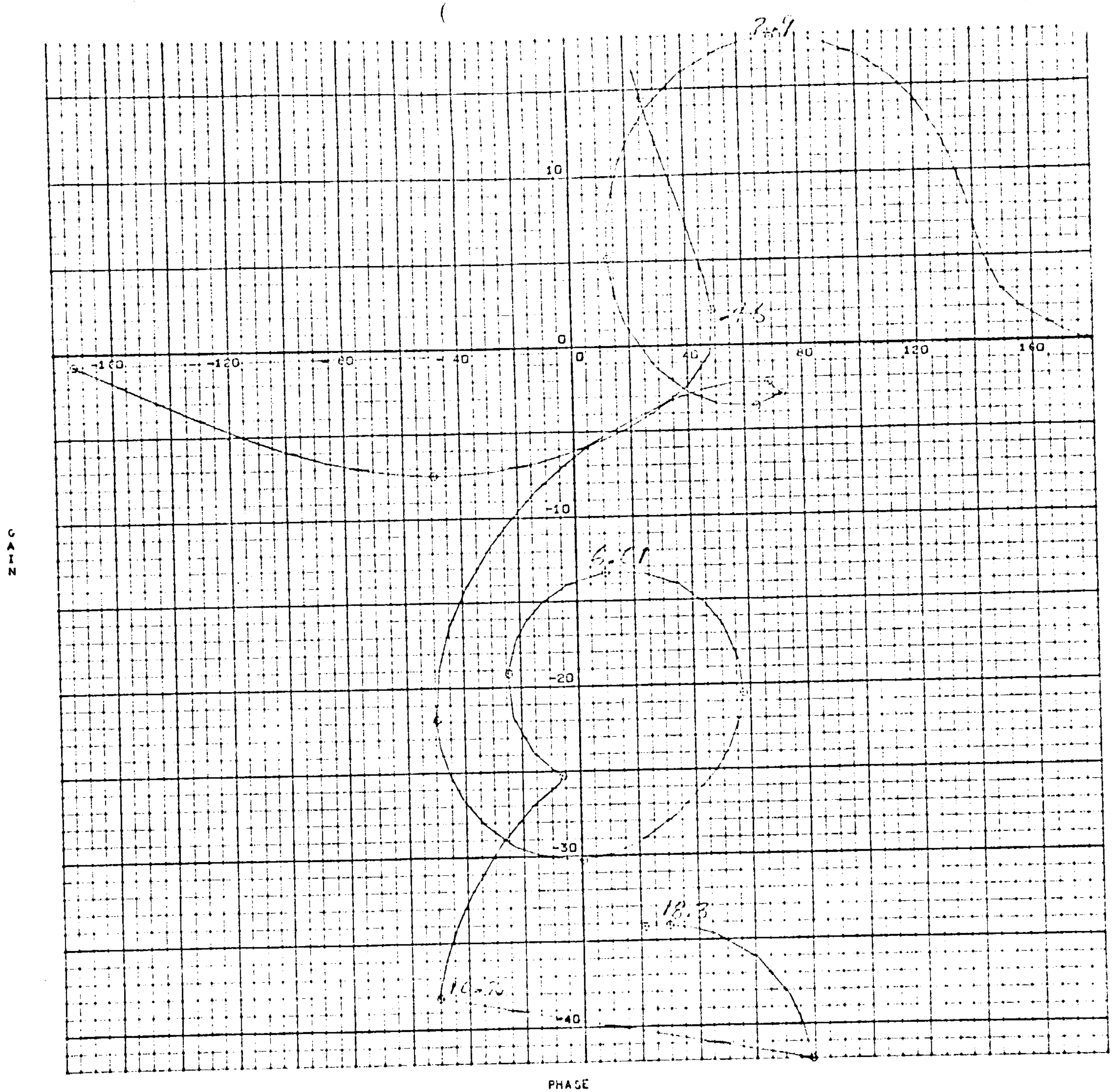

Figure 28. Gain-Phase t = 157 sec, Compensation Configuration #2

1st Mode Zero 3 % High

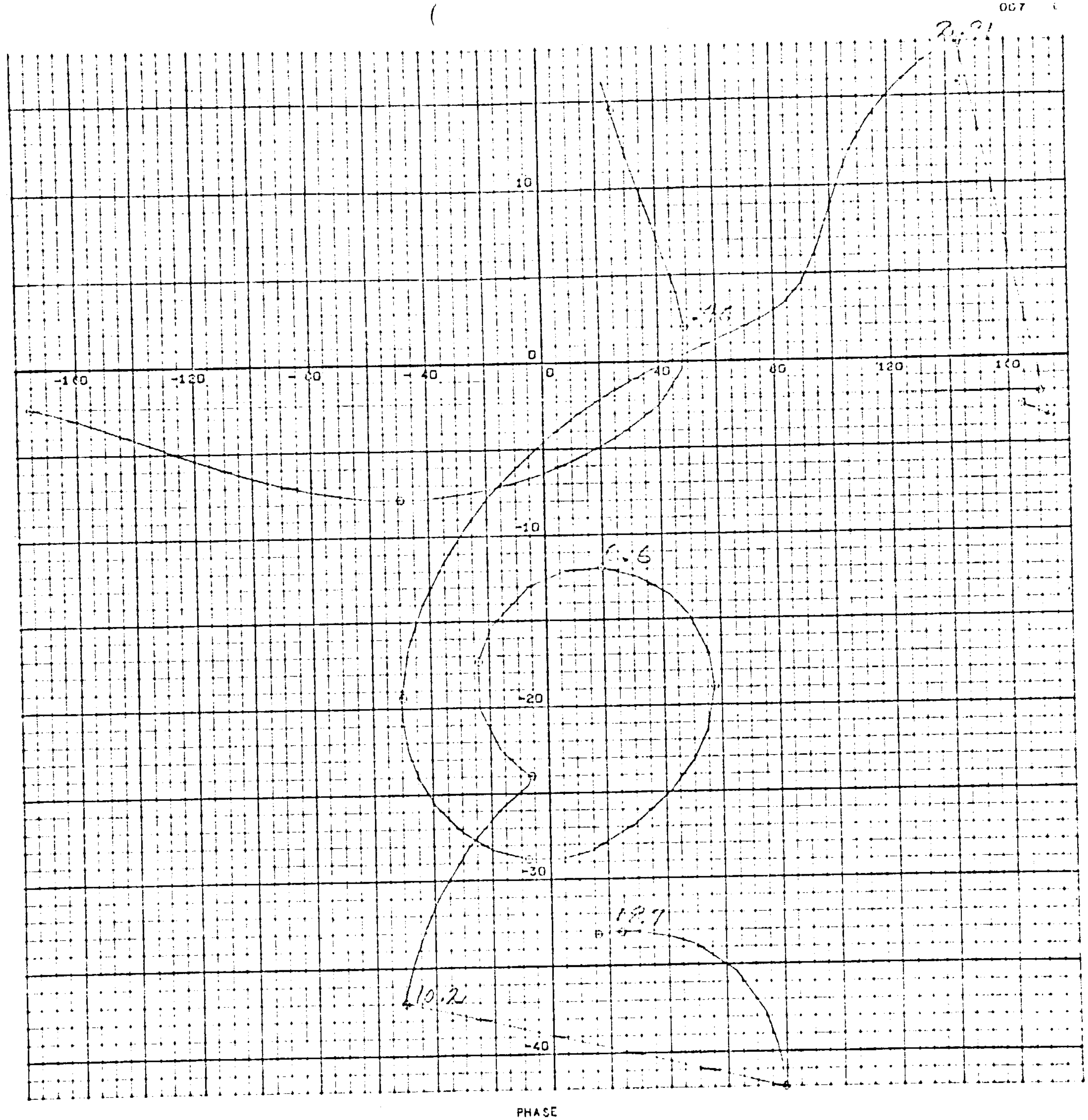

Figure 29. Gain-Phase t = 157 sec, Compensation Configuration #2
1st Mode Zero 3 % Low

2143-(
011

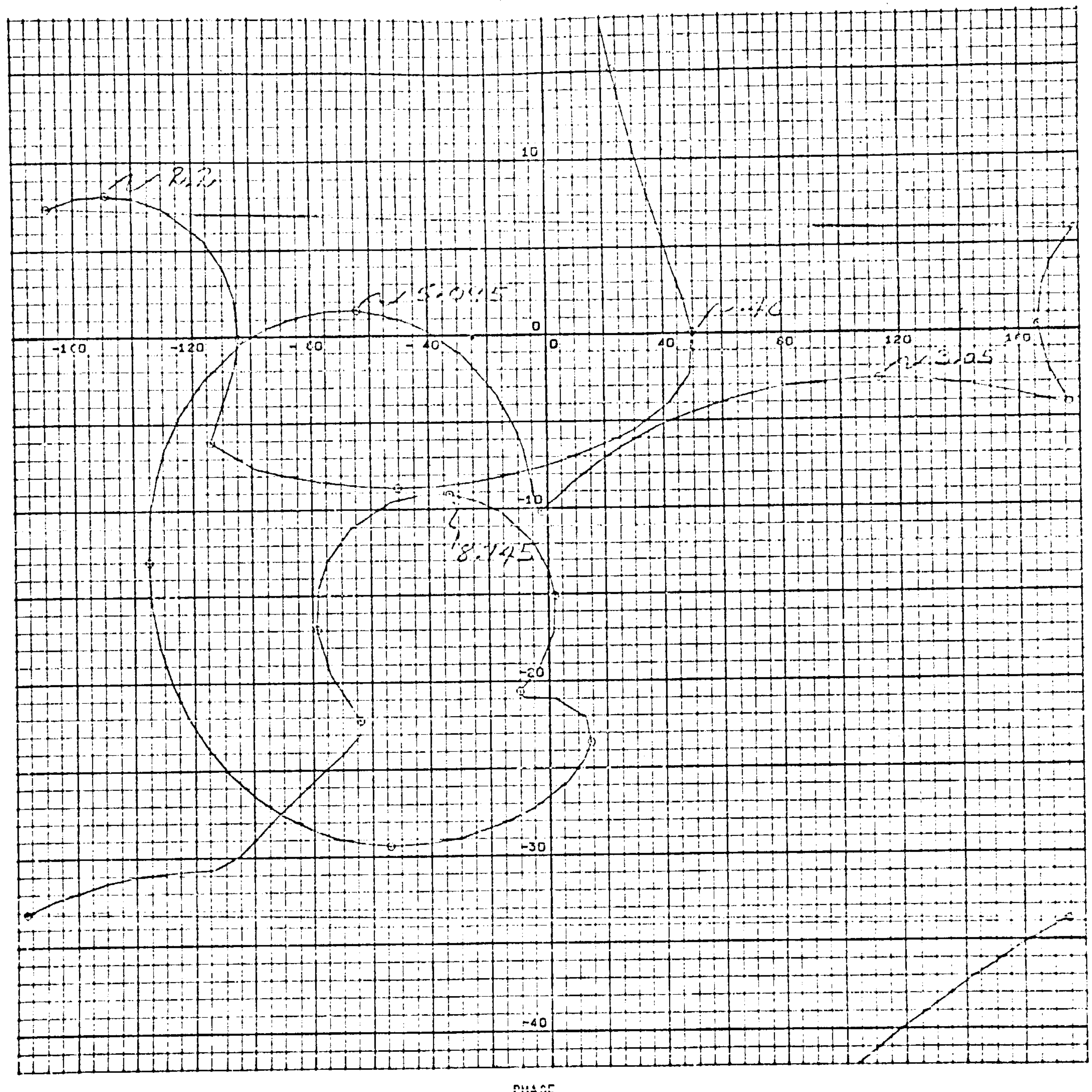

Figure 30. Gain-Phase t = 8 sec, Compensation Configuration #2

2nd Mode Zero 5 % High

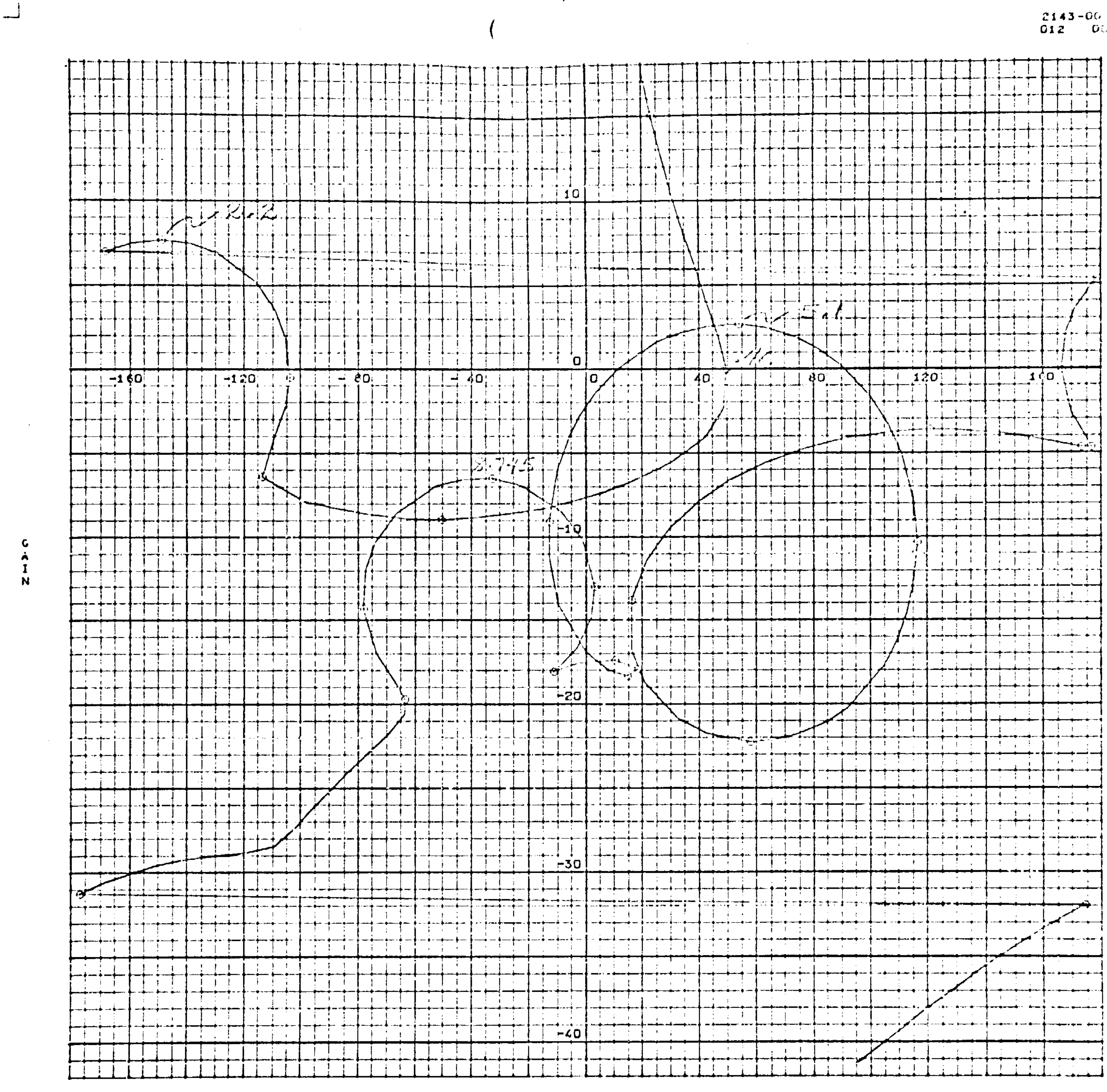

Figure 31. Gain-Phase t = 8 sec, Compensation Configuration #2

2nd Mode zero 5 % Low

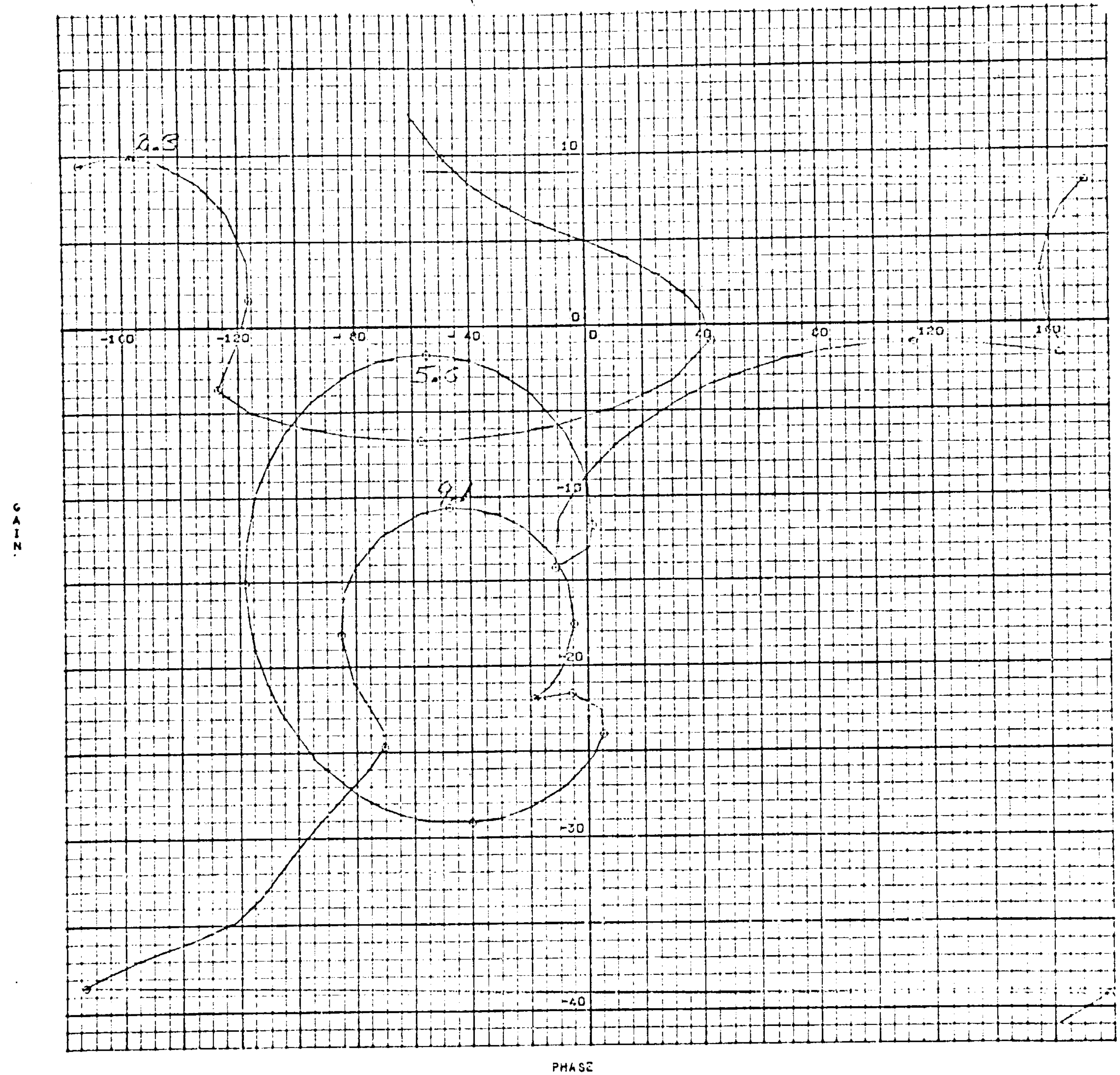

Figure 32. Gain-Phase t = 78 sec, Compensation Configuration #2

2nd Mode Zero 5 % High

2143-00 005 00

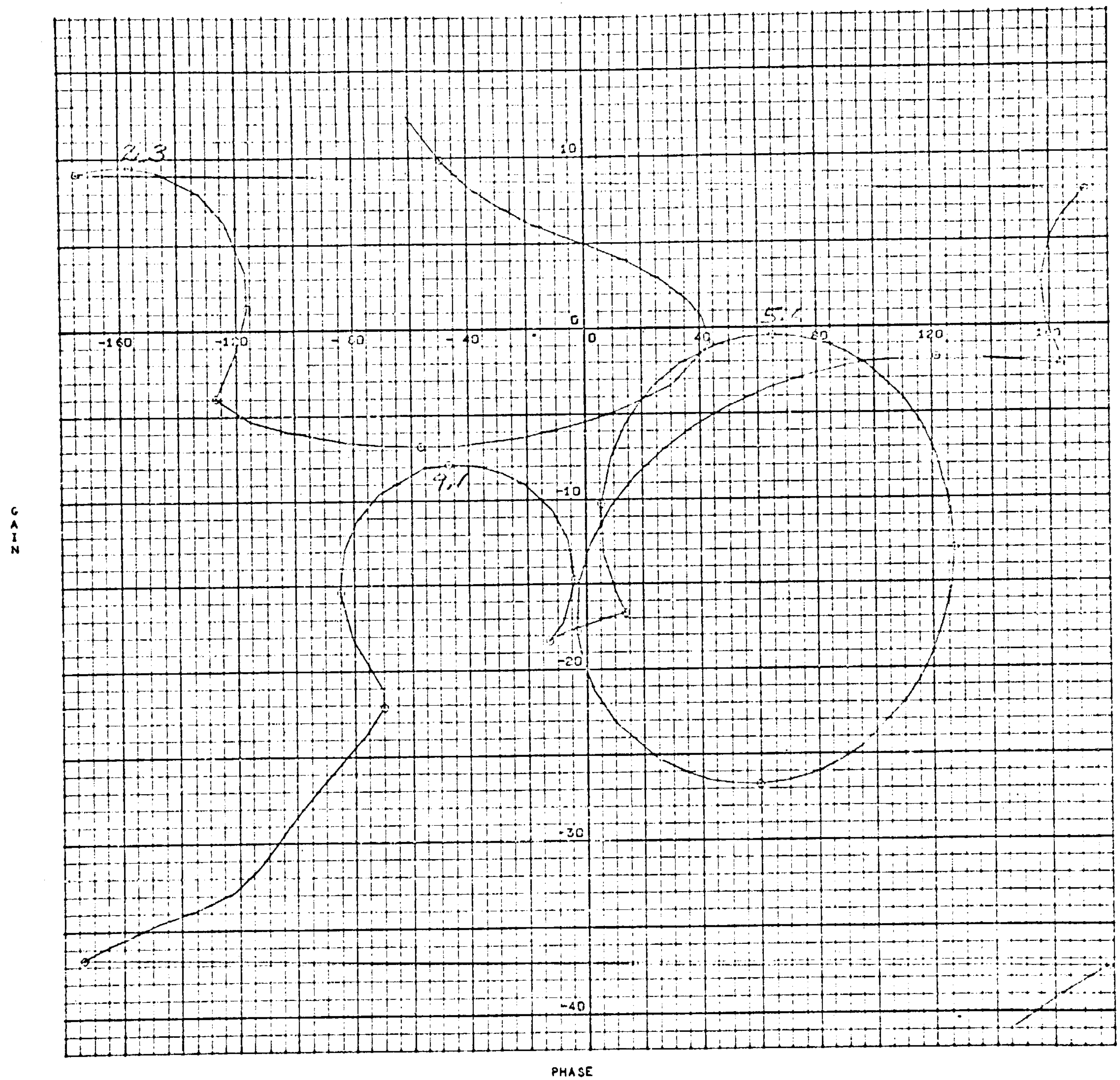

Figure 33. Gain-Phase t = 78 sec, Compensation Configuration #2

2nd Mode Zero 5 % Low

2143-G
008 000

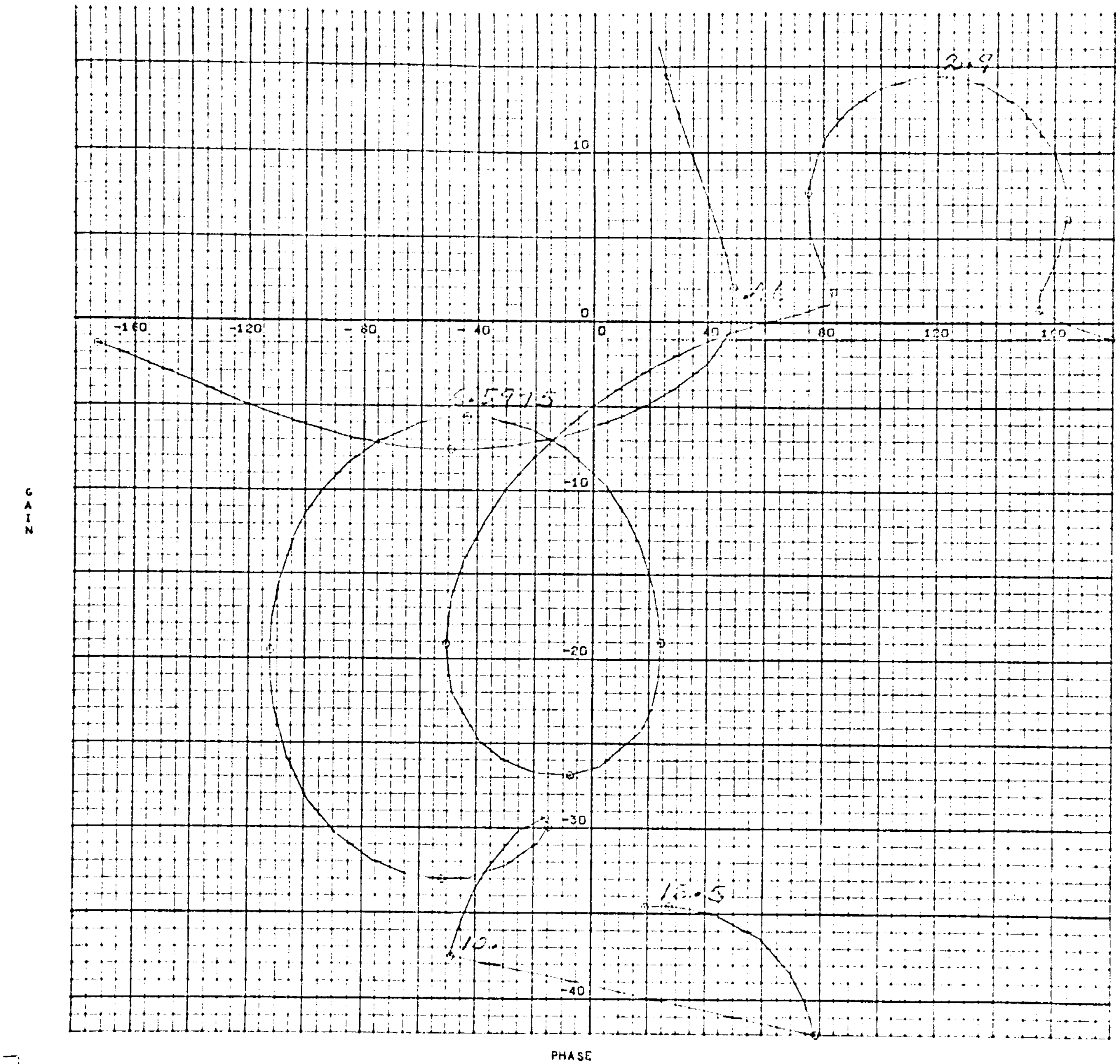

Figure 34. Gain-Phase t = 157 sec, Compensation Configuration #2

2nd mode Zero 5 % High

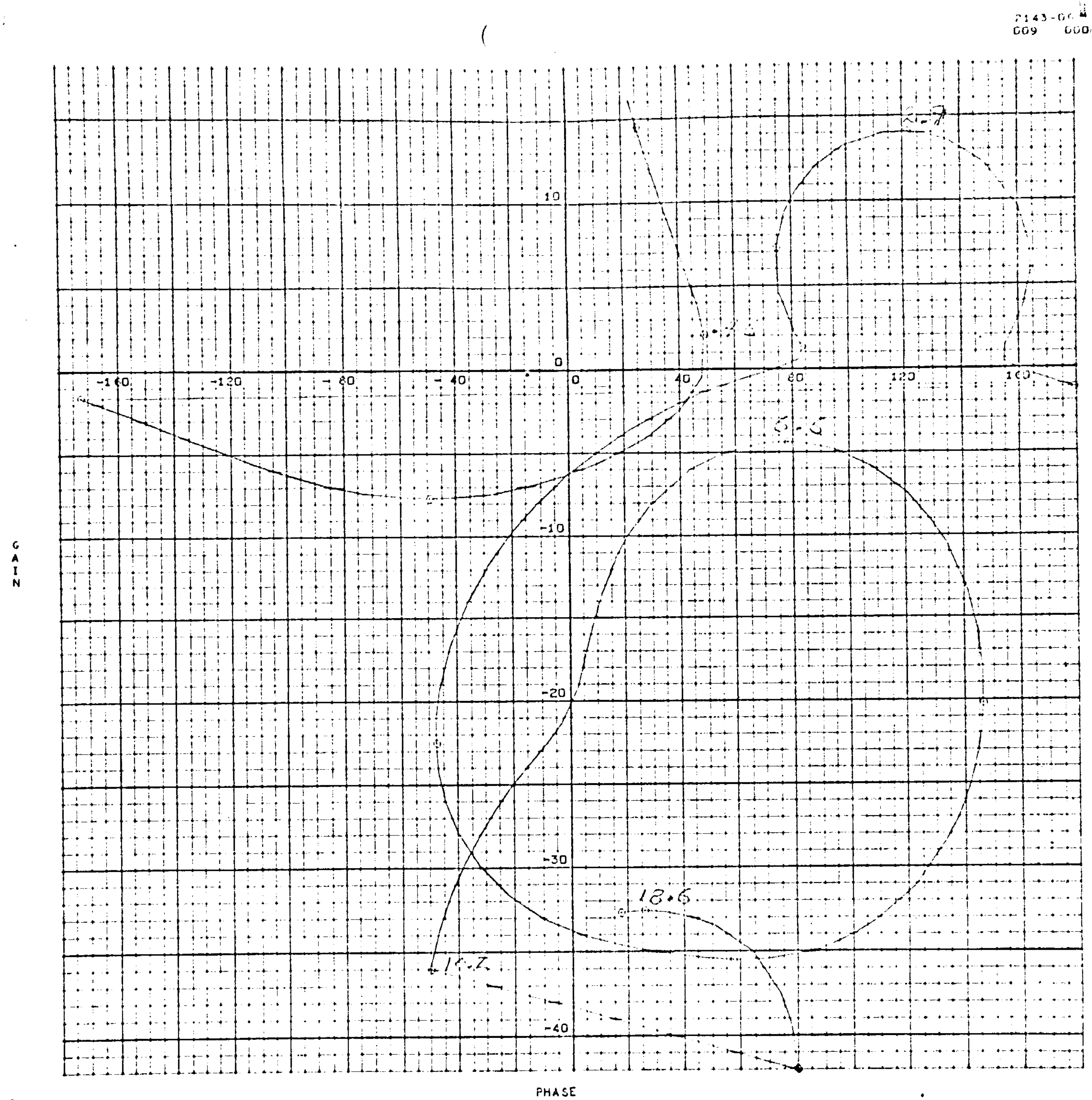

Figure 35. Gain-Phase t = 157 sec, Compensation Configuration #2
2nd Mode Zero 5 % Low

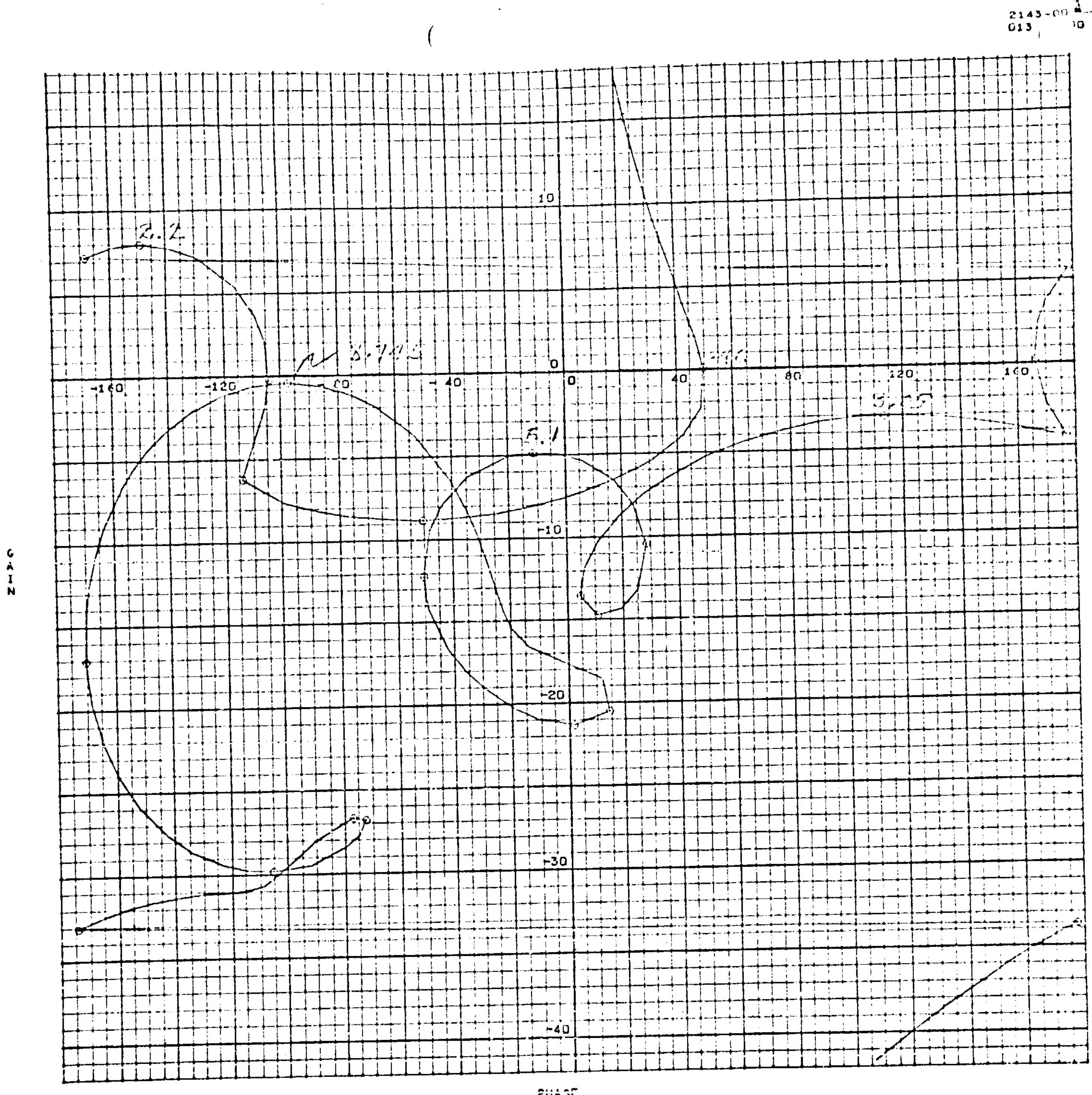

Figure 36. Gain-Phase t = 8 sec, Compensation Configuration #2
3rd Mode Zero 5 % High

2143-00
014 C

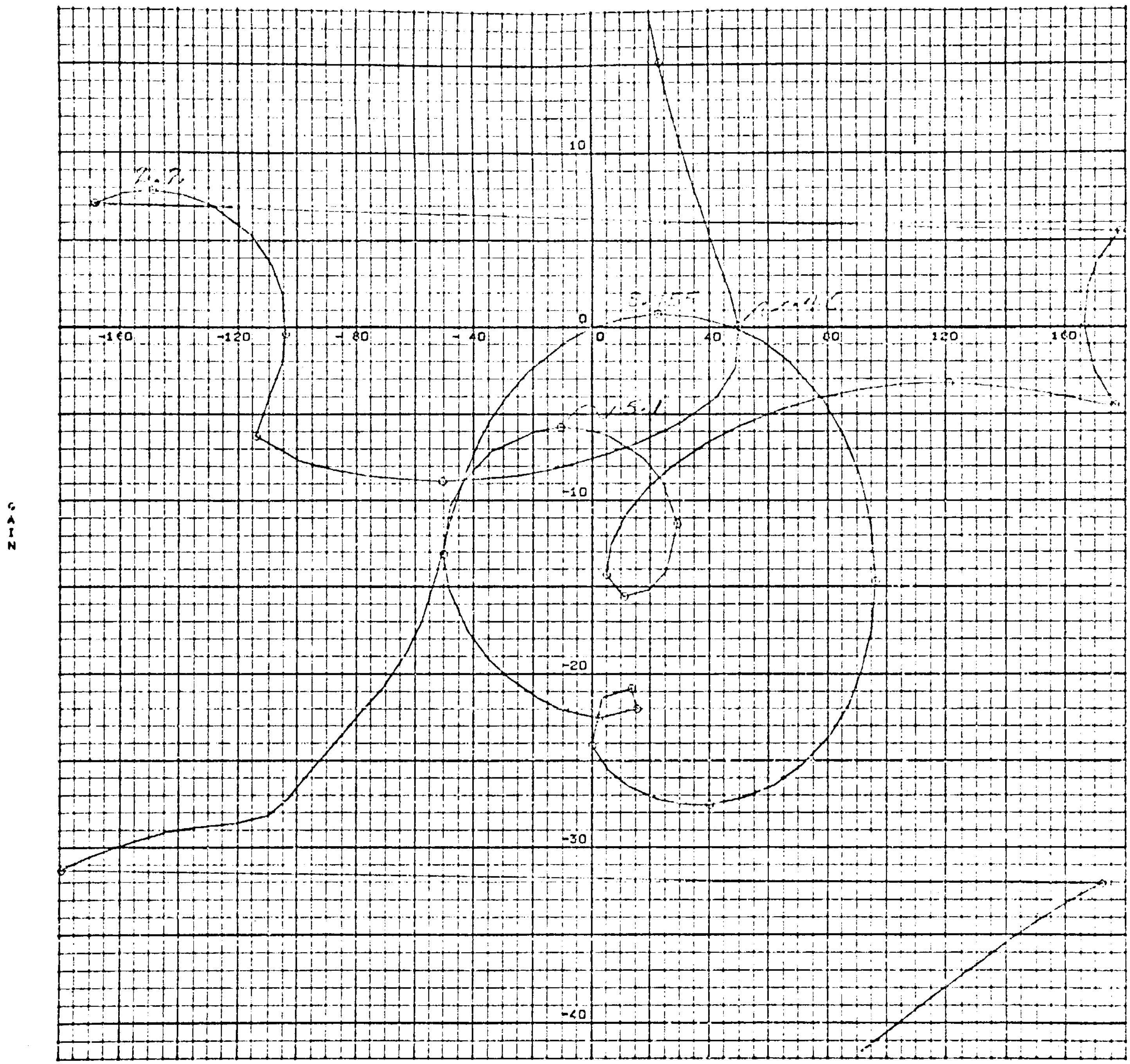

Figure 37. Gain-Phase t = 8 sec. Compensation Configuration #2
3rd Mode Zero 5 % Low

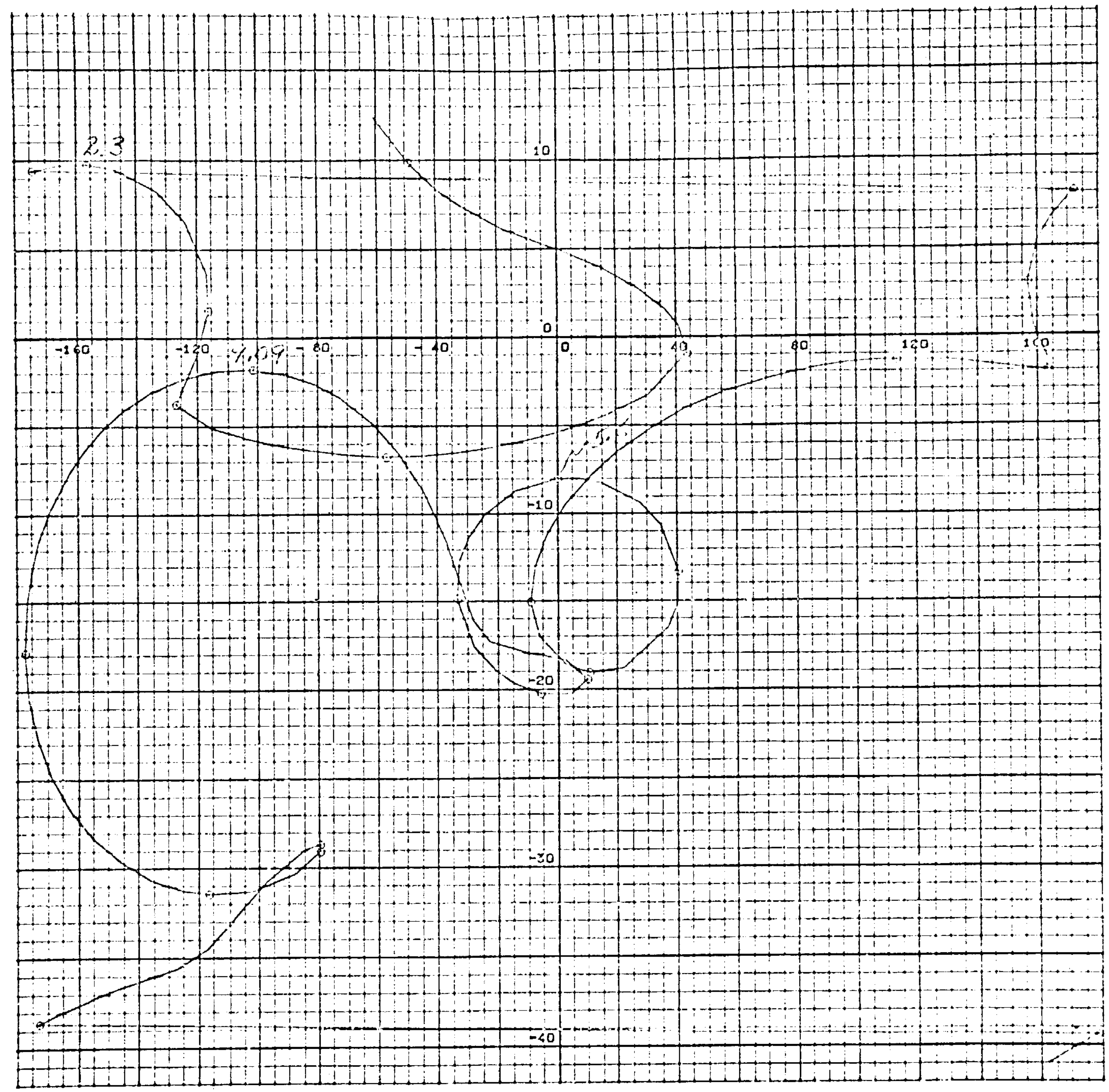

Figure 38. Gain-Phase t = 78 sec, Compensation Configuration #2

3rd Mode Zero 5 % High

2143-00
007 1

Figure 39. Gain-Phase t = 78 sec, Compensation Configuration #2
3rd Mode Zero 5 % Low

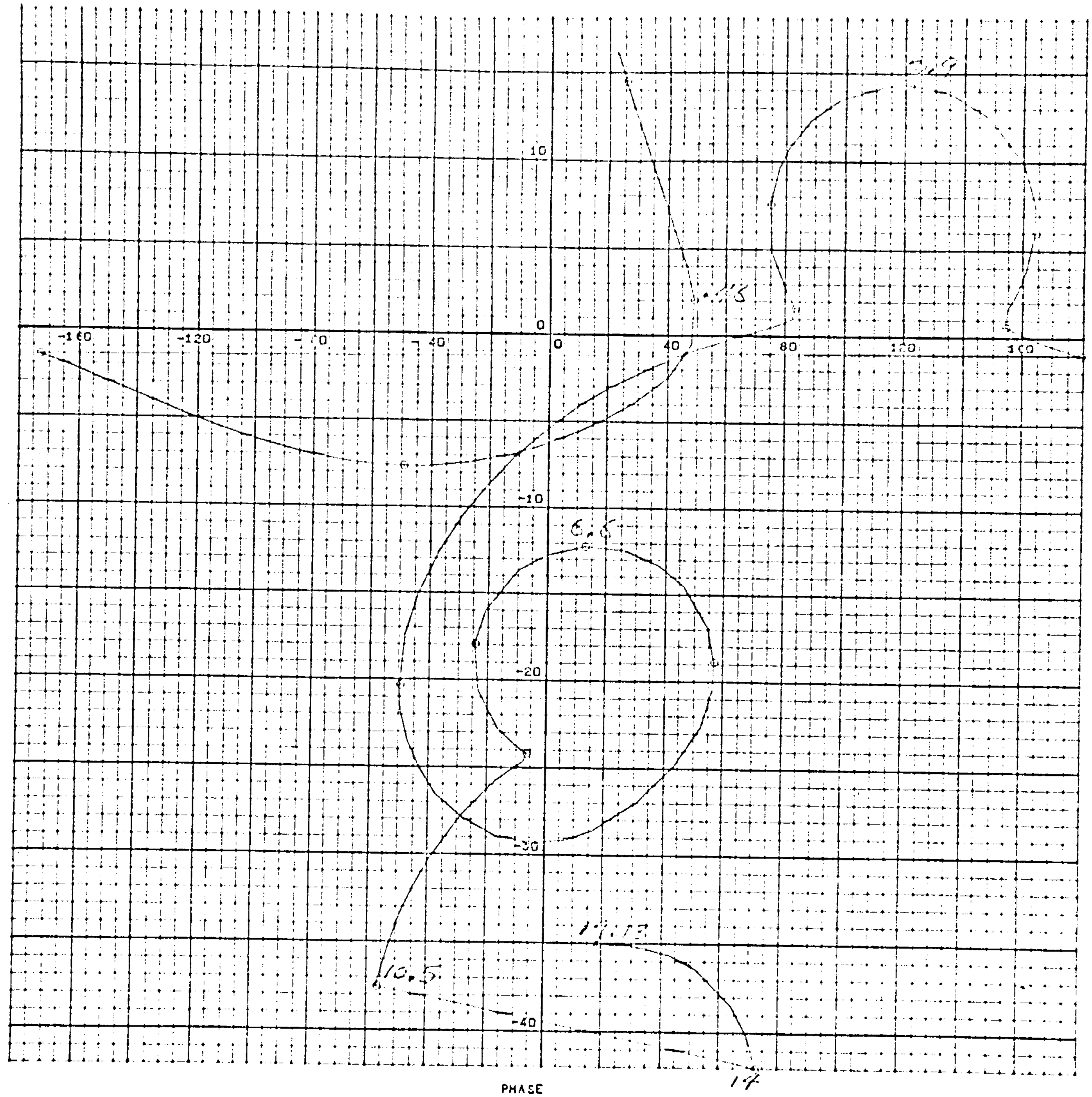

Figure 40. Gain-Phase t = 157 sec, Compensation Configuration #2
3rd Mode Zero 5 % High

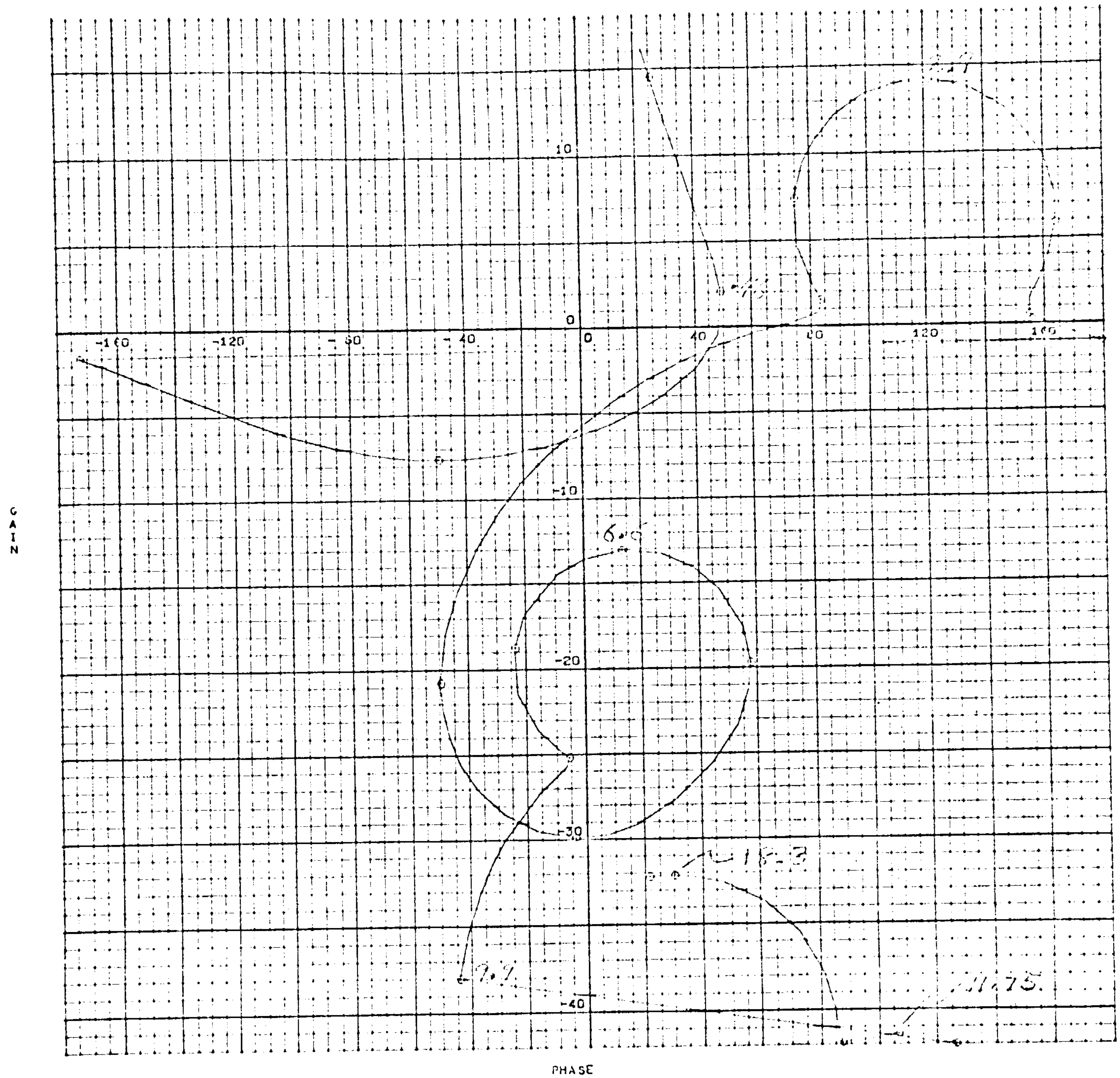

Figure 41. Gain-Phase t = 157 sec, Compensation Configuration #2

3rd Mode Zero 5 % Low

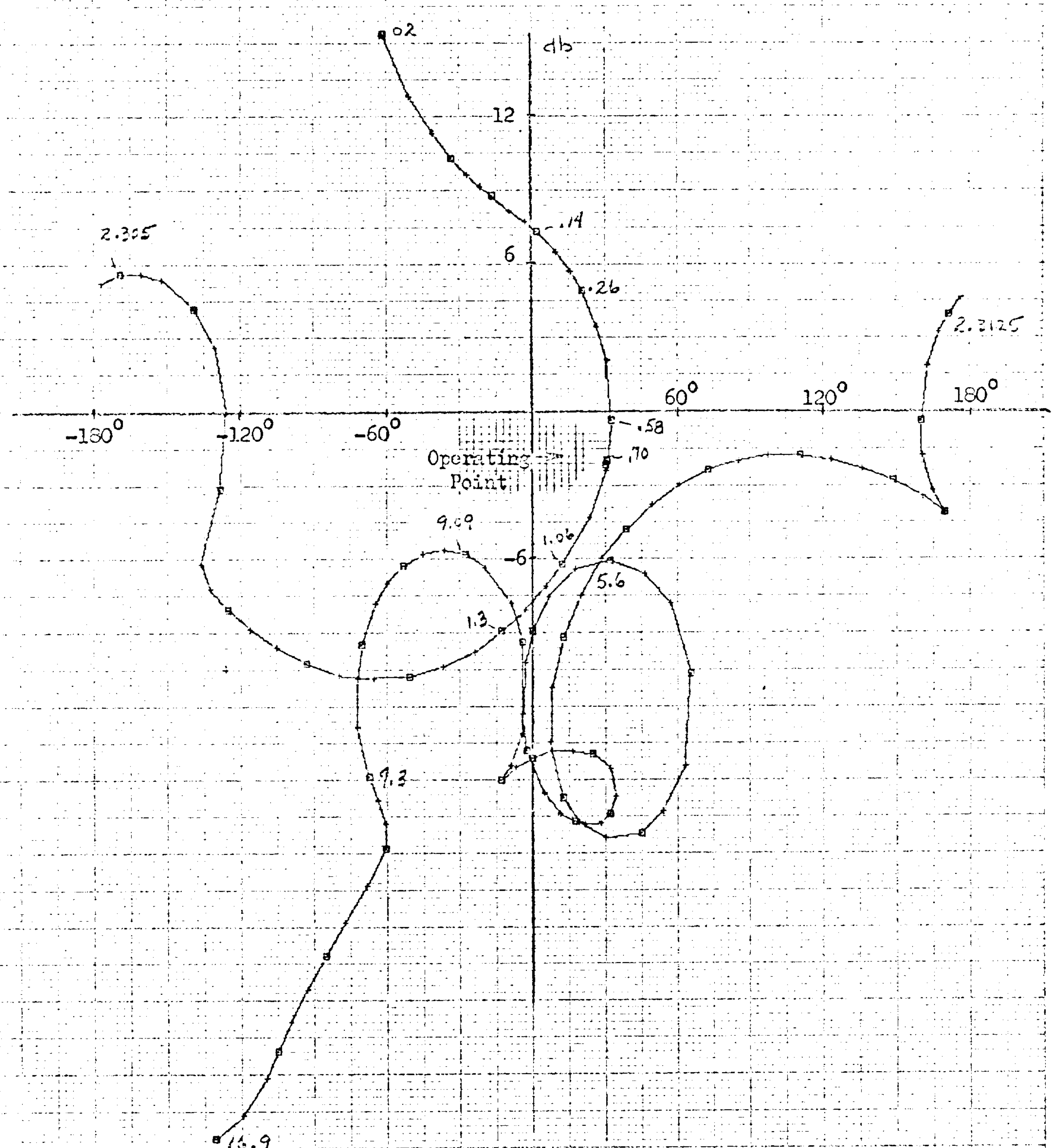

Figure 42 Gain-Phase t = 78 sec.

Compensation Configuration #3

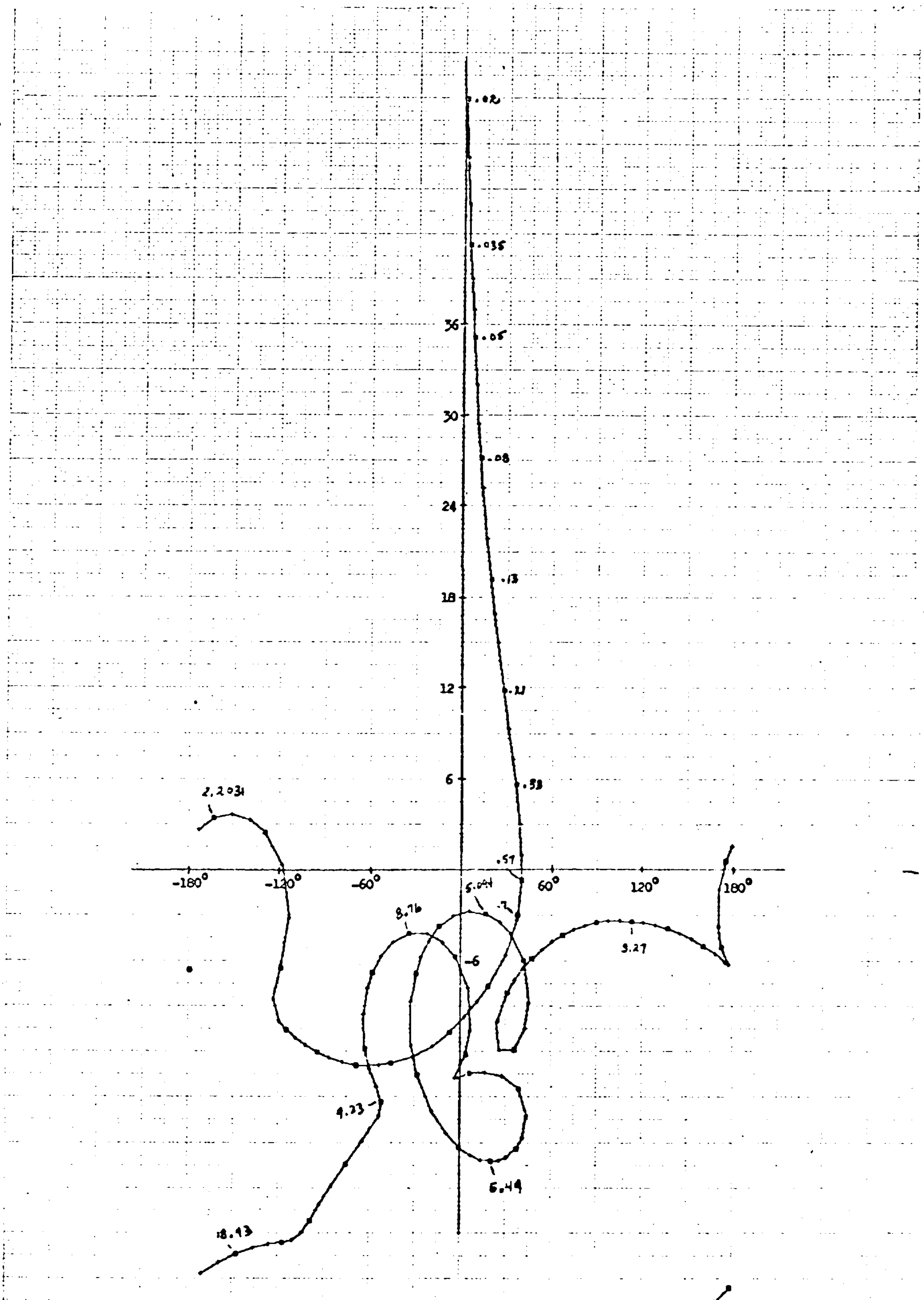

Figure 43. Gain-Phase t = 8 sec.

Compensation configuration #3 Applied Directly to 8 sec Flight Case

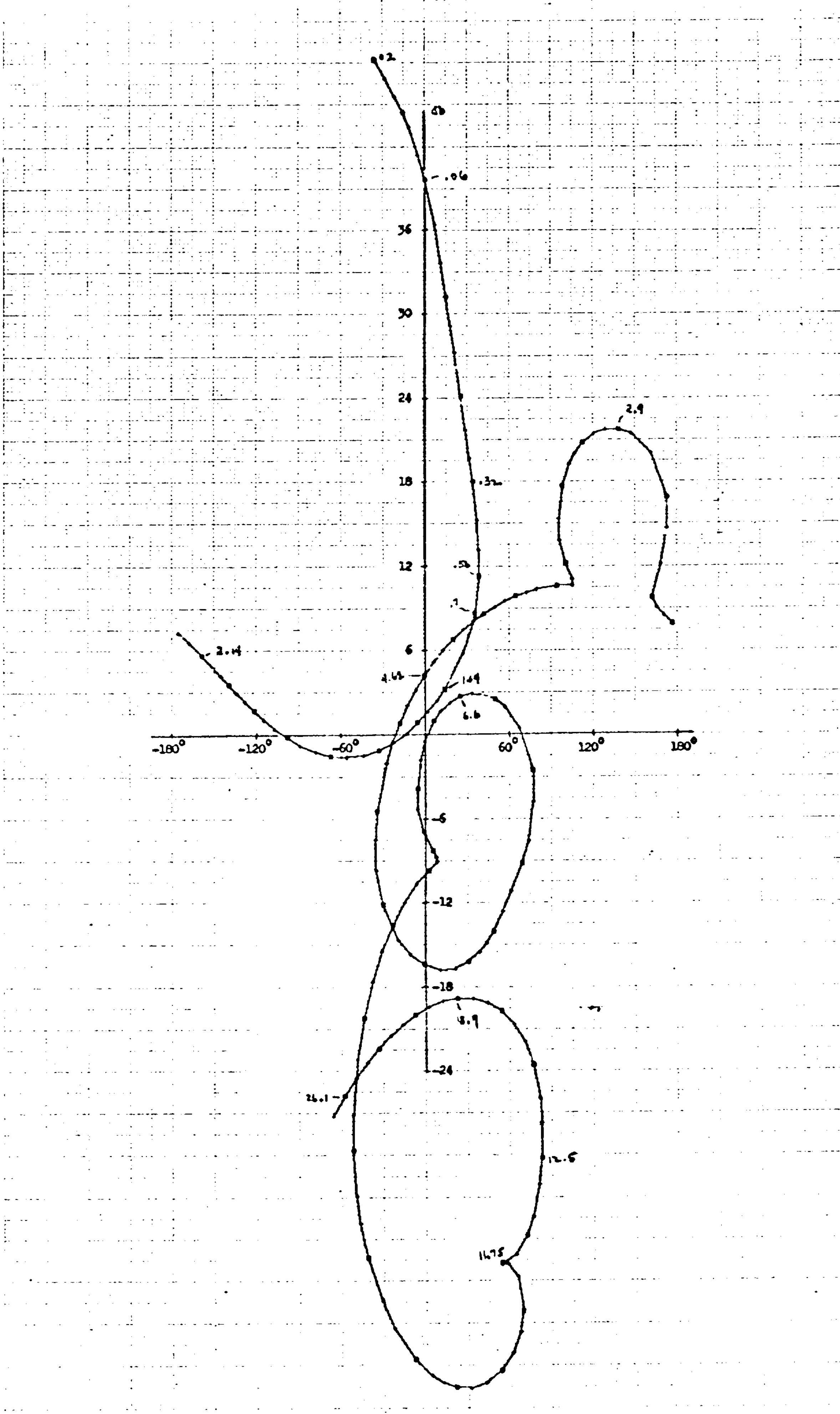

Figure 14. Gain-Phase t = 157 sec, Compensation Configuration #3 Applied Directly to 157 sec Flight Case

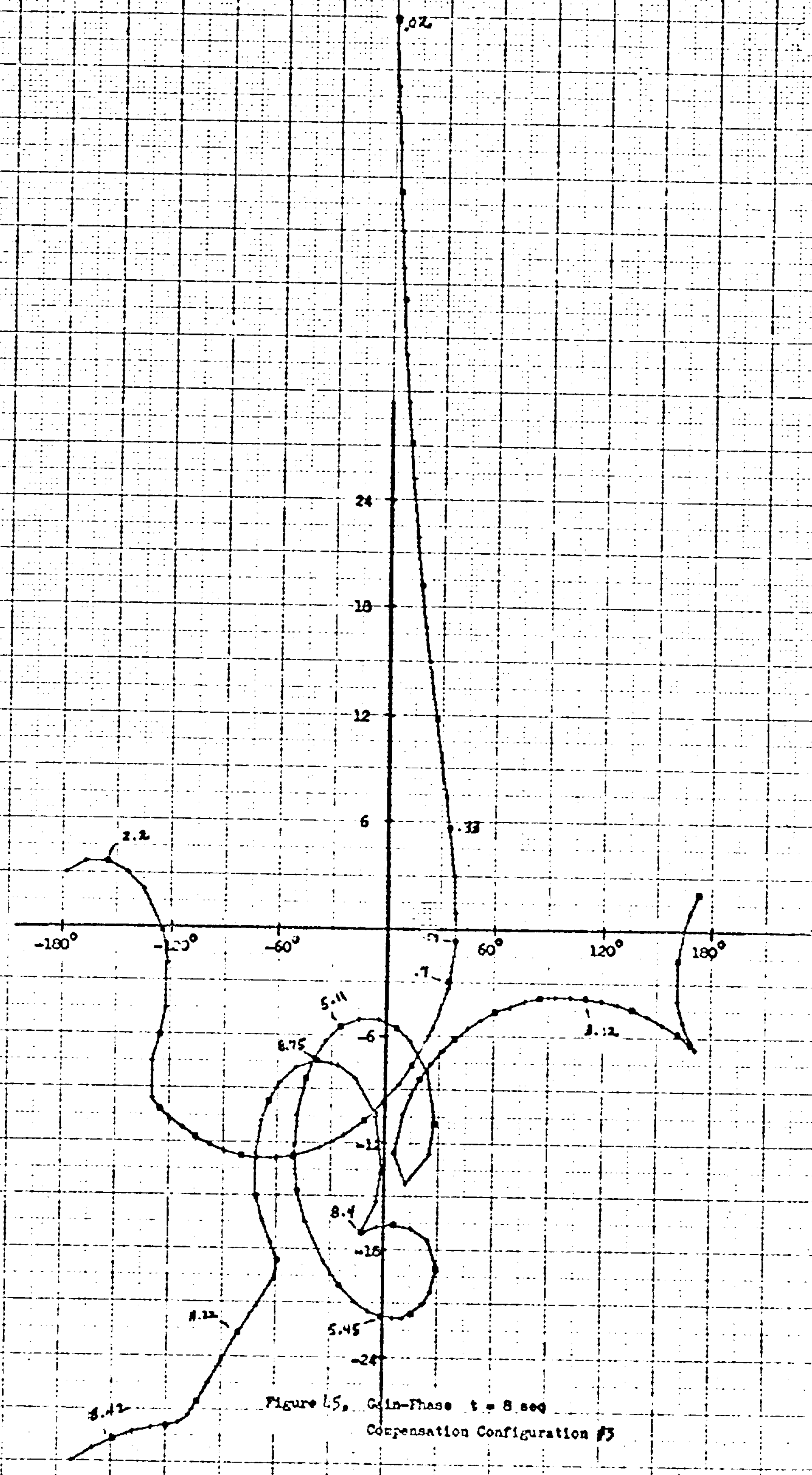

Figure 45, Gain-Phase t = 8 sec

Compensation Configuration #3

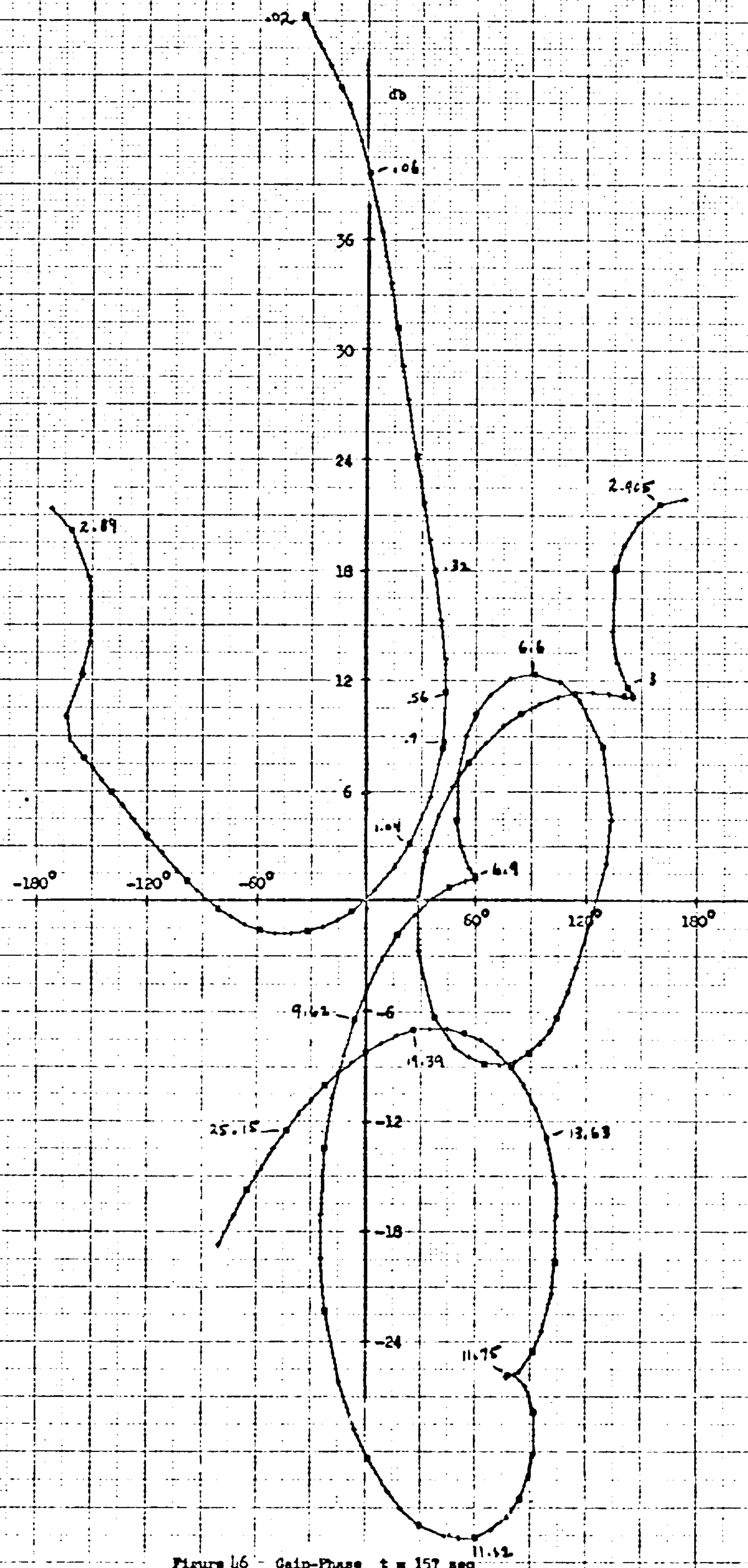

Figure 46 Gain-Phase t = 157 sec

Compensation Configuration 3

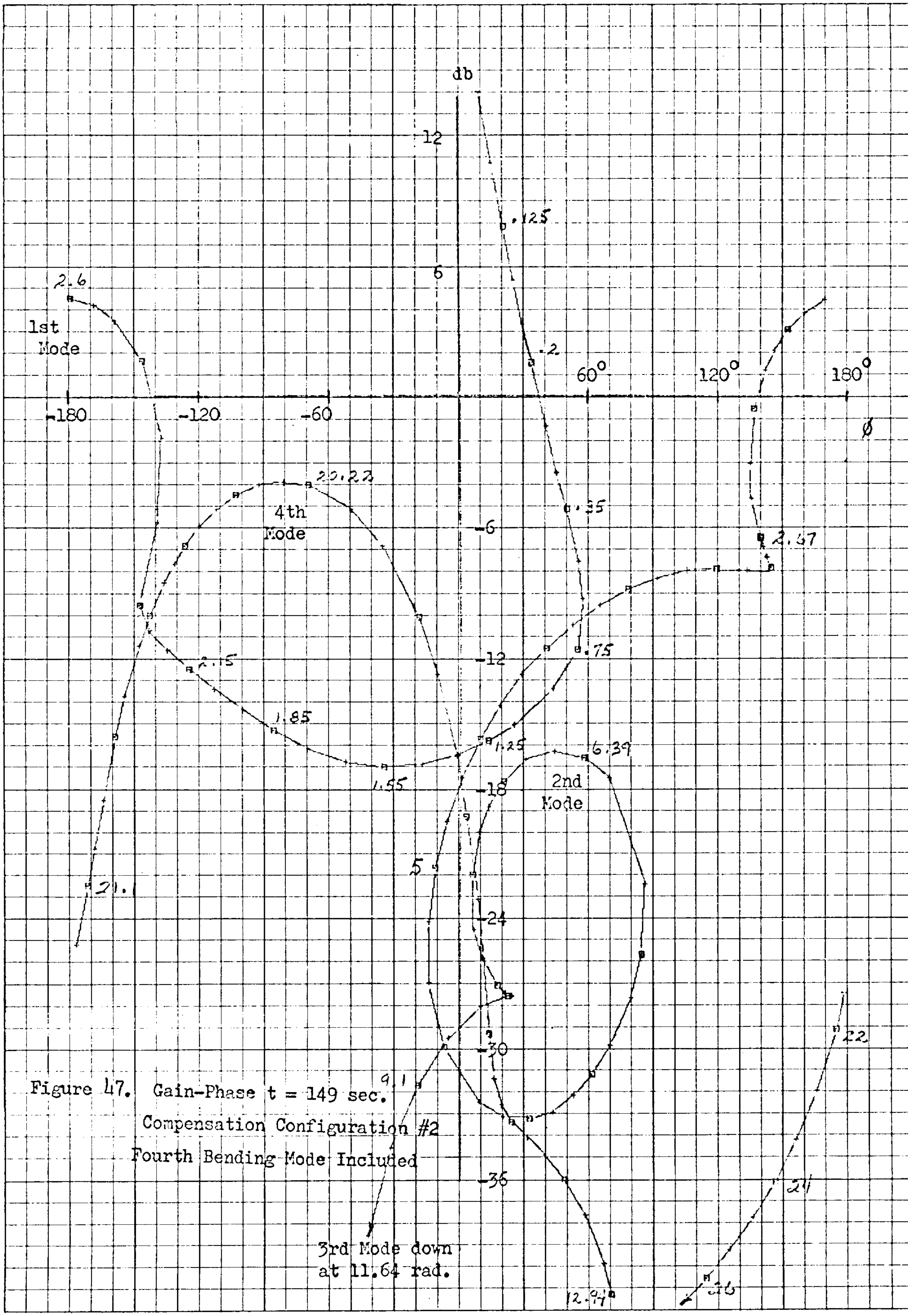

Figure 47. Gain-Phase t = 149 sec.
Compensation Configuration #2
Fourth Bending Mode Included

Figure 48. Gain-Phase t = 8 sec

Compensation Configuration #2

With Fuel Slosh, With Baffles

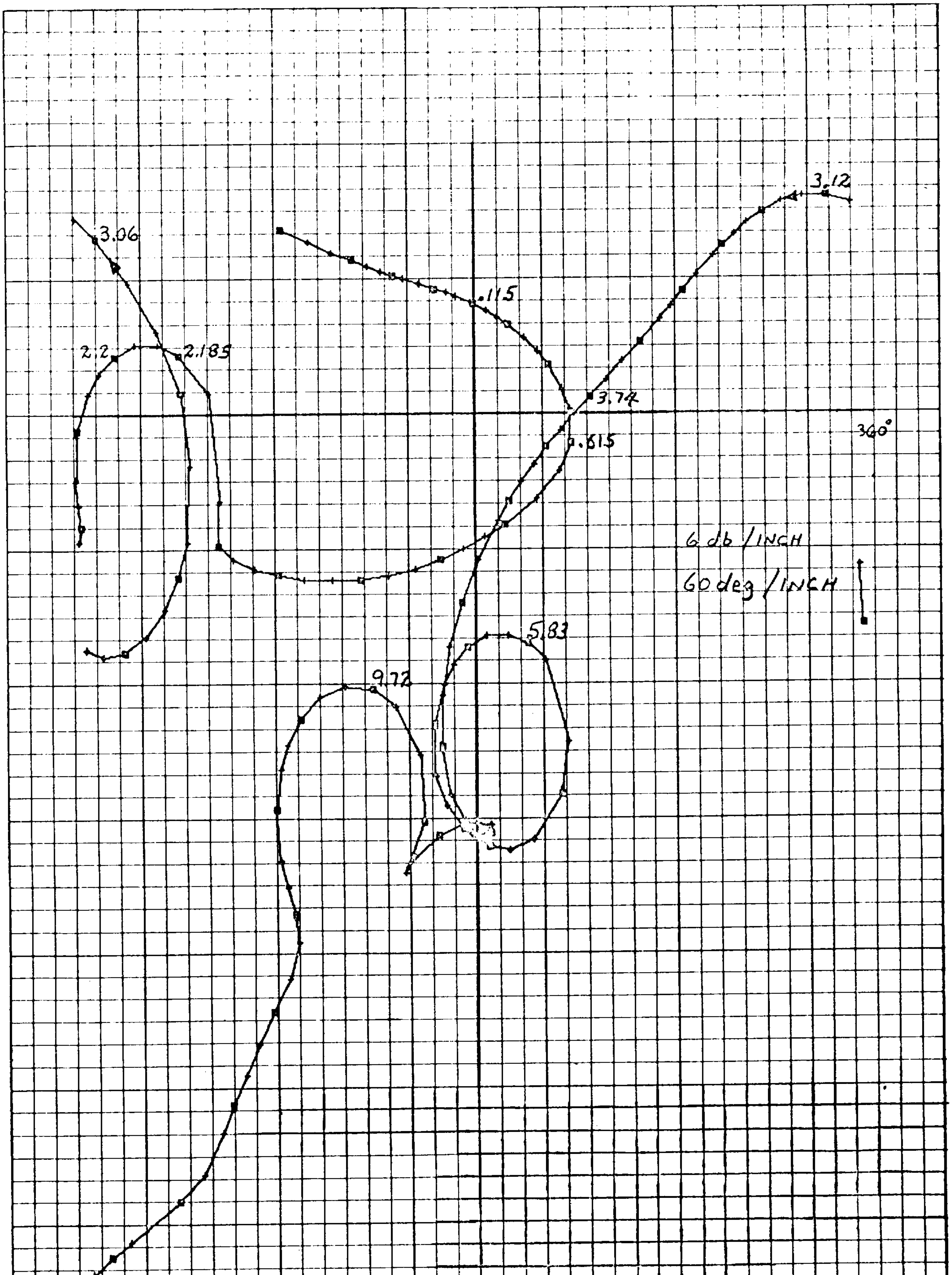

Figure 49. Gain-Phase t = 78 sec

Compensation Configuration #2
With Fuel Slosh, With Baffles

10/30/65 #3

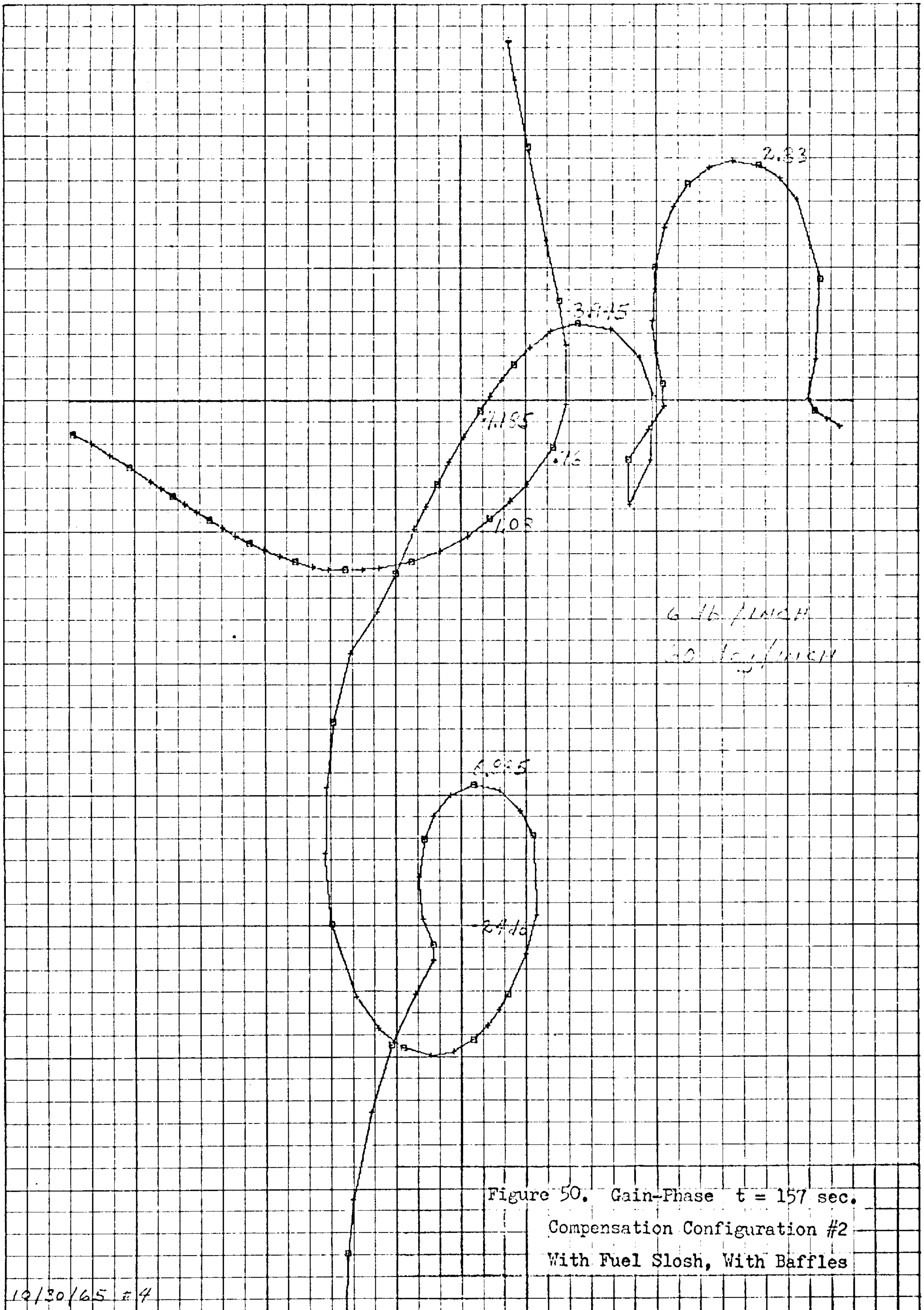

Figure 50. Gain-Phase t = 157 sec.
Compensation Configuration #2
With Fuel Slosh, With Baffles

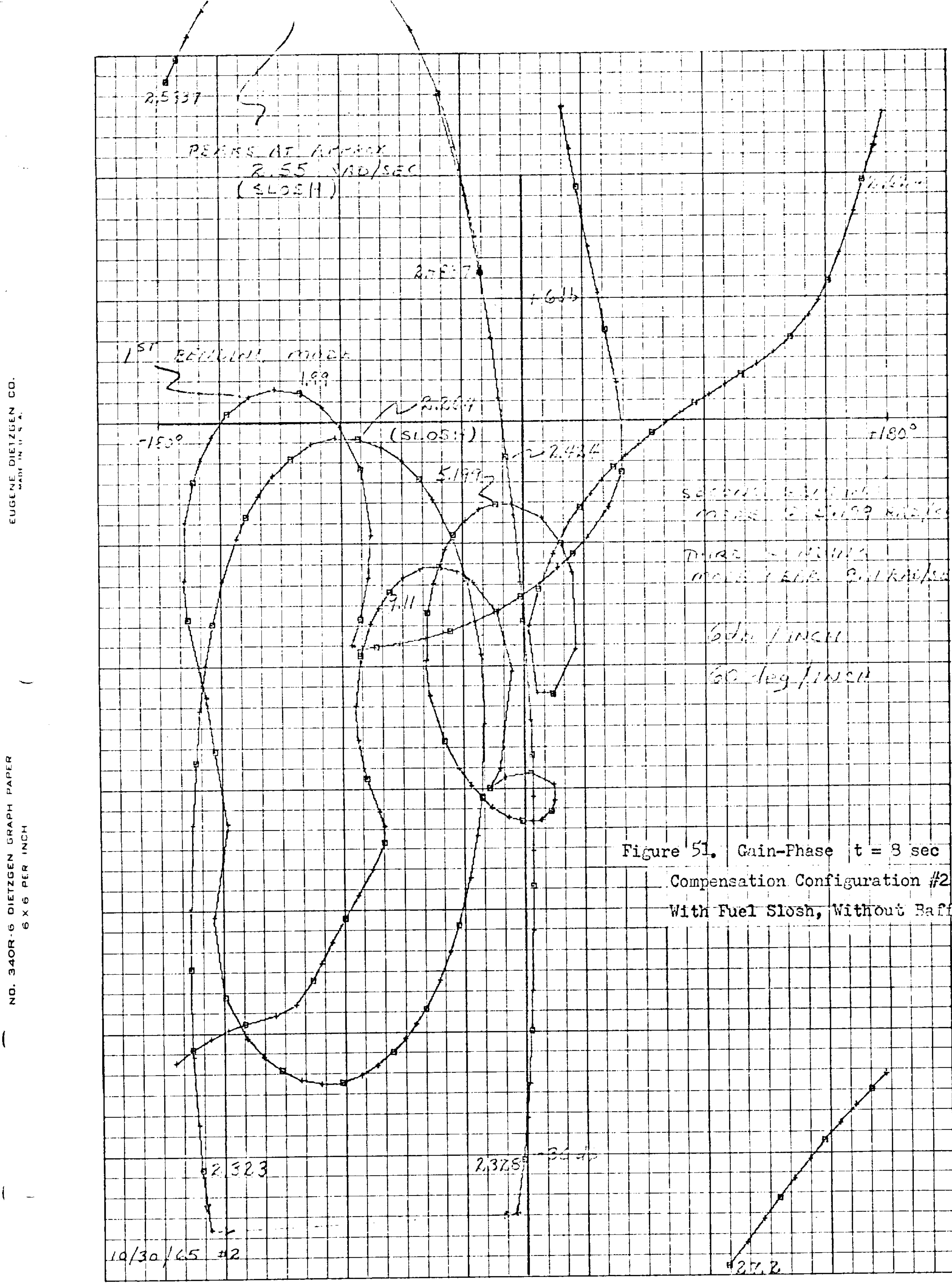

Figure 51. Gain-Phase t = 8 sec
Compensation Configuration #2
With Fuel Slosh, Without Baffles

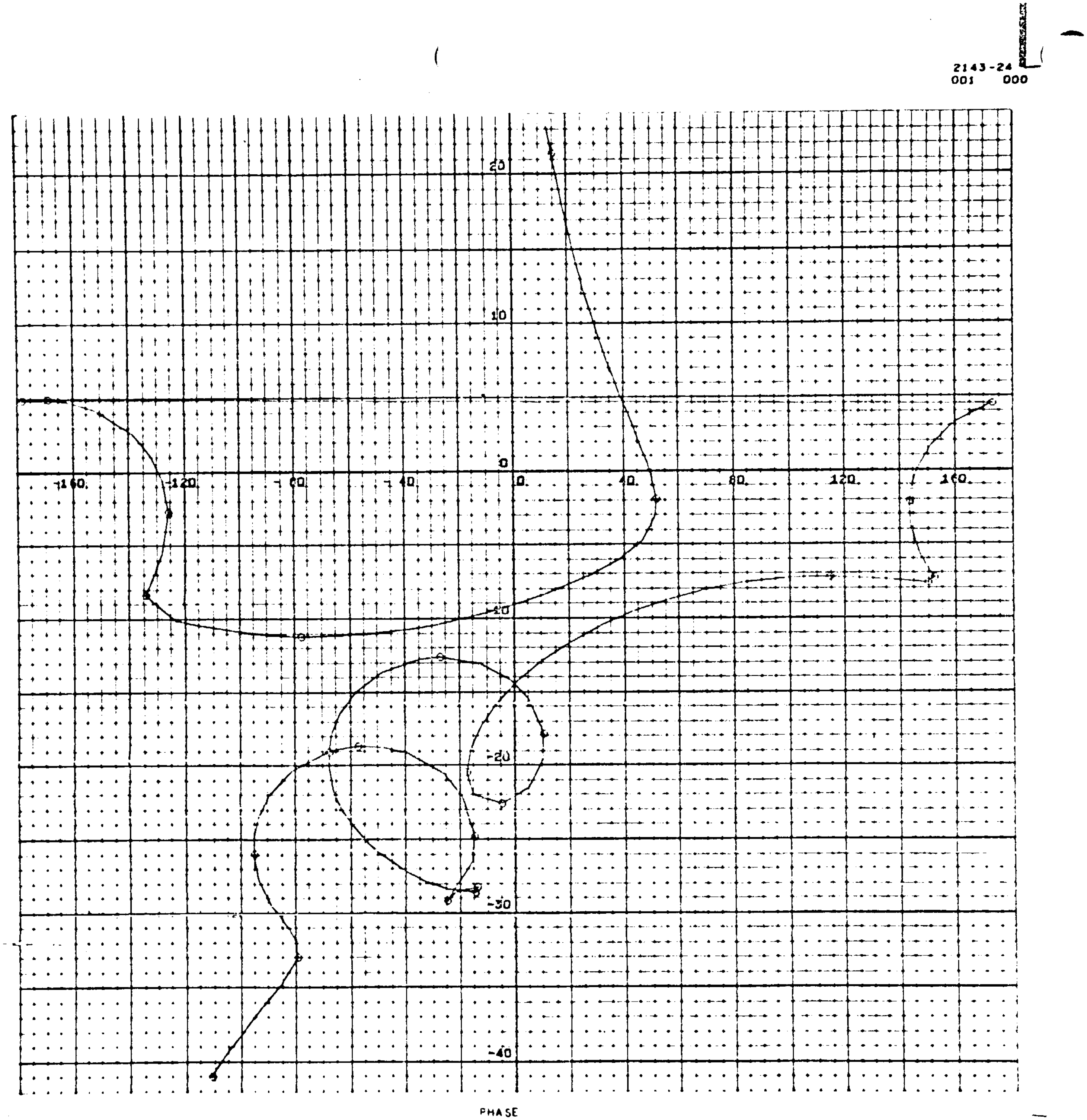

Figure 52. 8 sec. Worst Case Configuration #1

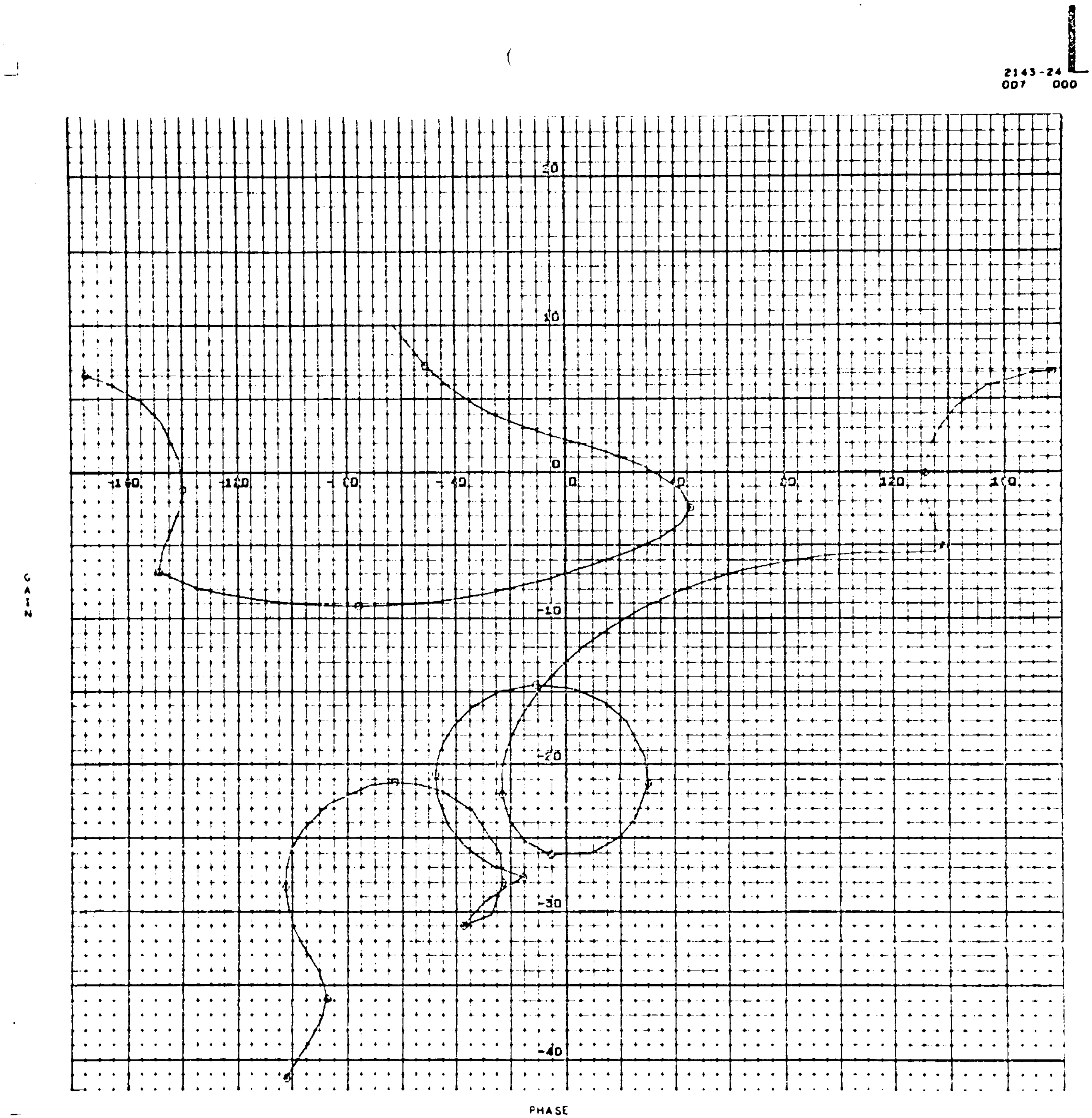

Figure 53. 78 sec. Worst Case Configuration #1

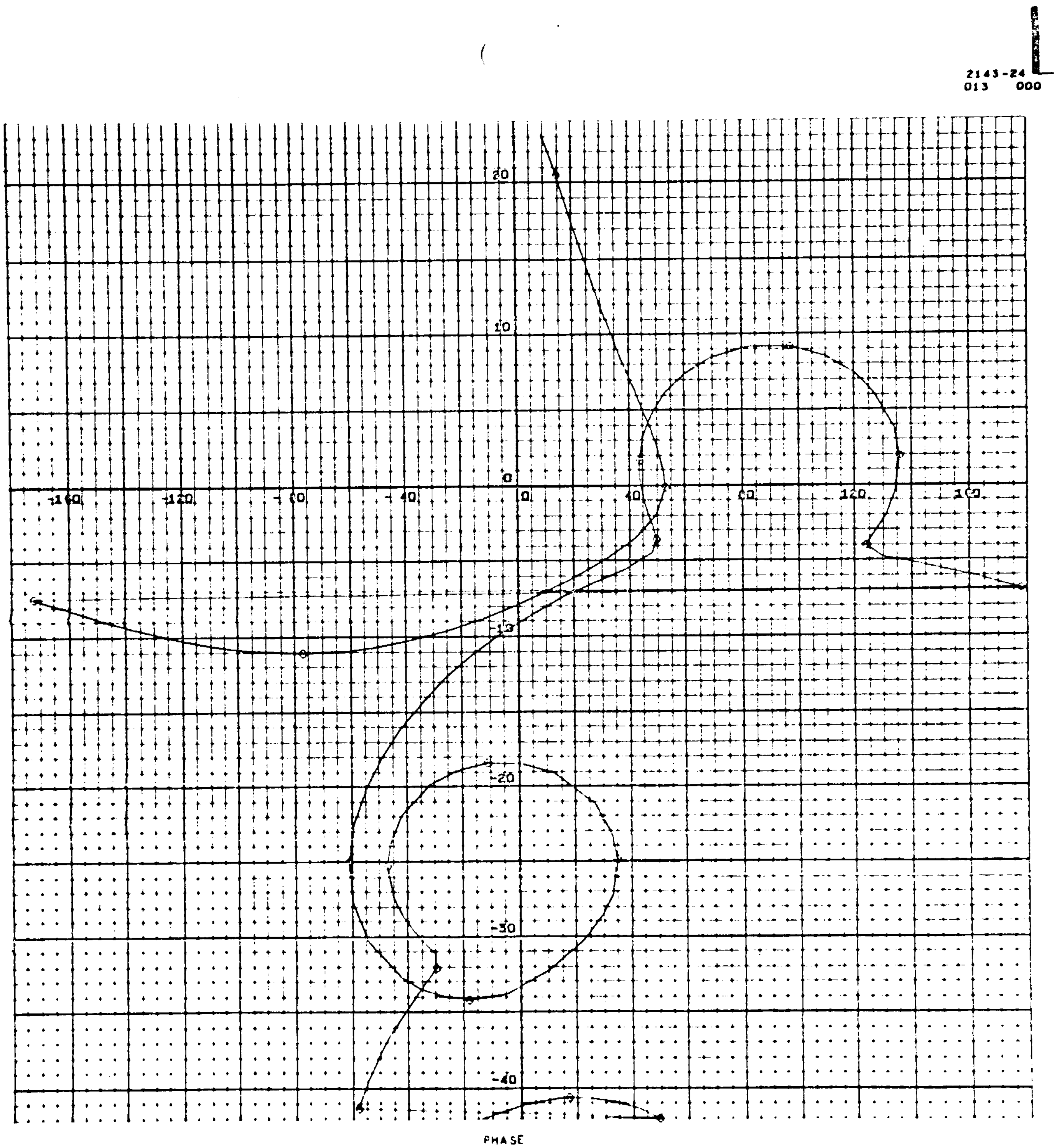

Figure 54. 157 sec. Worst Case Configuration #1

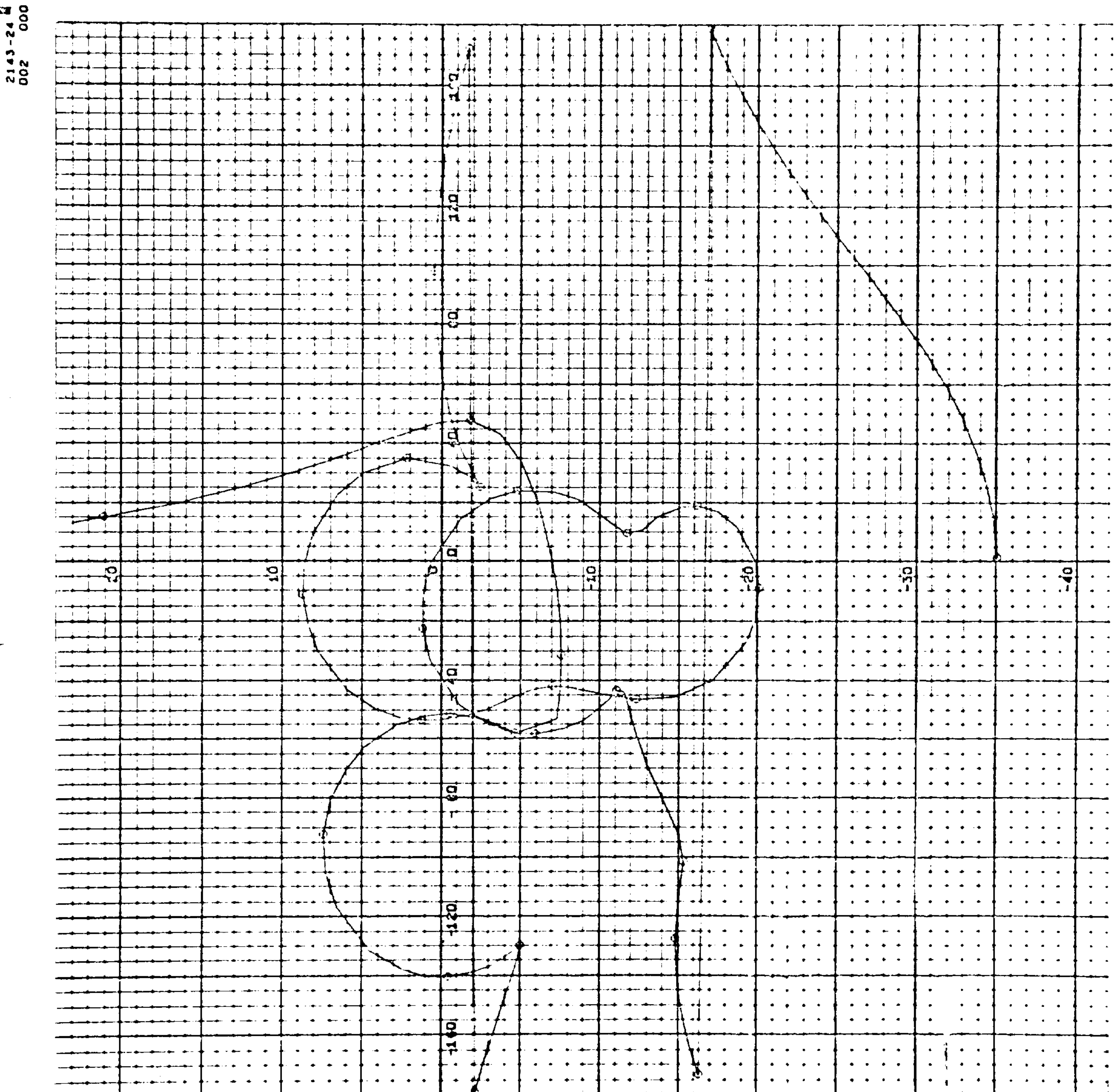

Figure 55. 8 sec. Worst Case Configuration #2

2143-24 008 000

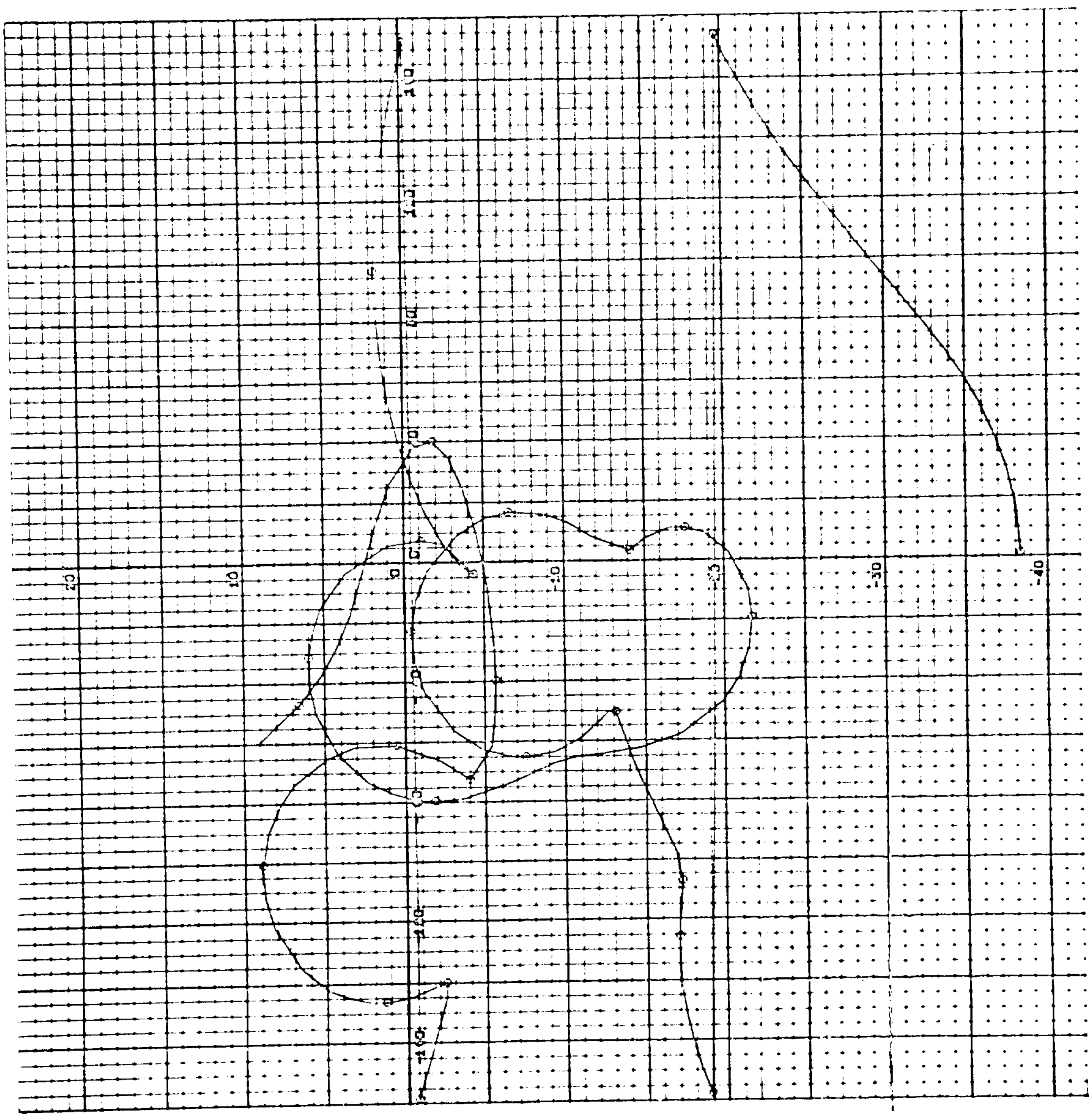

Figure 56. 78 sec. Worst Case Configuration #2

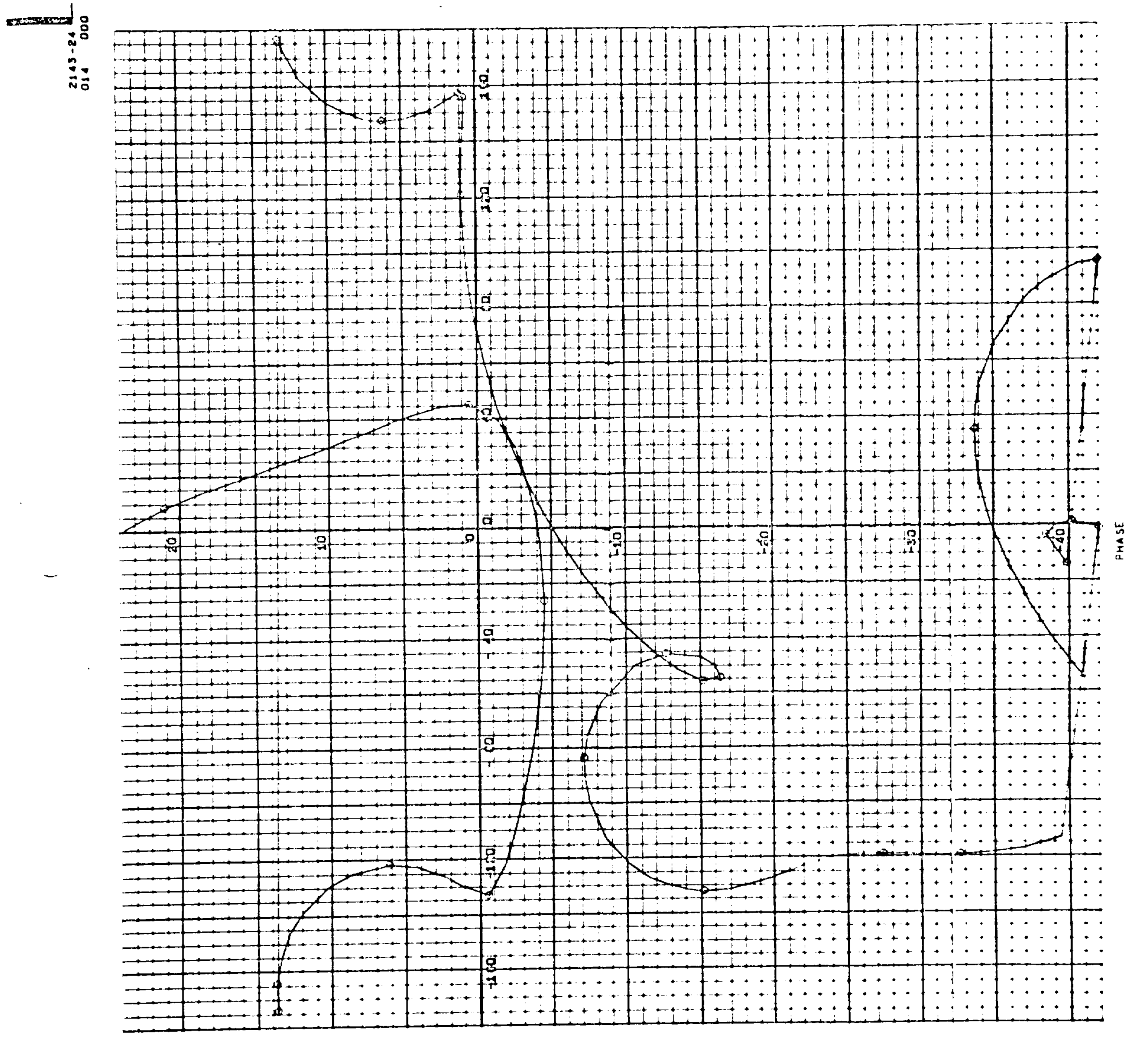

Figure 57. 157 sec. Worst Case Configuration #2

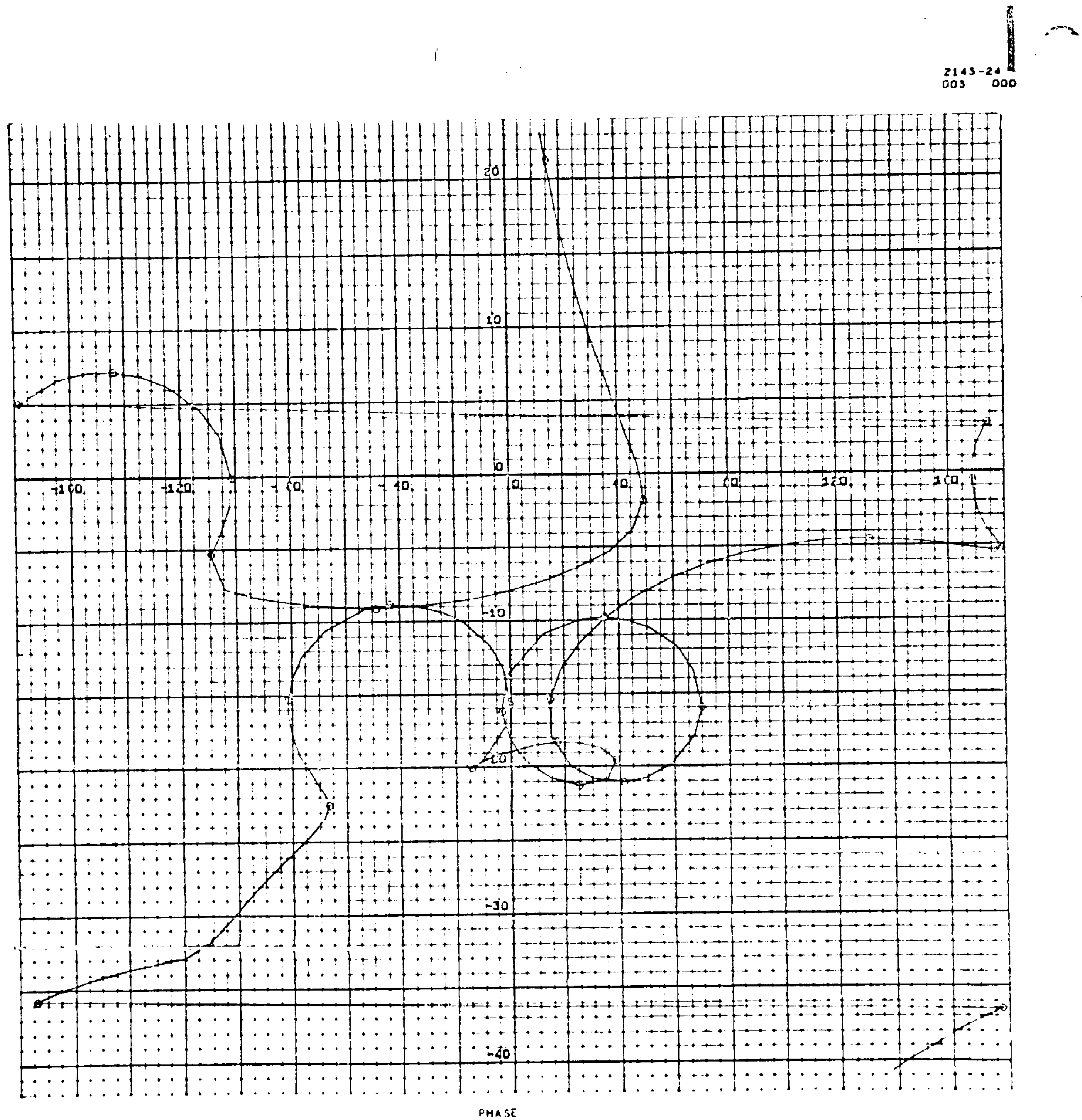

Figure 58. 8 sec. Worst Case Configuration #3

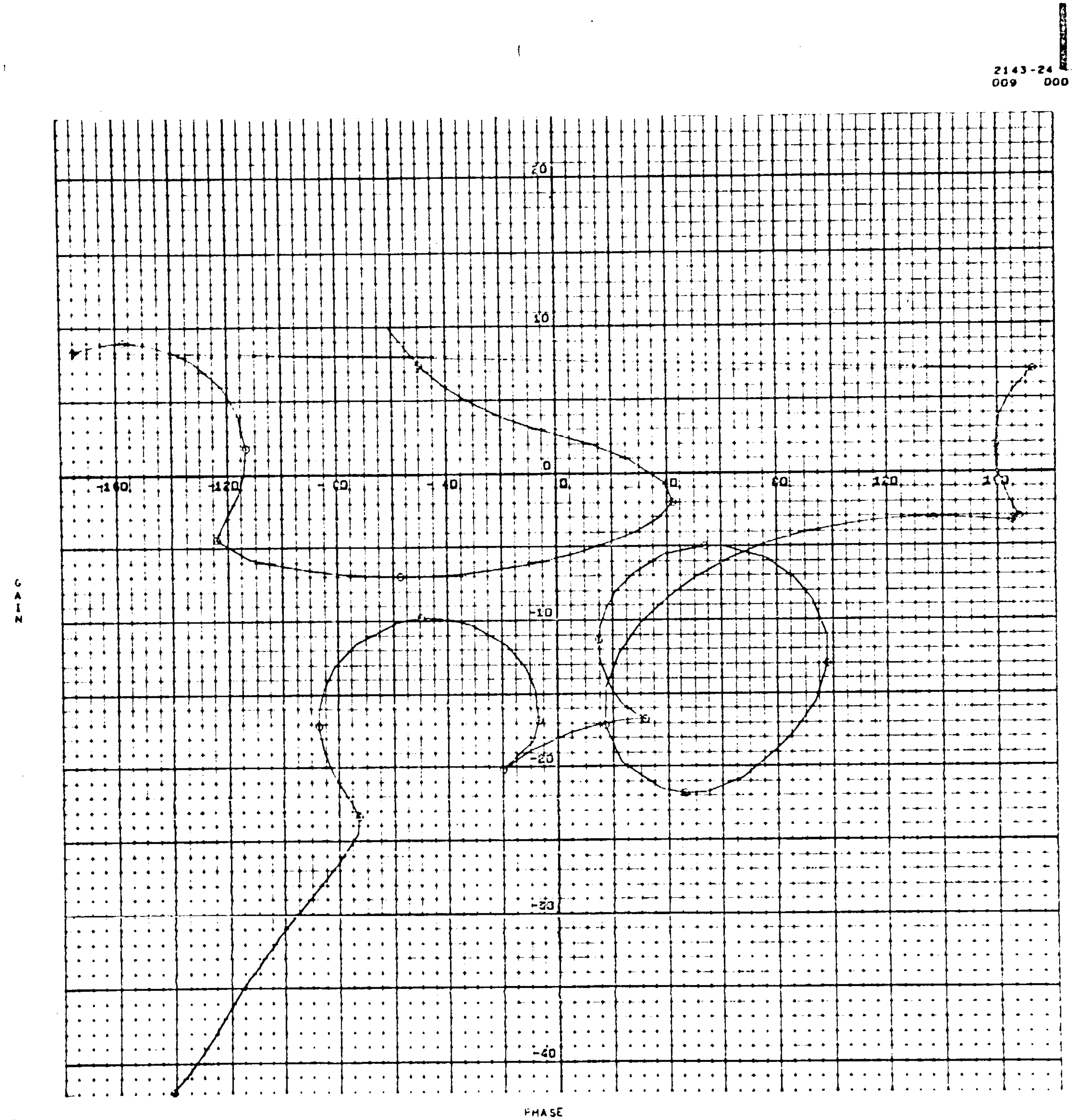

Figure 59. 78 sec. Worst Case Configuration #3

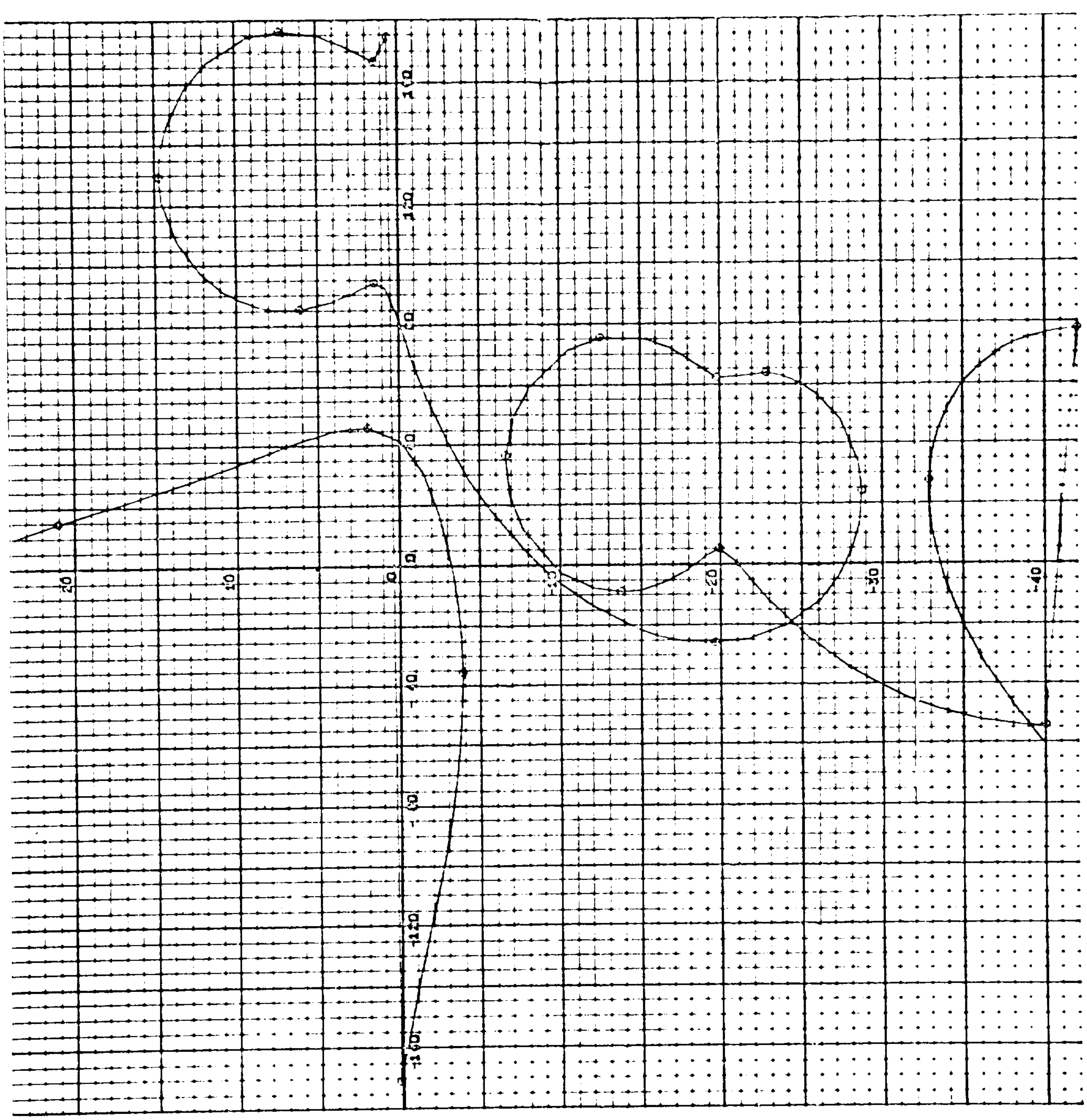

Figure 6Q. 157 sec. Worst Case Configuration #3

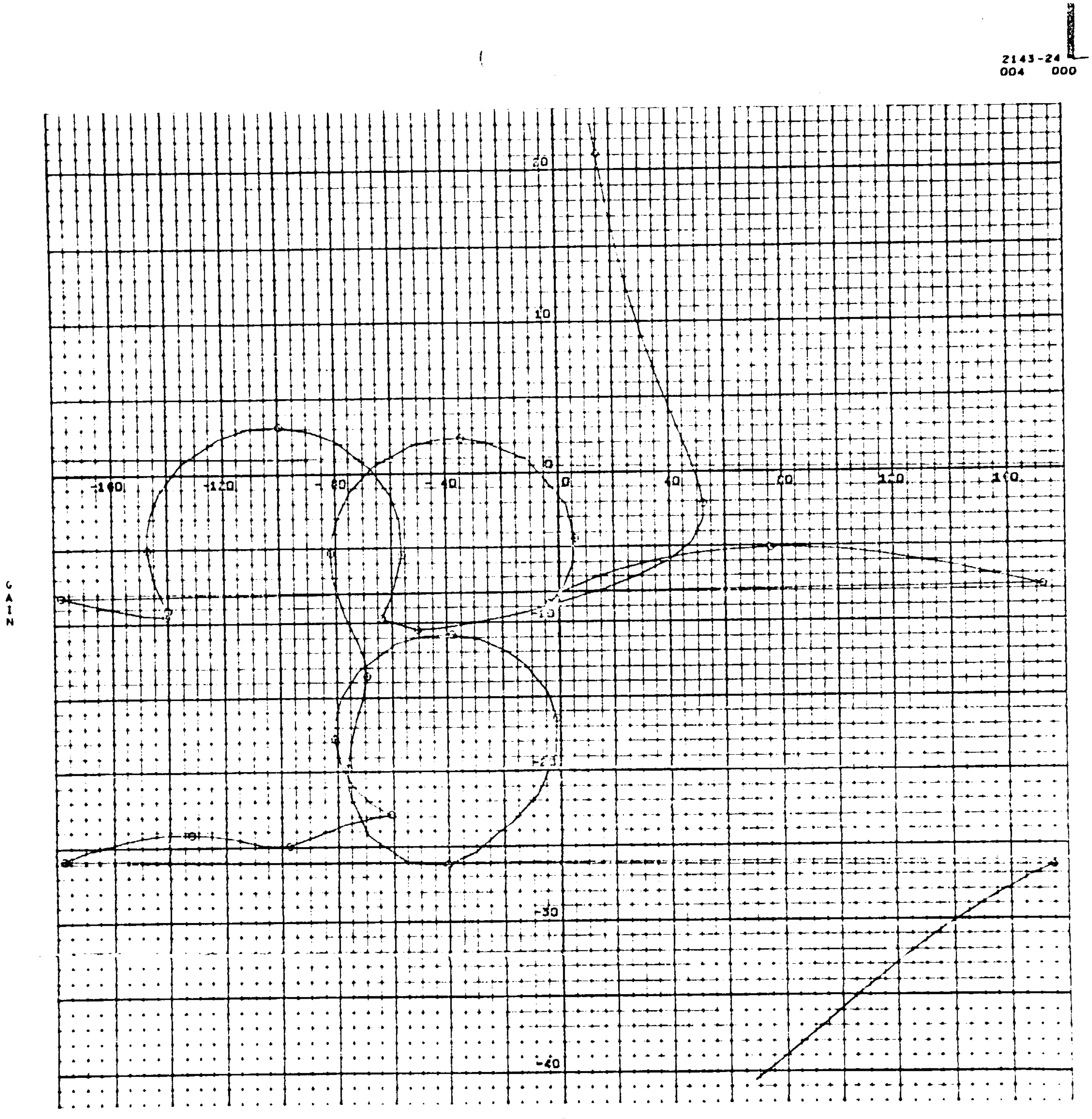

Figure 61. 8 sec. Worst Case Configuration #4

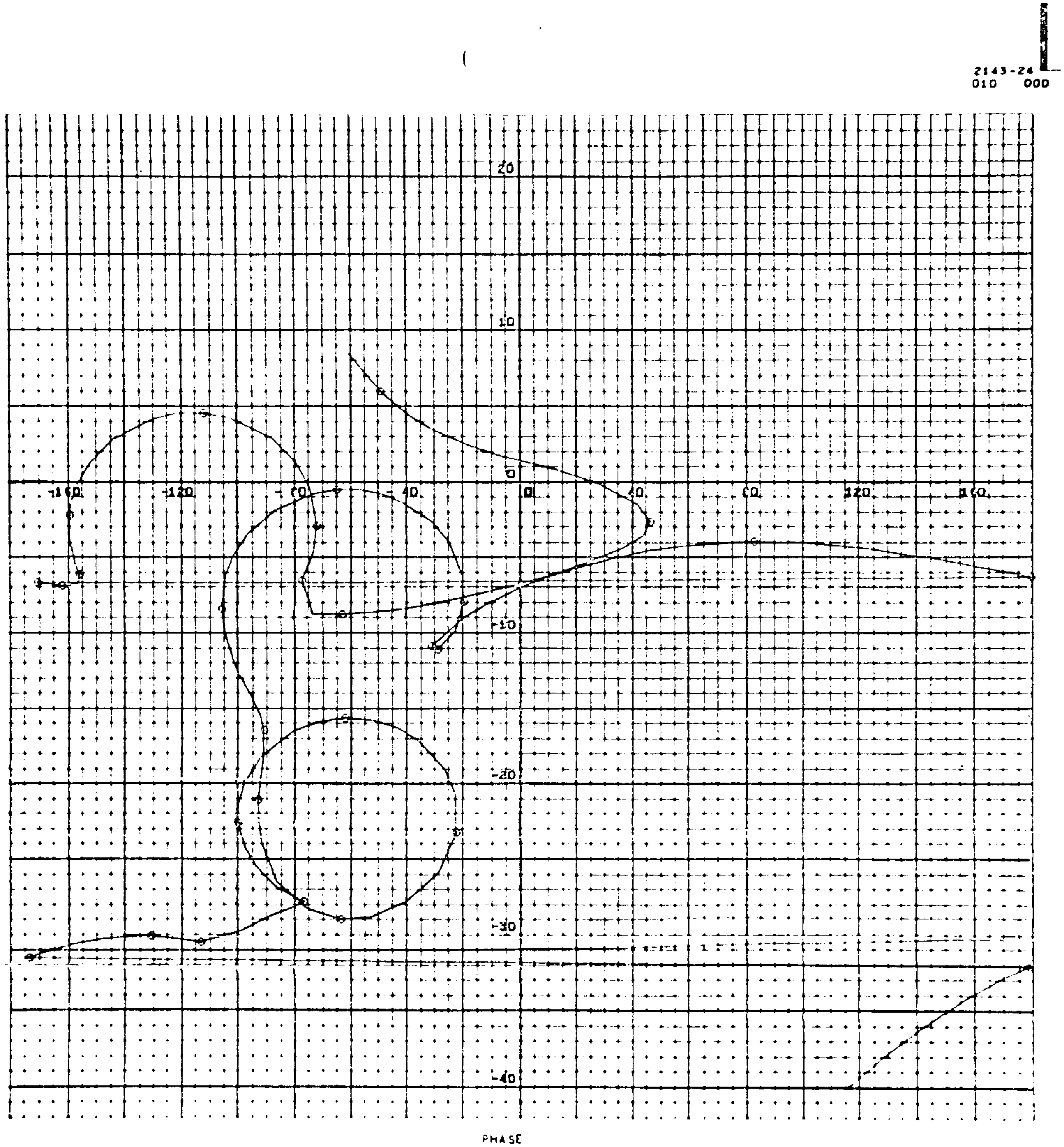

Figure 62. 78 sec. Worst Case Configuration #4

2143-24
016 000

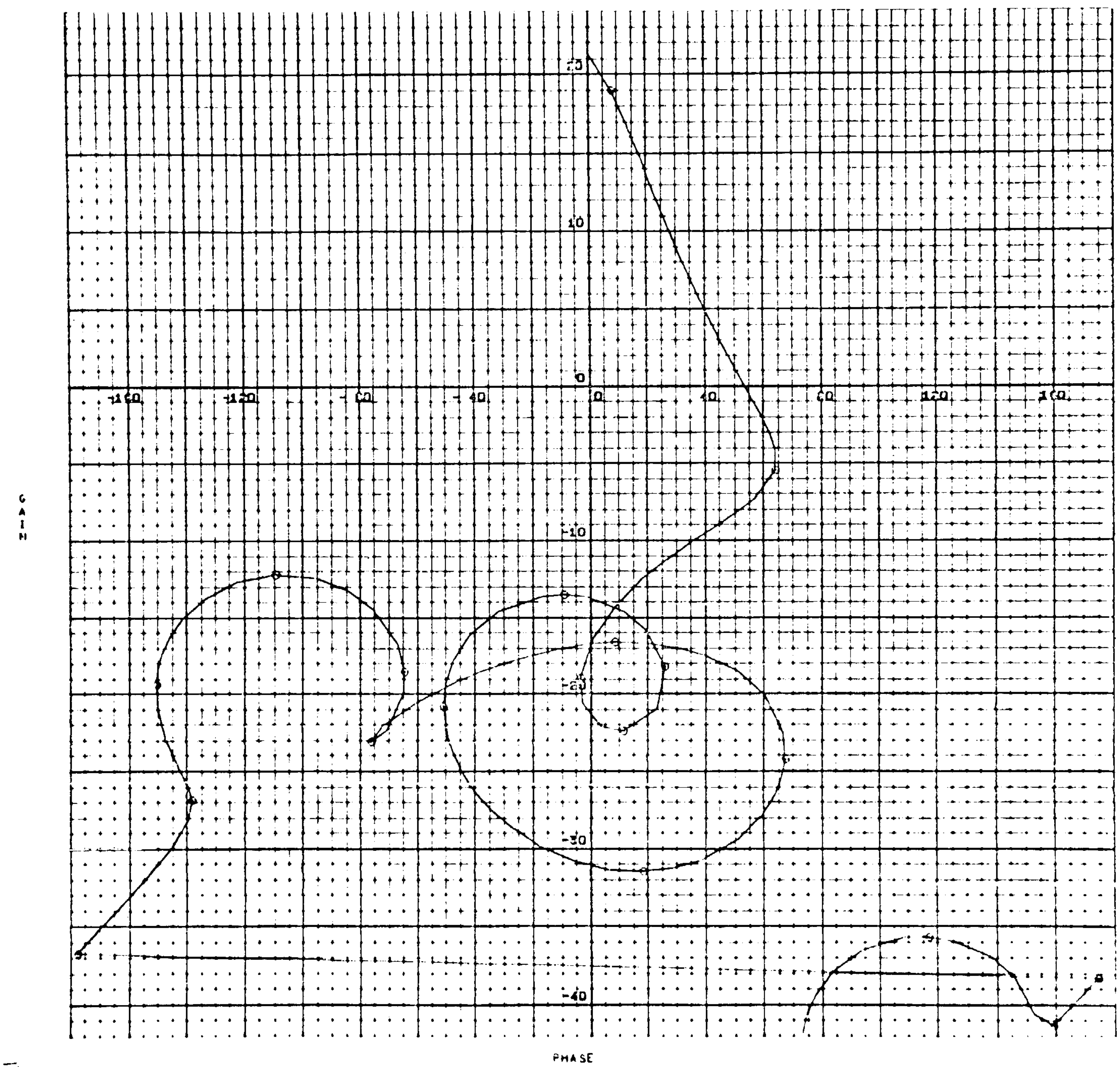

Figure 63. 157 sec. Worst Case Configuration #4

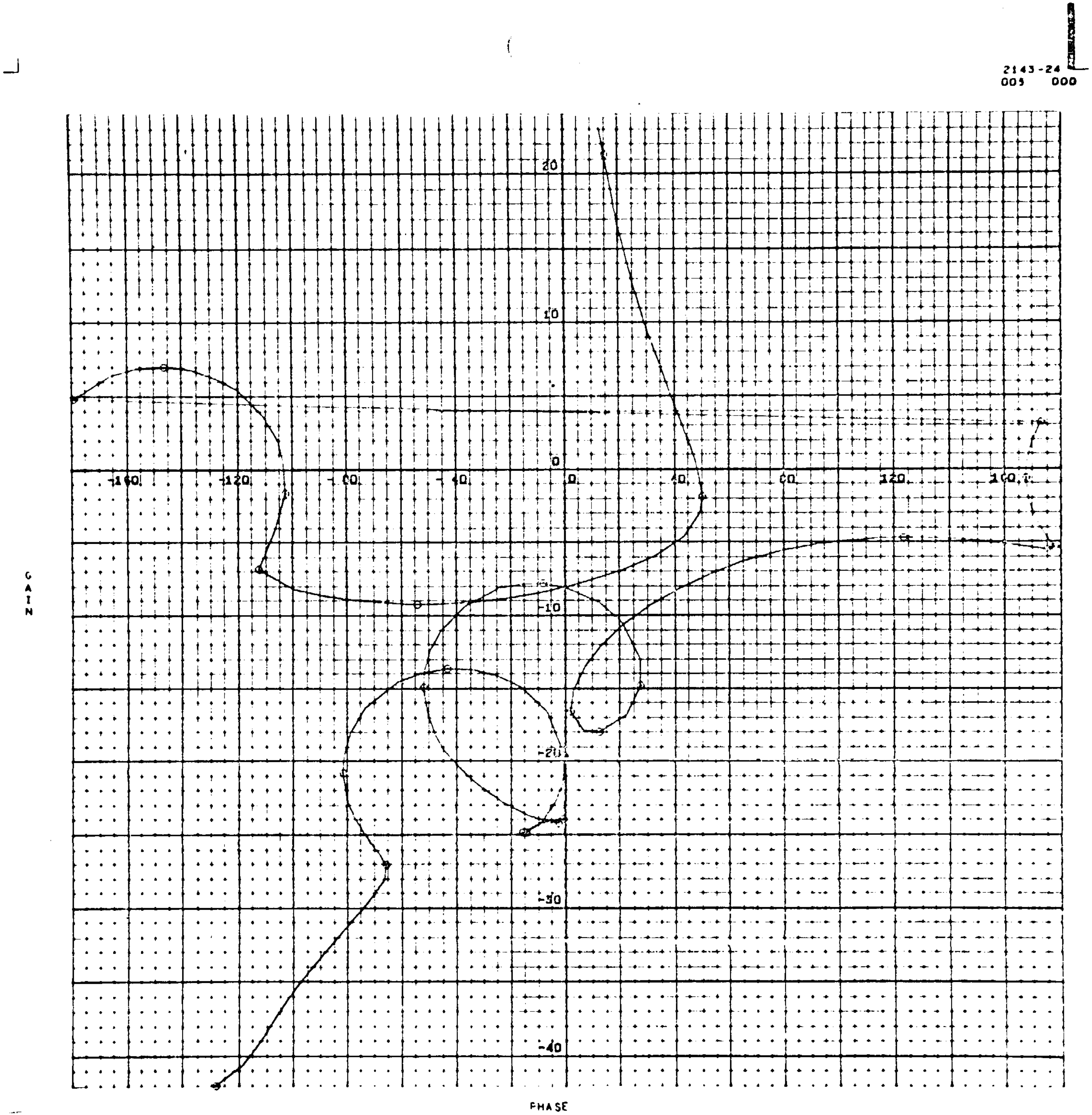

Figure 64. 8 sec. Worst Case Configuration #5

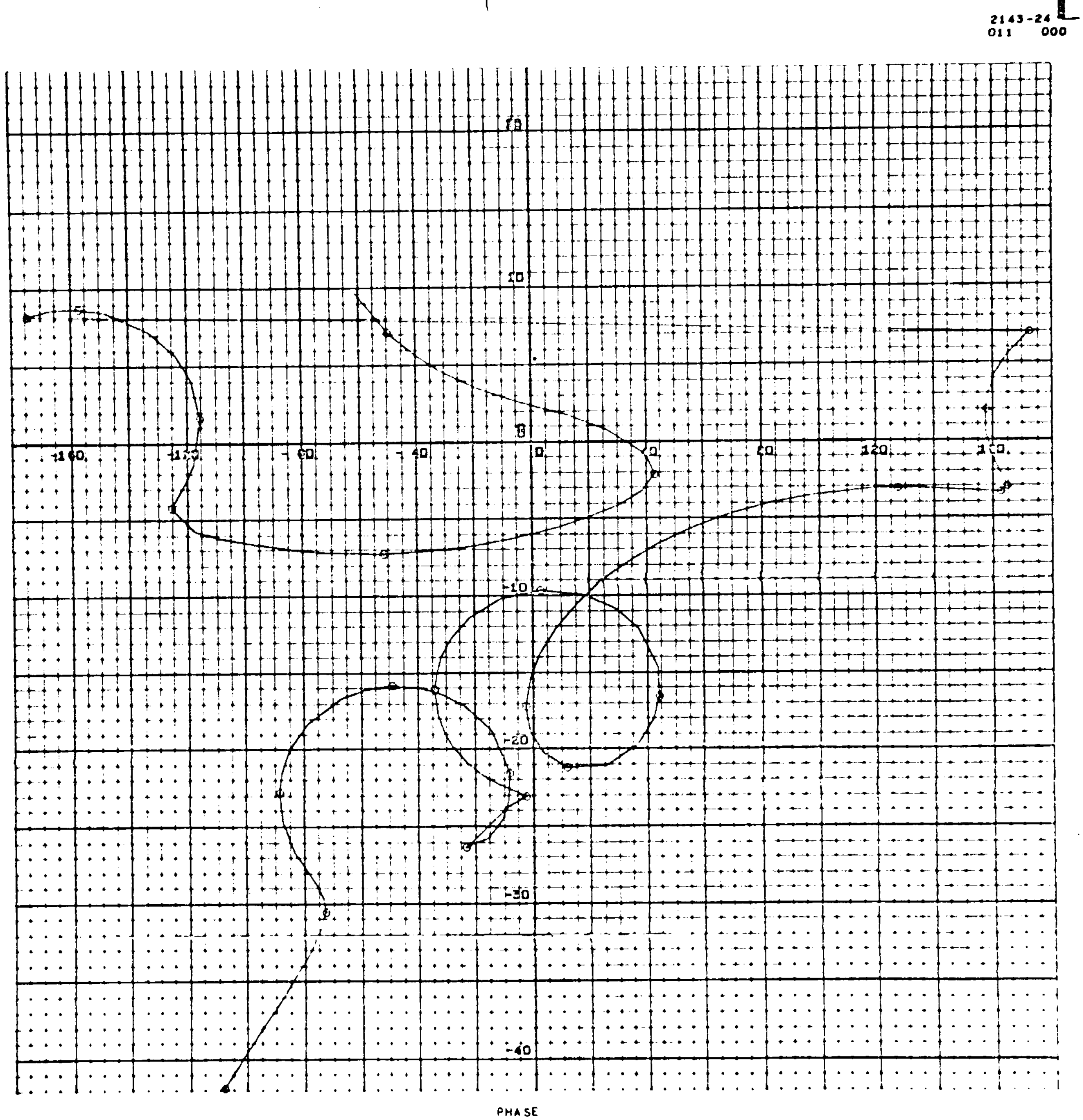

Figure 65. 78 sec. Worst Case Configuration #5

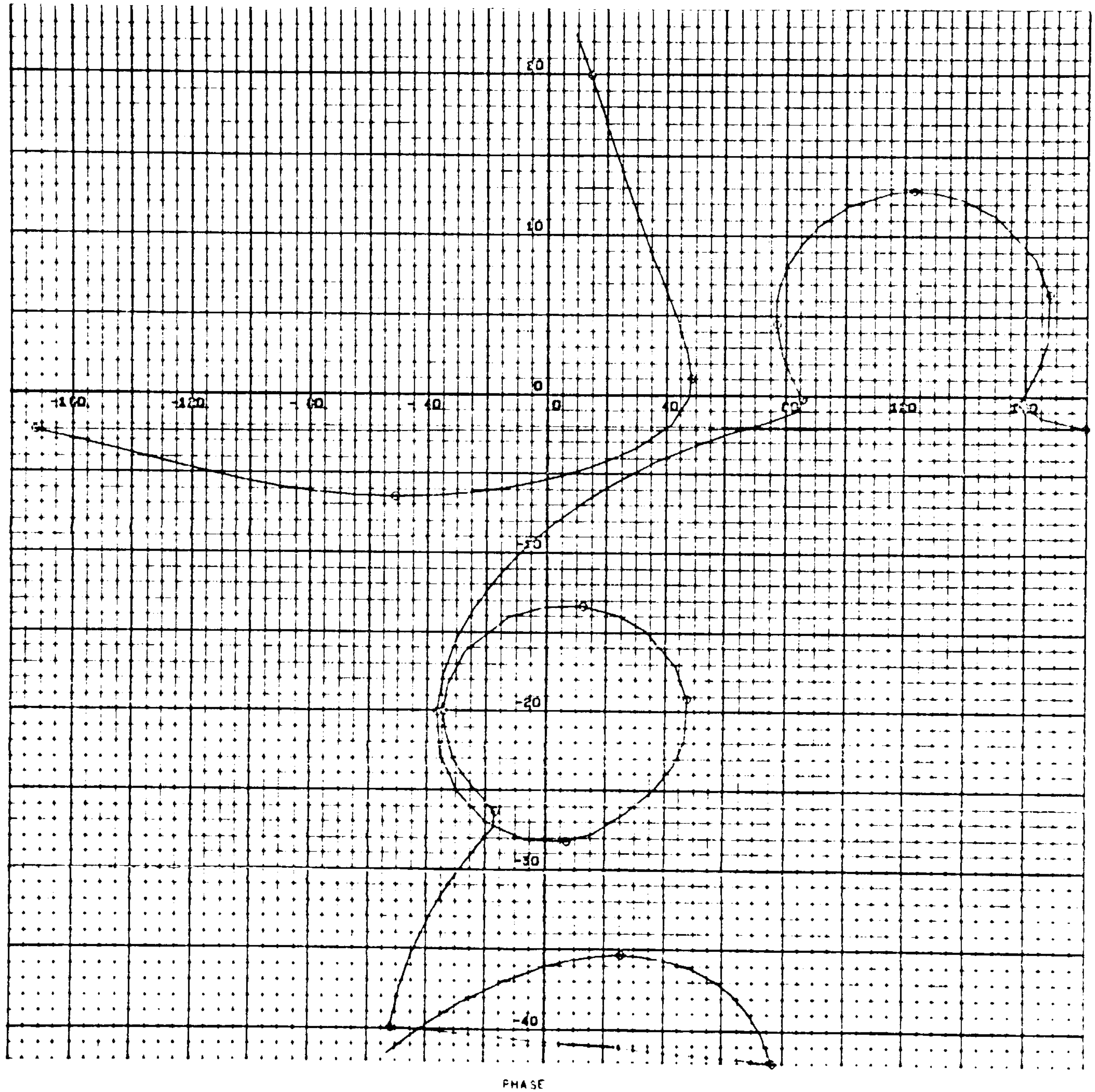

Figure 66. 157 sec. Worst Case Configuration #5

2143-24
006 000

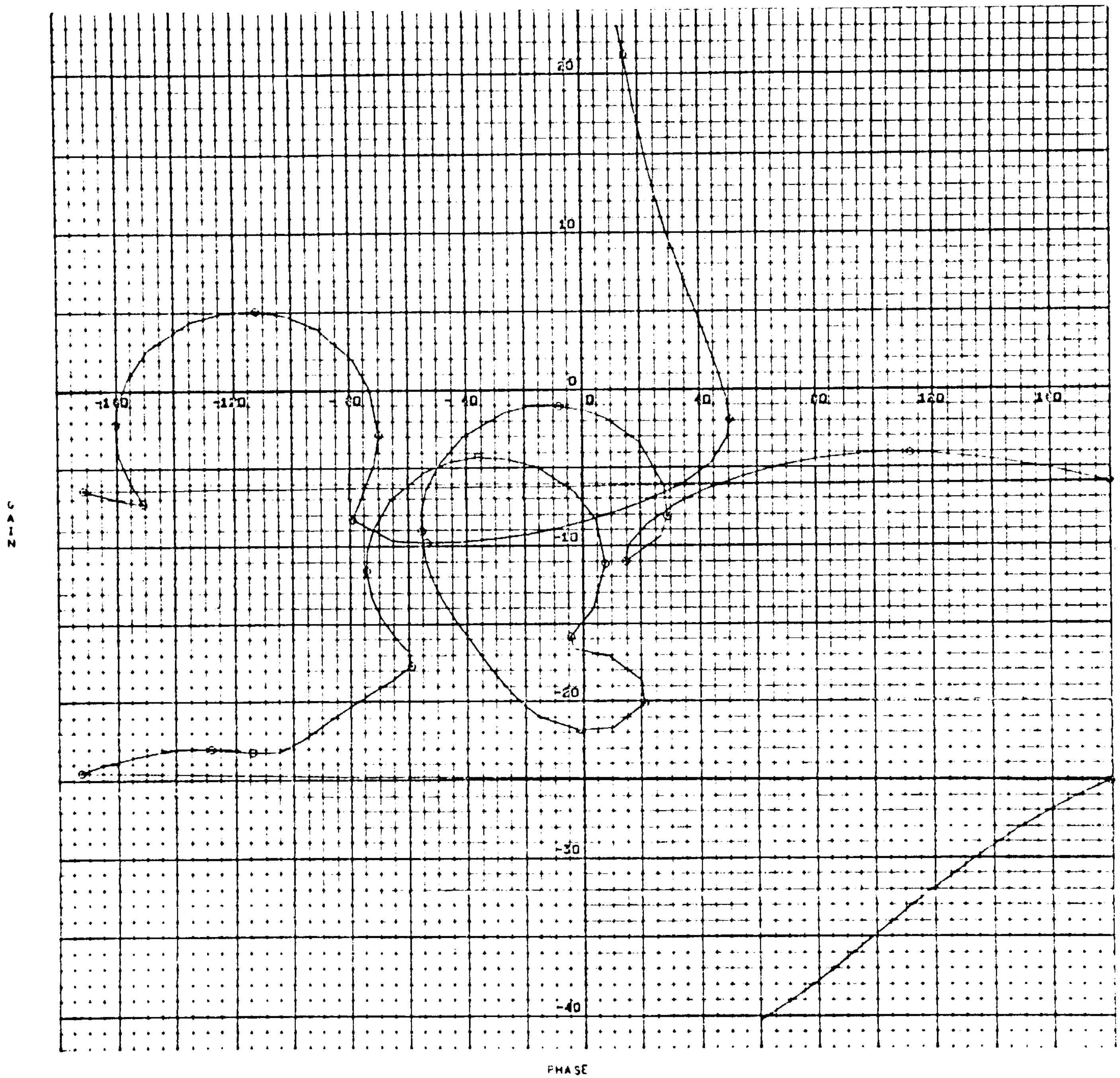

Figure 67. 8 sec. Worst Case Configuration #6

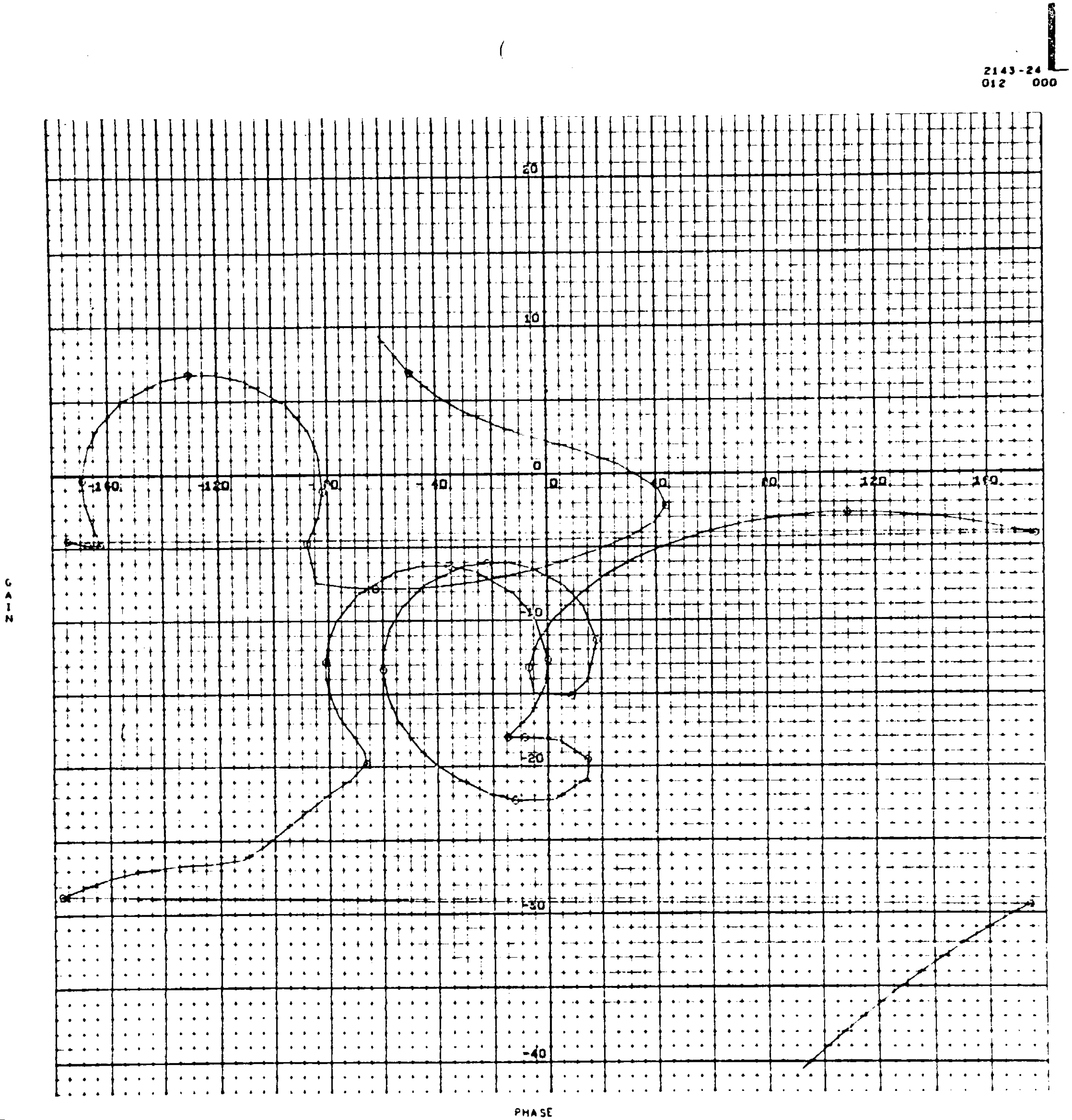

Figure 68. 78 sec. Worst Case Configuration #6

2143-24
018 000

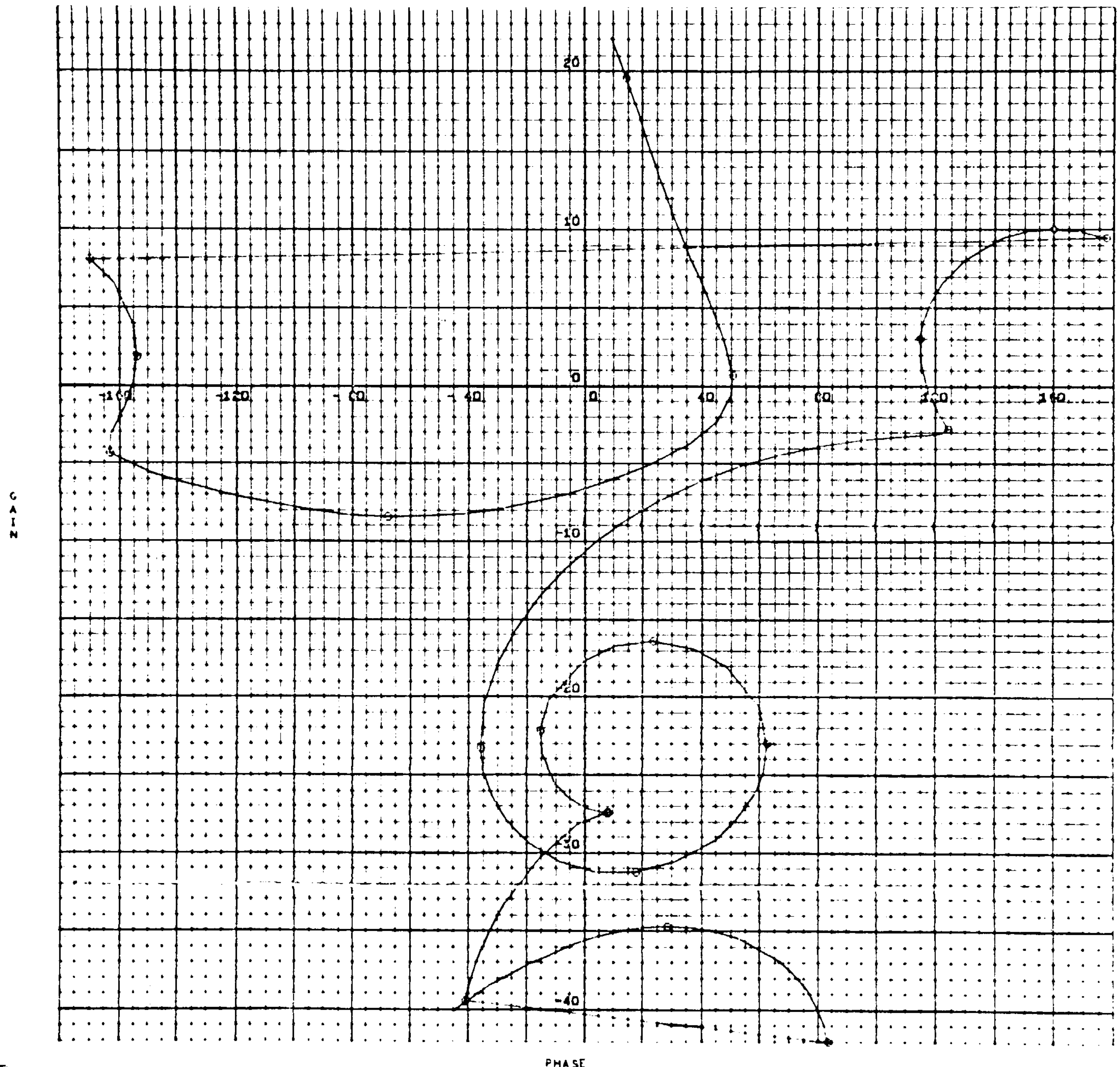

Figure 69. 157 sec. Worst Case Configuration #6

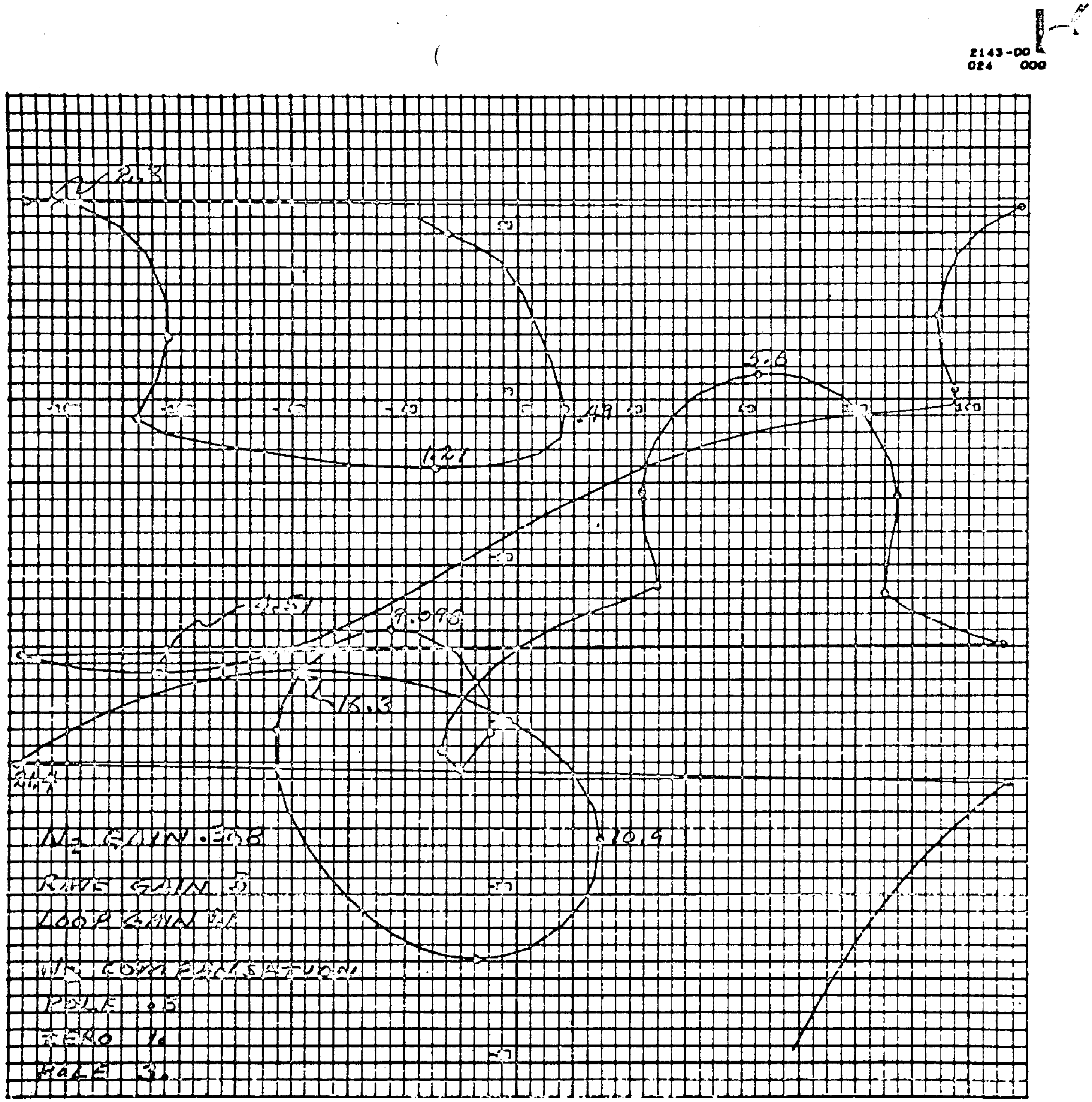

Figure 70. Gain-Phase t = 78 sec, Compensation Configuration #2, N_z Loop Closed

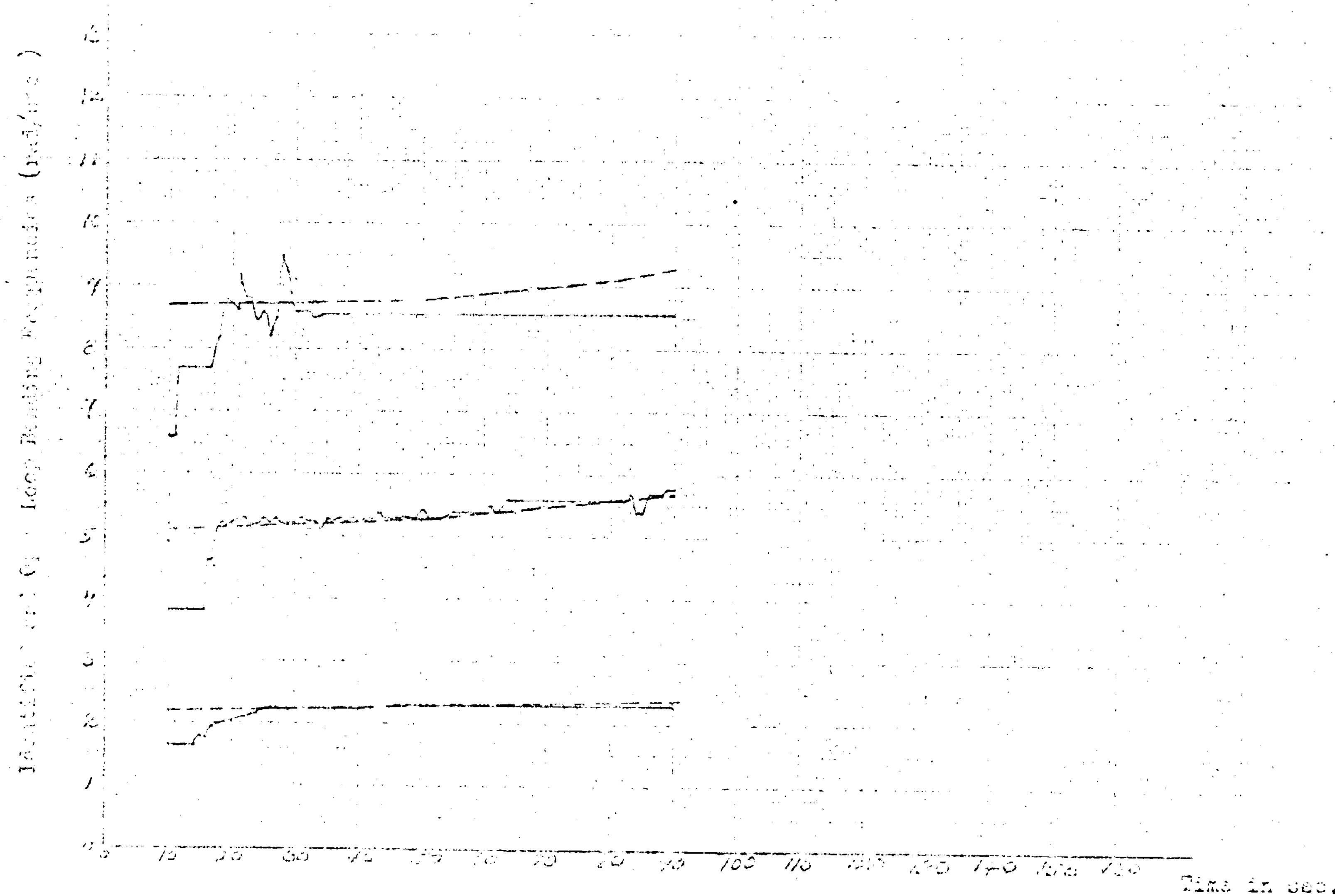
Time in sec.

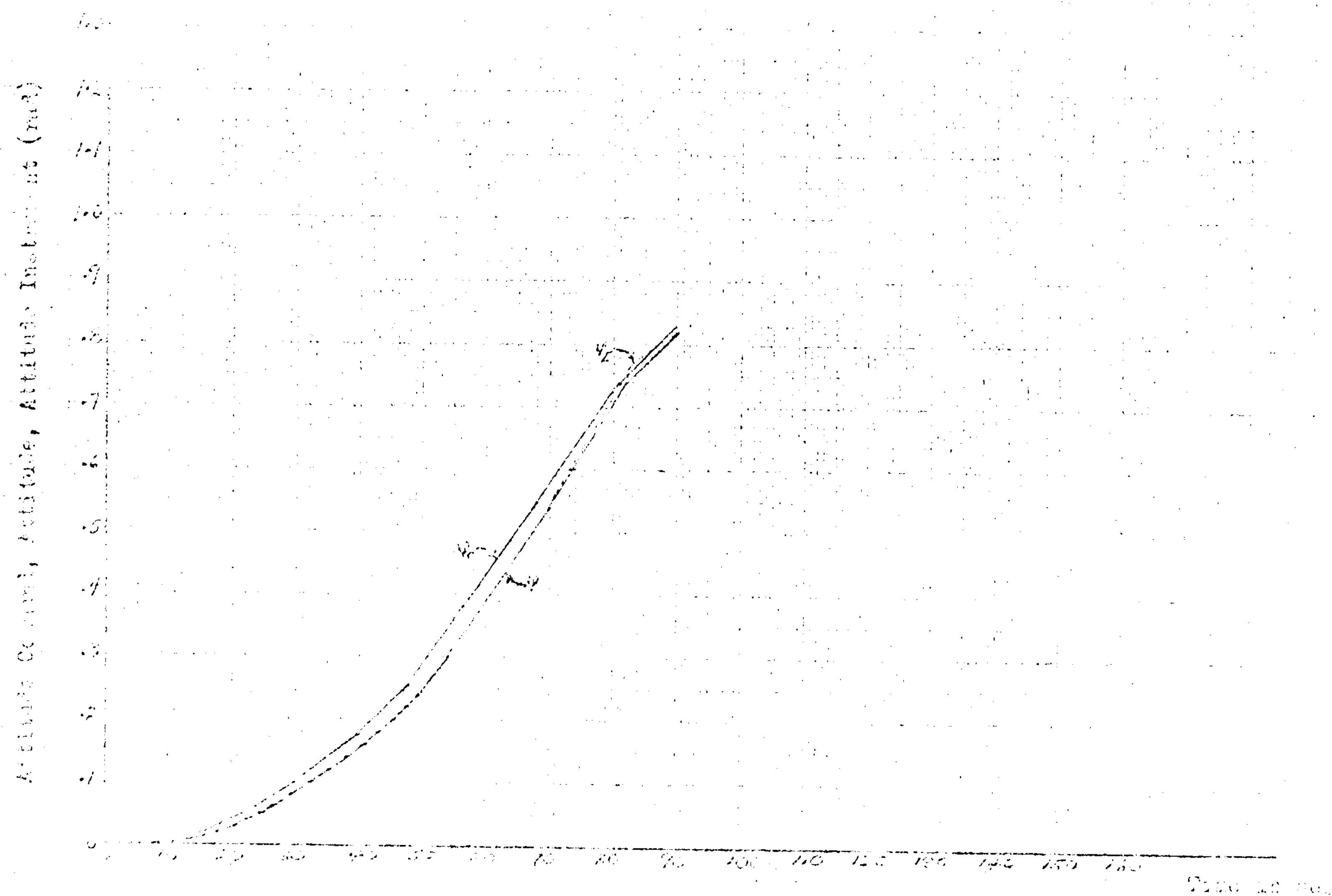
Attitude Control, Attitude, Attitude Instrument
Time in sec.

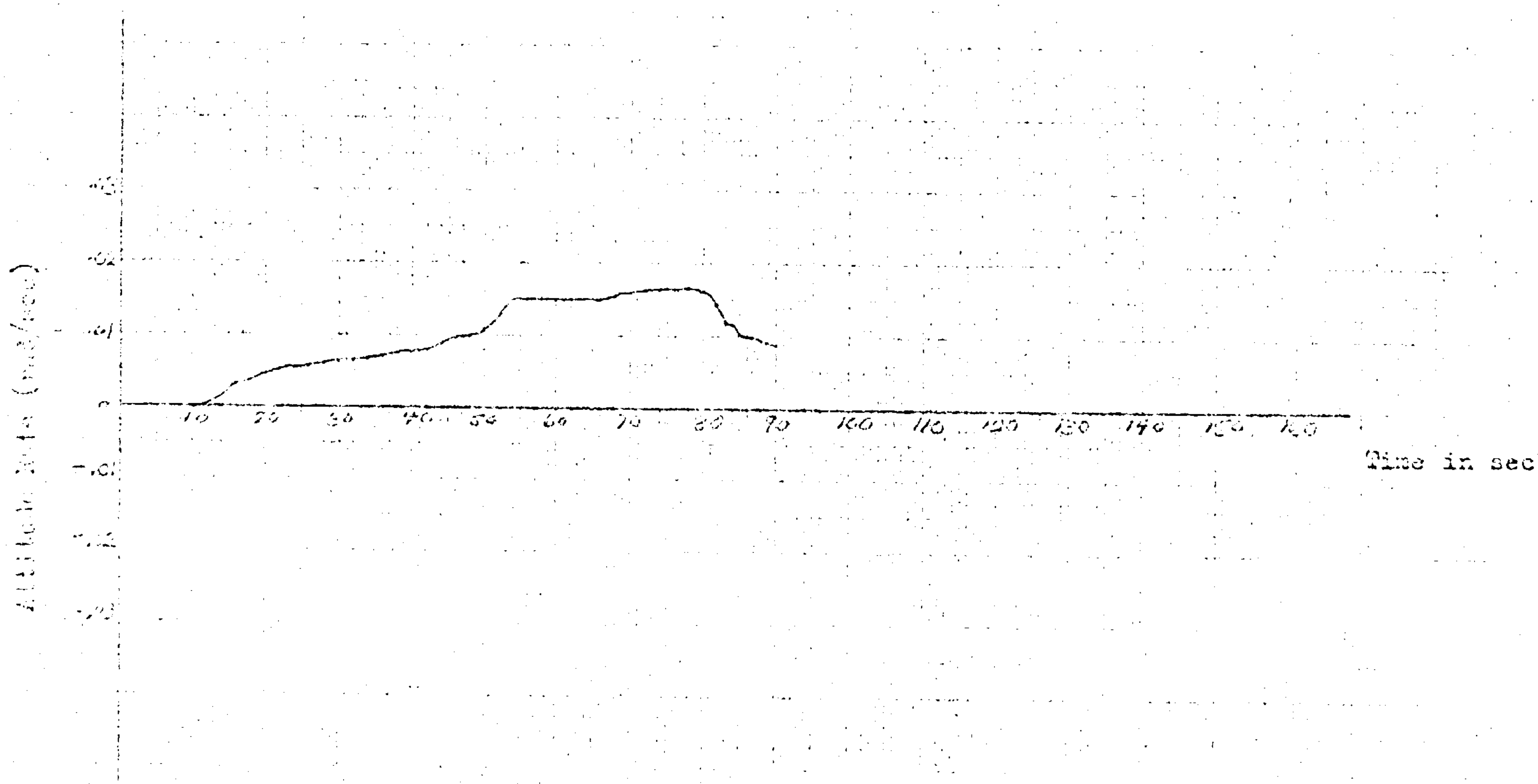
Time in sec.
0
10
20
30
40
50
60
70
80
90
100
110
120
130
140
150
160
.01
.02
.03
-.01
-.02
-.03

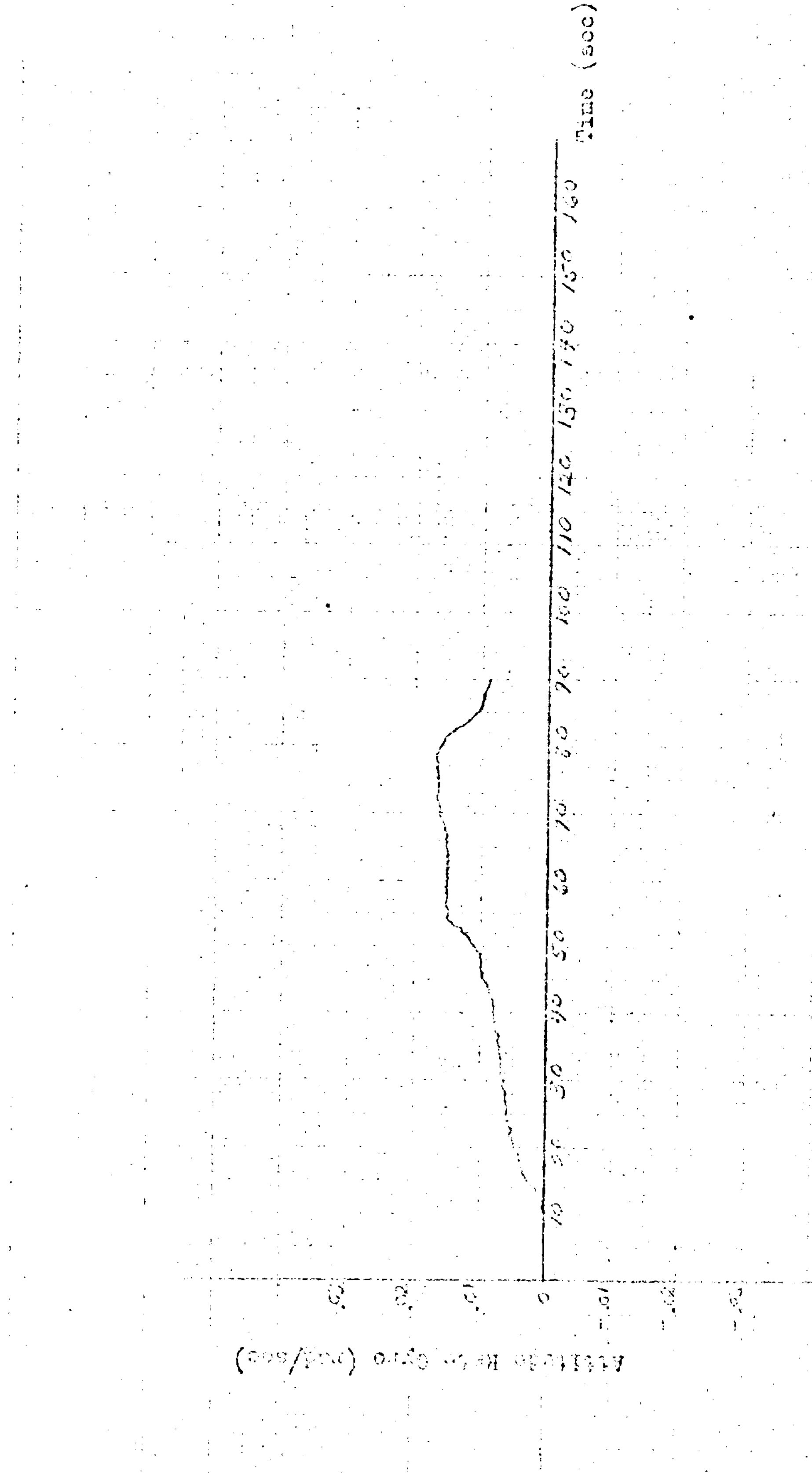
Time (sec)
10
20
30
40
50
60
70
80
90
100
110
120
130
140
150
160
.03
.02
.01
0
-.01
-.02
-.03

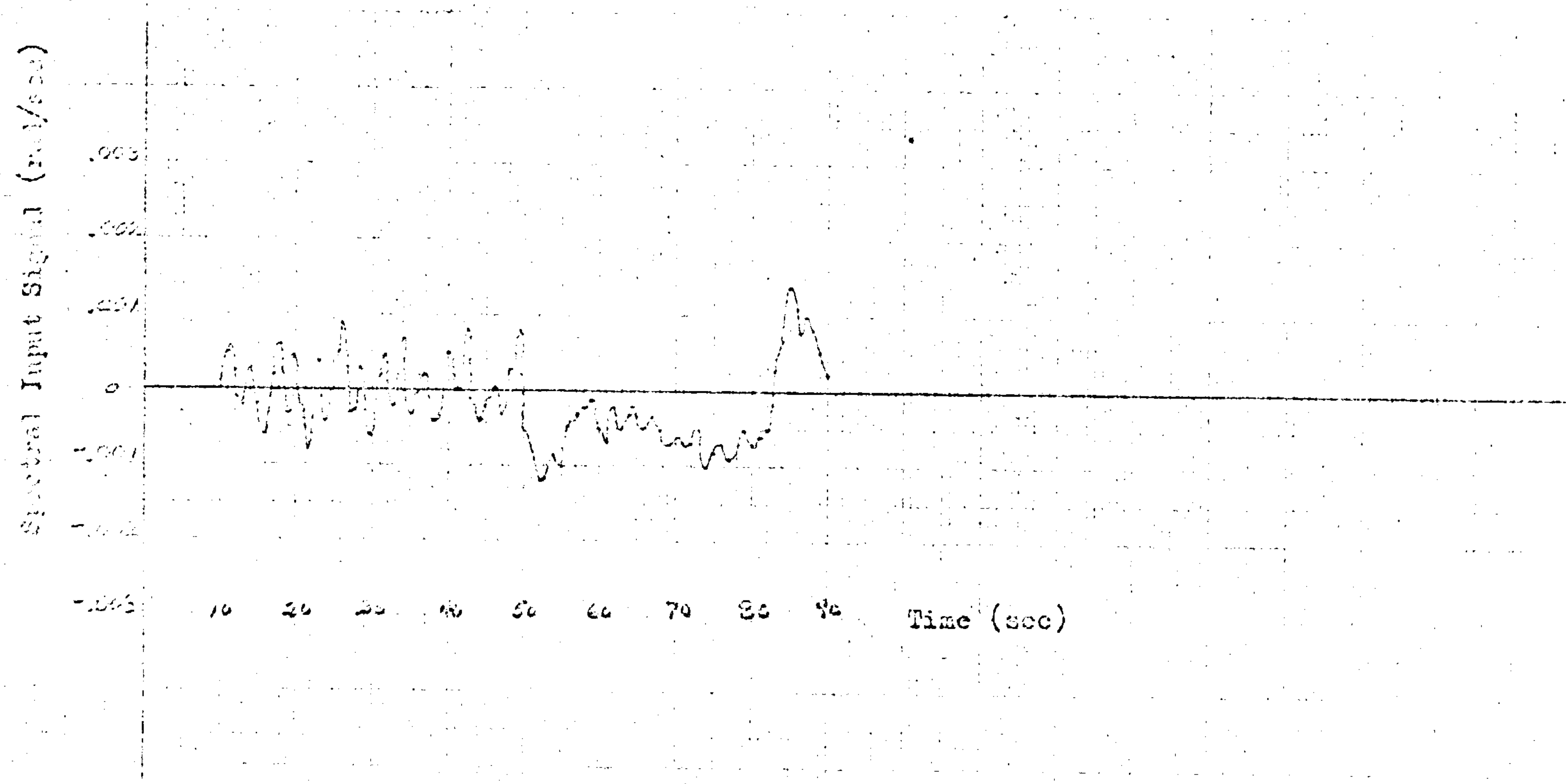
Spectral Input Signal (rad/sec)
.003
.002
.001
0
-.001
-.002
-.003
10
20
30
40
50
60
70
80
90
Time (sec)

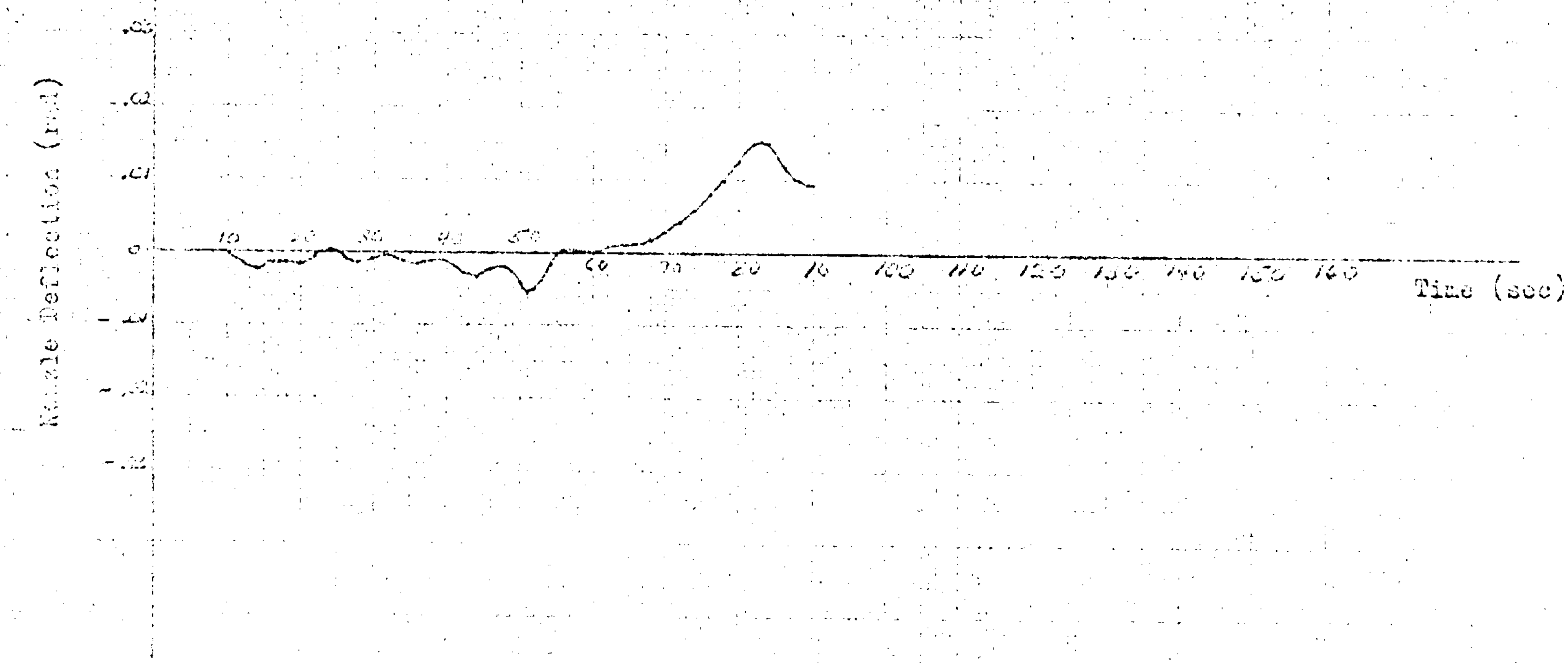
Nozzle Deflection (rad)
Time (sec)
.03
.02
.01
0
-.01
-.02
-.03
10
20
30
40
50
60
70
80
90
100
110
120
130
140
150
160

[illegible]

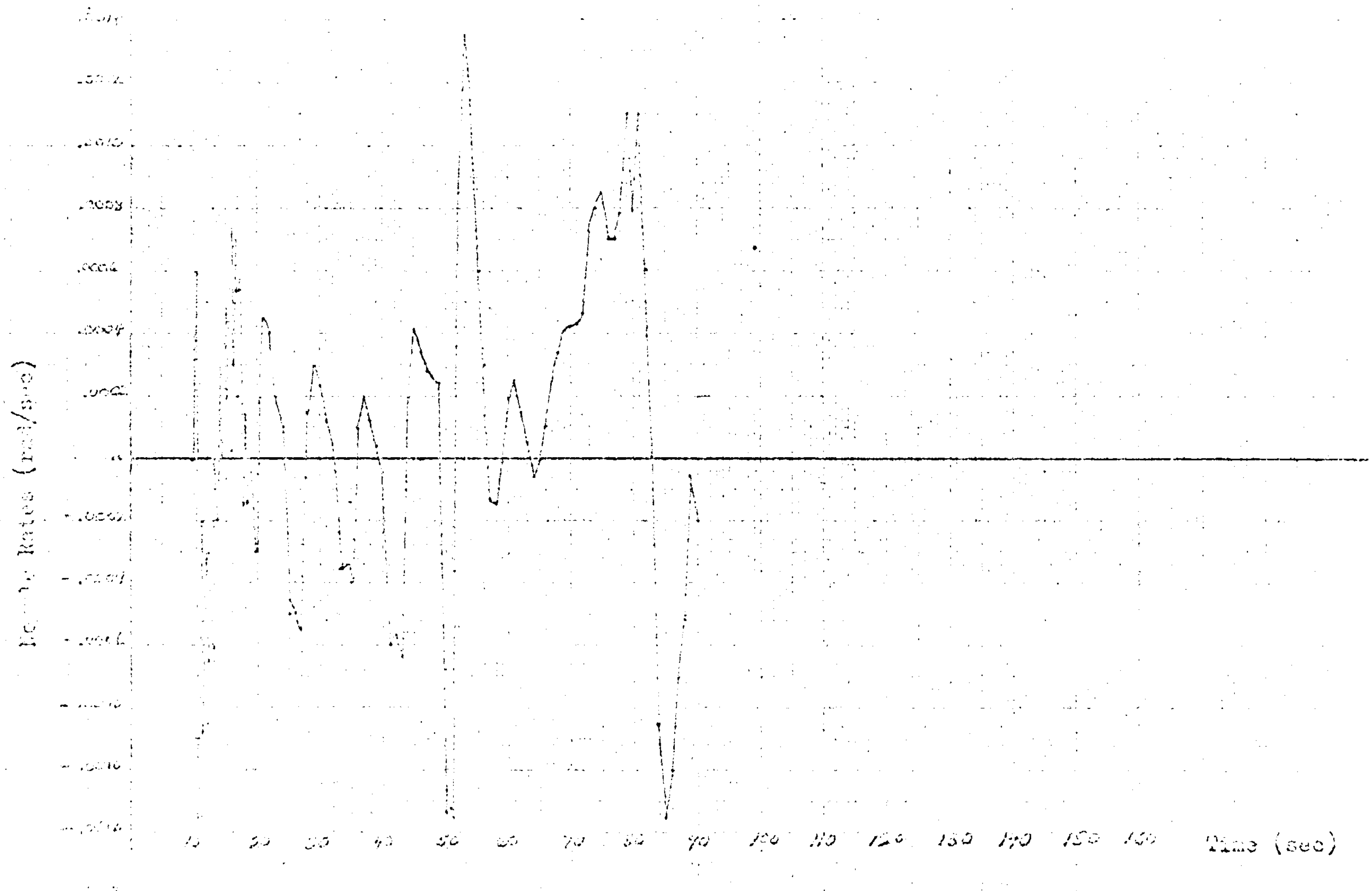
Time (sec)

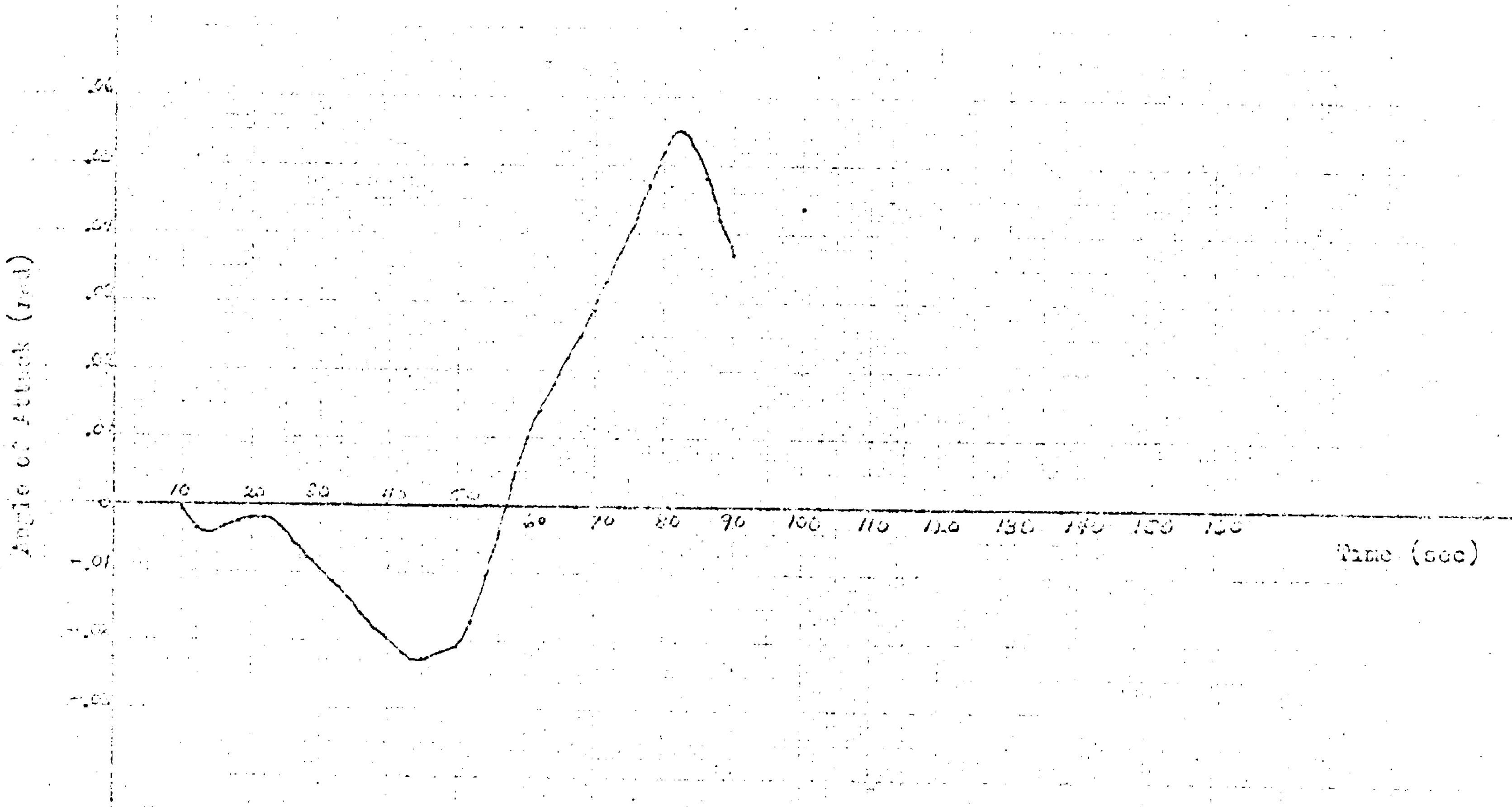
Angle of Attack (rad)
Time (sec)

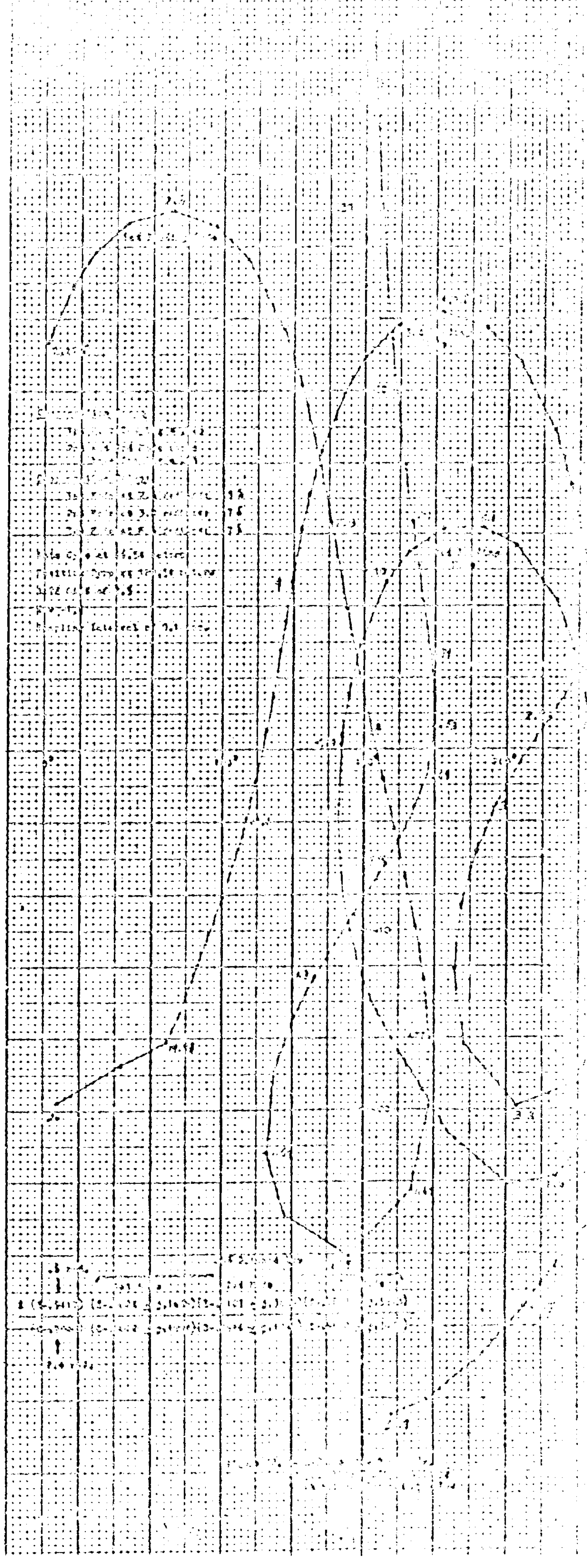

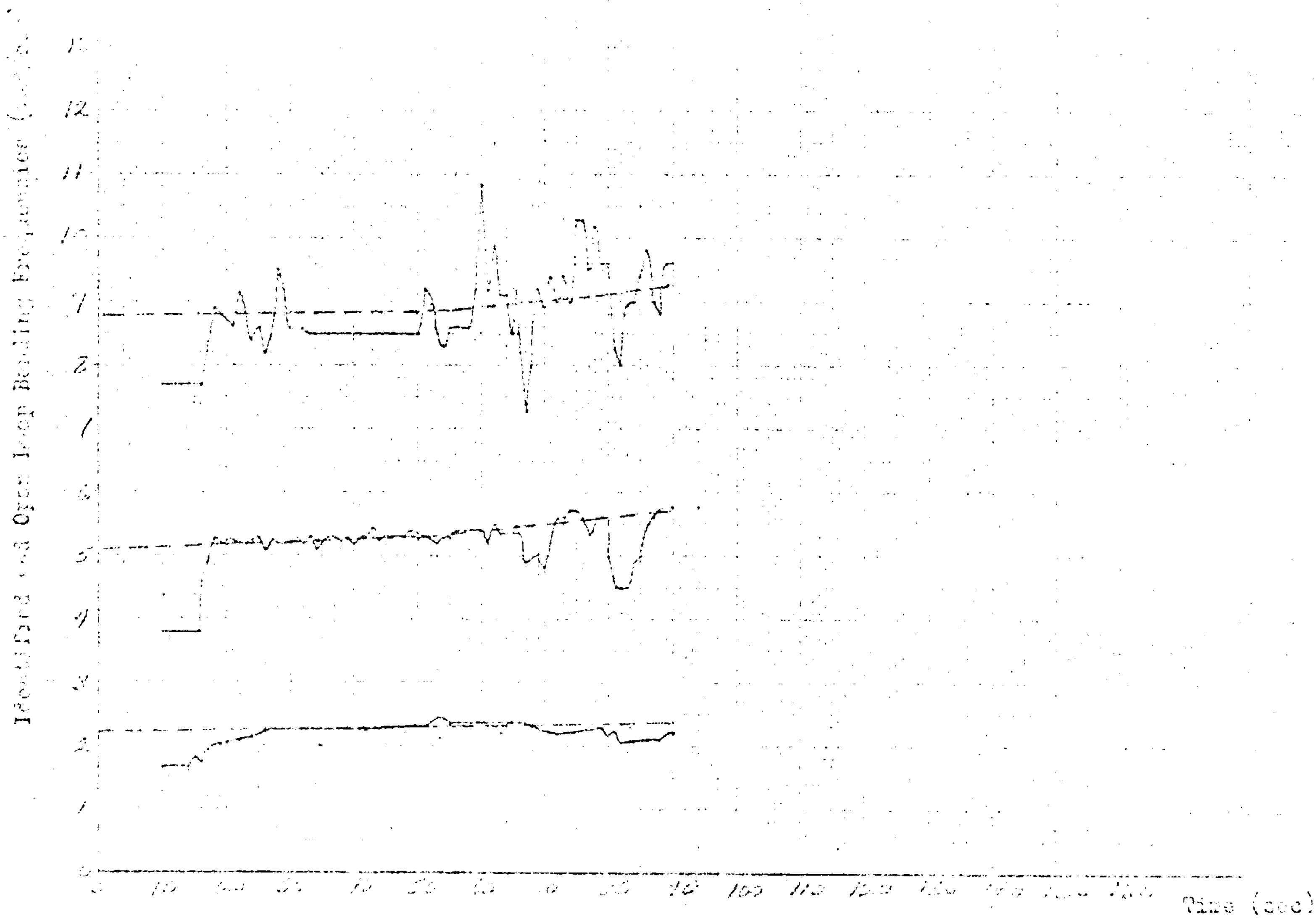
Identified and Open Loop Bending Frequencies
Time (sec)

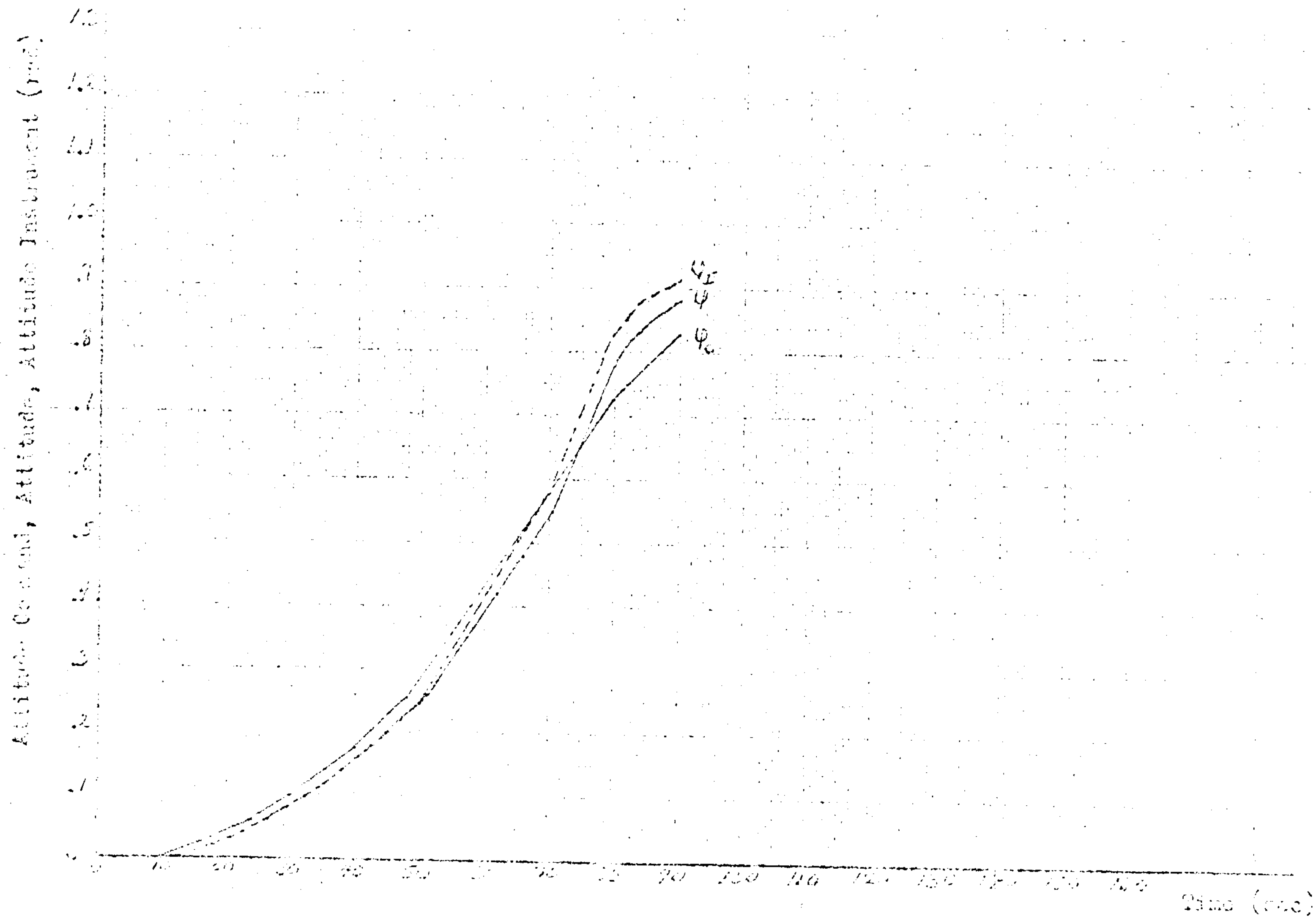
Attitude Command, Attitude, Attitude Instrument (rad)
Time (sec)
φ_I
φ
φ_c

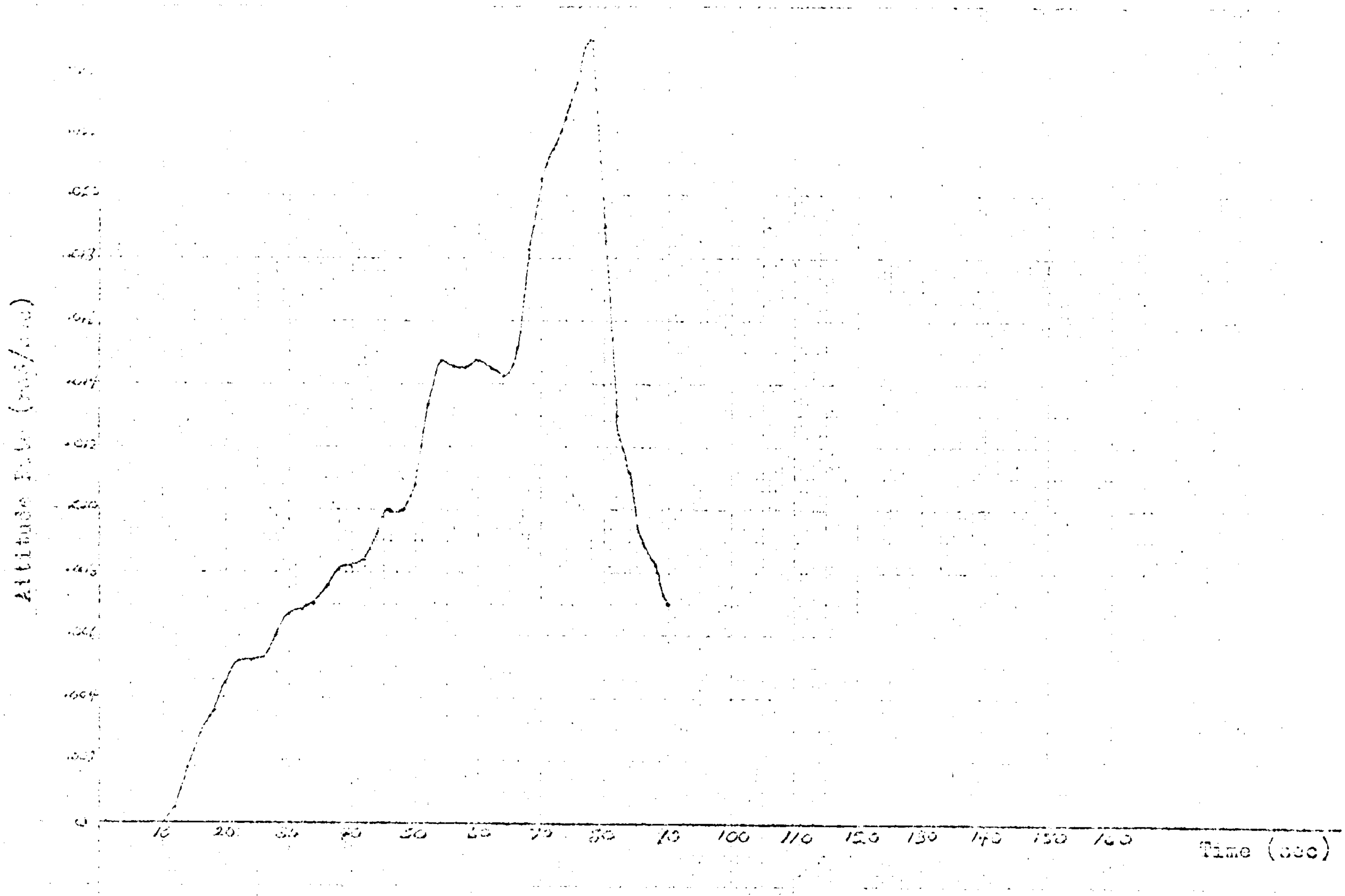

Figure [illegible] Configuration [illegible]

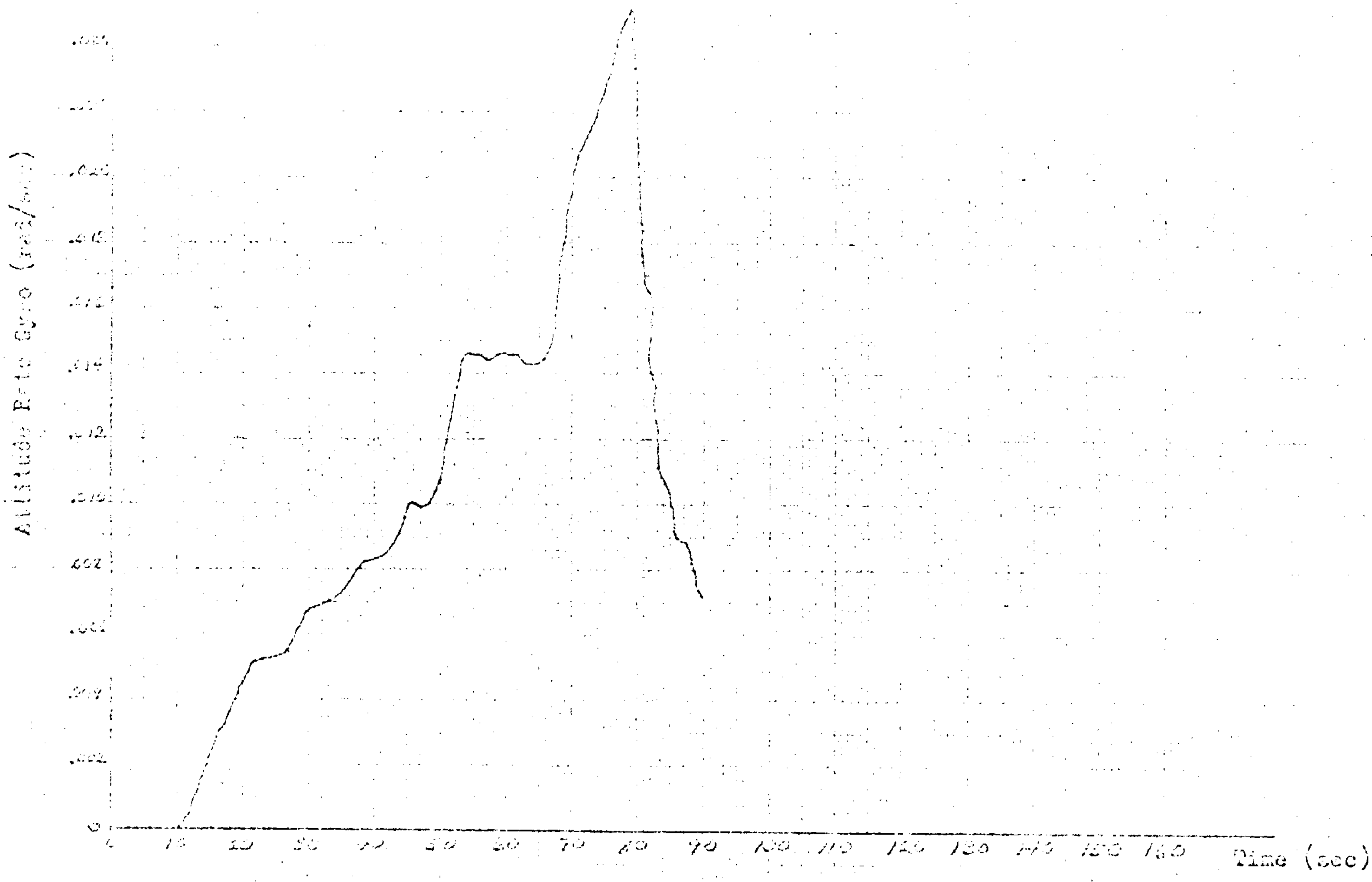

Time (sec)

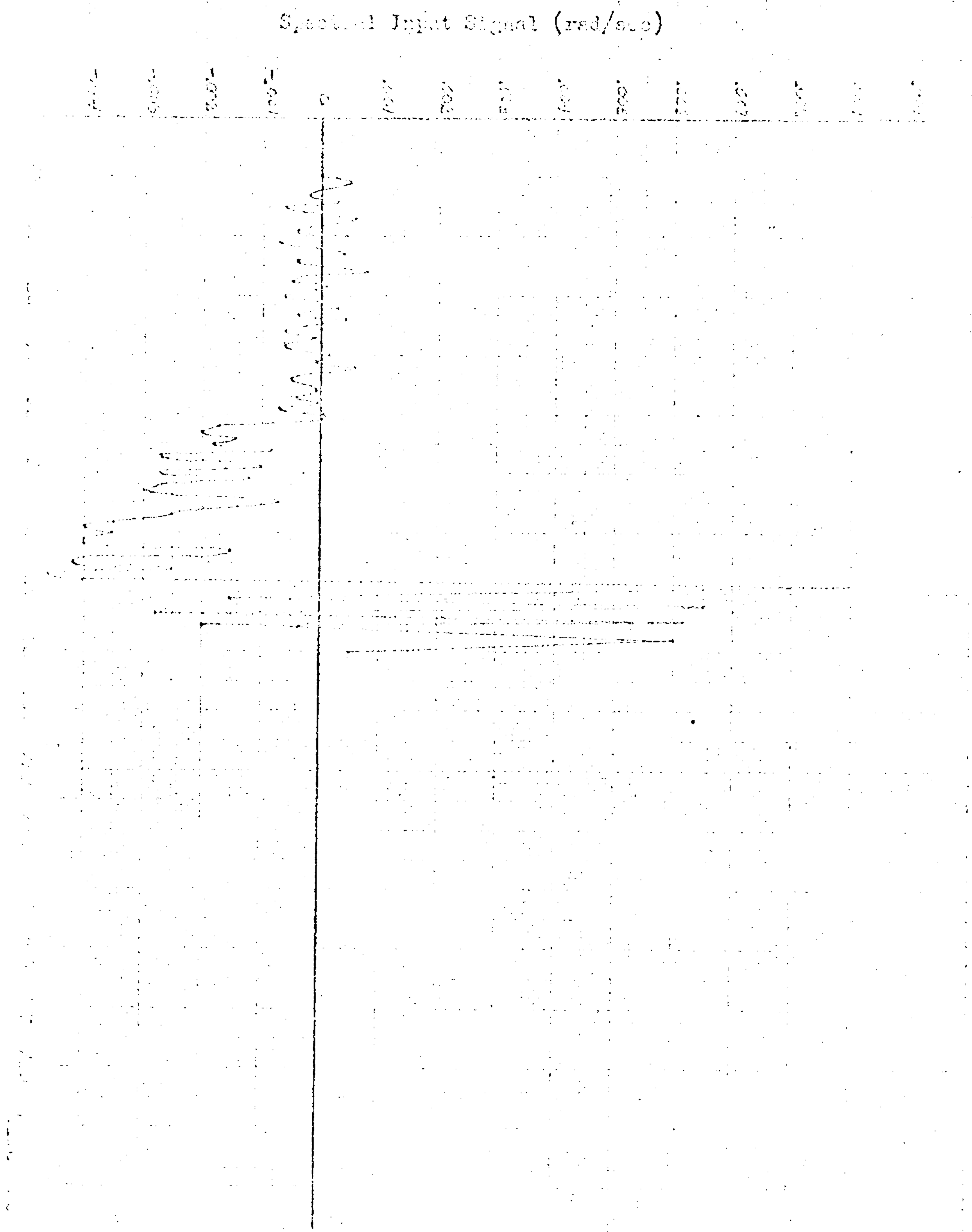
Spectral Input Signal (rad/sec)

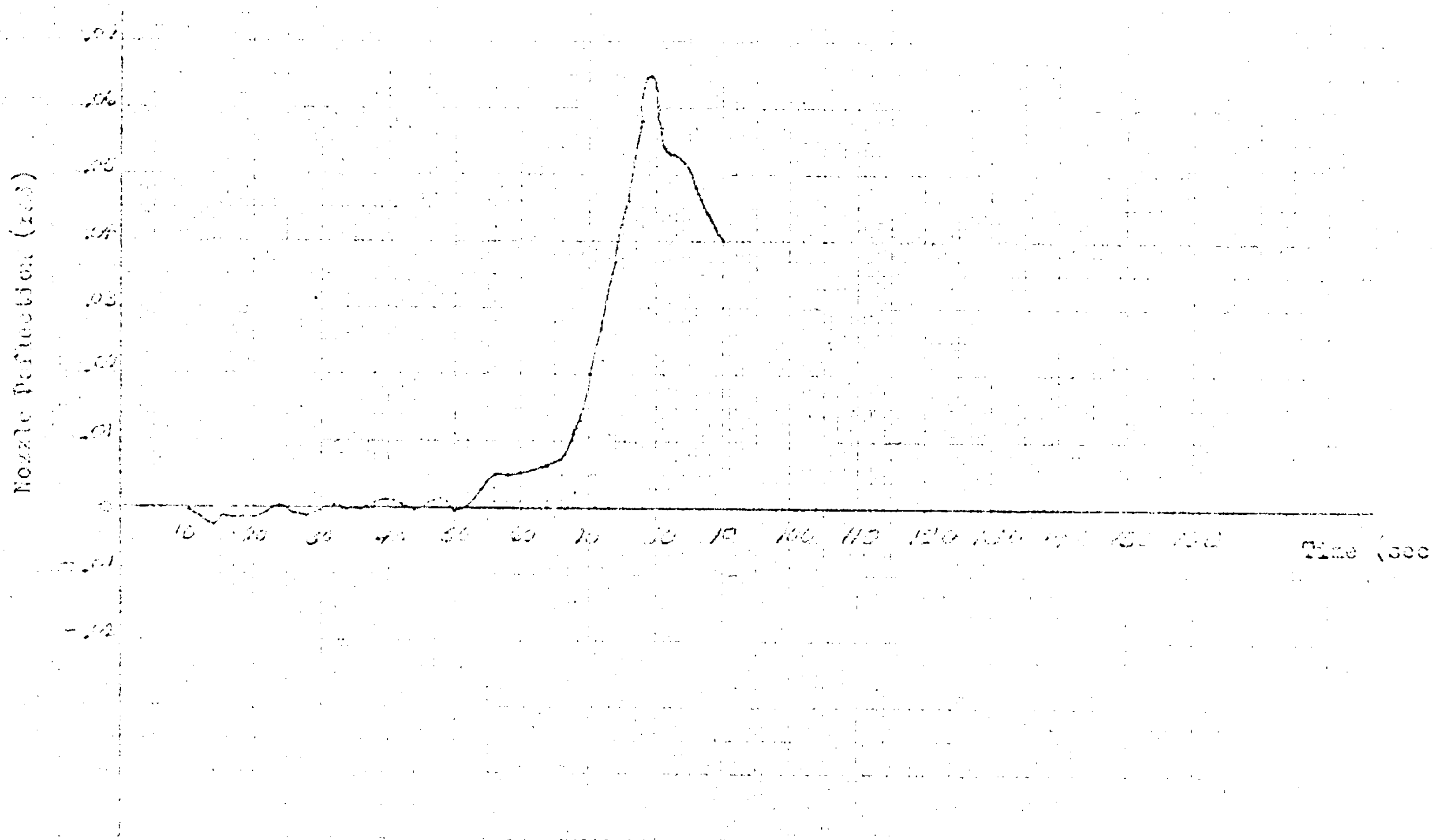
Nozzle Deflection (rad)
Time (sec)

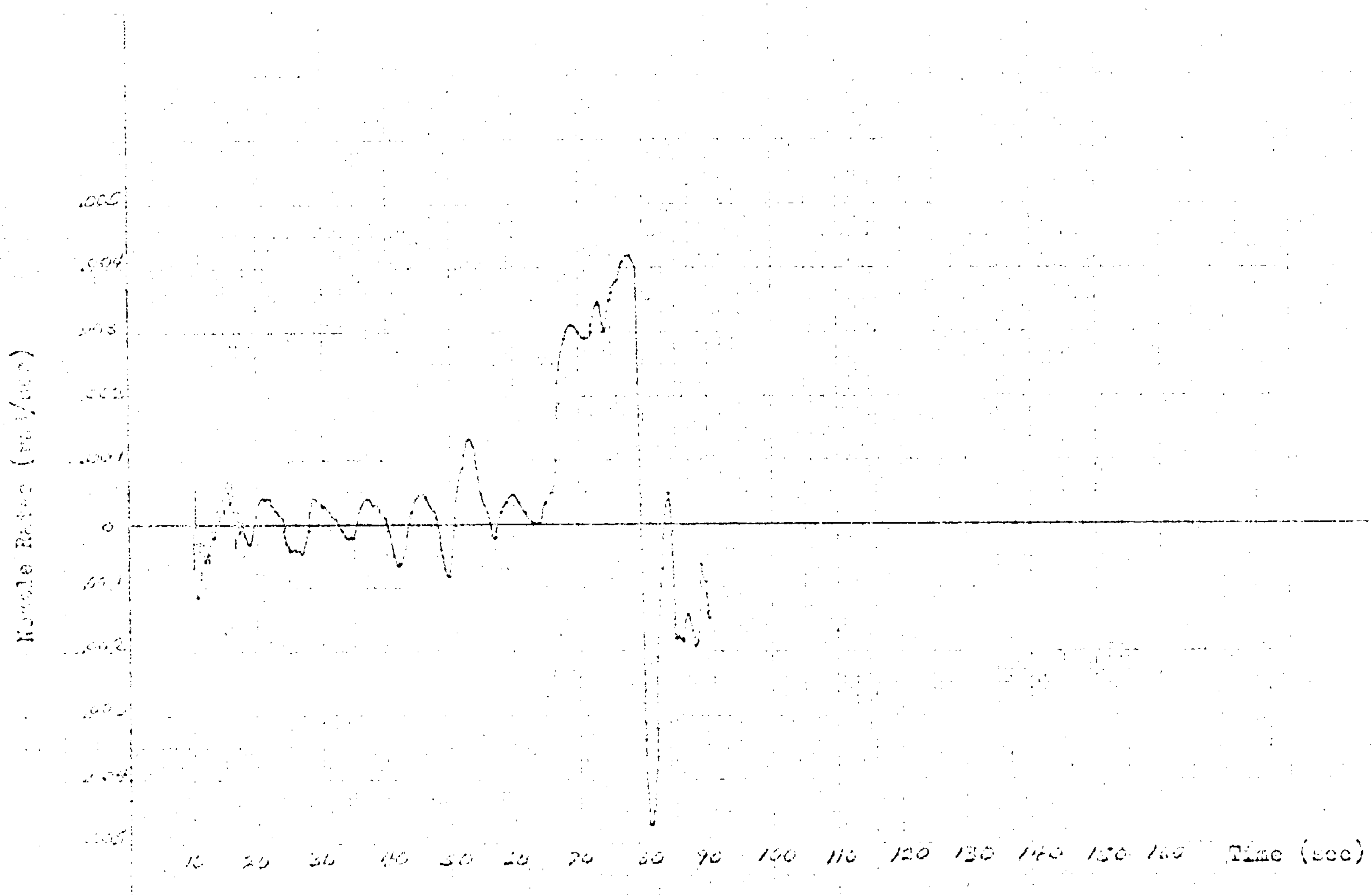
Time (sec)

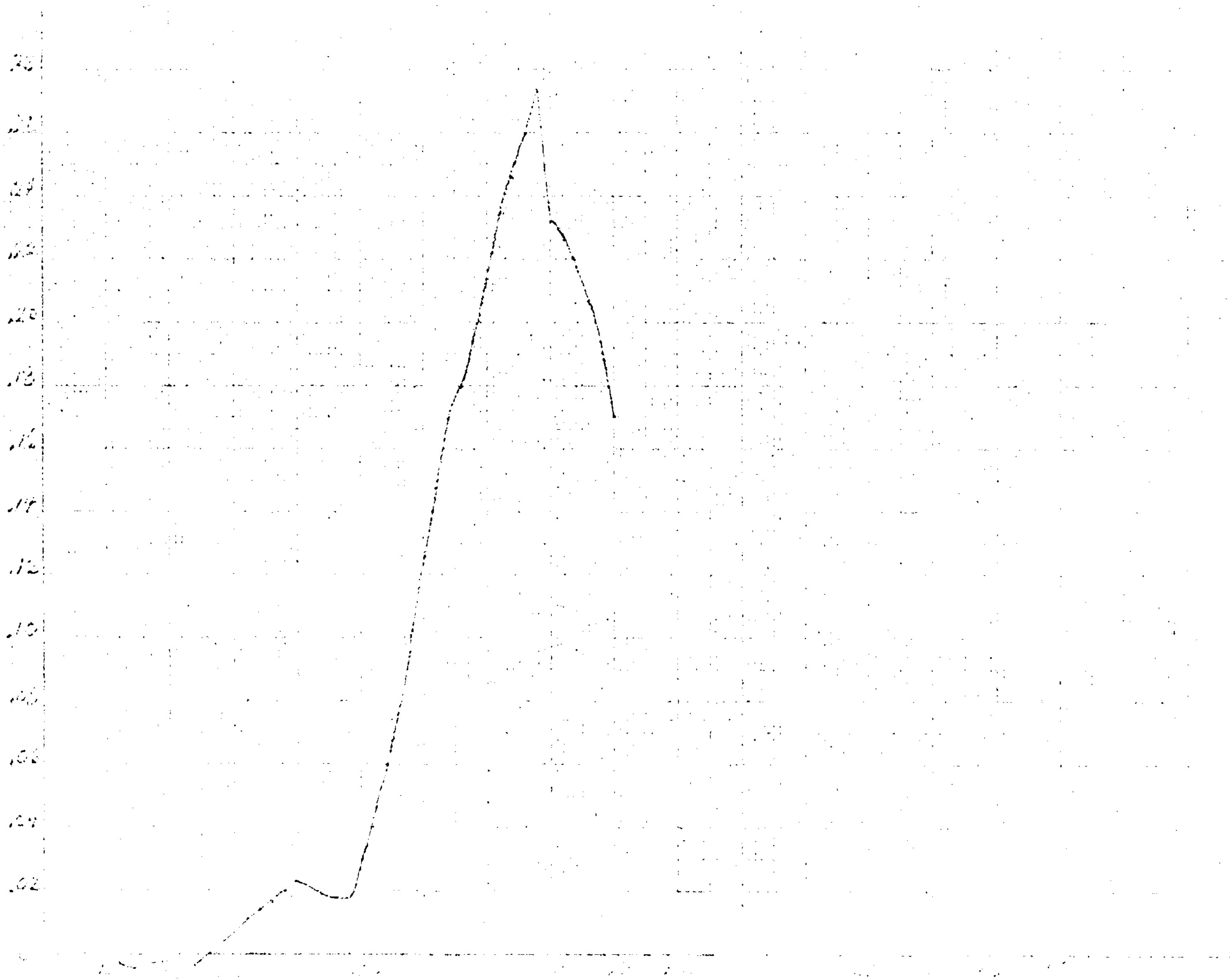
Angle of Attack (deg)

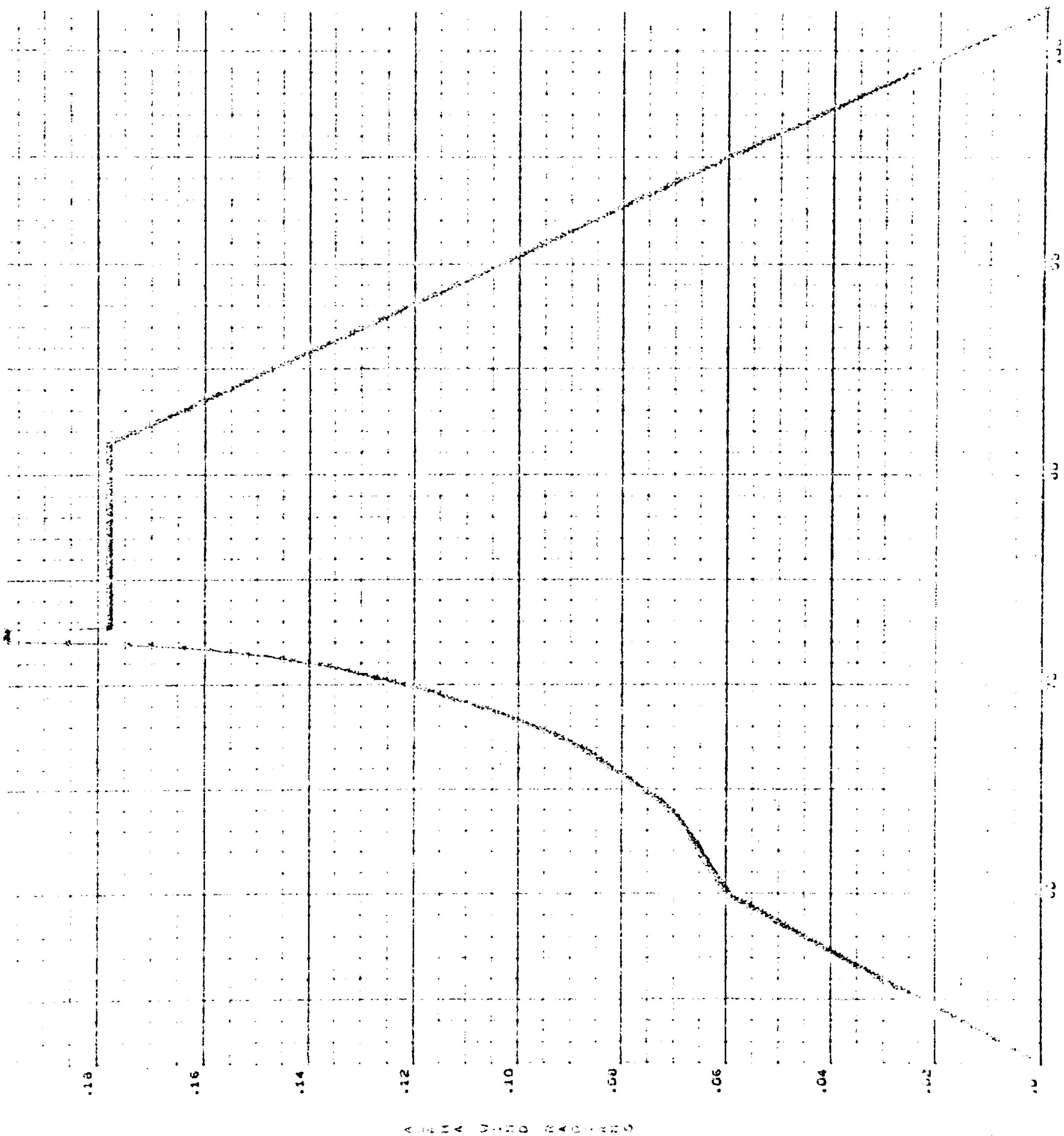
.18
.16
.14
.12
.10
.08
.06
.04
.02
0

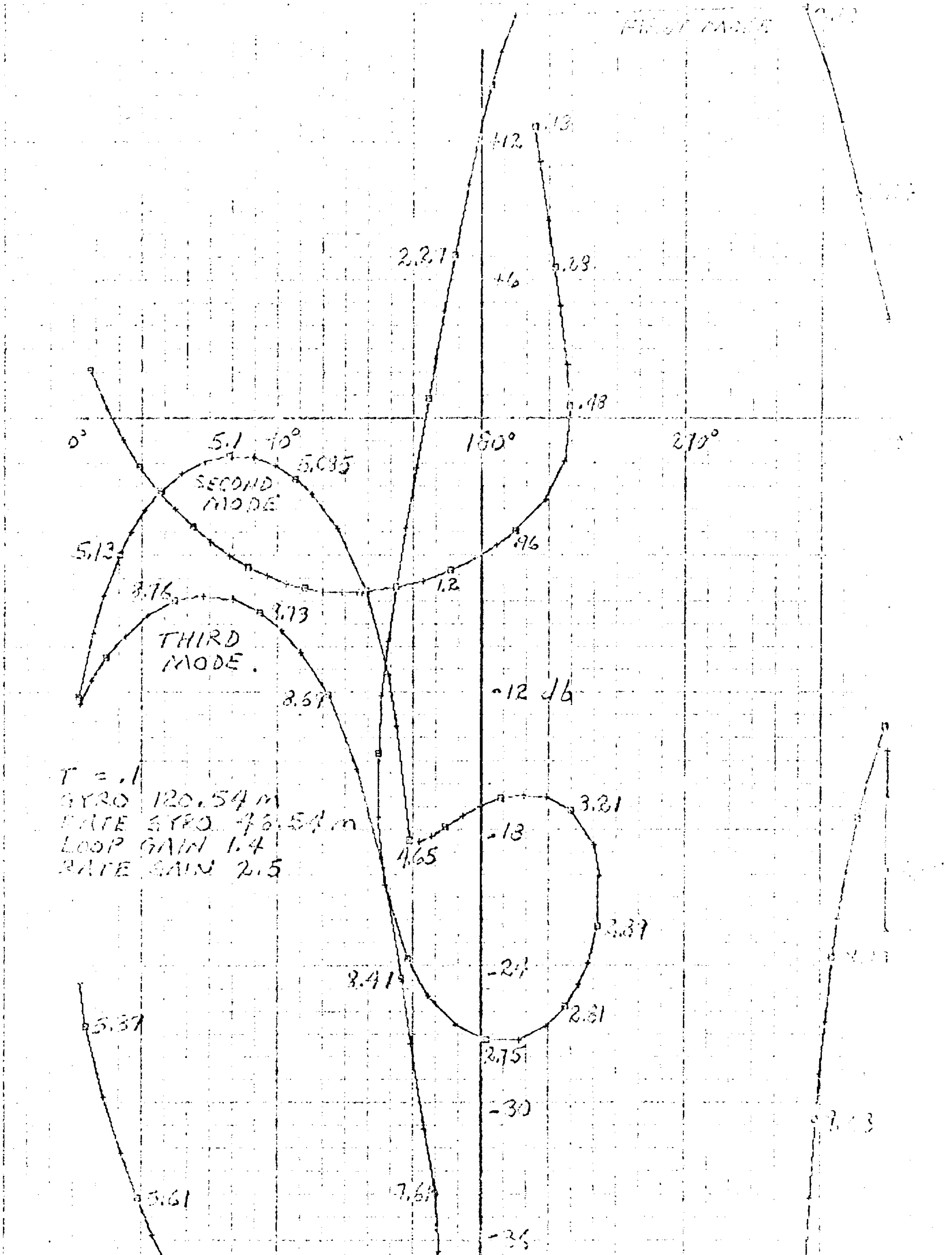

Figure 75. Gain-Phase
t = 3 seconds
[illegible]
[illegible]

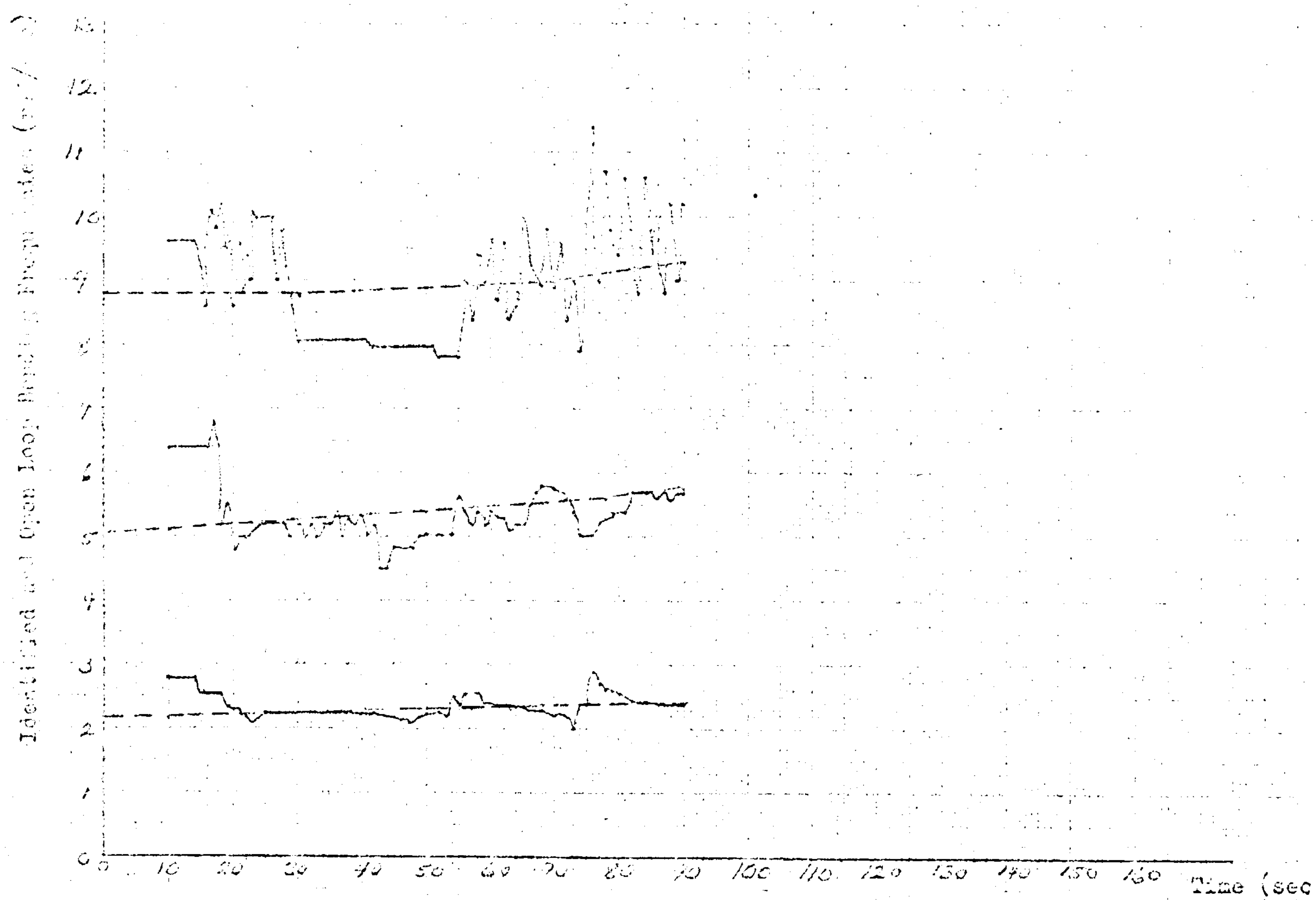

Figure 7b-1. Compensation Configuration [illegible]

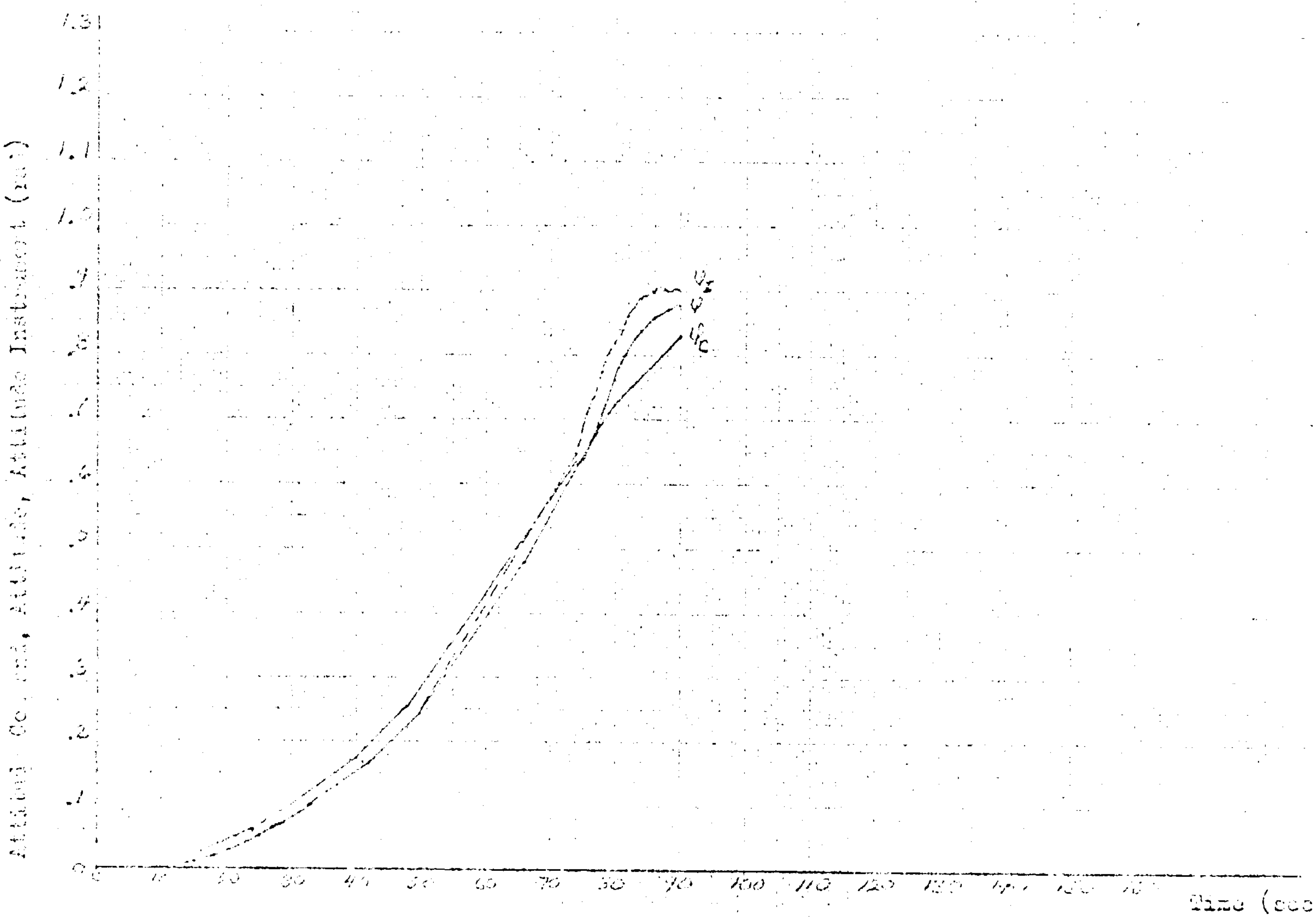
Time (sec)

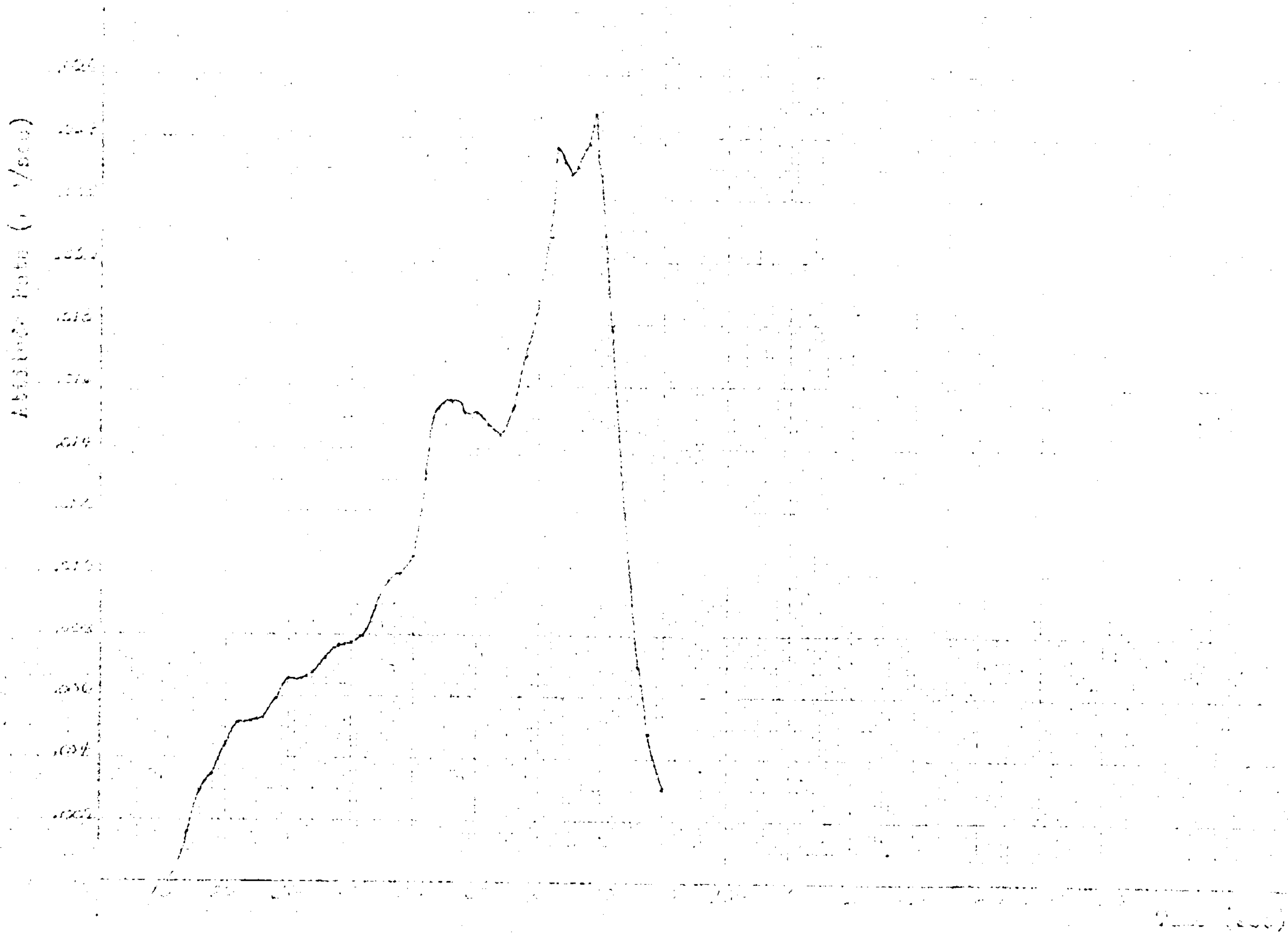

Figure 7a-3. Compensation Configuration #1, Boron Initially 25% High


Attitude Rate Gyro (rad/sec)
.020
.018
.016
.014
.012
.010
.006

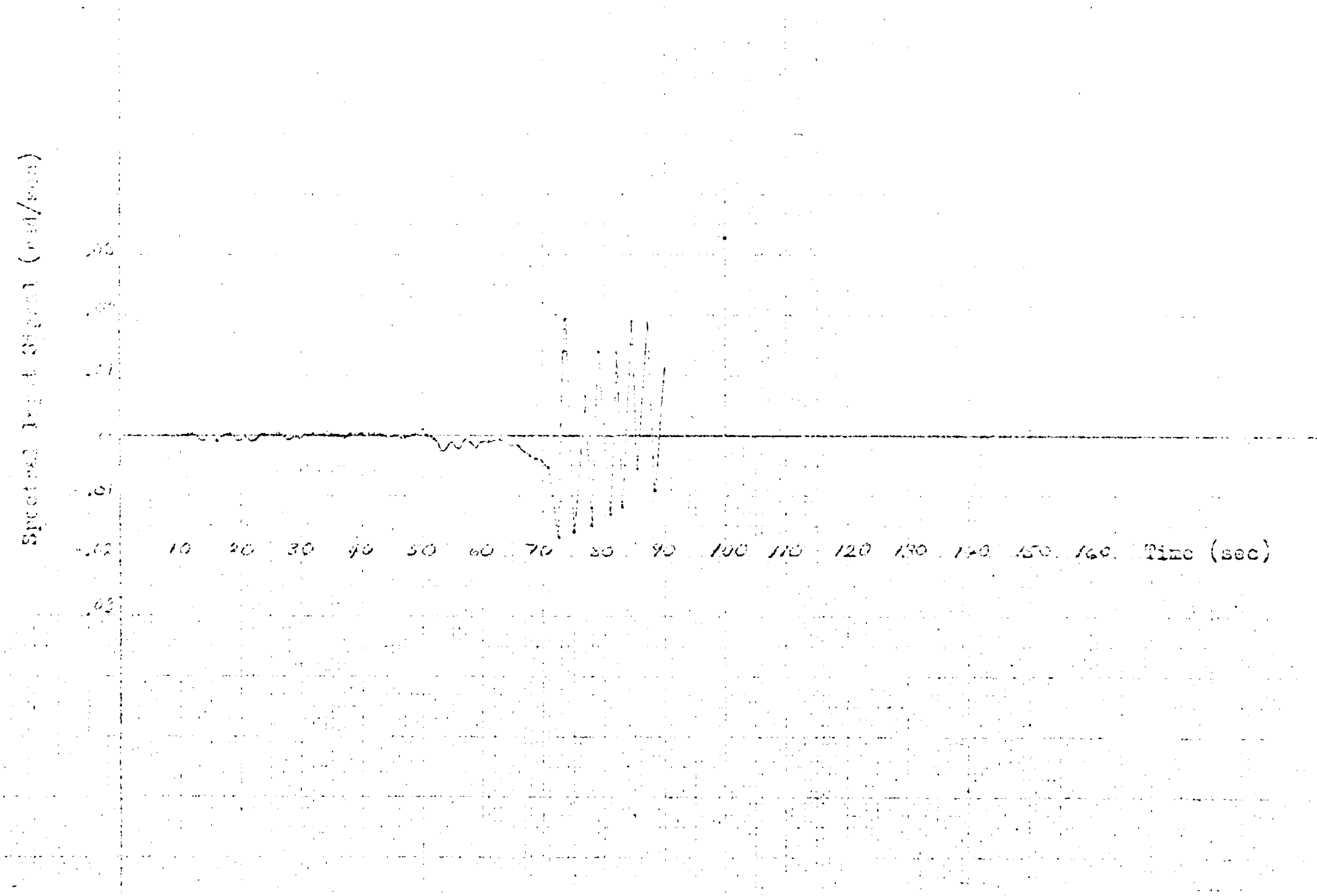

Figure 76-5. Compensation Configuration #1, [illegible]

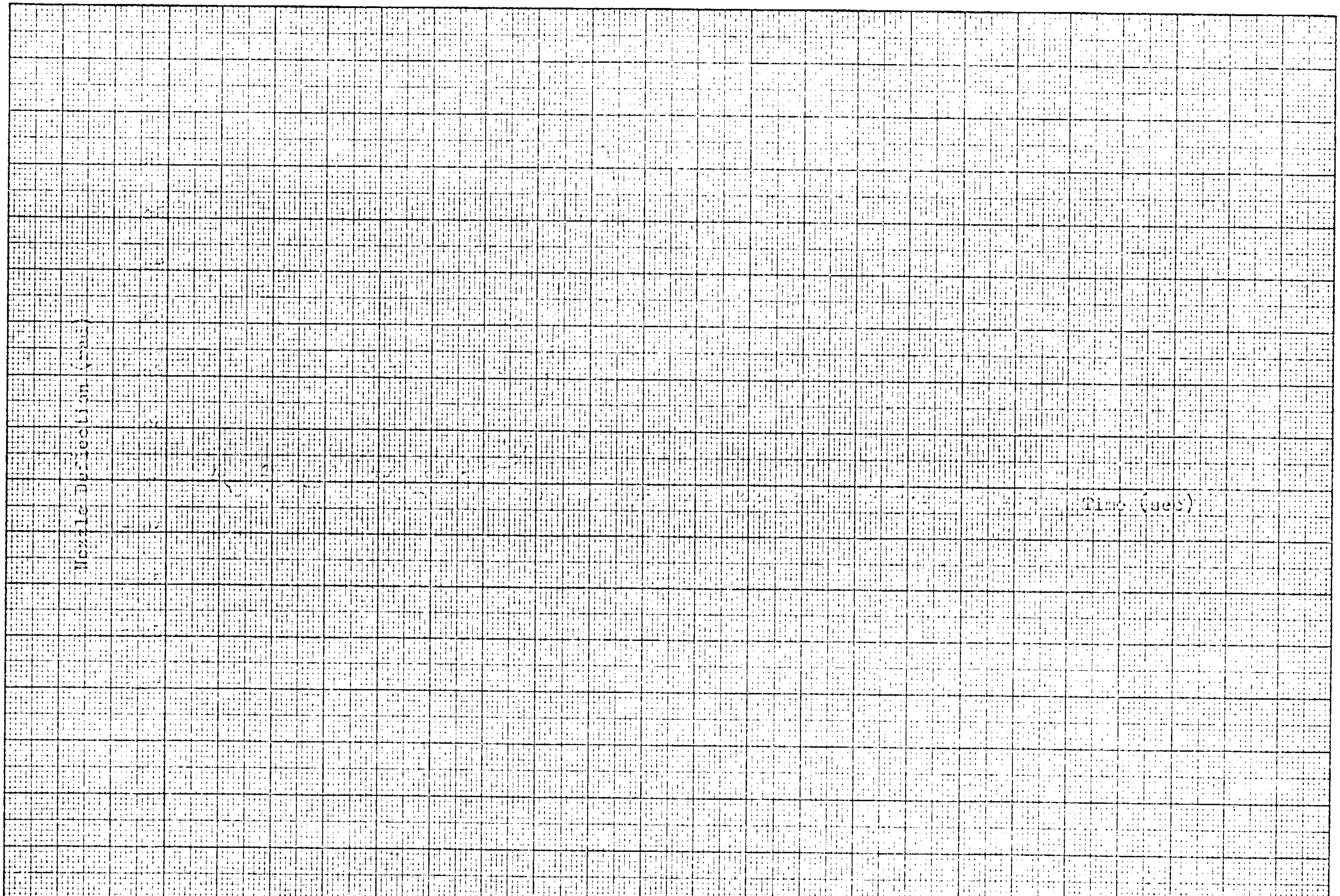

[illegible] Compensation Configuration [illegible] Zeros Initially [illegible] High

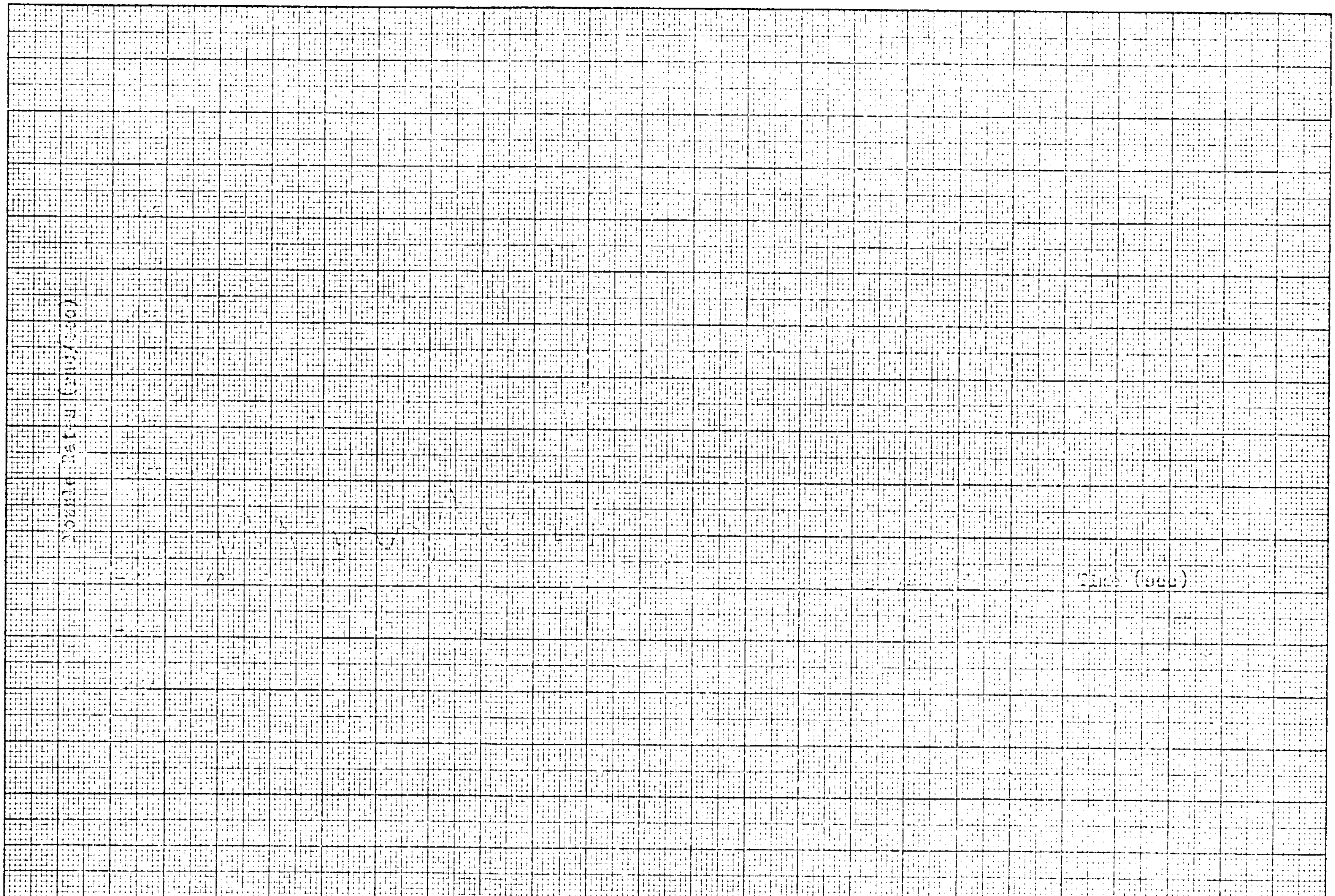

Figure [illegible]. Compensation Configuration #1, Zeros Initially 25 Hz

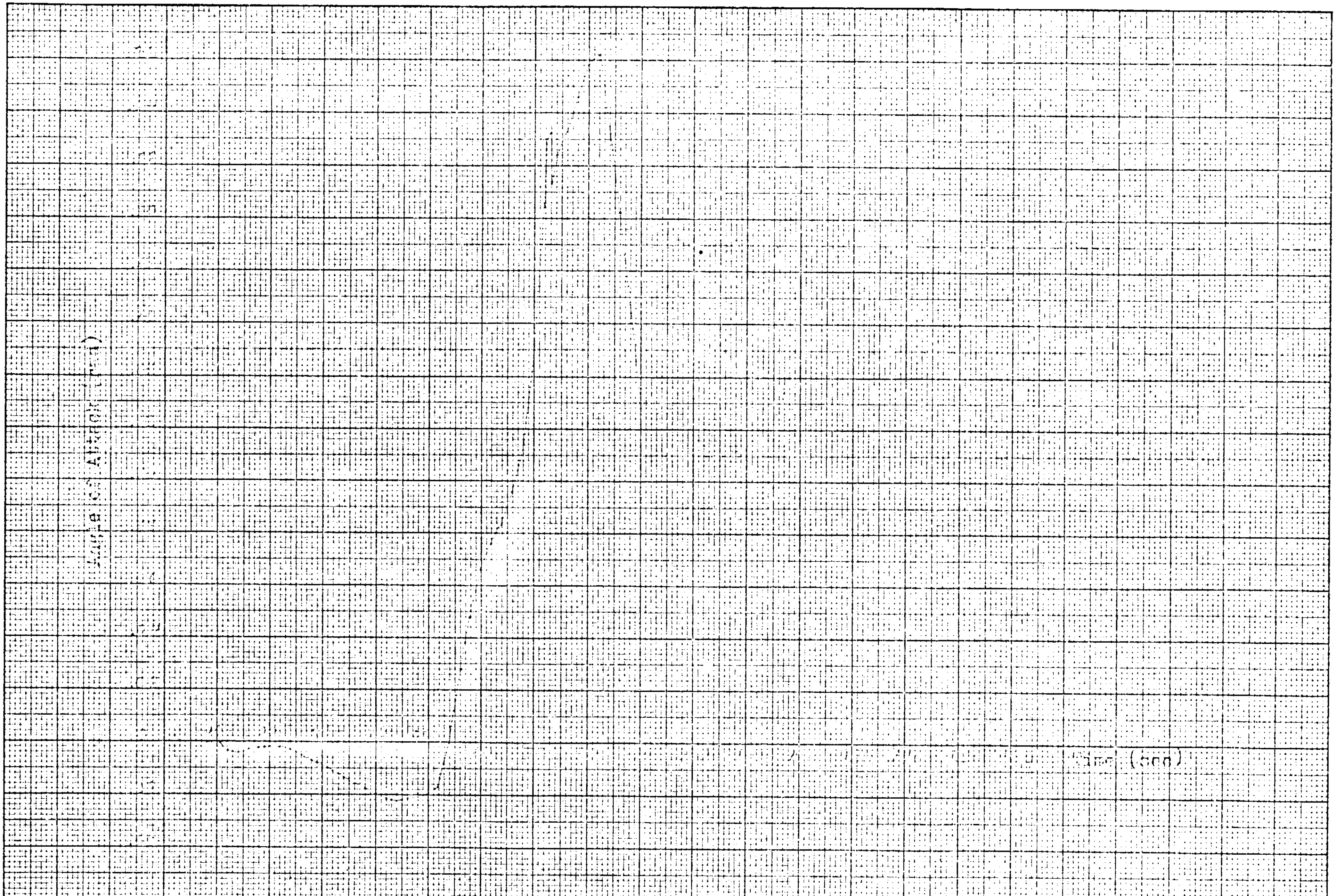

Figure 75-8. Compensation Configuration #1, Zeros Initially 25% High

2143-G
003

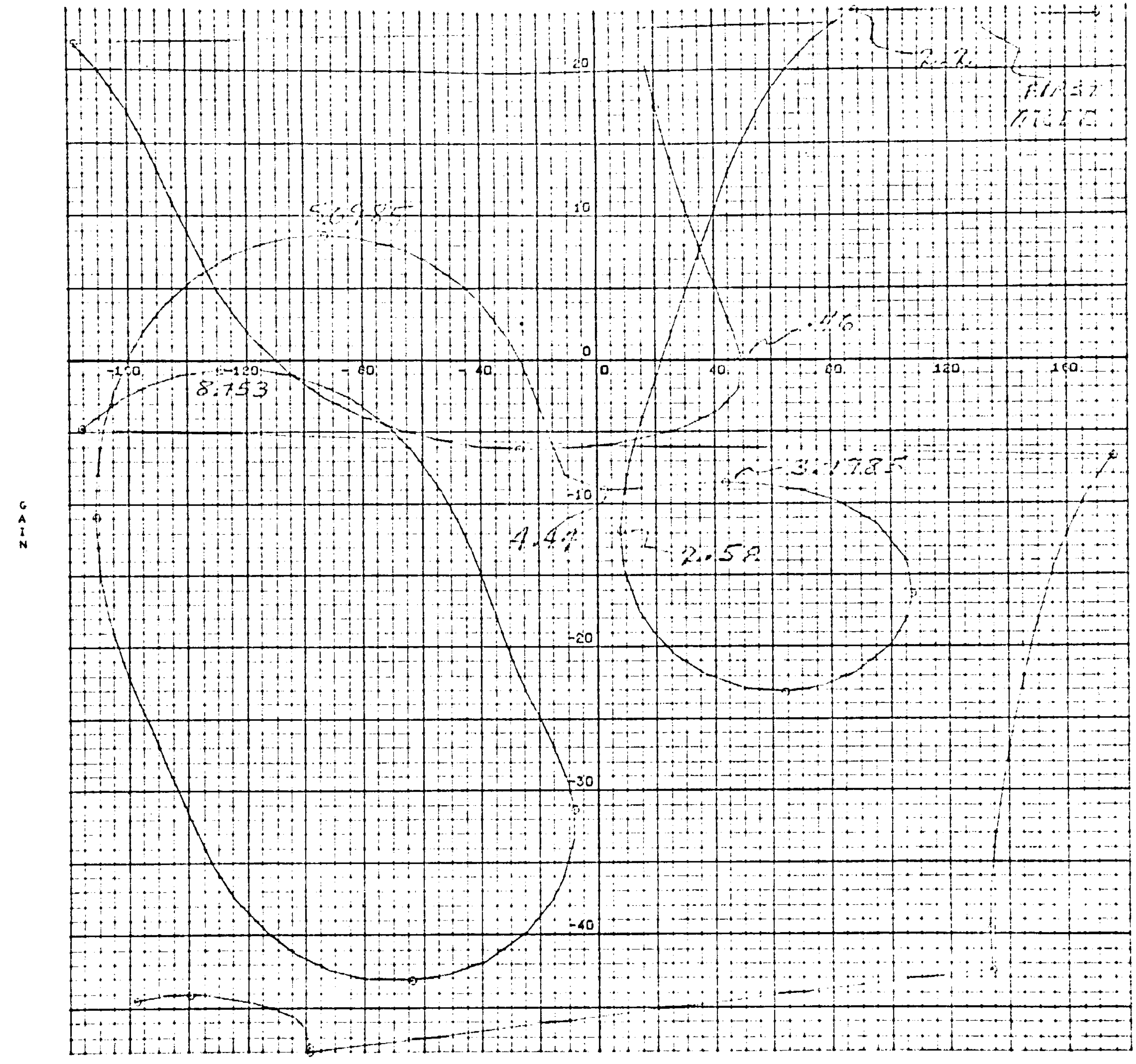

Figure 77. Gain-Phase t = 8 sec, Compensation Configuration #2
All Zeros 25 % High

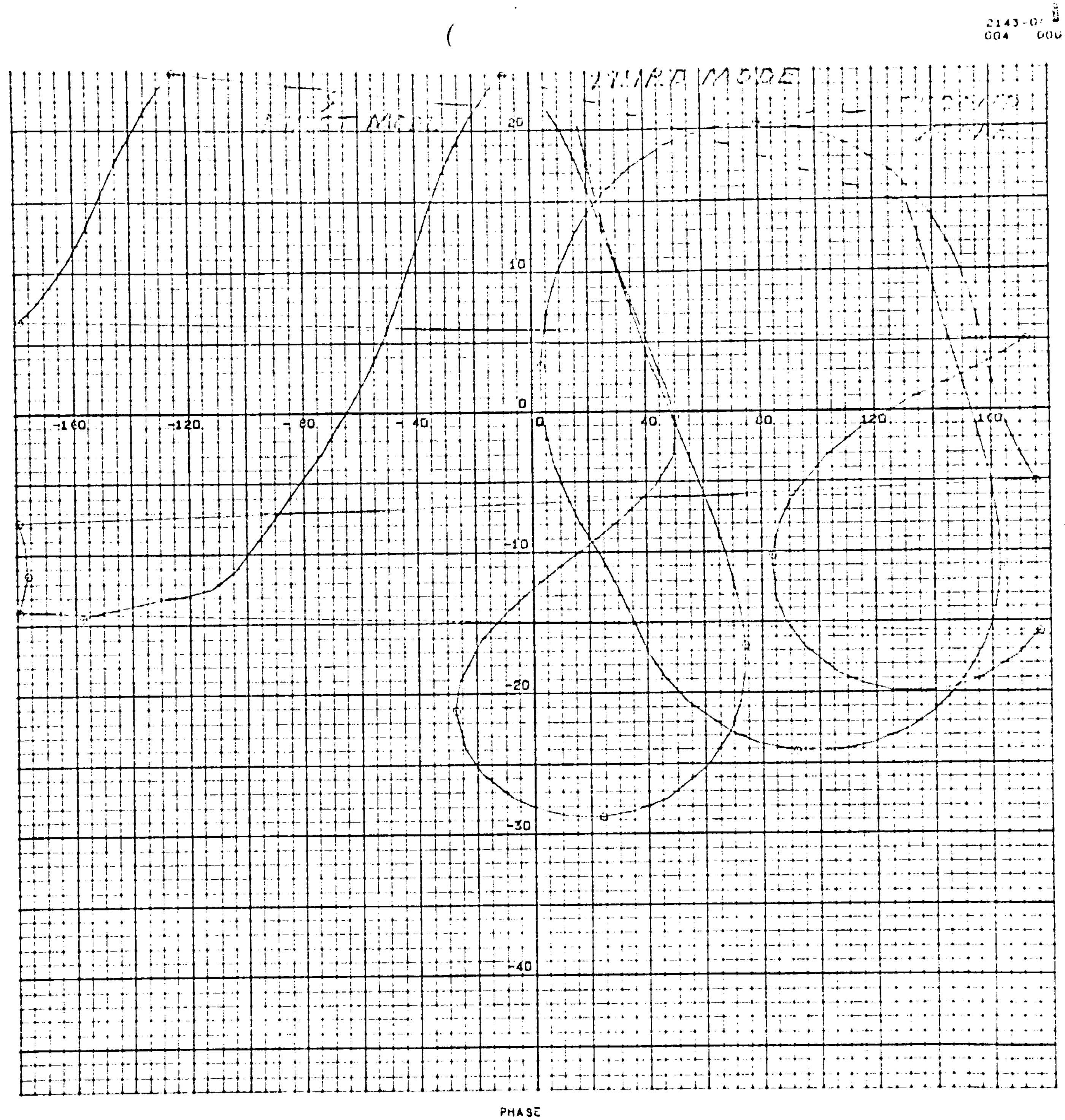

Figure 78. Gain-Phase t = 8 sec, Compensation Configuration #2

All Zeros 25 % Low

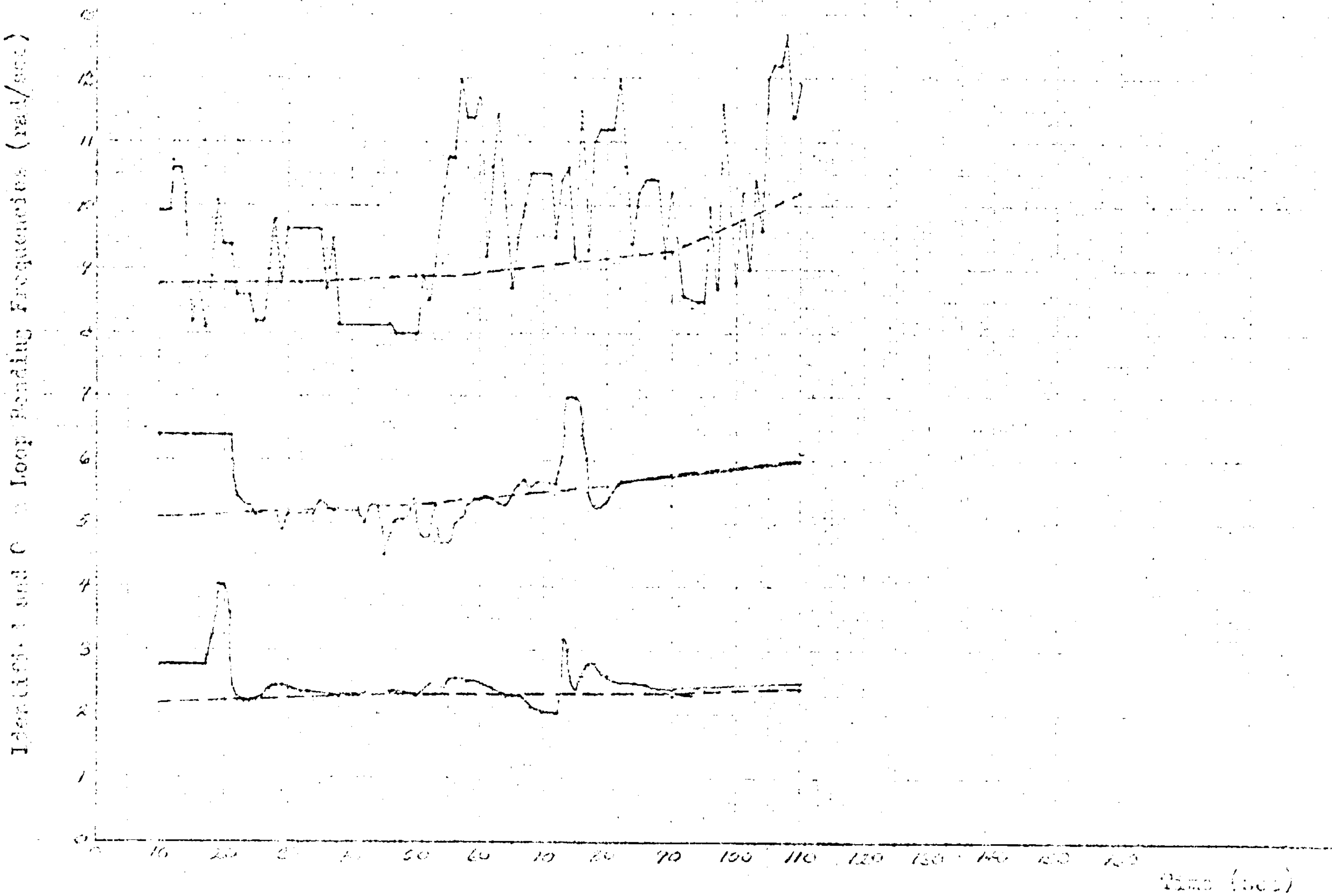
Identified and ... Loop Bending Frequencies (rad/sec)
Time (sec)

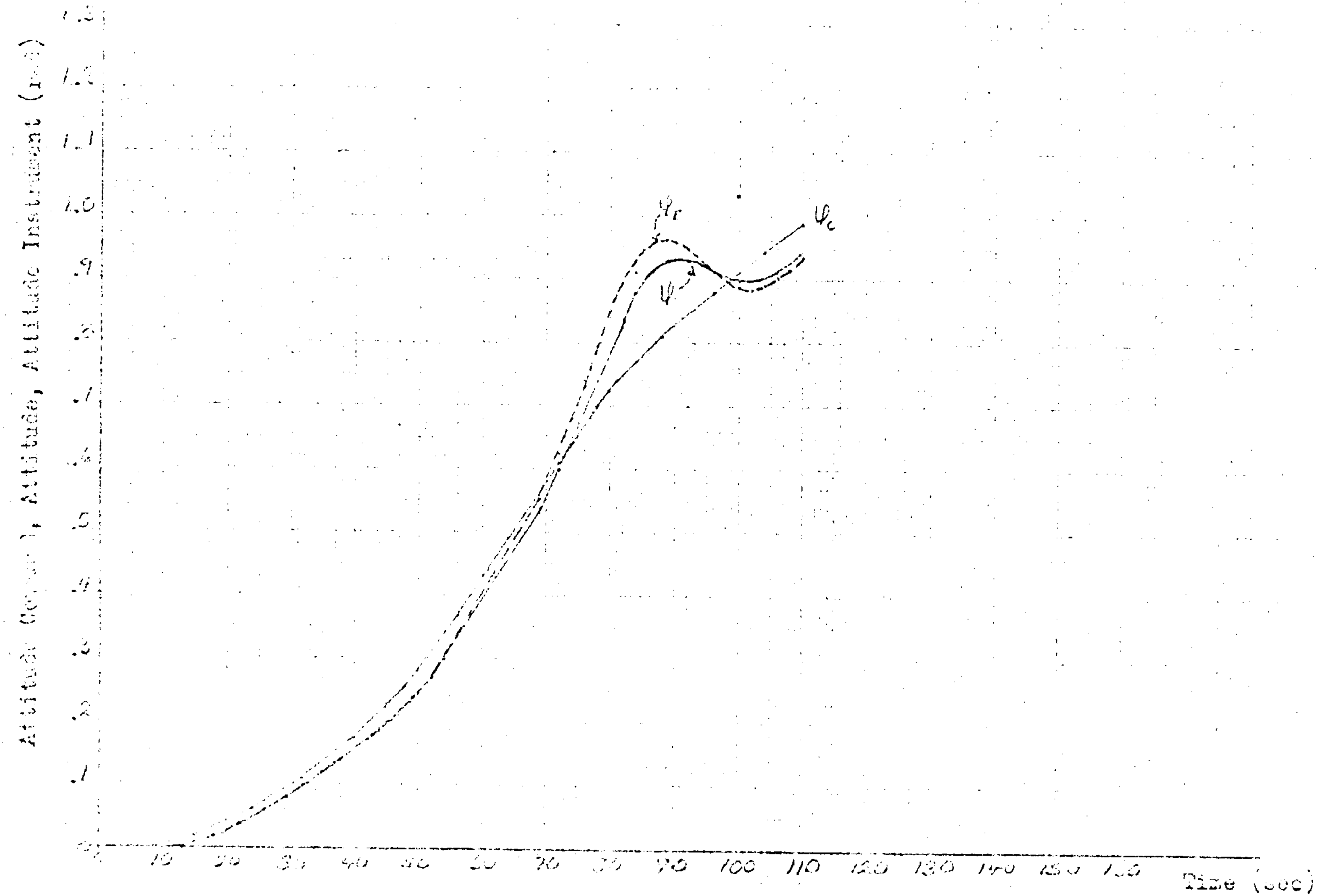
Attitude Command, Attitude, Attitude Instrument (rad)
Time (sec)
ψ_r
ψ_c
ψ
10
20
30
40
50
60
70
80
90
100
110
120
130
140
150
160
.1
.2
.3
.4
.5
.6
.7
.8
.9
1.0
1.1
1.2
1.3

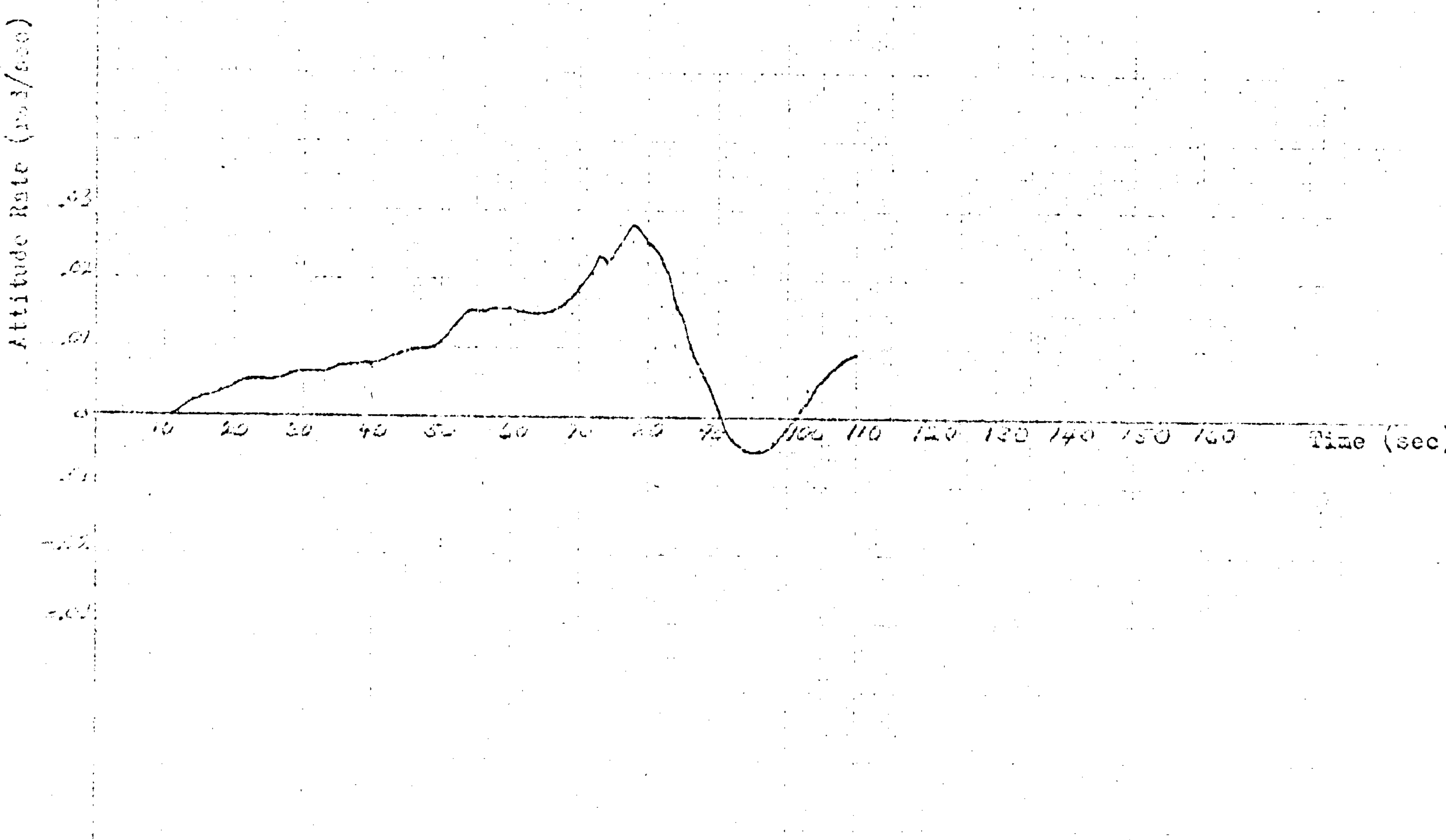
Attitude Rate (rad/sec)
.03
.02
.01
0
10
20
30
40
50
60
70
80
90
100
110
120
130
140
150
160
Time (sec)

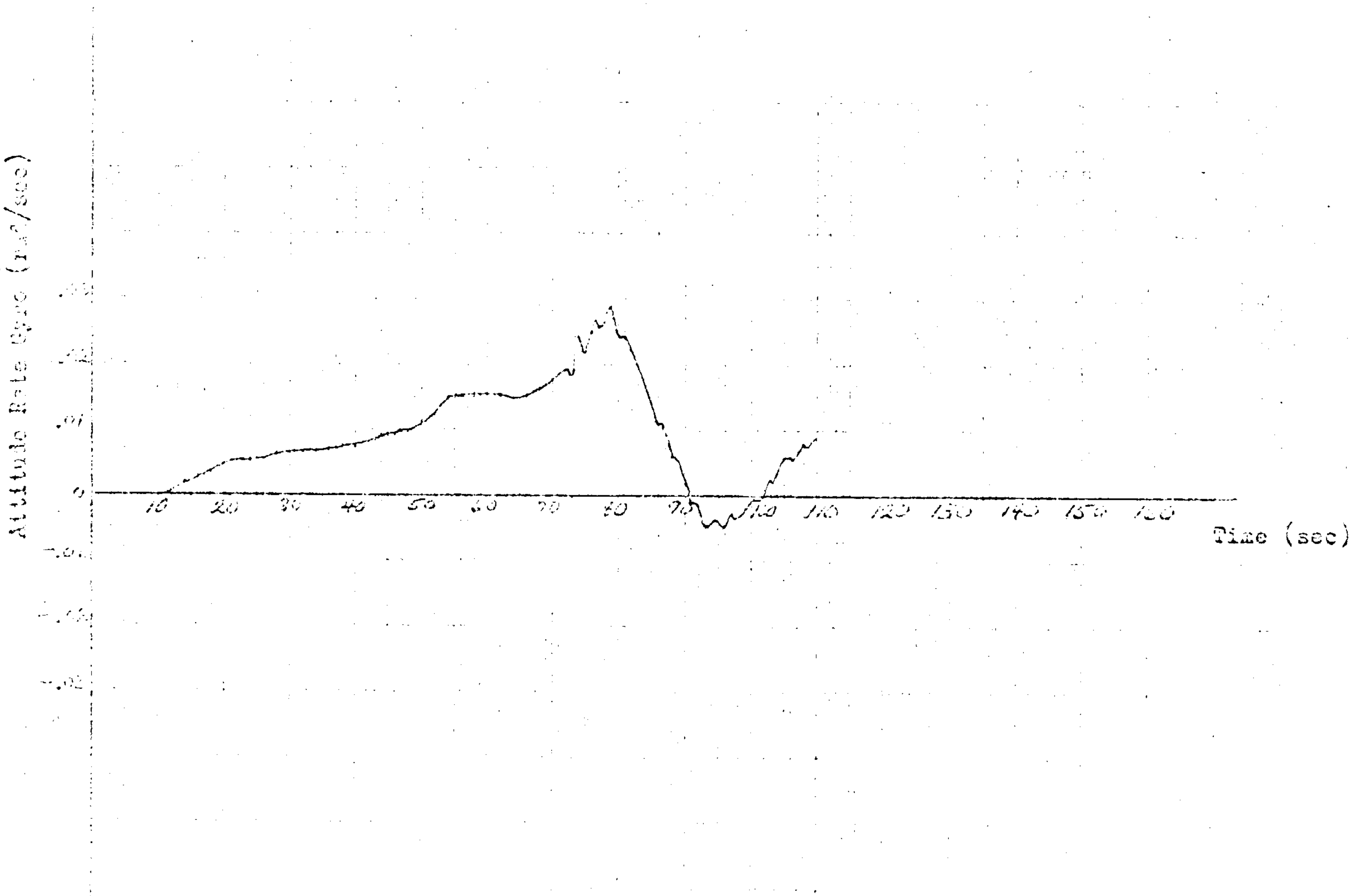

[illegible] Configuration [illegible]

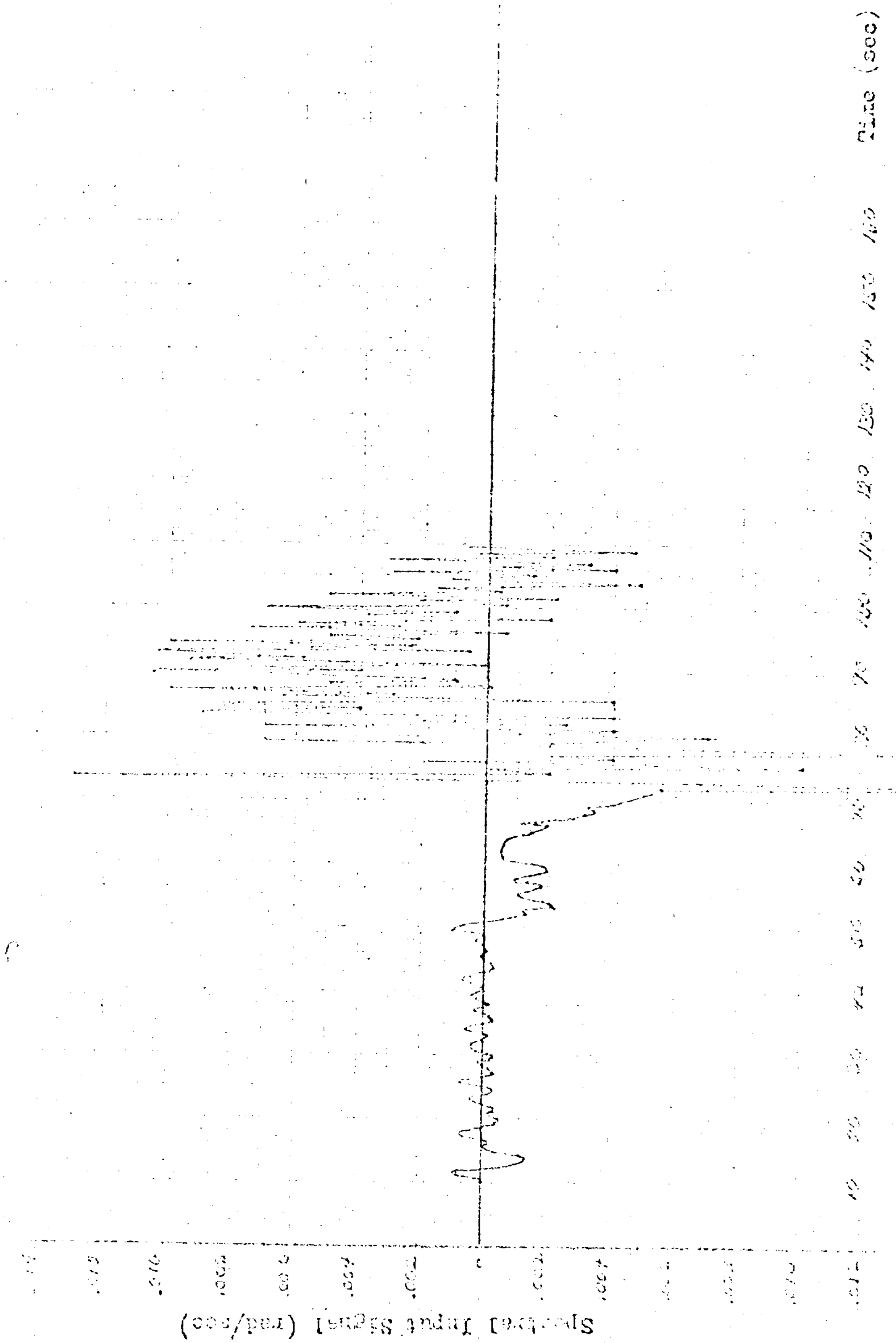
Spectral Input Signal (rad/sec)
Time (sec)

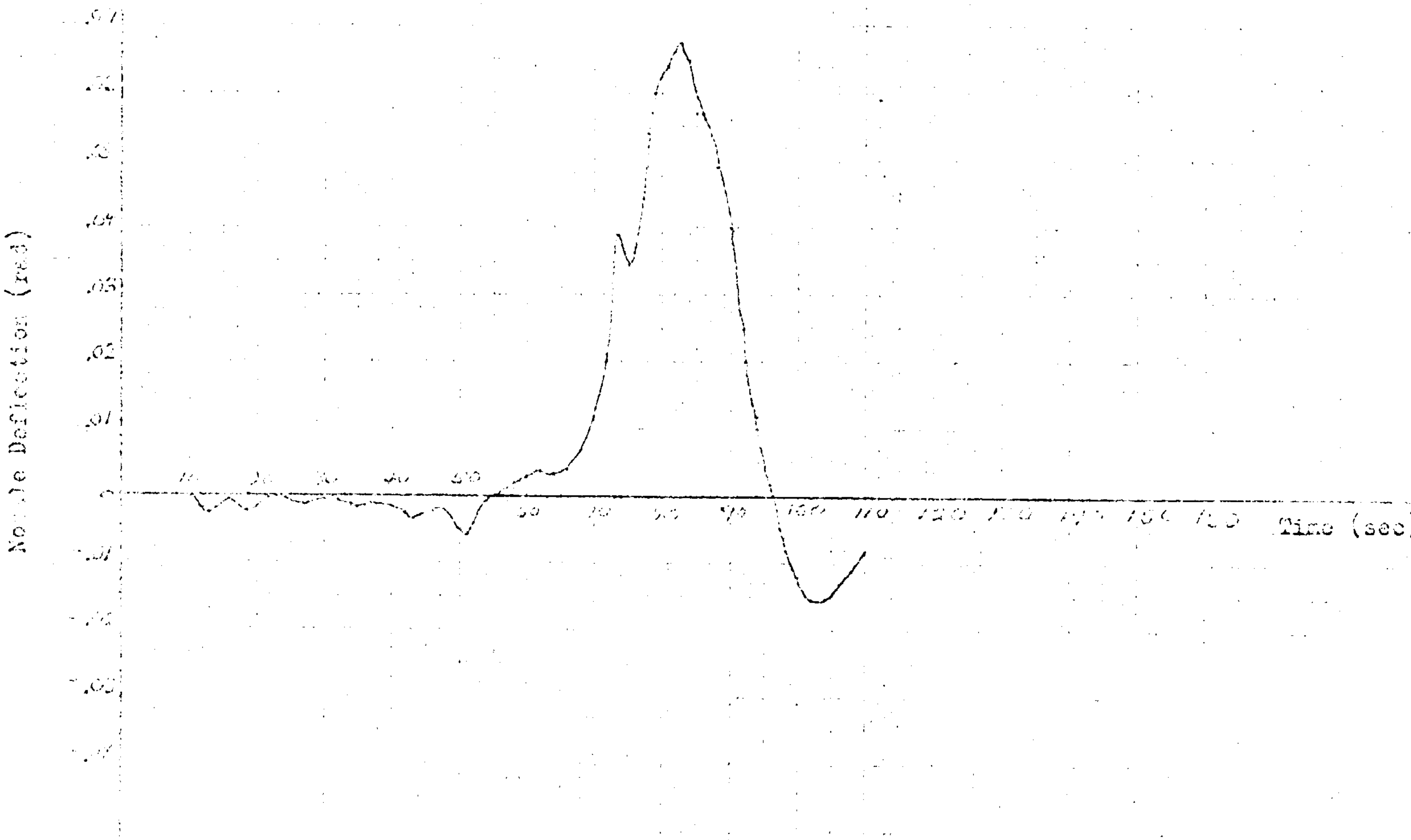

Time (sec)

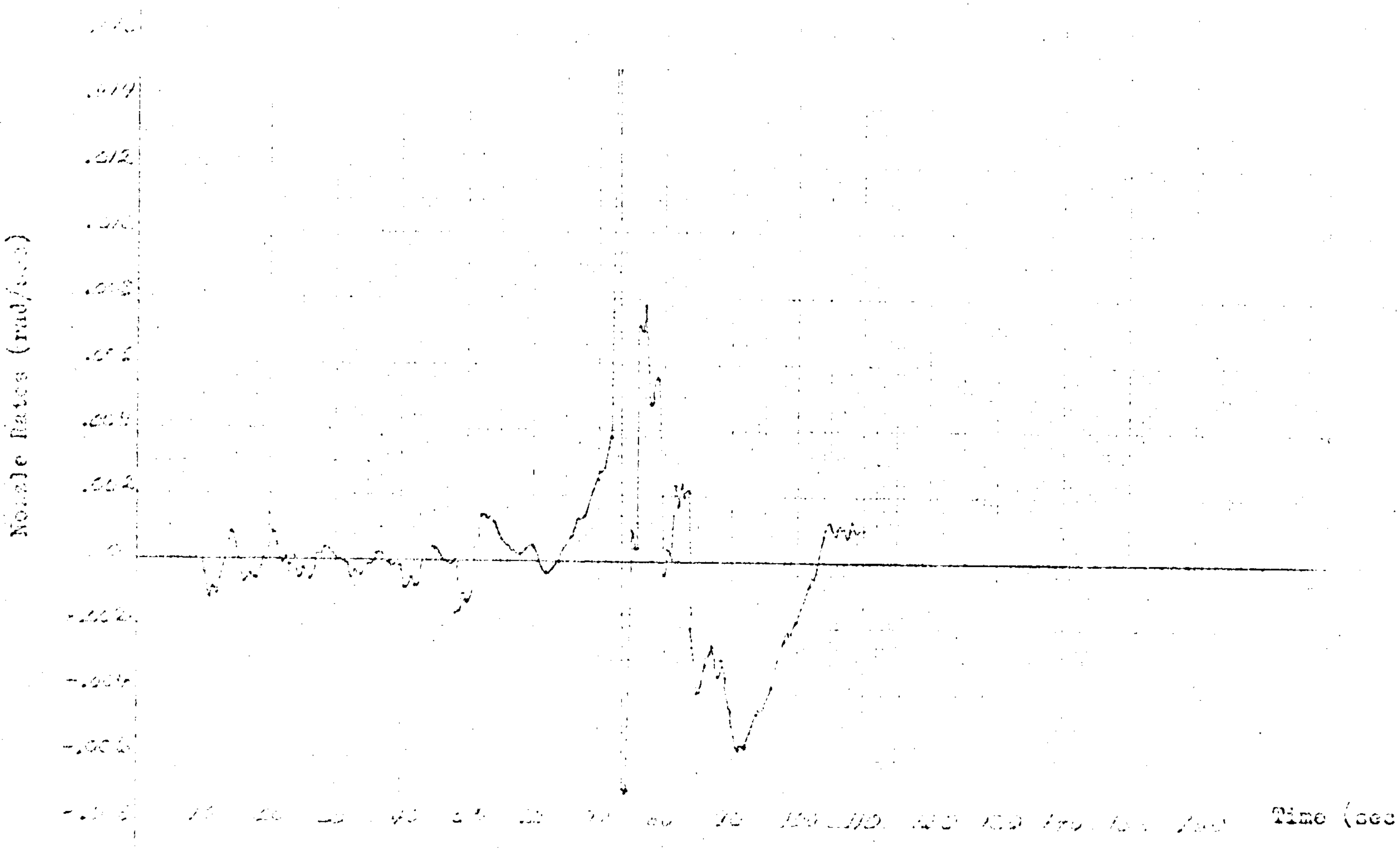
Nozzle Rates (rad/sec)
.014
.012
.010
.008
.006
.004
.002
0
-.002
-.004
-.006
Time (sec)

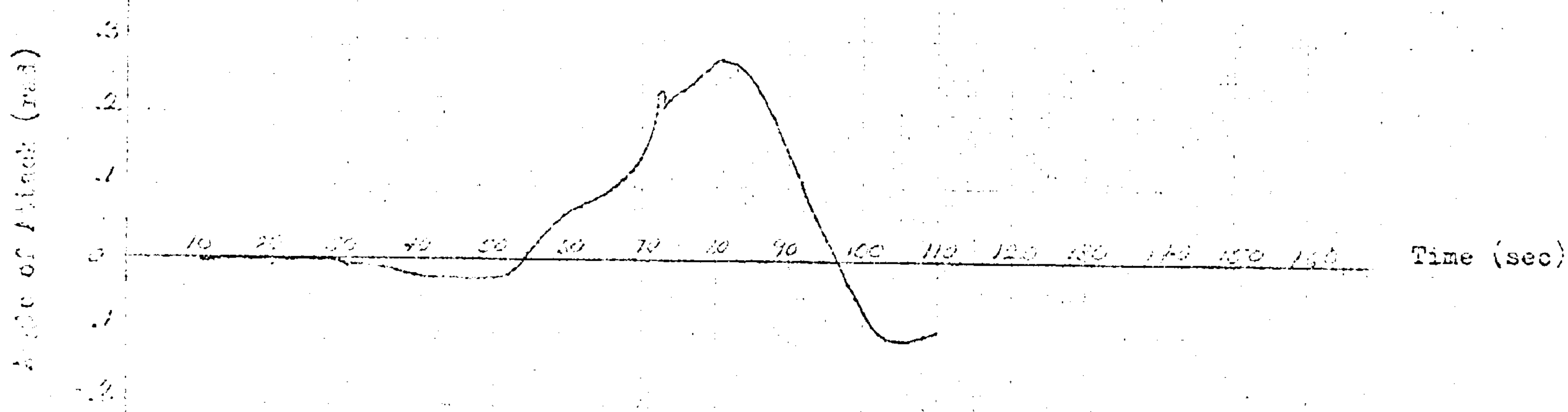
Time (sec)
10 20 30 40 50 60 70 80 90 100 110 120 130 140 150 160
.3 .2 .1 0 -.1 -.2

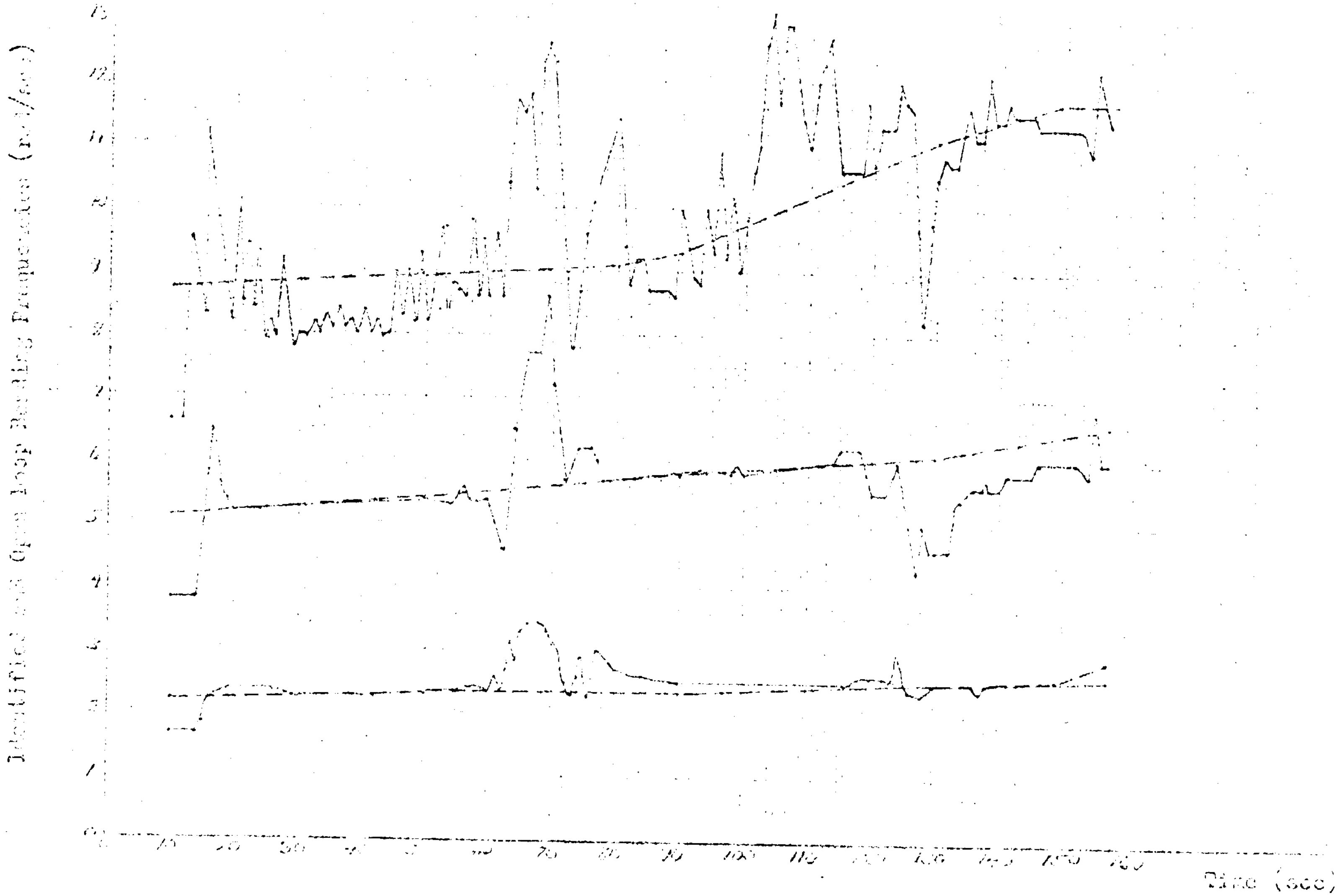
Identified and Open Loop Bending Frequencies (rad/sec)
Time (sec)

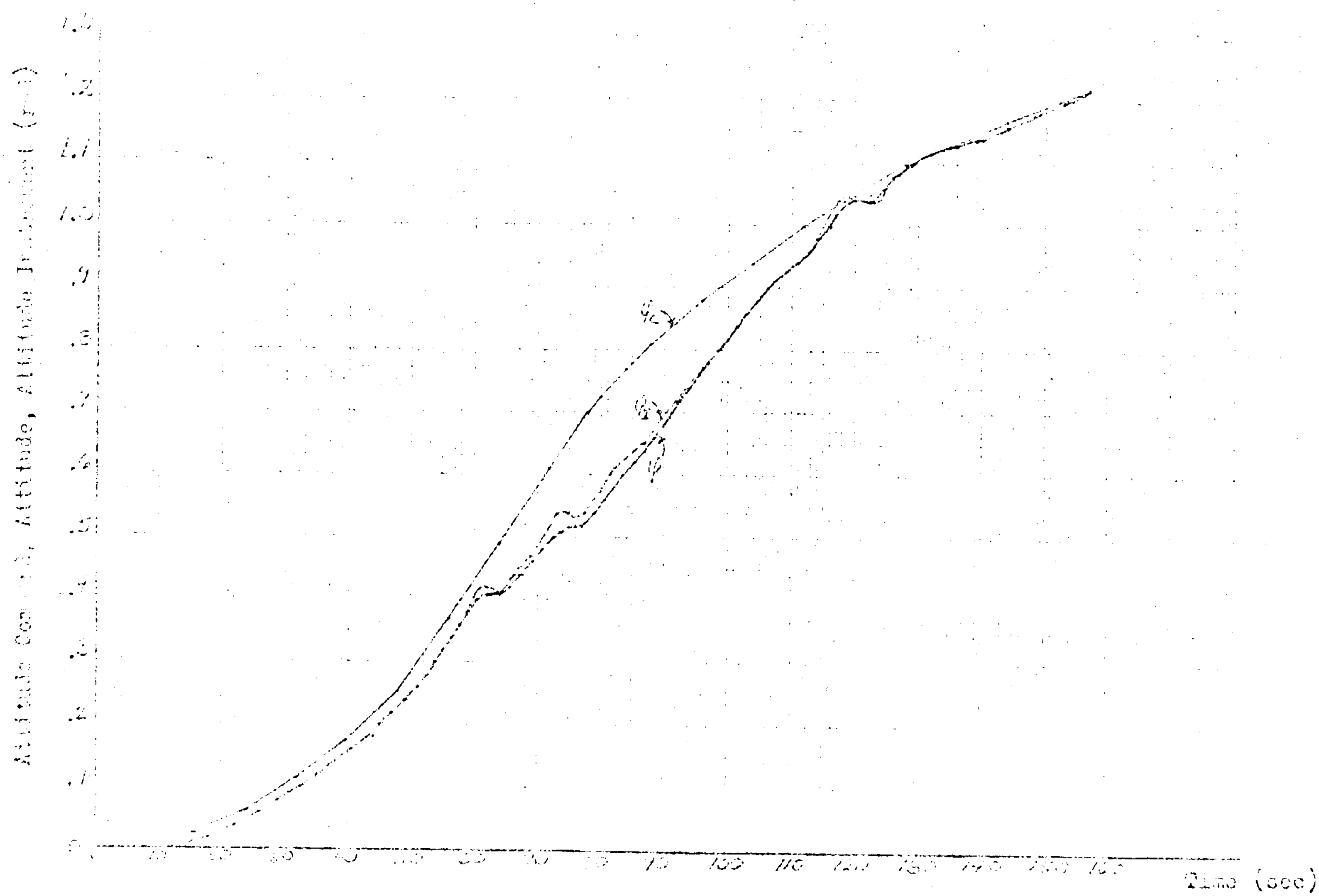

Figure [illegible]. [illegible] Configuration [illegible]

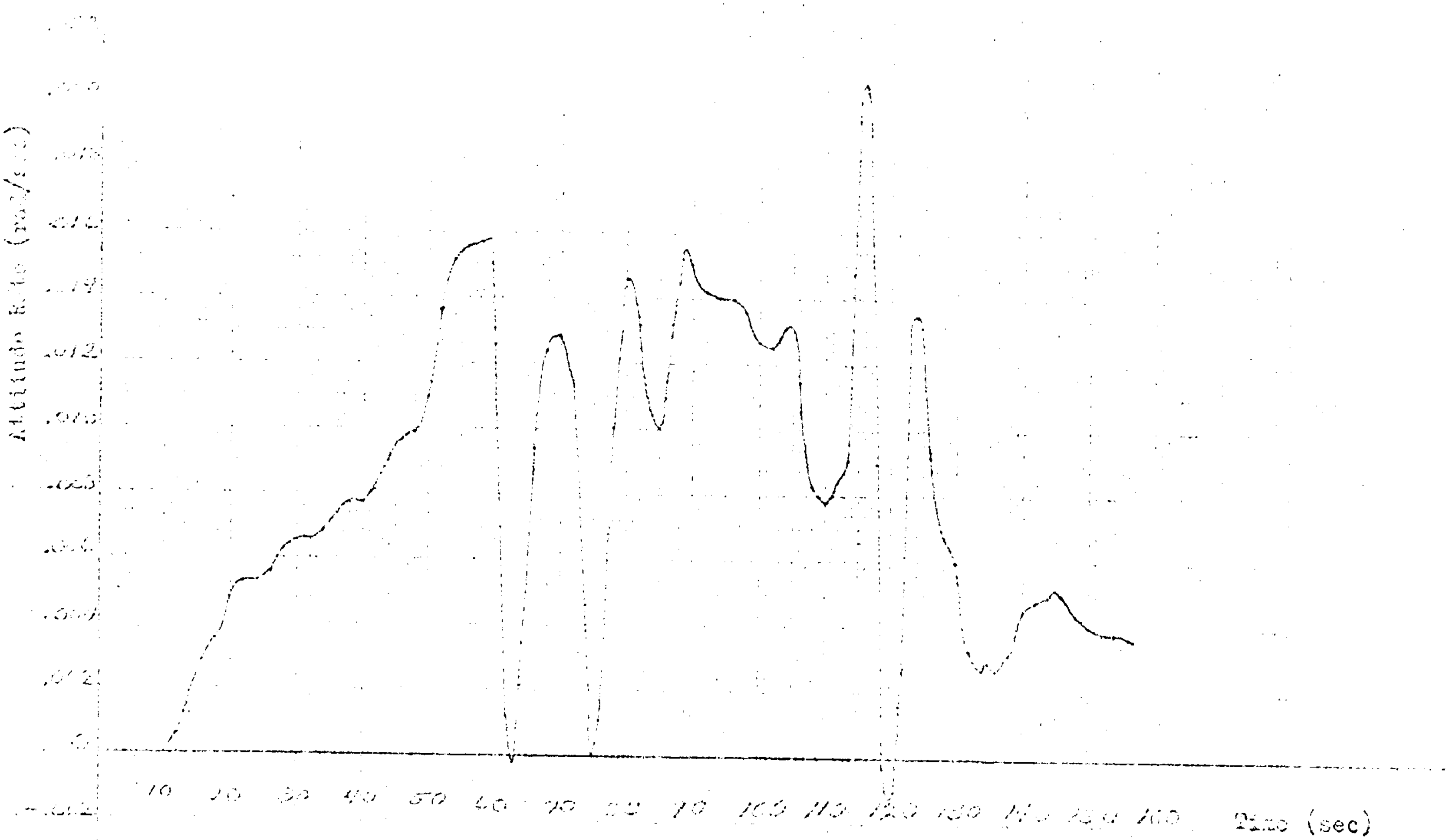
Attitude Rate (rad/sec)
Time (sec)

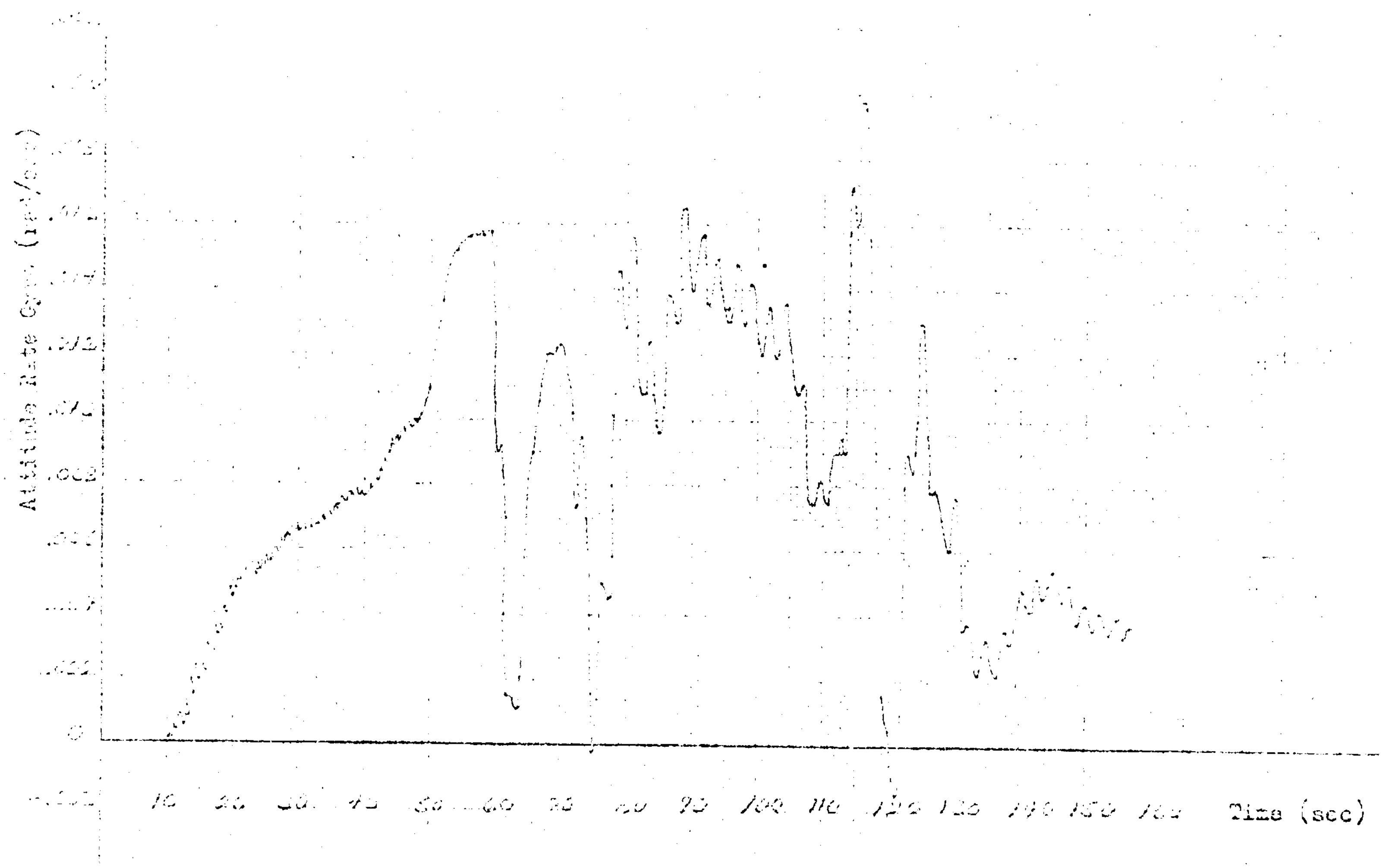
Attitude Rate Gyro (rad/sec)
Time (sec)

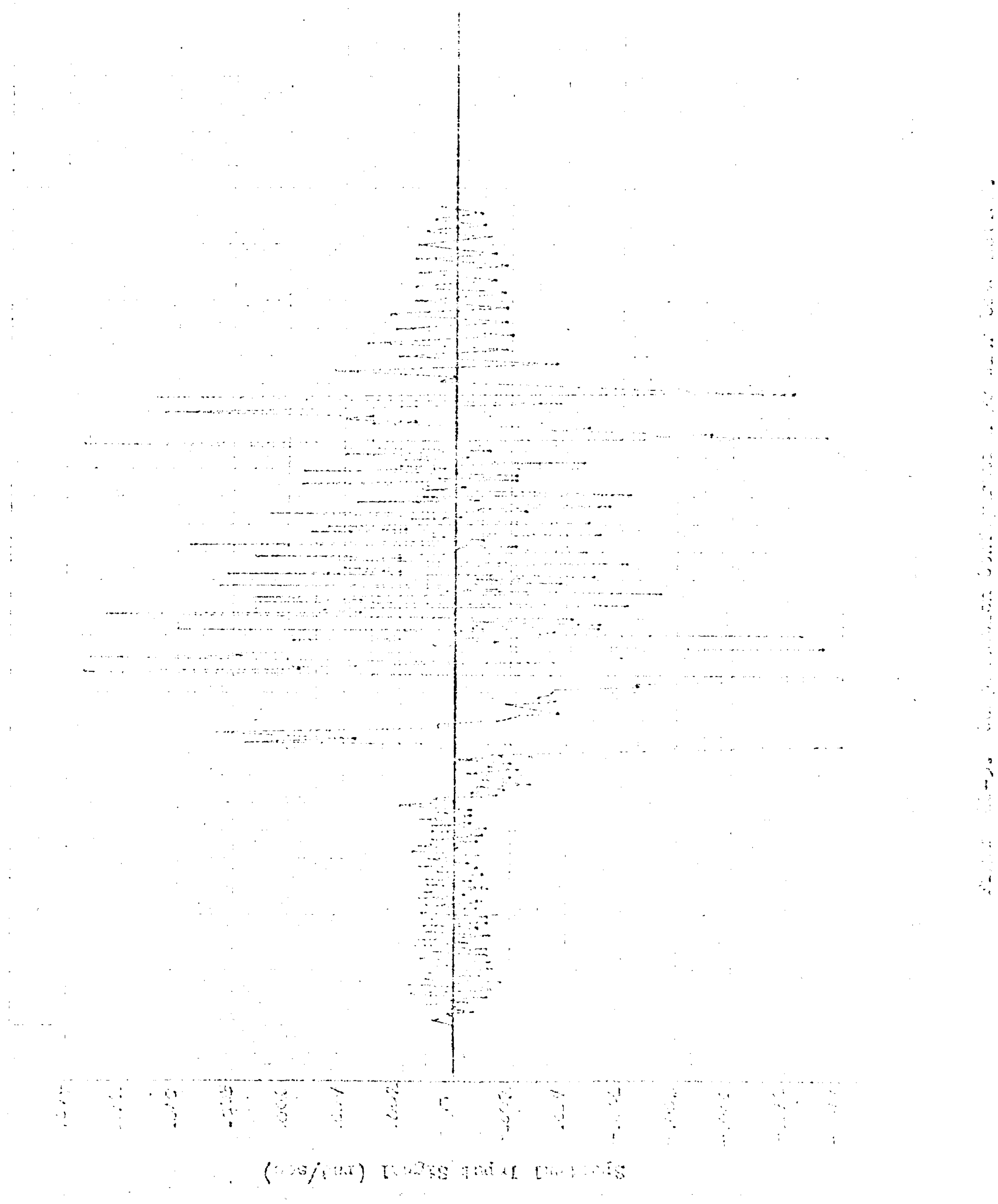

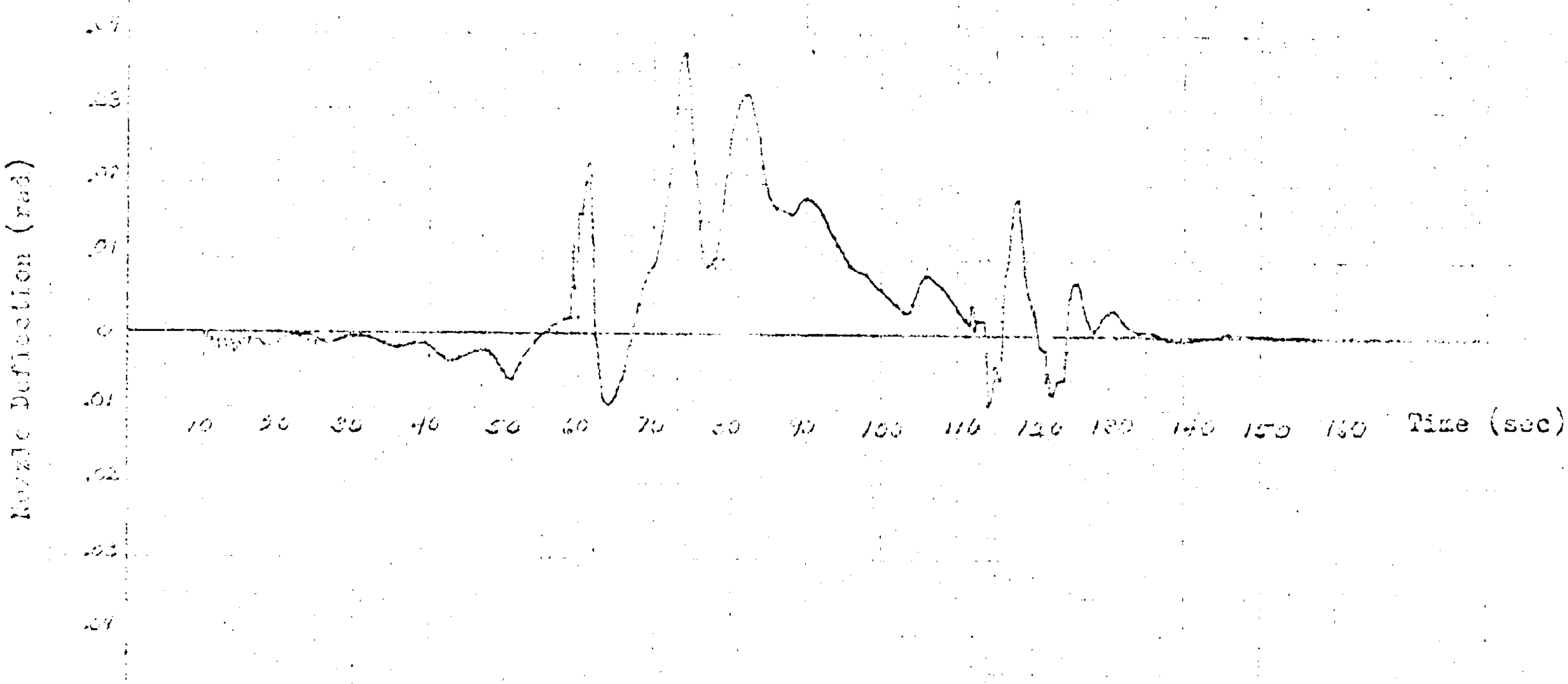
Nozzle Deflection (rad)
.04
.03
.02
.01
0
.01
.02
.03
.04
10
20
30
40
50
60
70
80
90
100
110
120
130
140
150
160
Time (sec)

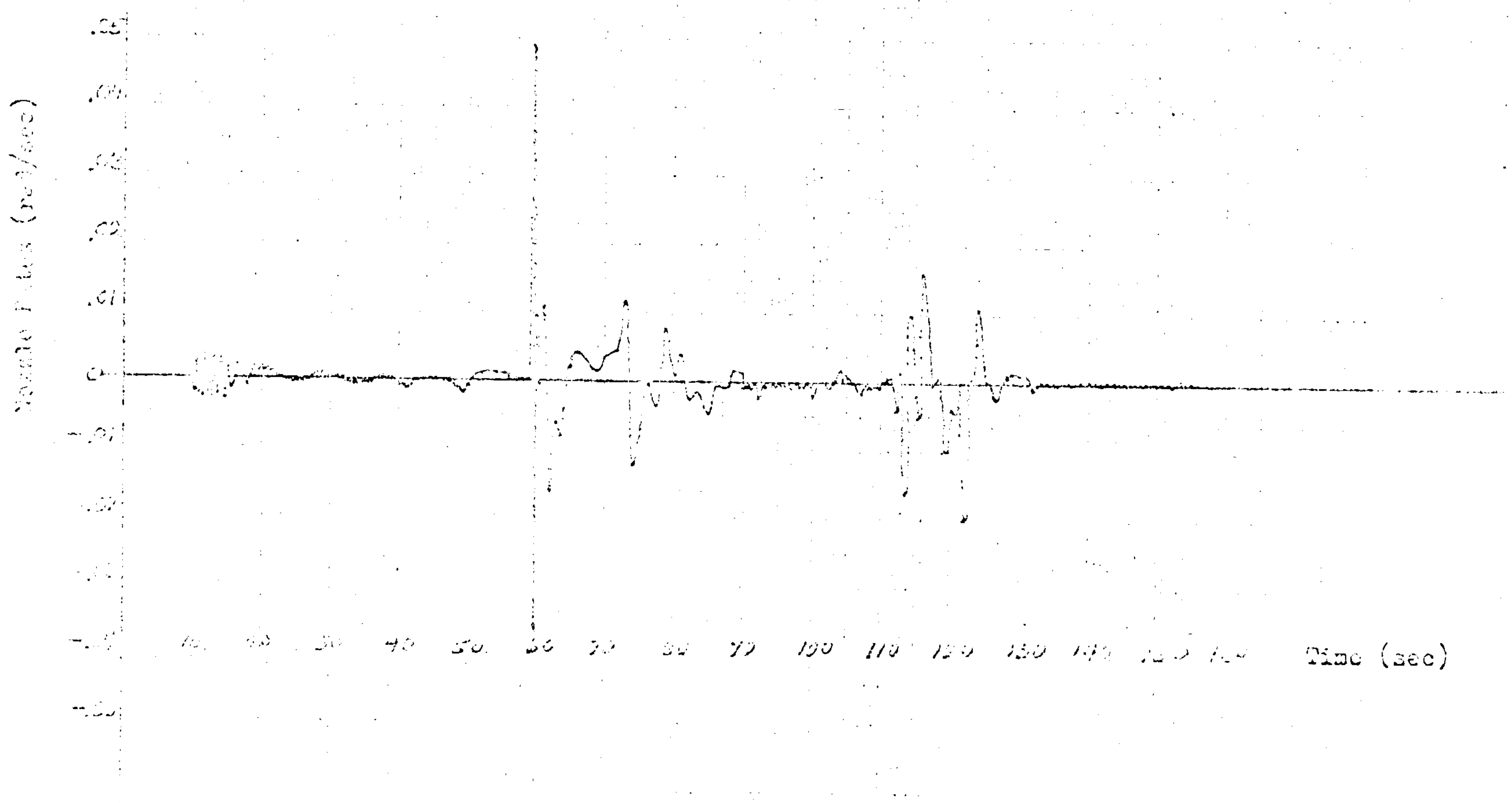
Time (sec)

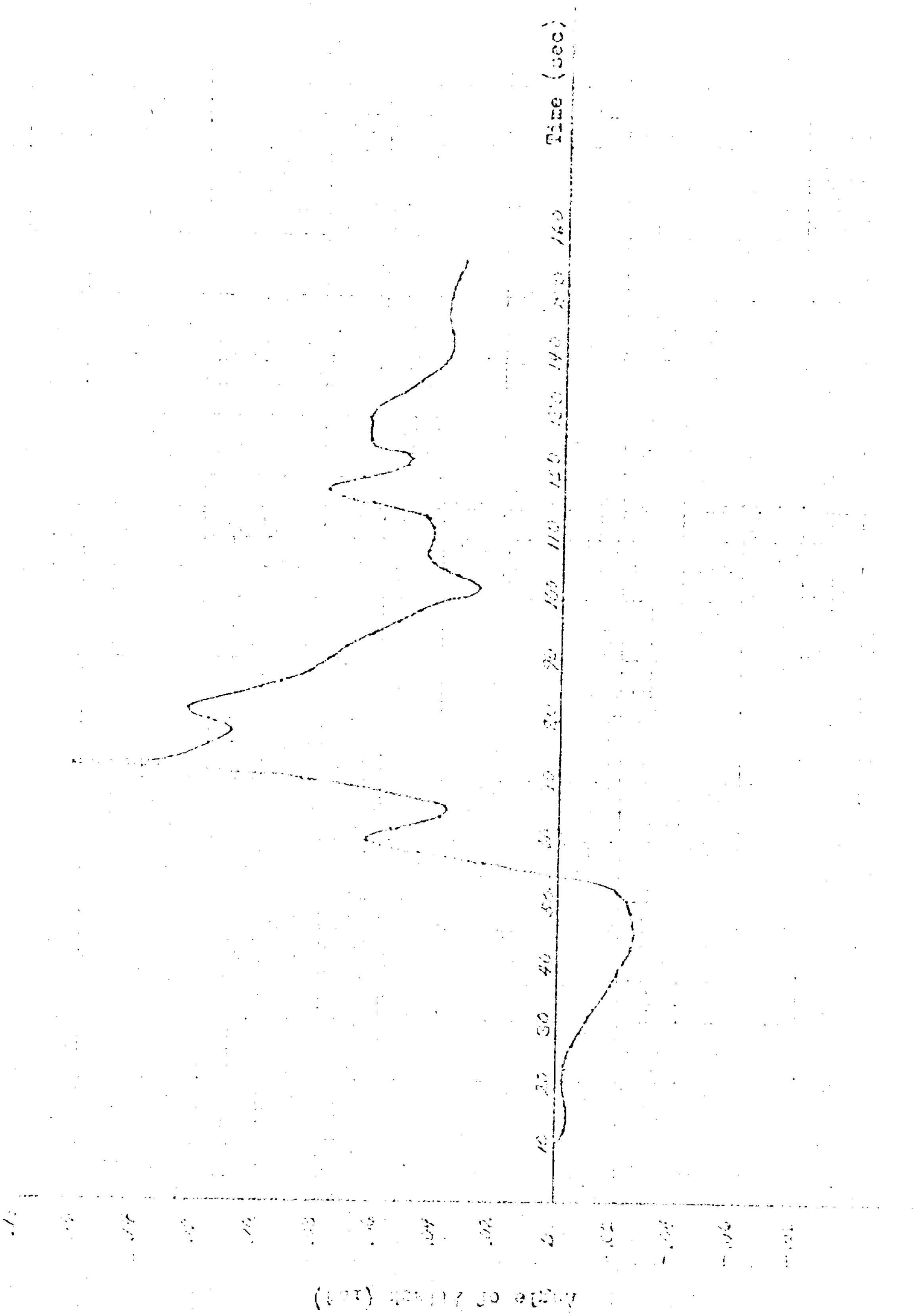
Time (sec)

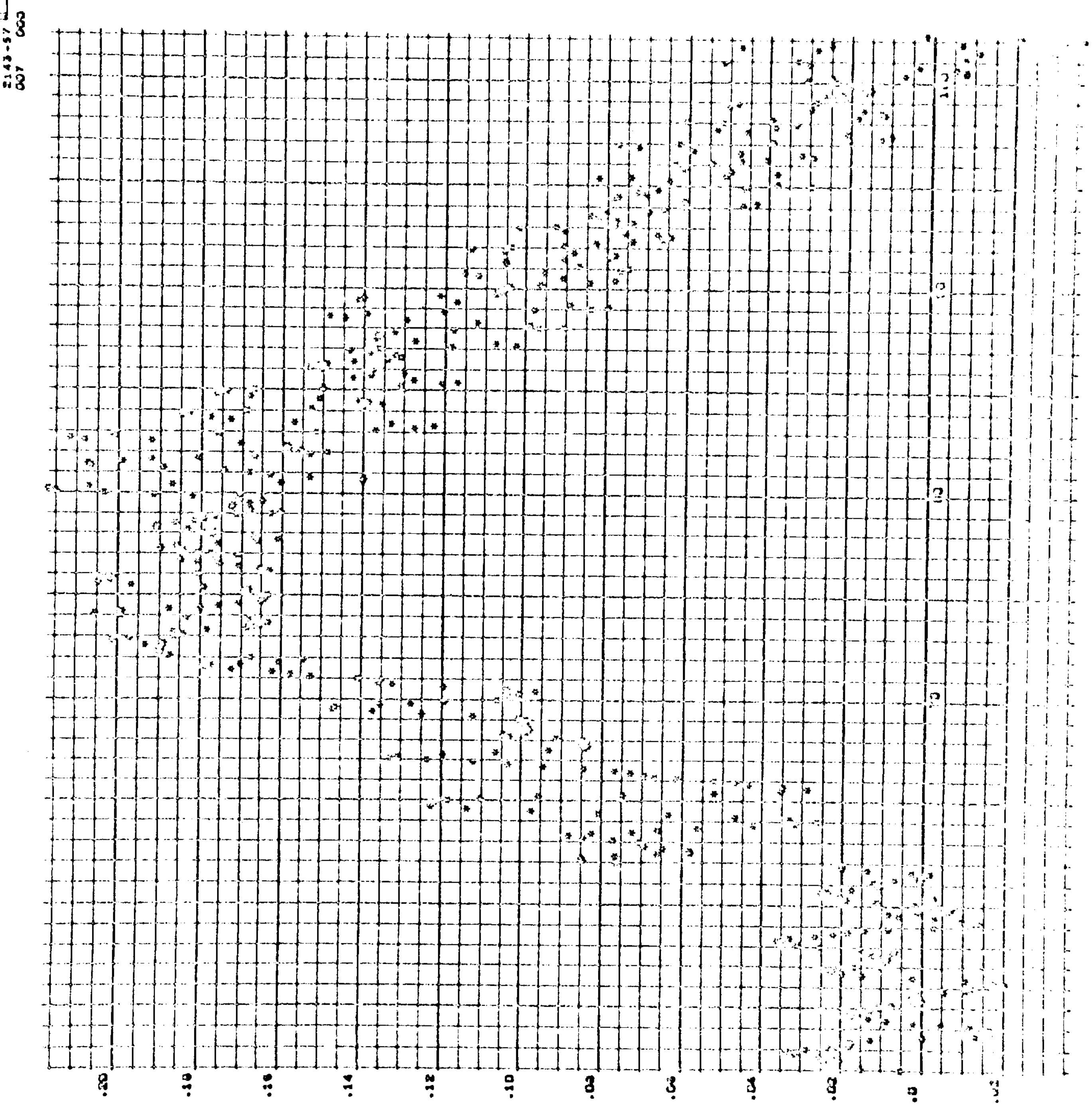

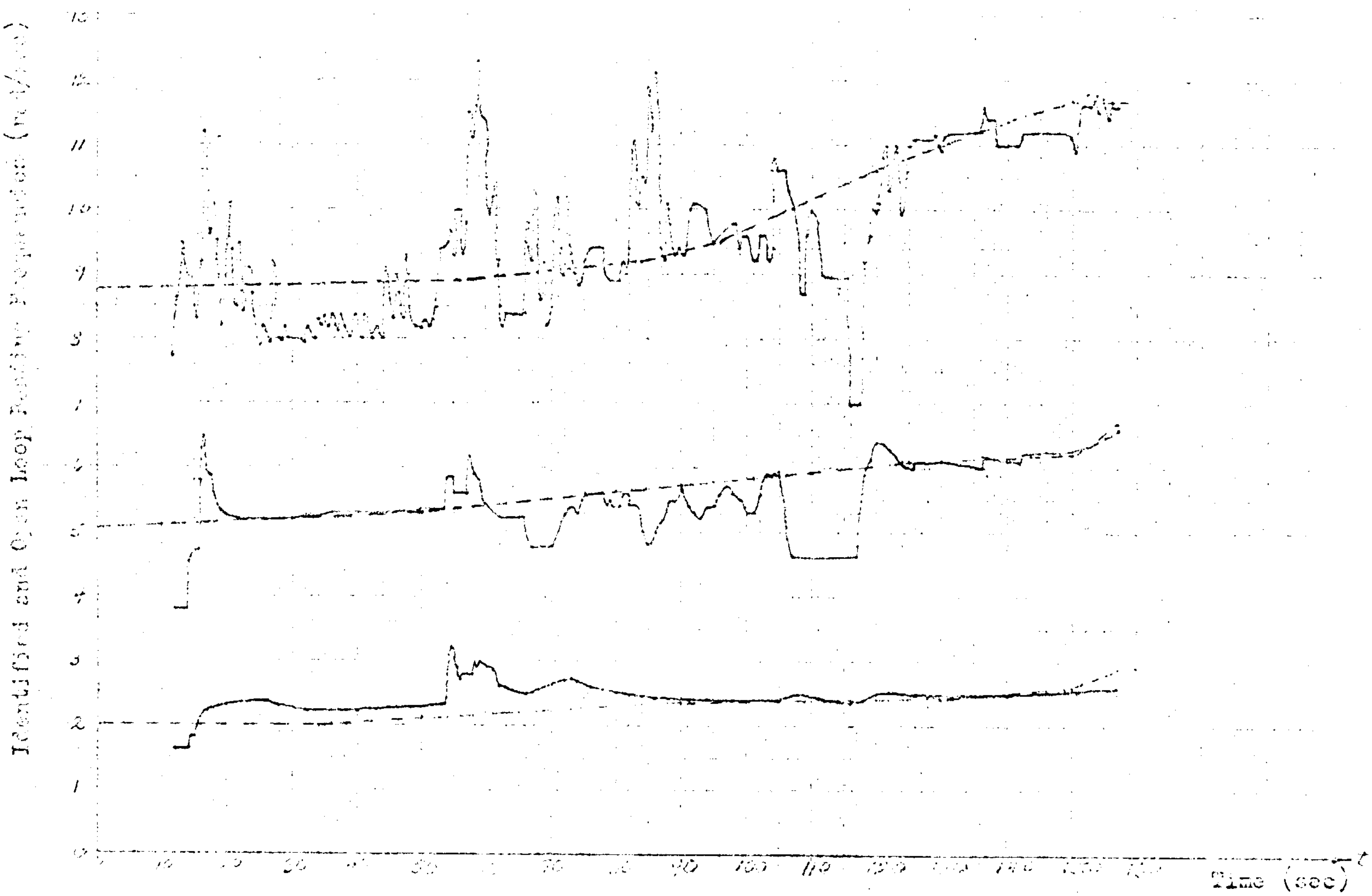
Identified and Open Loop Rolling Responses (rad/sec)
Time (sec)
t
0
1
2
3
4
5
6
7
8
9
10
11
12
13

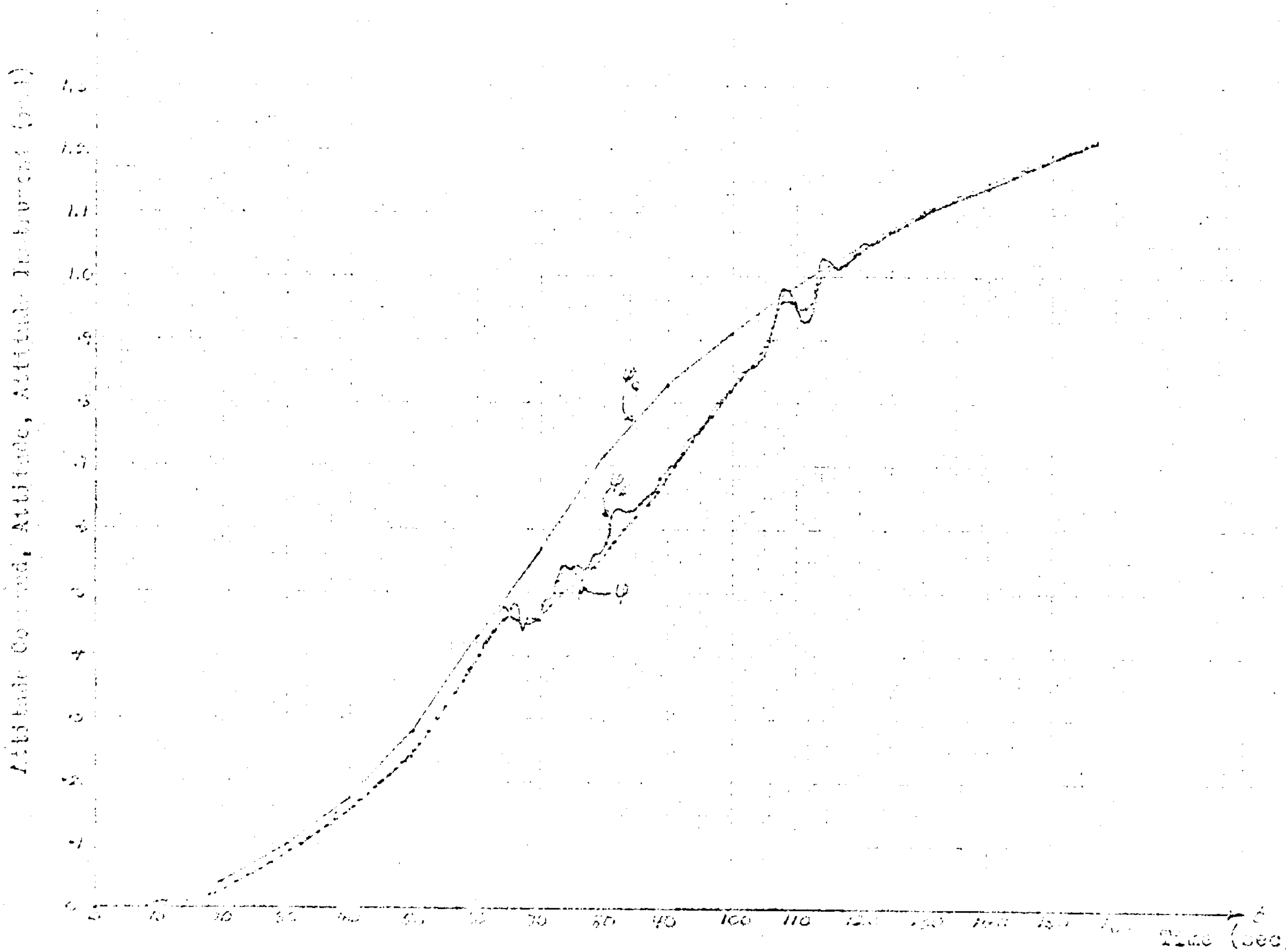
Time (sec)

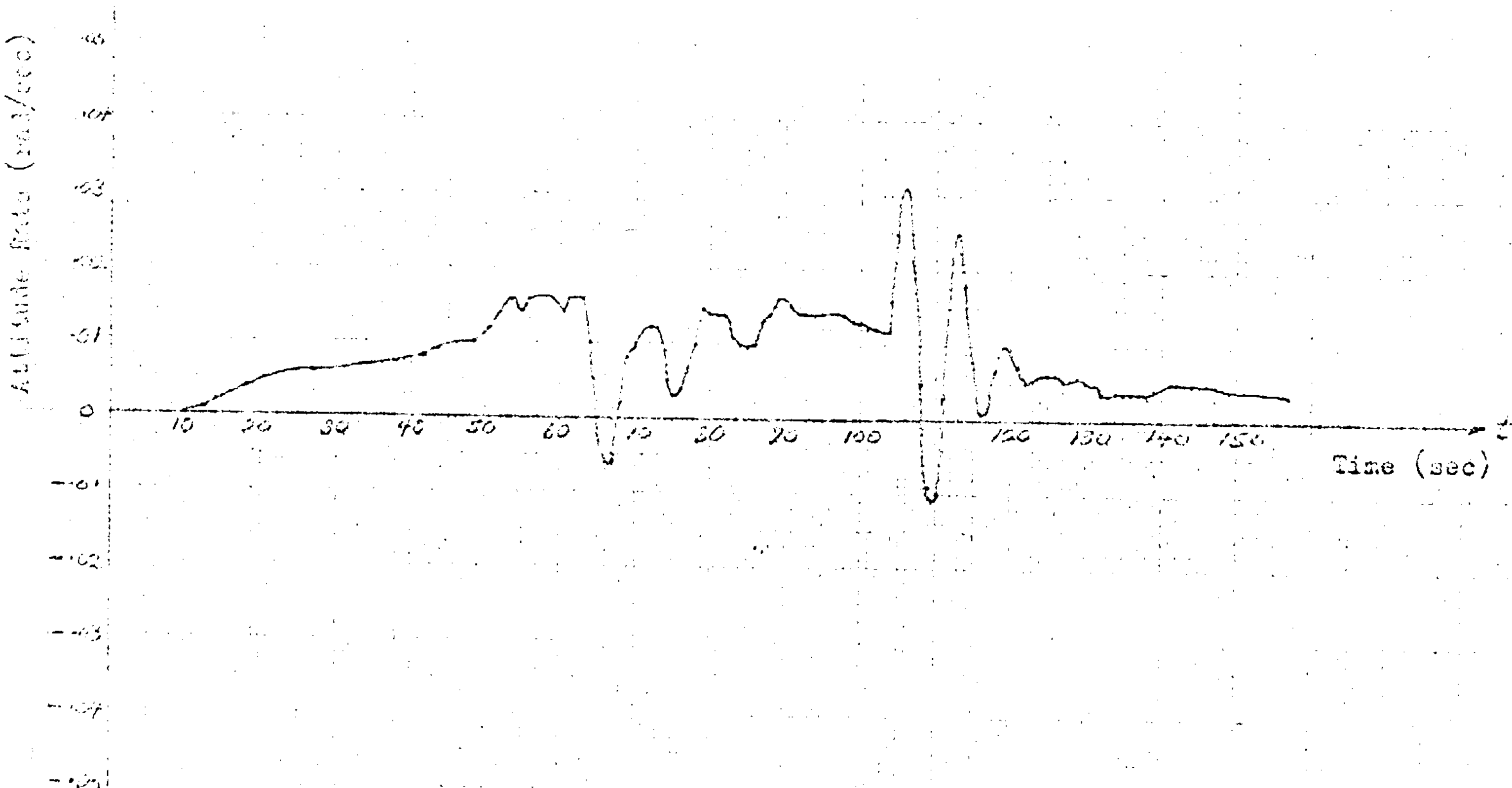
Attitude Rate (rad/sec)
.05
.04
.03
.02
.01
0
-.01
-.02
-.03
-.04
-.05
10
20
30
40
50
60
70
80
90
100
120
130
140
150
t
Time (sec)

[illegible]

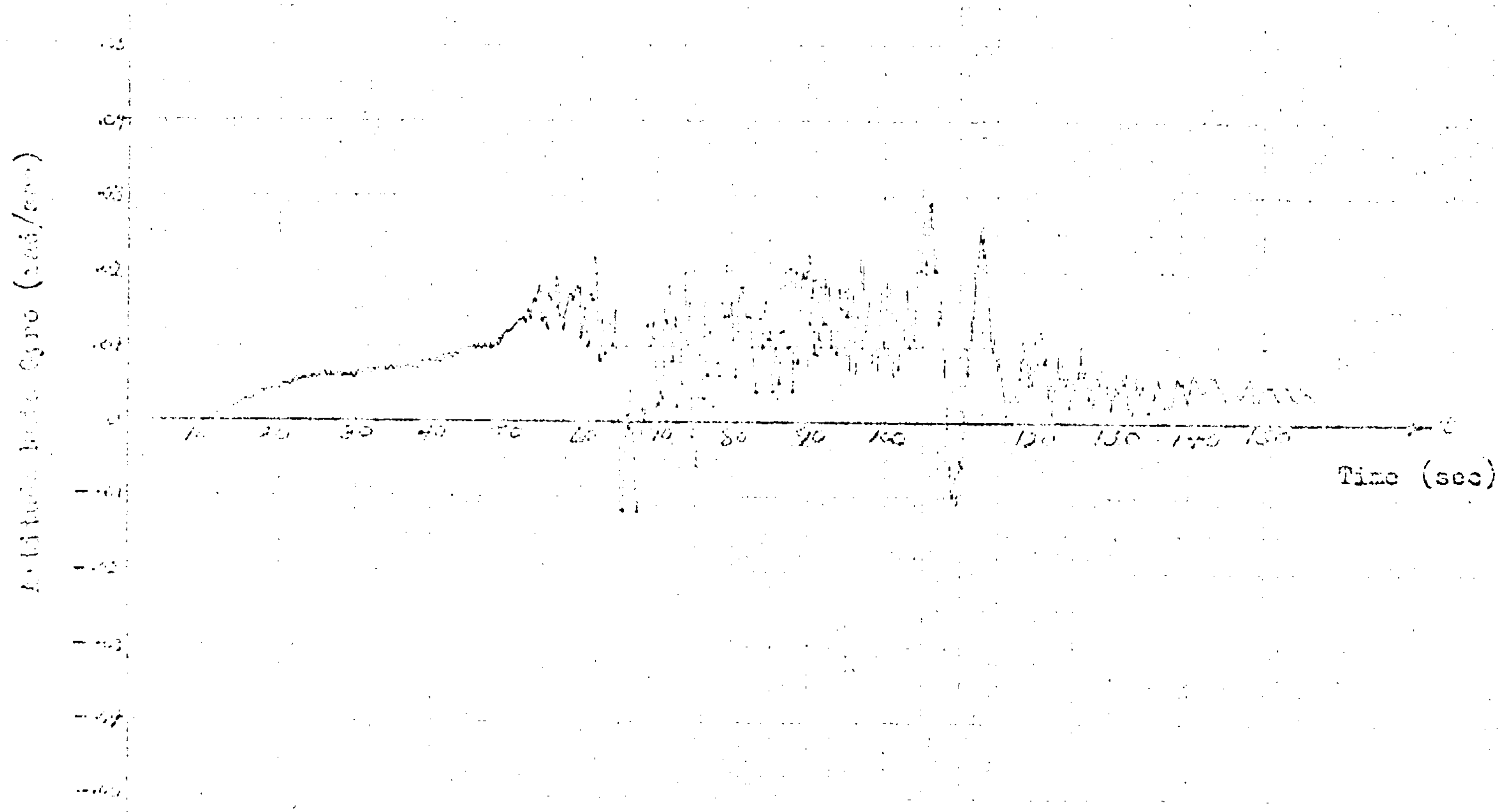
Time (sec)

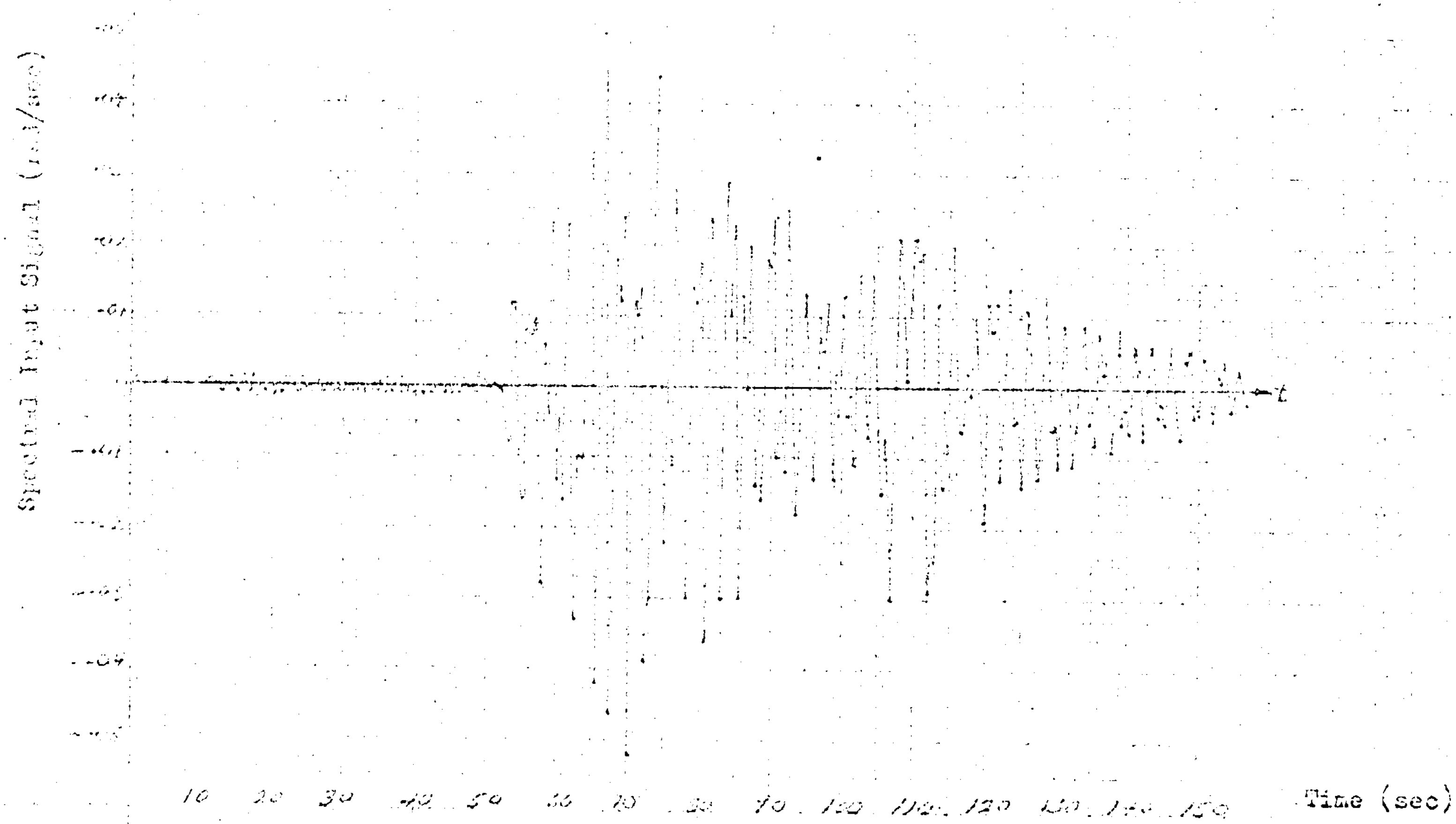
Spectral Input Signal (rad/sec)
t
10
20
30
40
50
70
Time (sec)

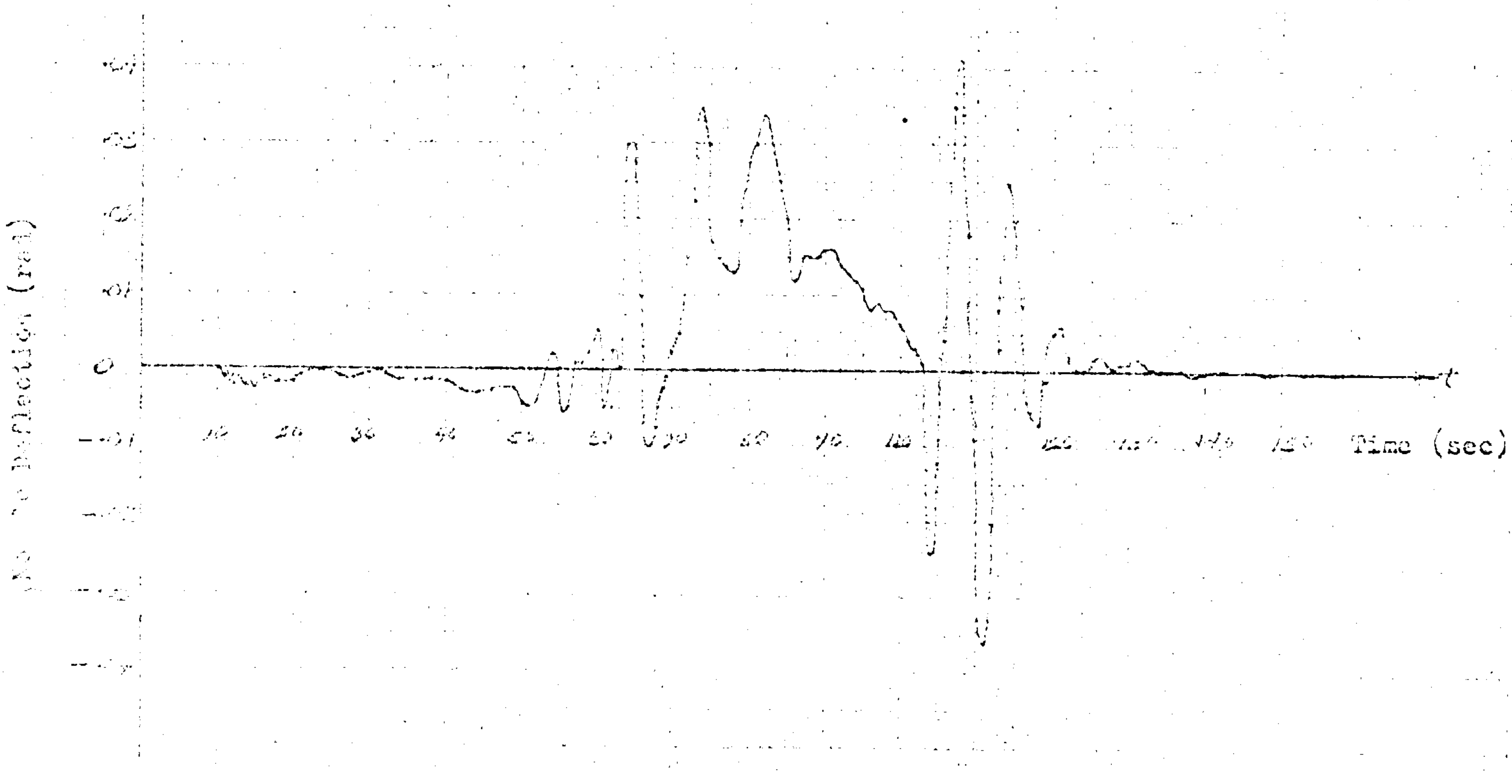
0
Time (sec)

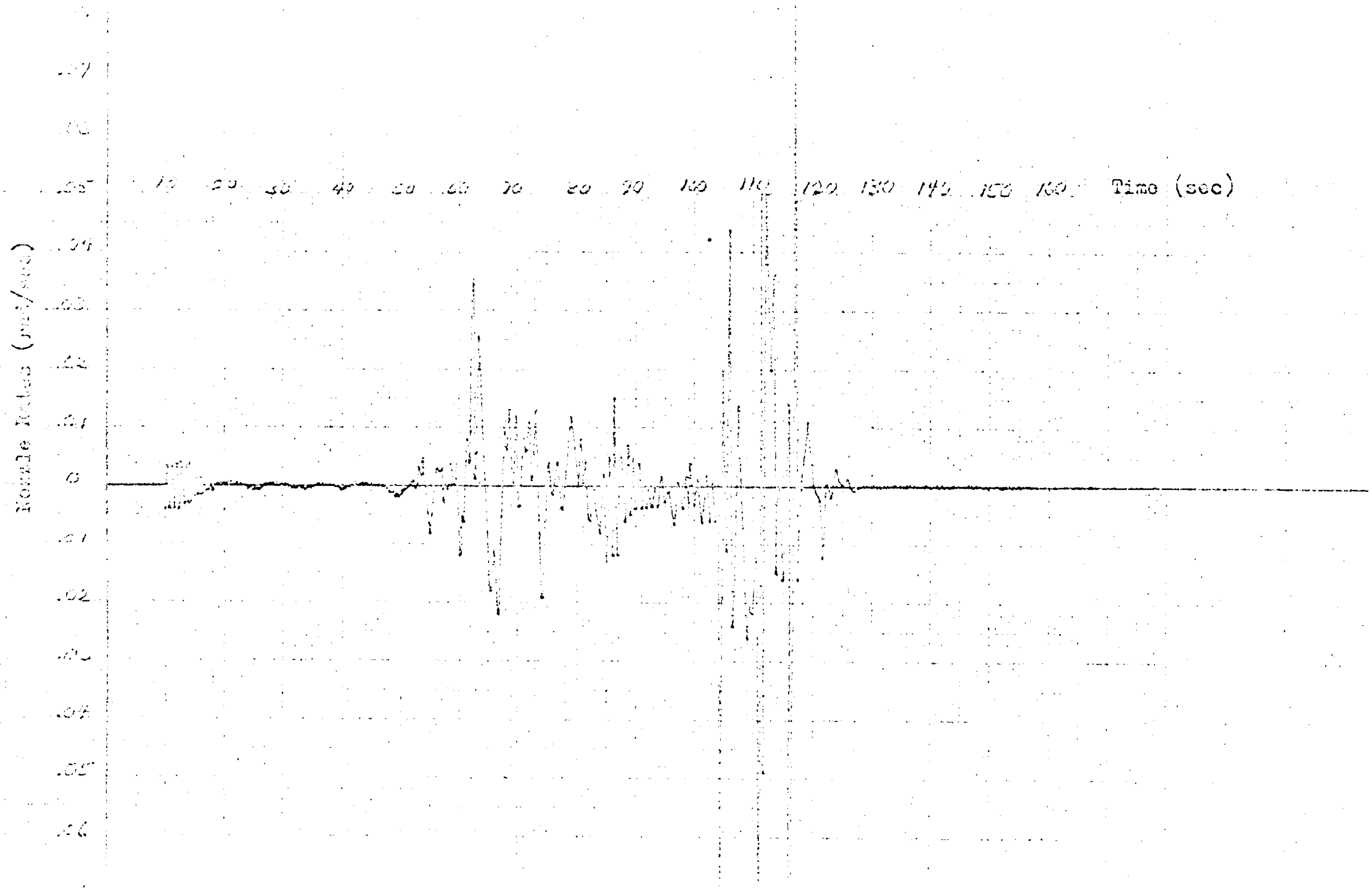

Time (sec)

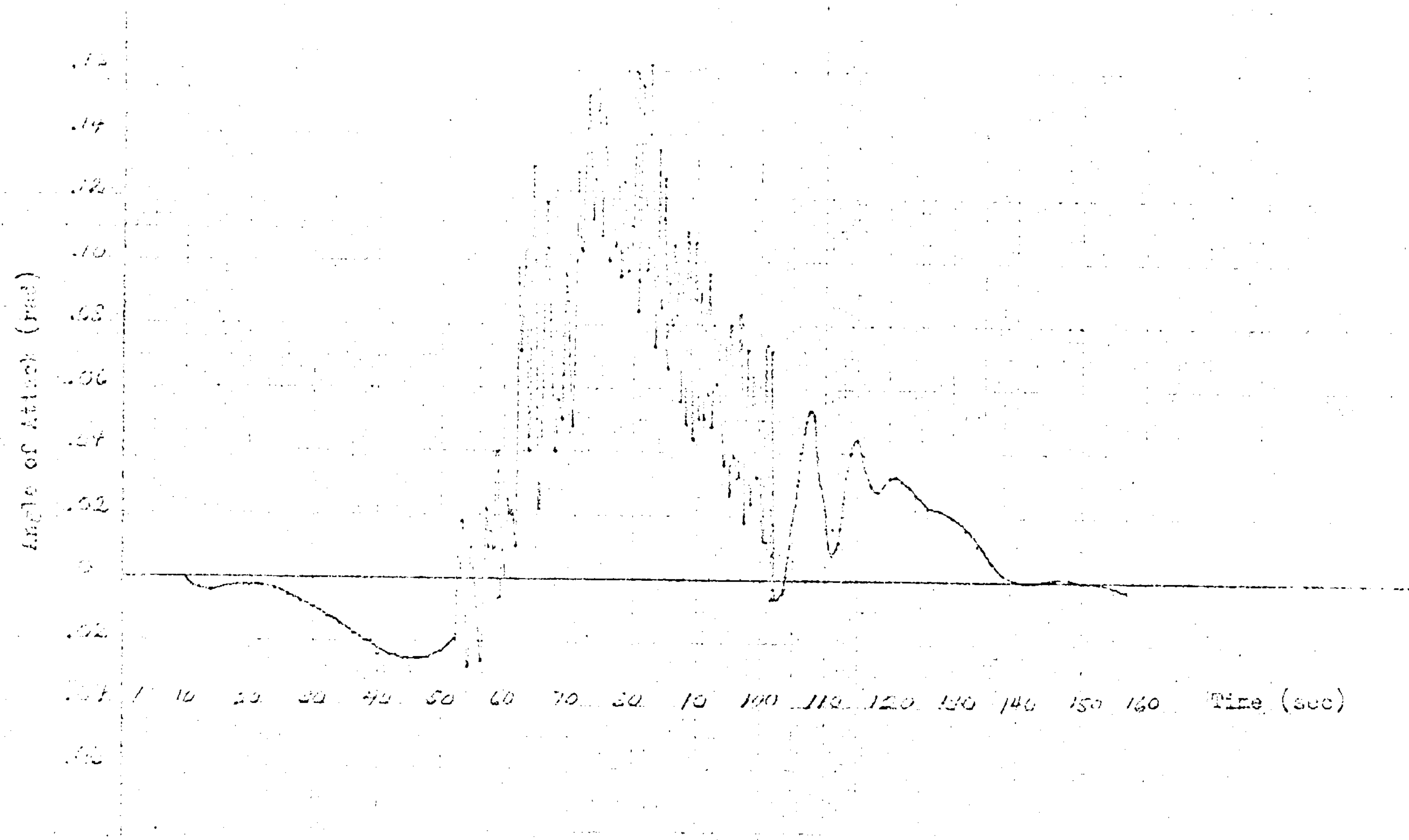
Angle of Attack (rad)
Time (sec)

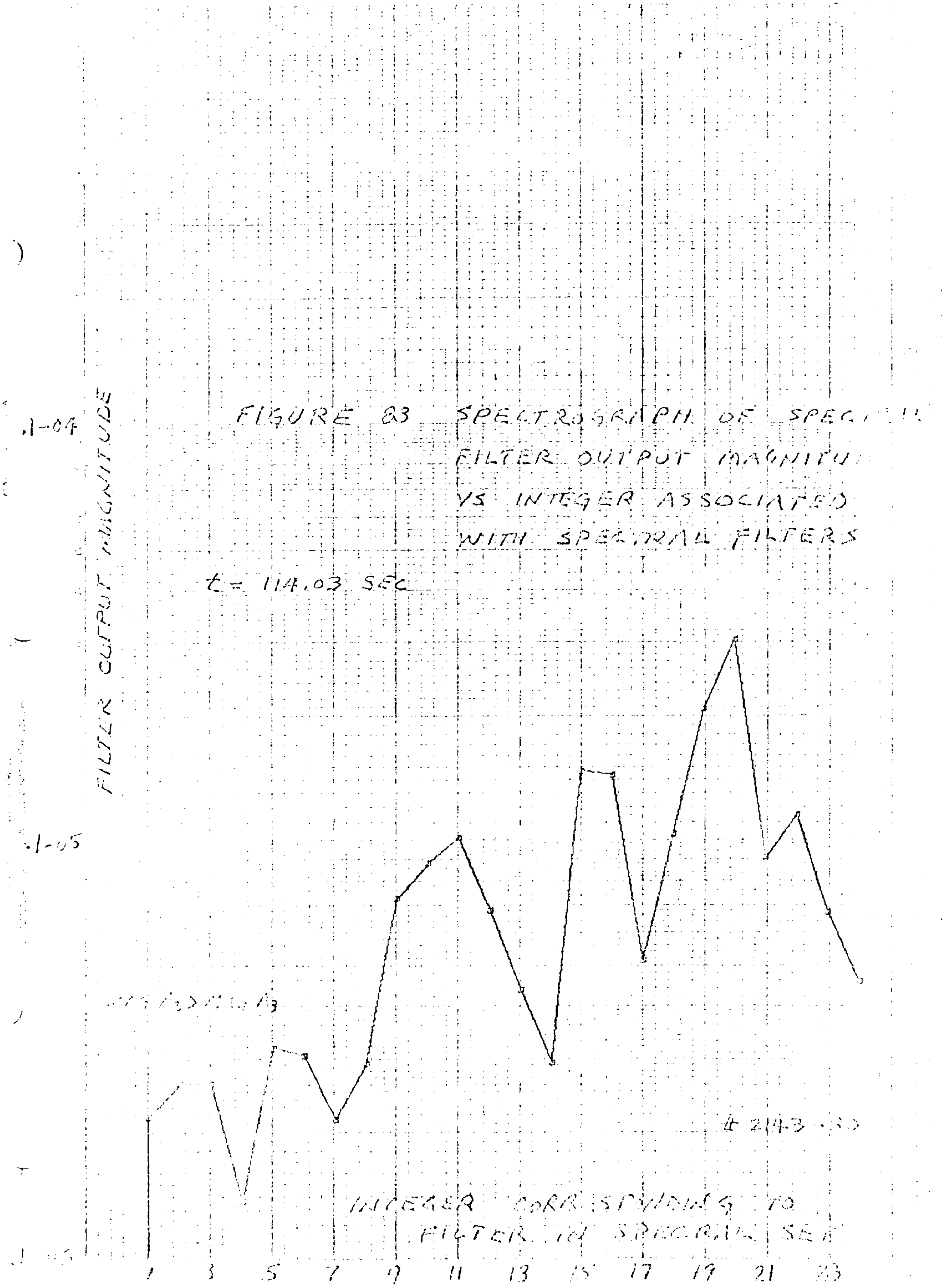
FIGURE 83 SPECTROGRAPH OF SPEC
FILTER OUTPUT MAGNITU
VS INTEGER ASSOCIATED
WITH SPECTRAL FILTERS
t = 114.03 SEC
FILTER OUTPUT MAGNITUDE
.1-04
.1-05
INTEGER CORRESPONDING TO
FILTER IN SPECTRAL SET
1
3
5
7
9
11
13
15
17
19
21
23

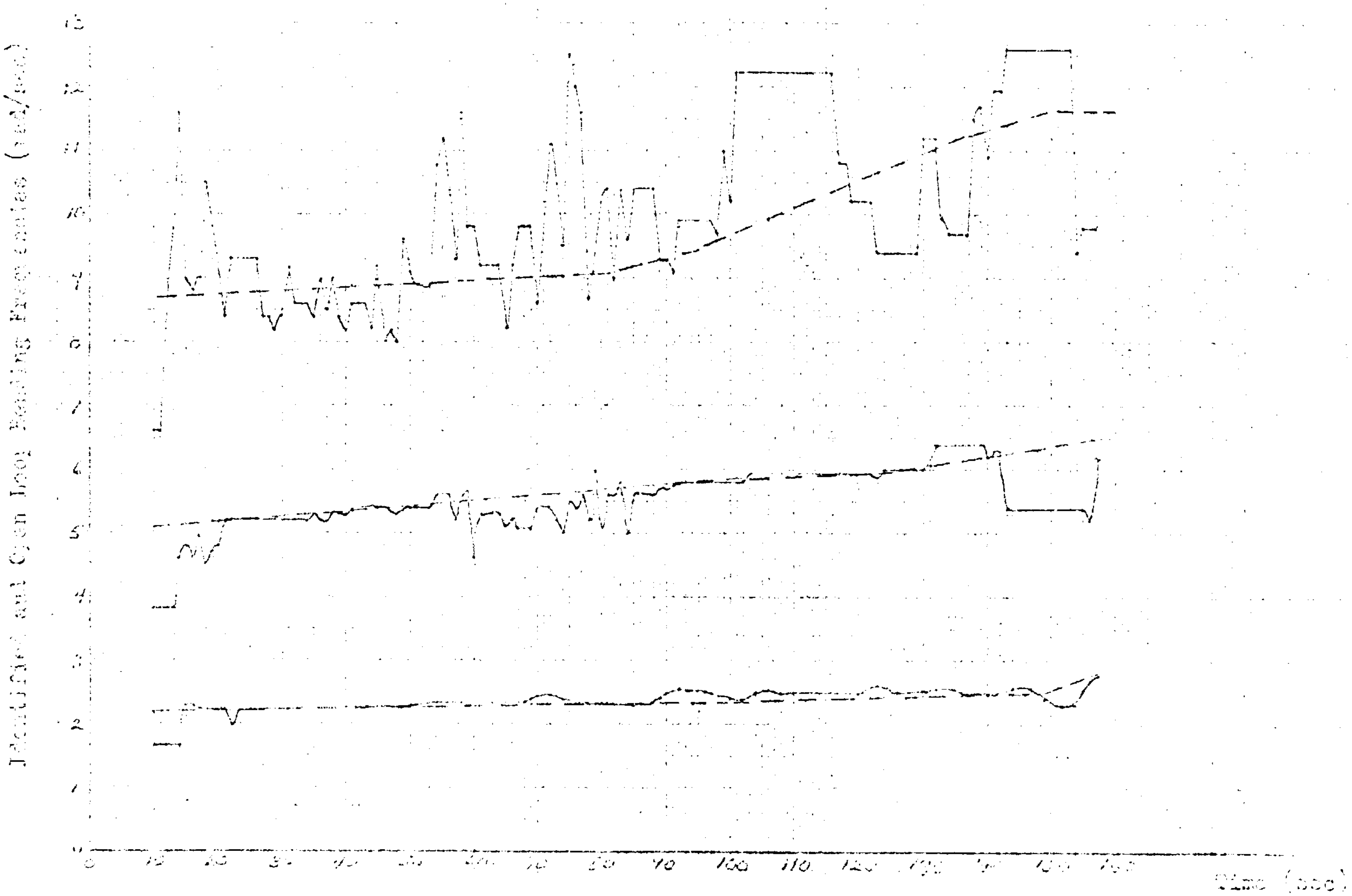
Identified and Open Loop Bending Frequencies (rad/sec)
Time (sec)

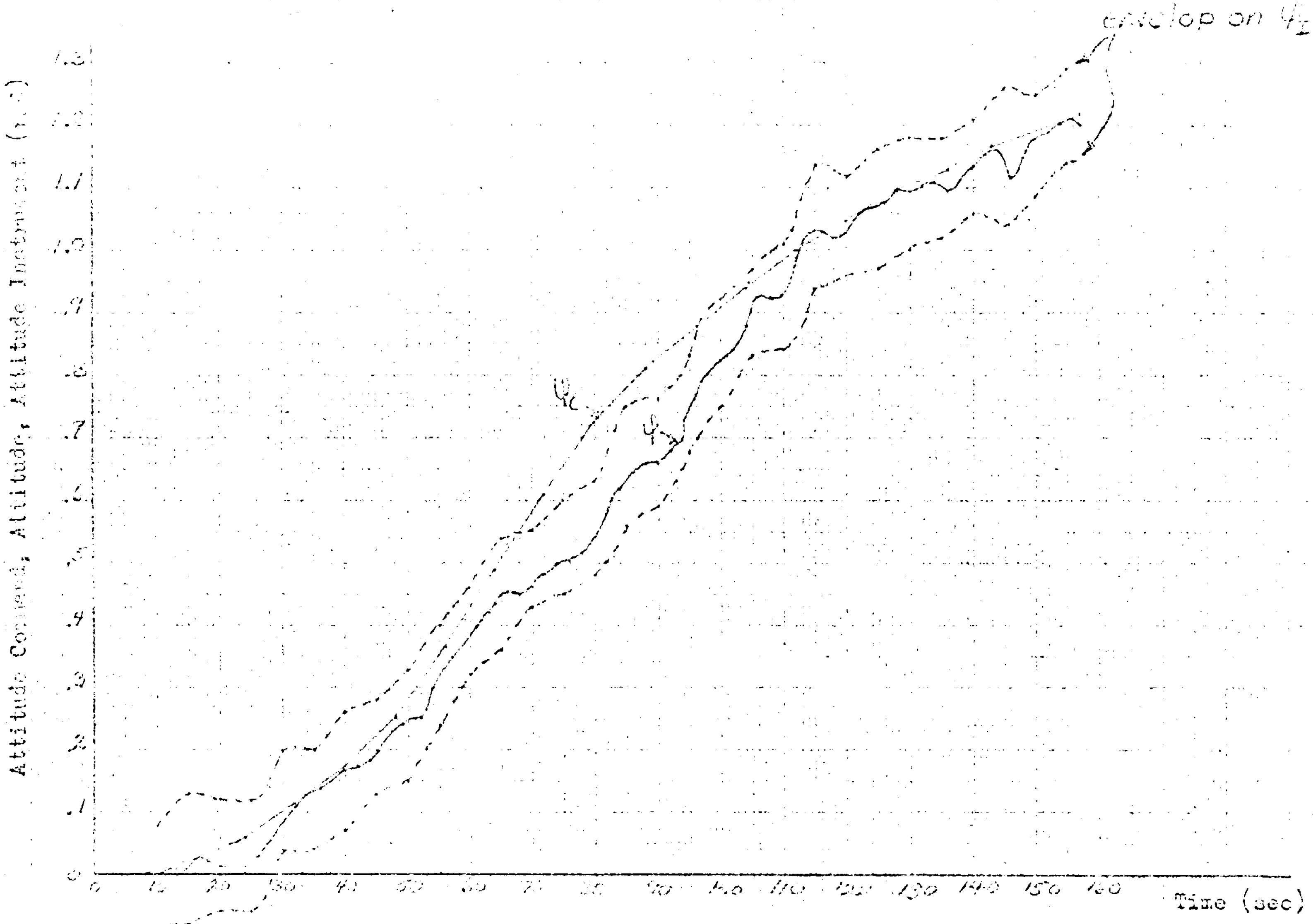

Figure [illegible]. [illegible] Configuration [illegible] with Instrument [illegible]

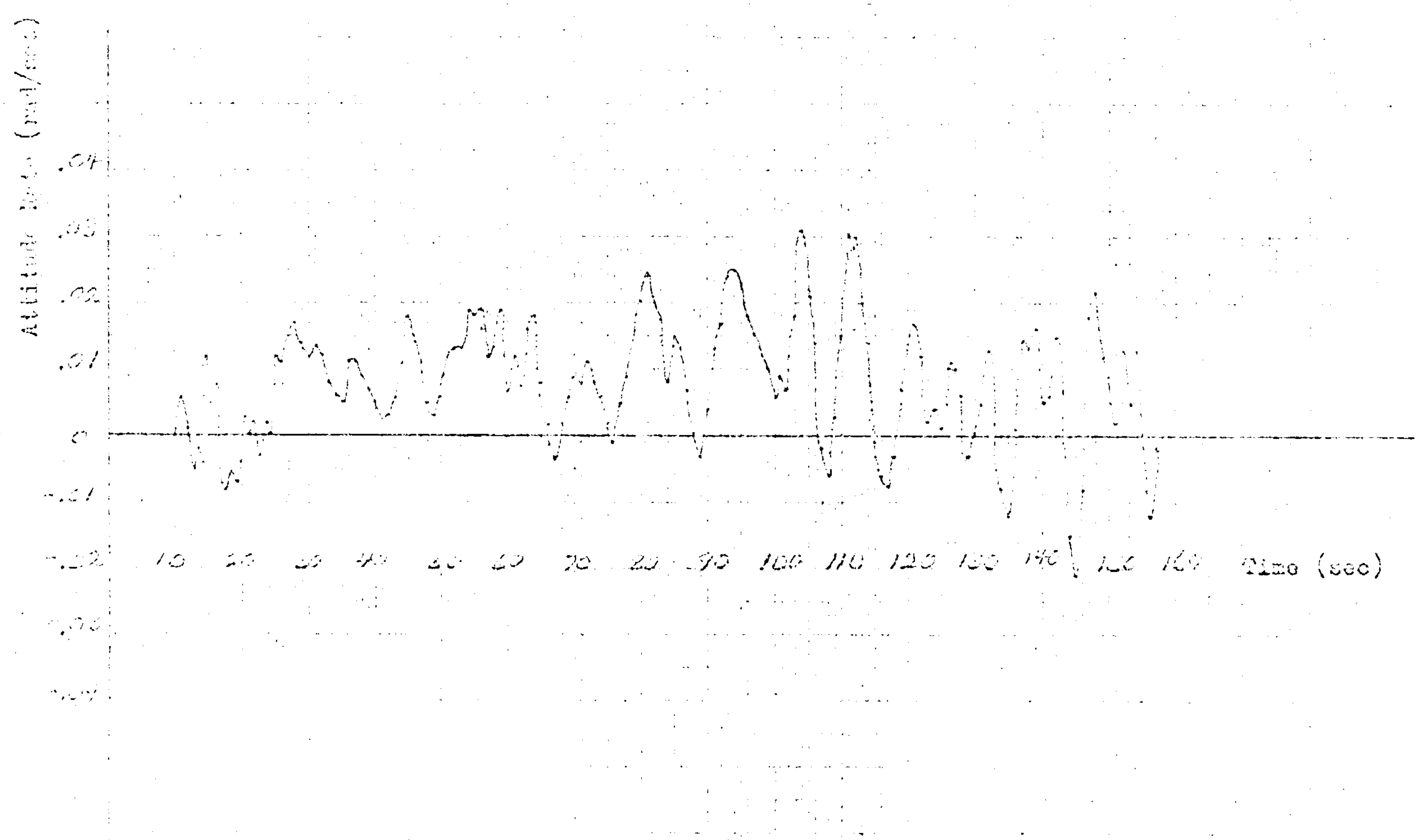
Attitude Rate (rad/sec)
.04
.03
.02
.01
0
-.01
-.02
10
20
30
40
50
60
70
80
90
100
110
120
130
140
150
160
Time (sec)

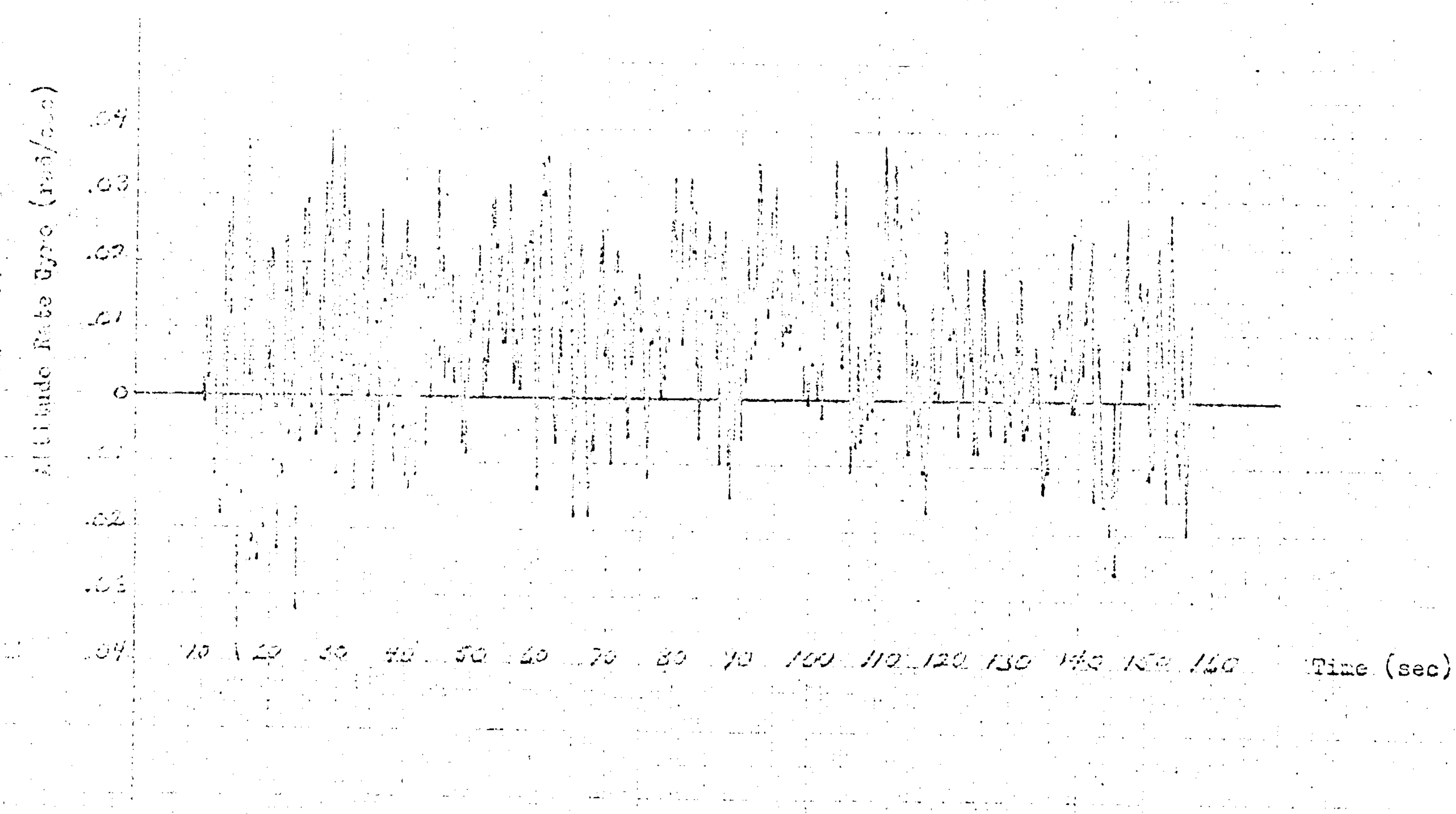

Figure 6-41 Compensated Configuration #2 with Instrument Noise

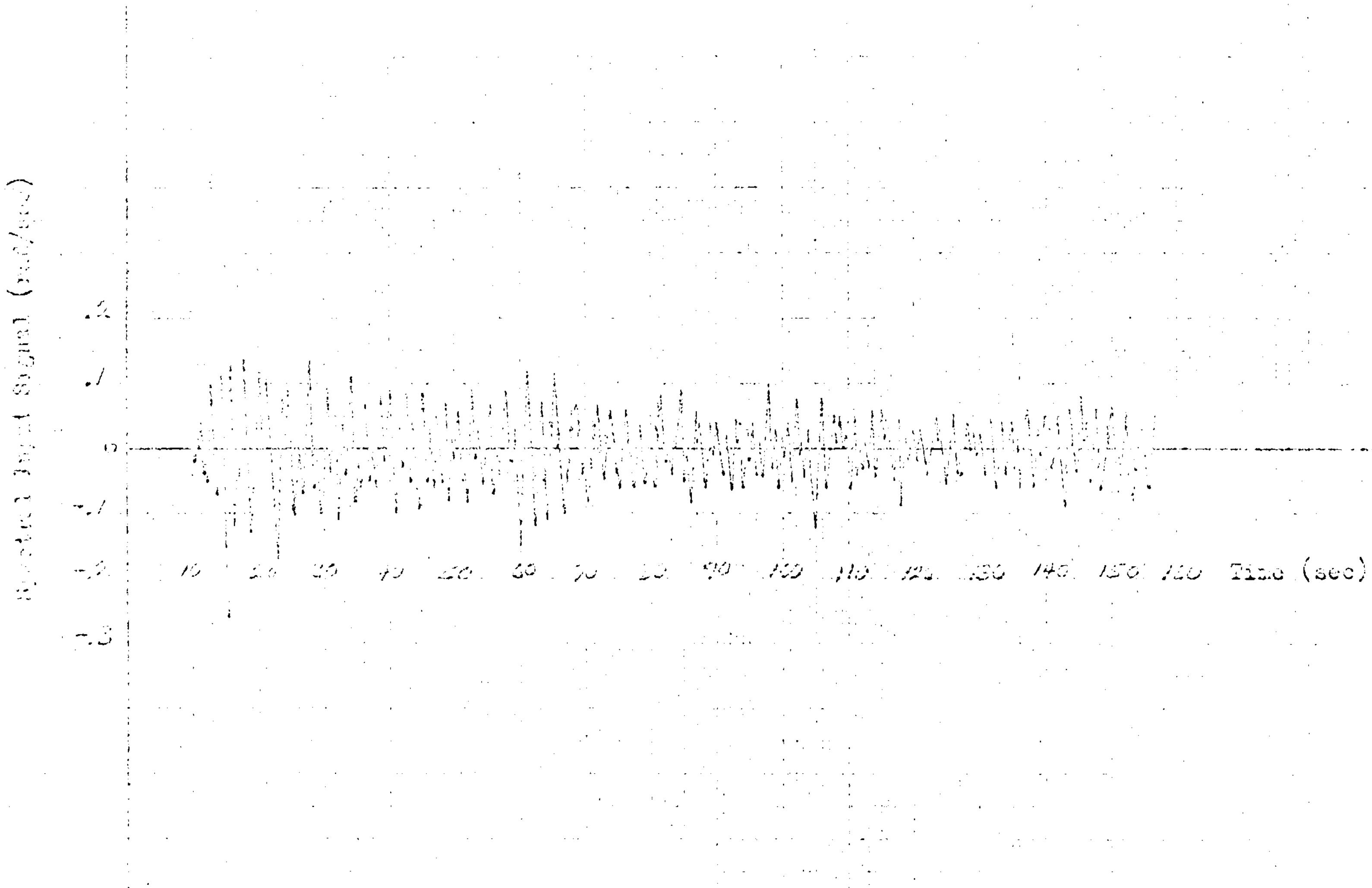
.2
.1
0
-.1
-.2
-.3
Time (sec)

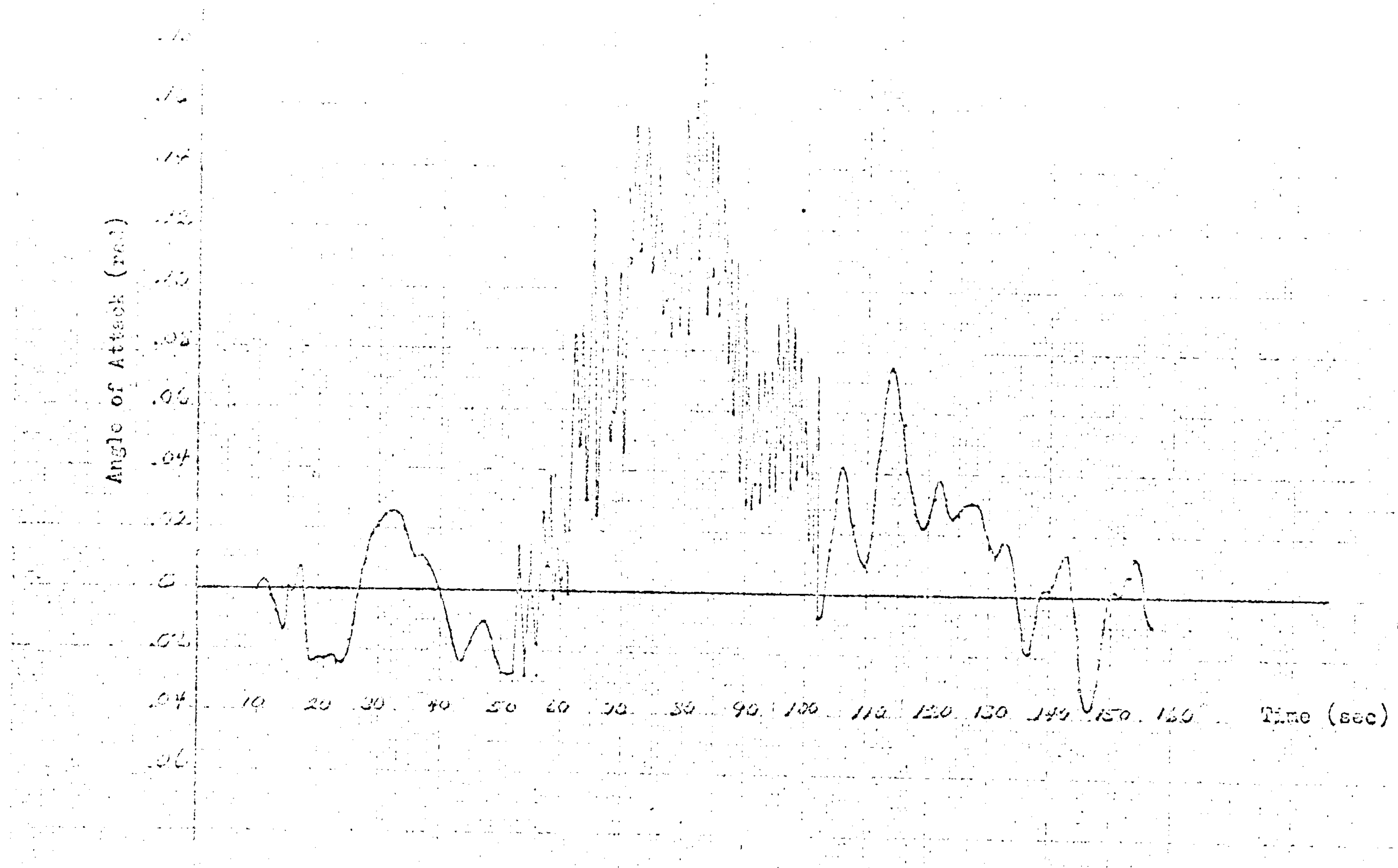

Figure B4-6. Compensation Configuration #2 with Instrument Noise

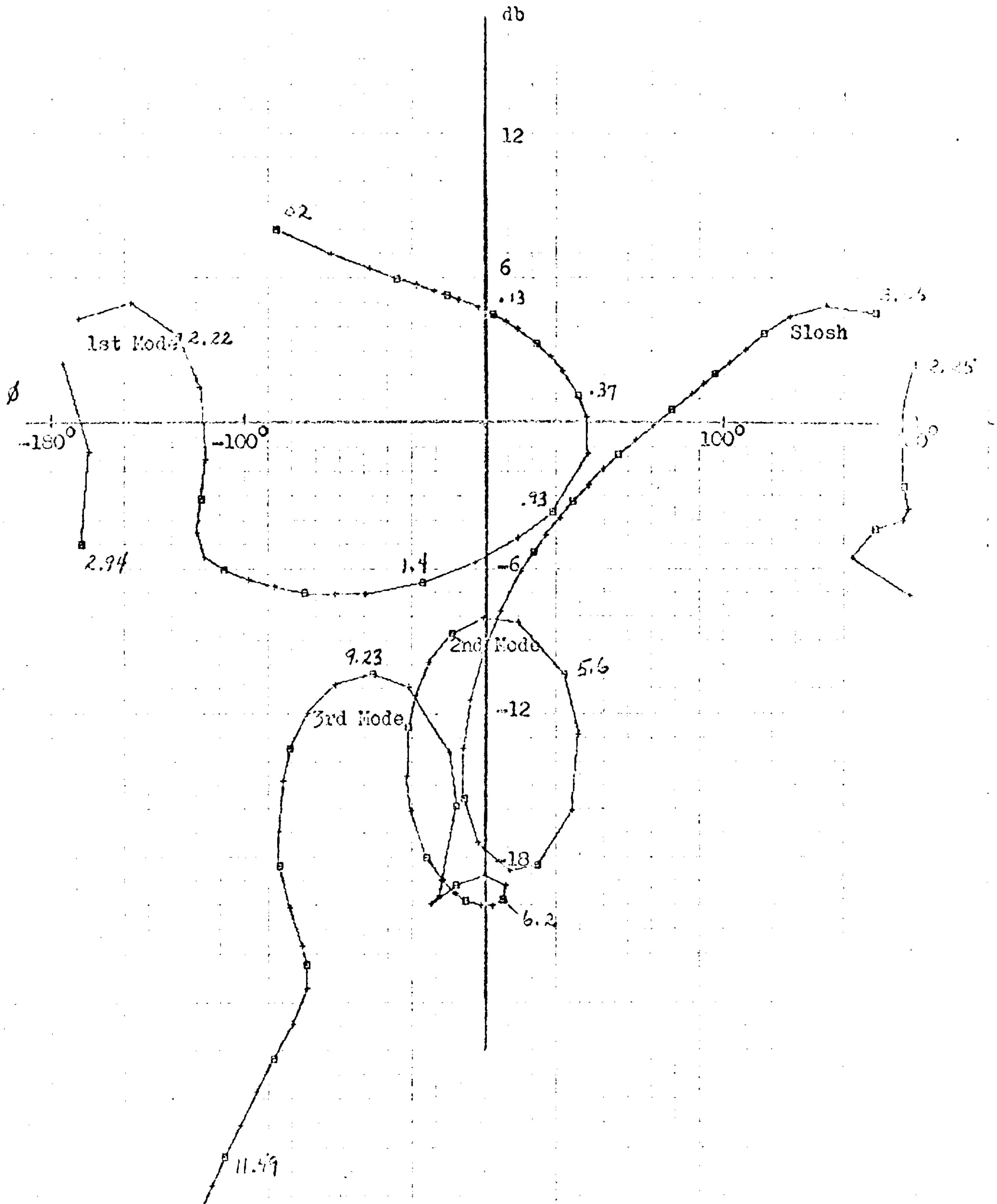

Figure 85, 78 Sec. Gain Phase Plot of the System with One Slosh Mode

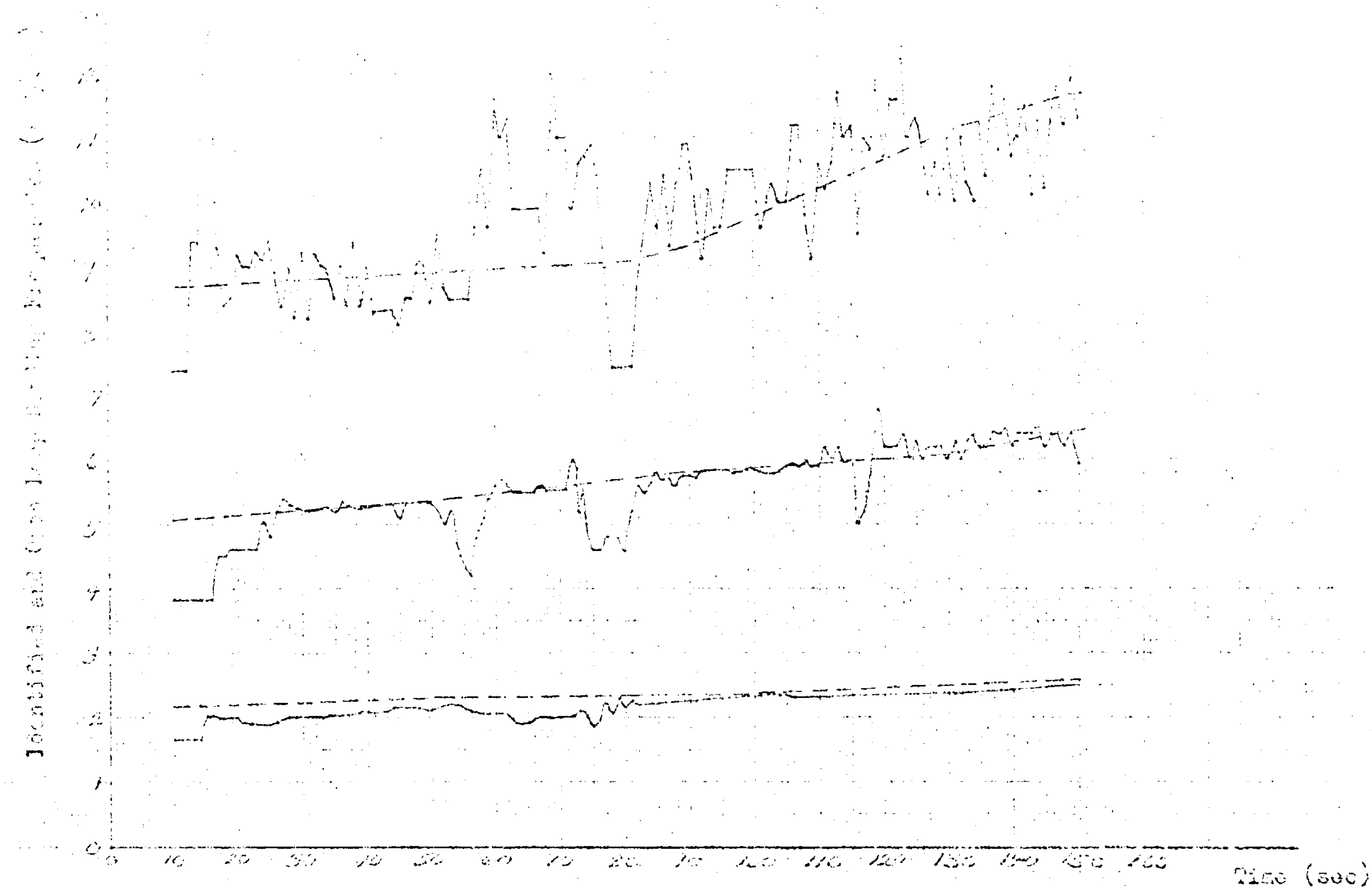

[illegible] Comparison [illegible] #2 with [illegible]

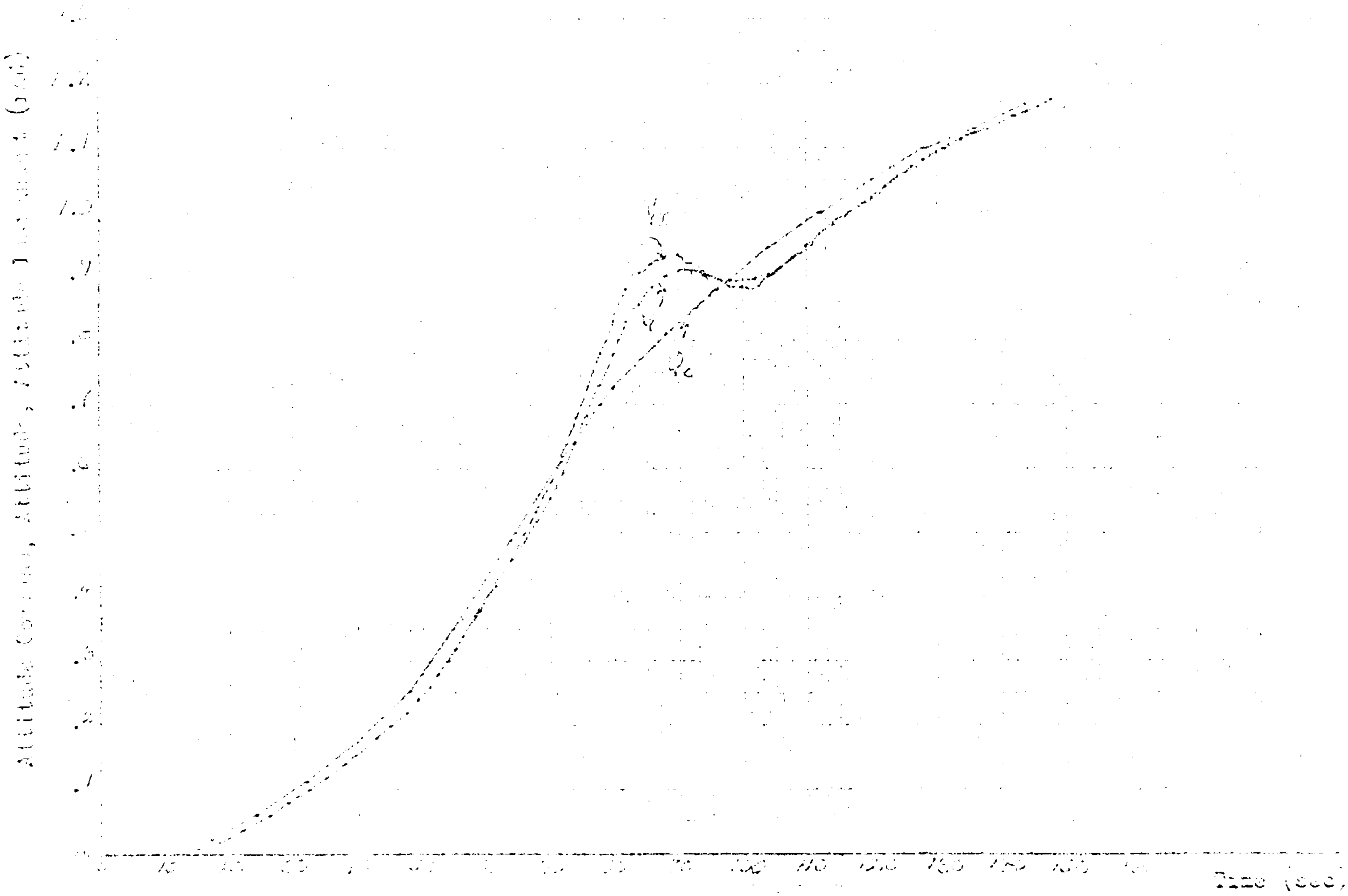
Time (sec)

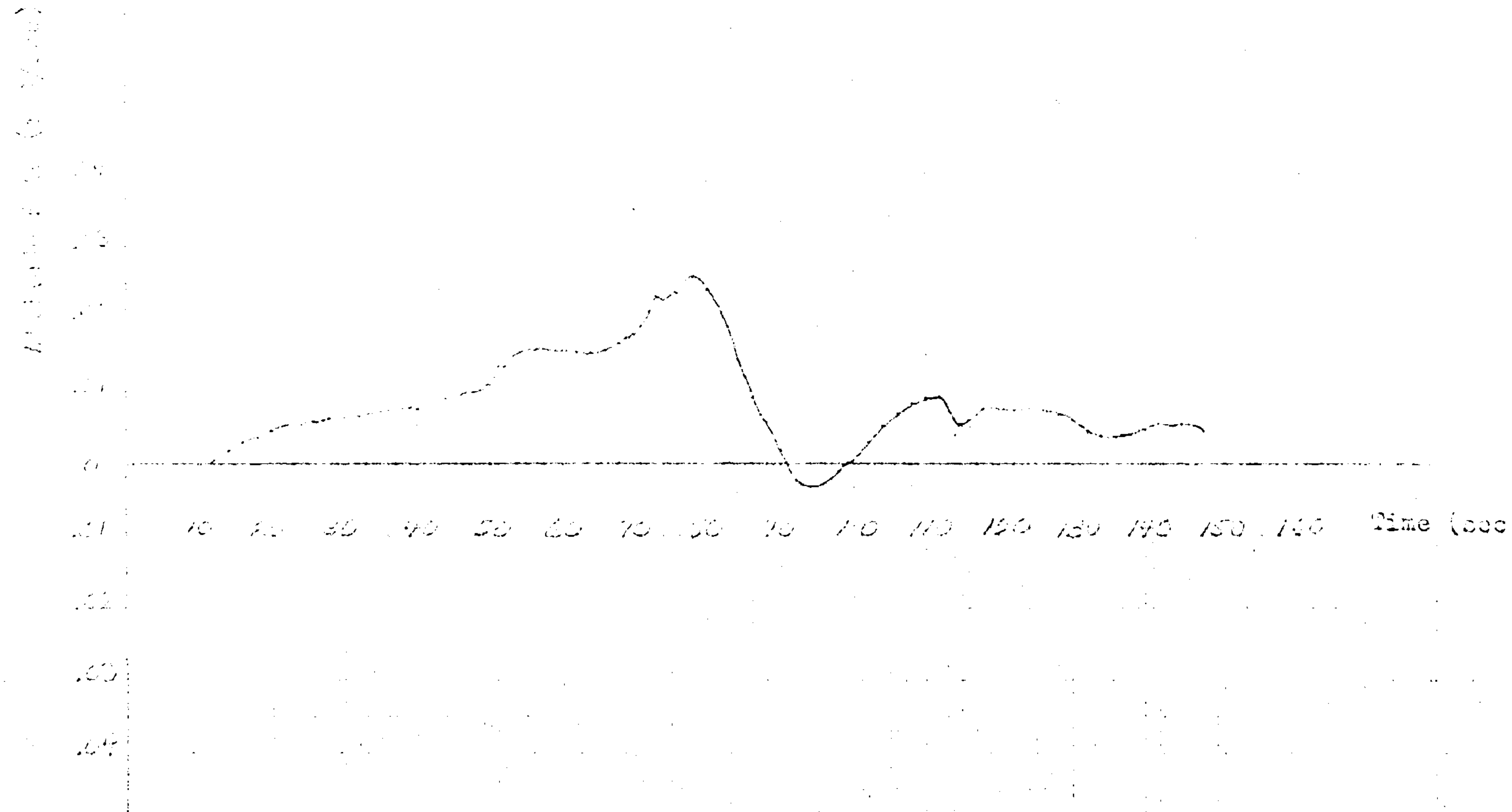

Figure [illegible]. Compensation Configuration #2 with Fuel Slosh

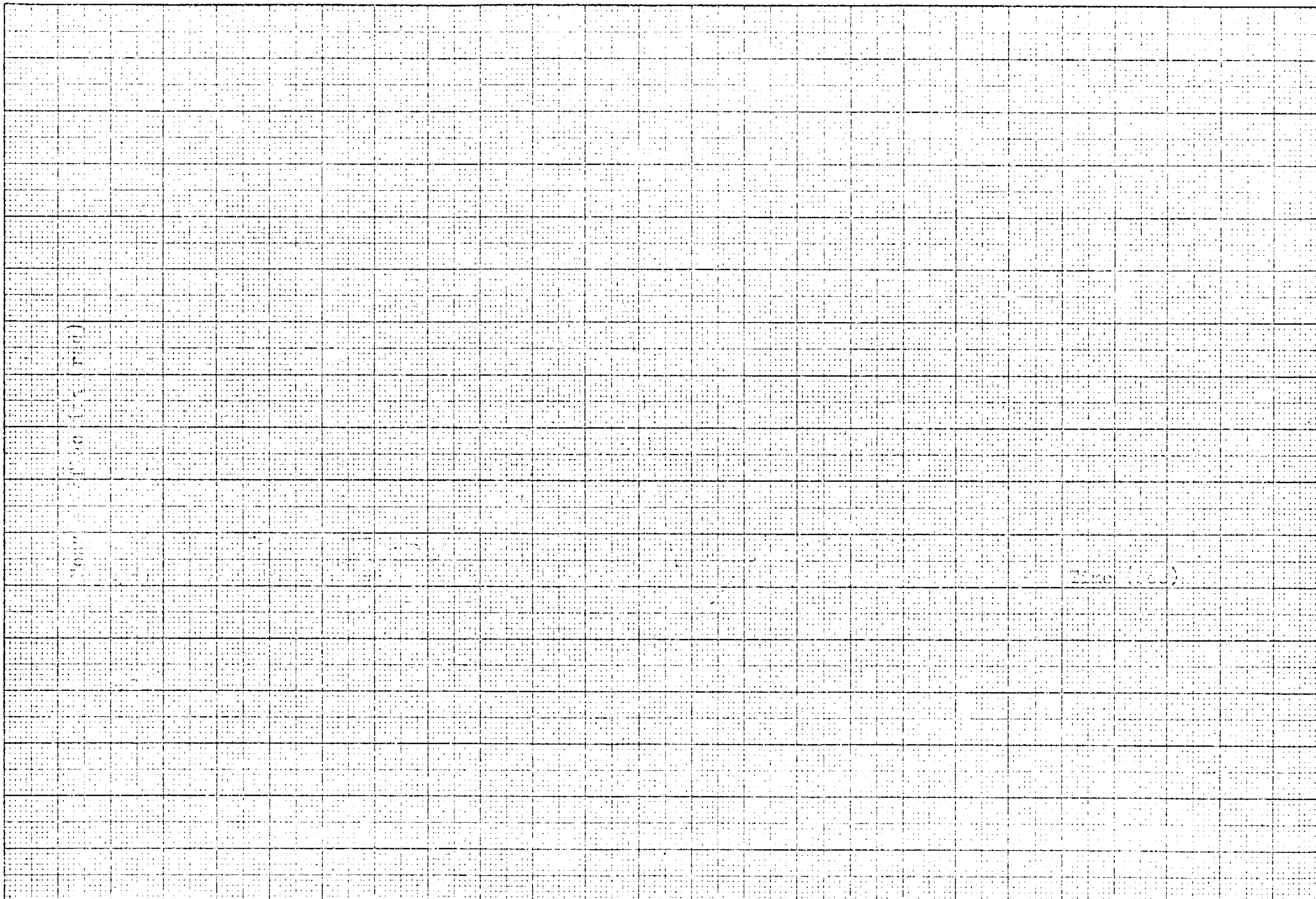

Figure 5-5. Compensation Configuration [illegible] Shock

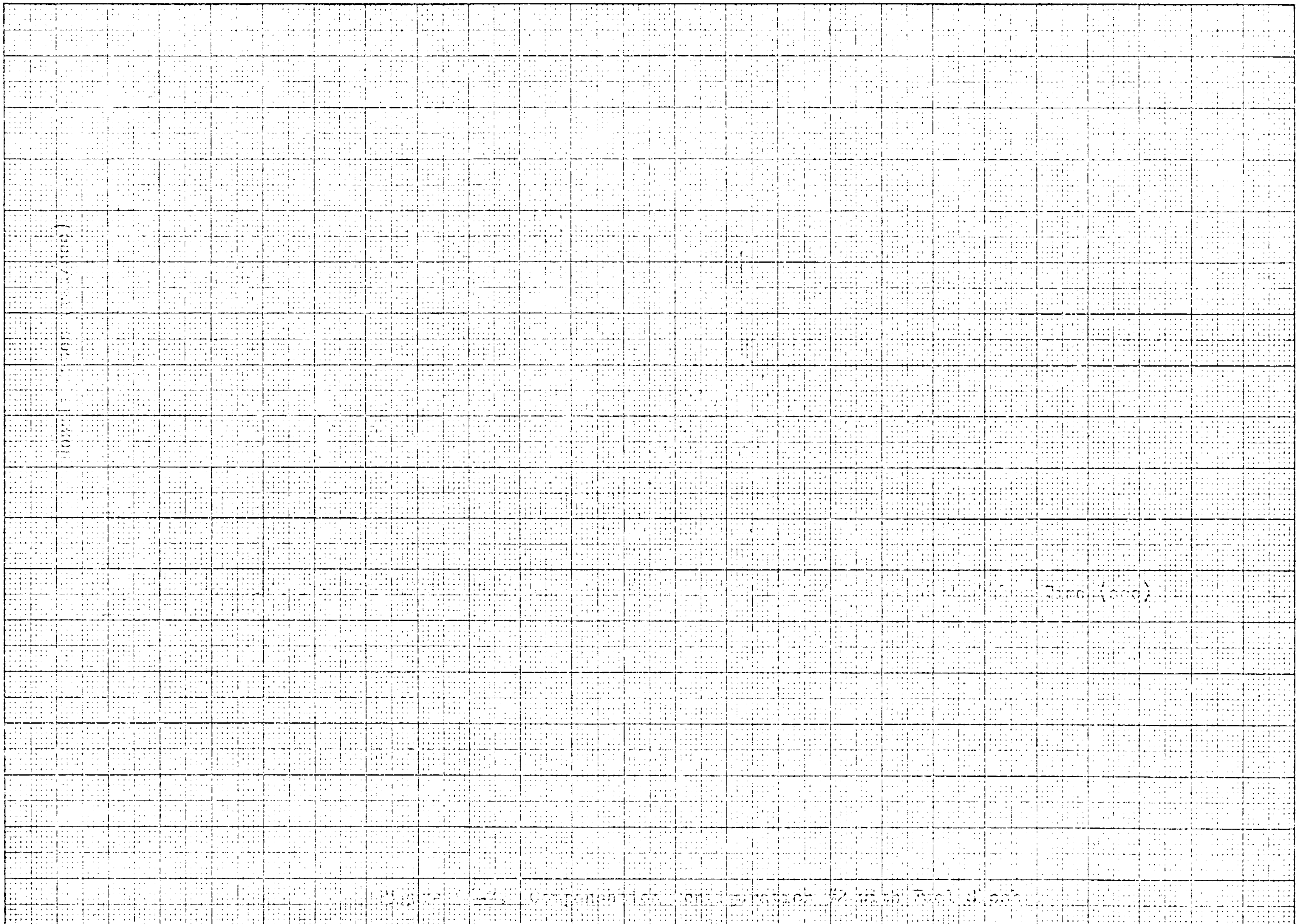
Time (sec)

10 X 10 TO THE CENTIMETER 46 1517
18 X 25 CM. • ALBANENE®
KEUFFEL & ESSER CO. MADE IN U.S.A.

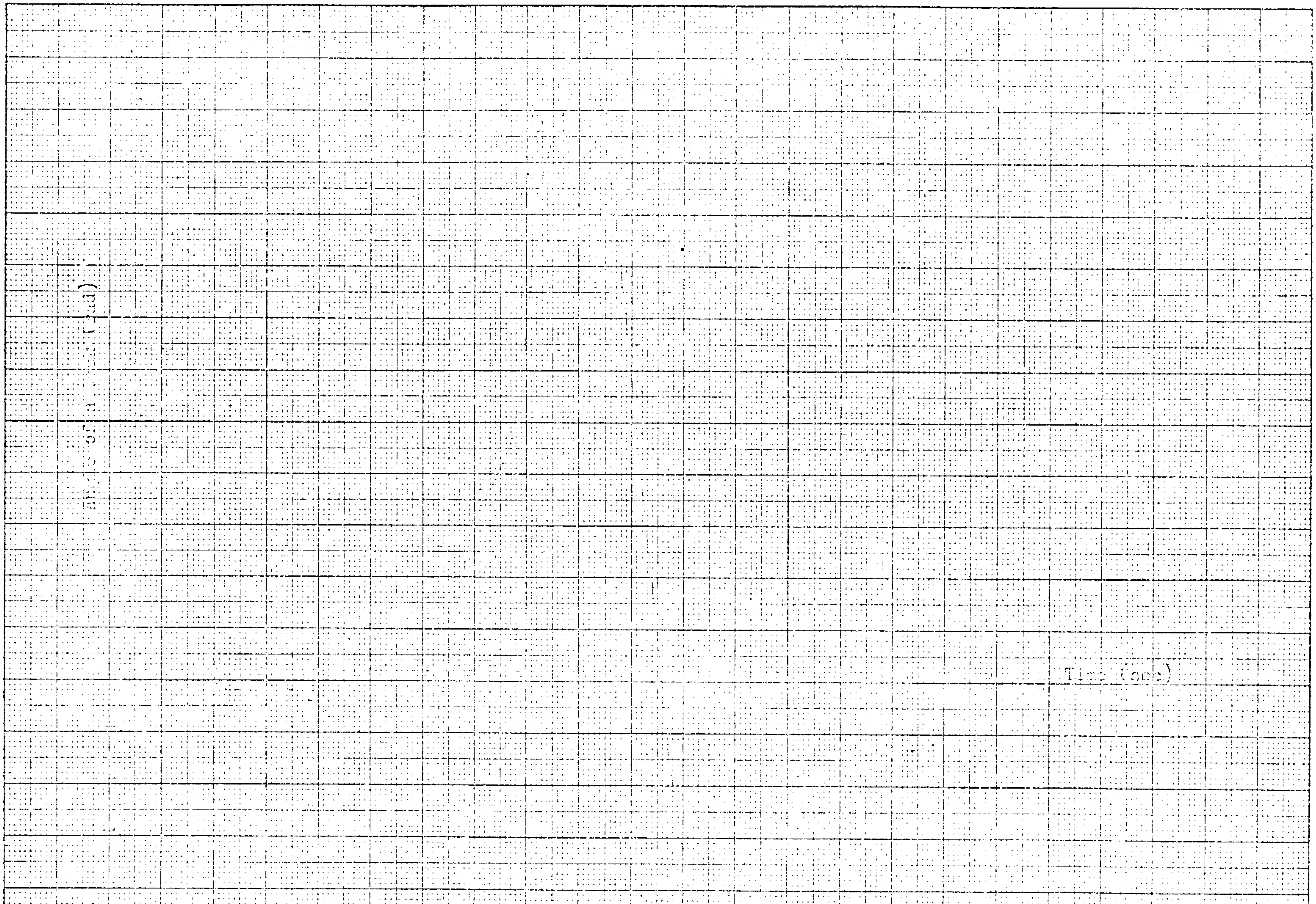

Figure 85-8. Compressor Configuration #2 with [illegible]

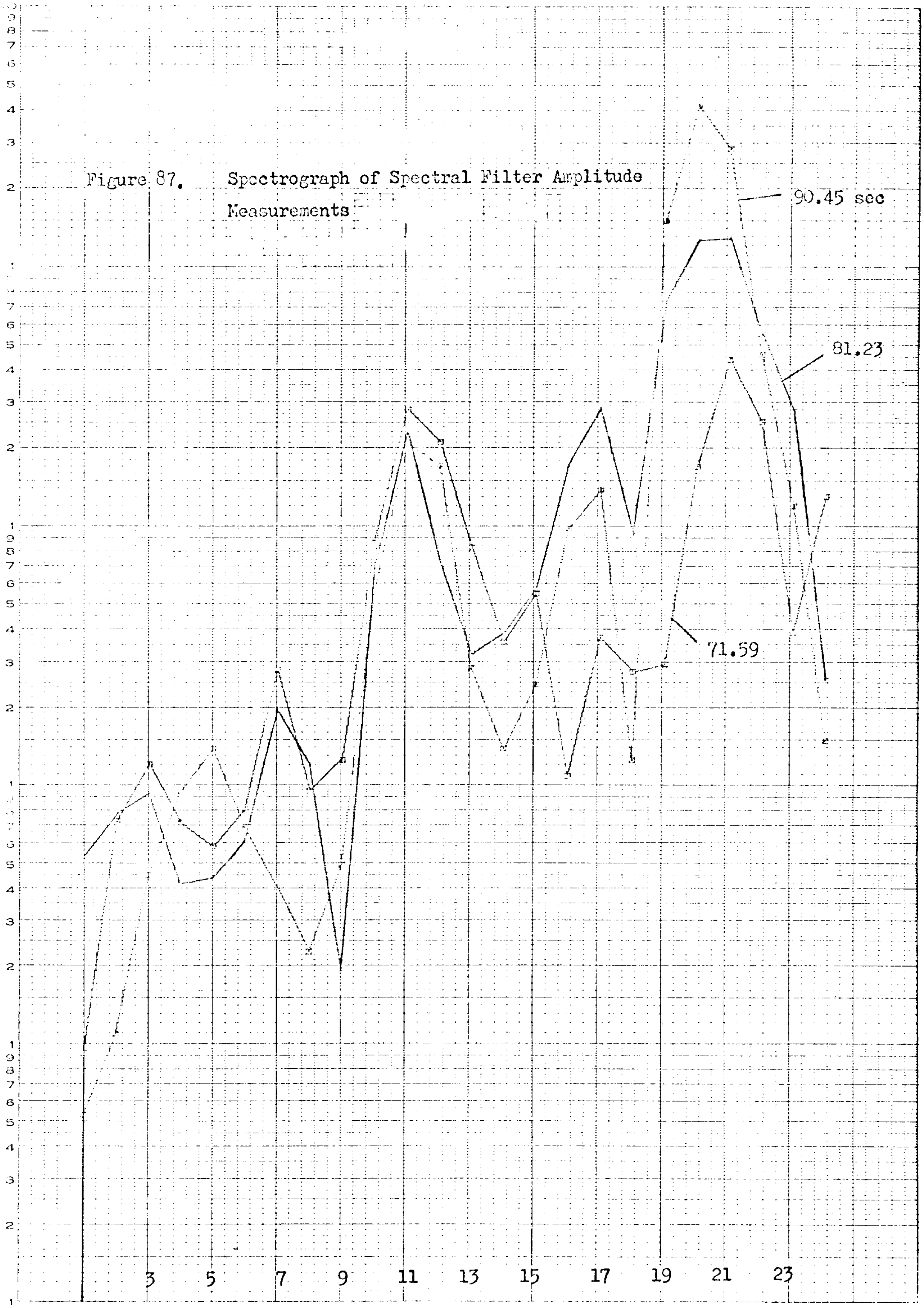

Figure 87. Spectrograph of Spectral Filter Amplitude Measurements

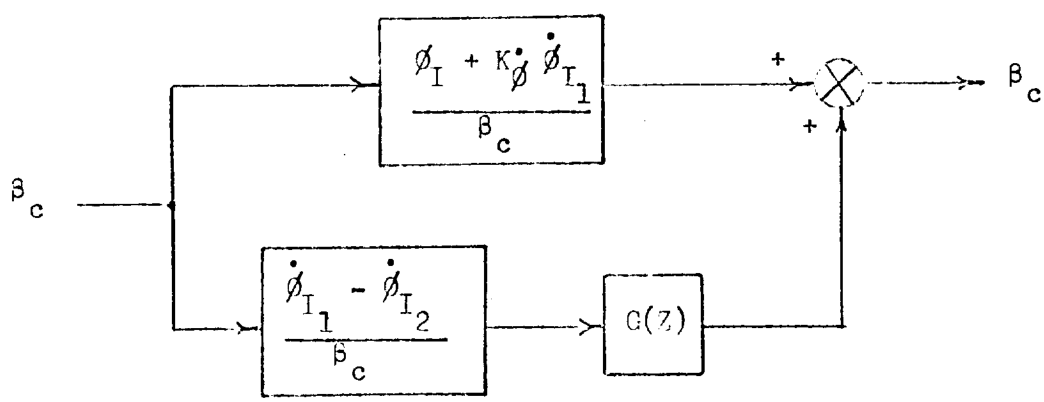

Figure 88. General Active Control Block Diagram

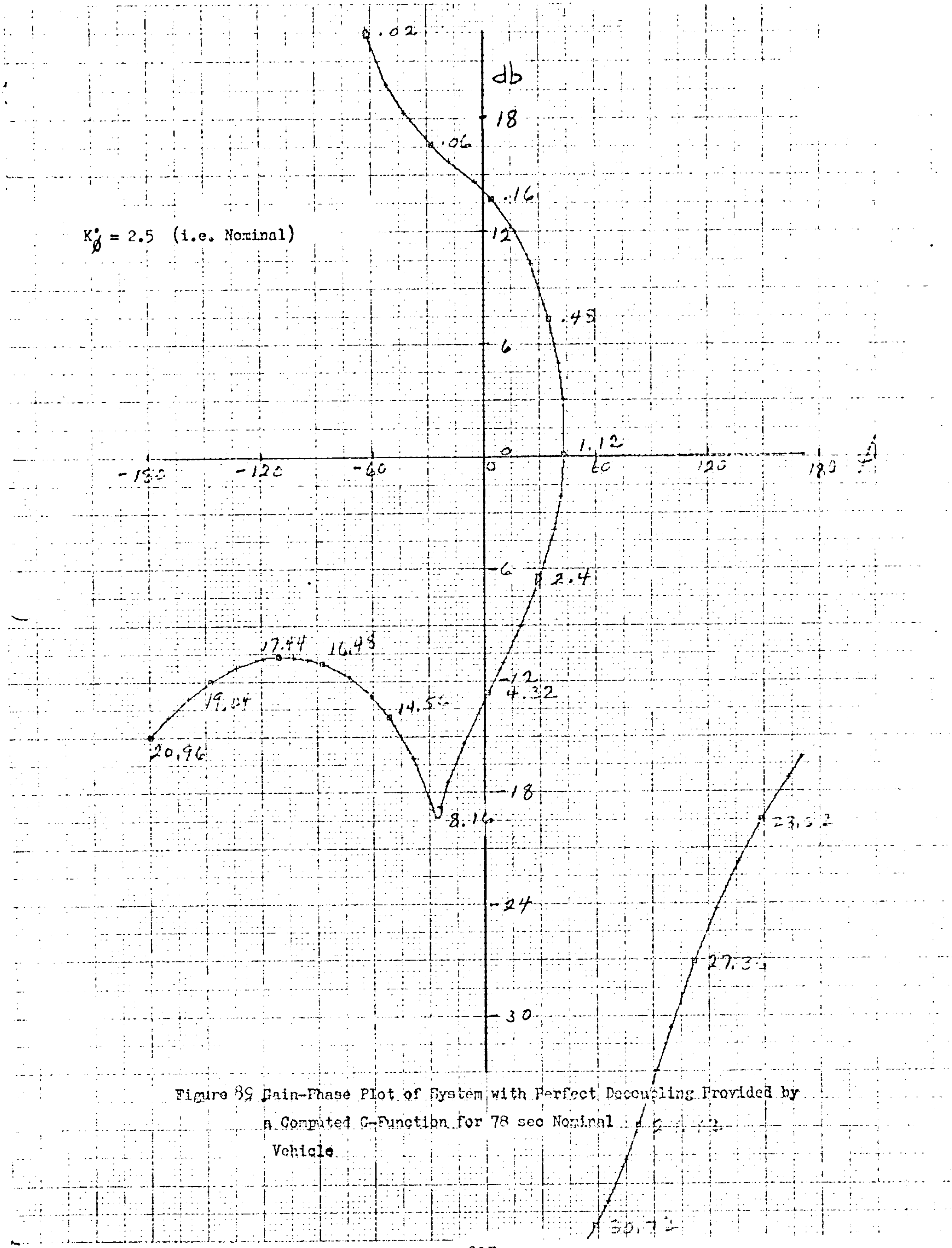

Figure 89 Gain-Phase Plot of System with Perfect Decoupling Provided by a Computed G-Function for 78 sec Nominal Vehicle

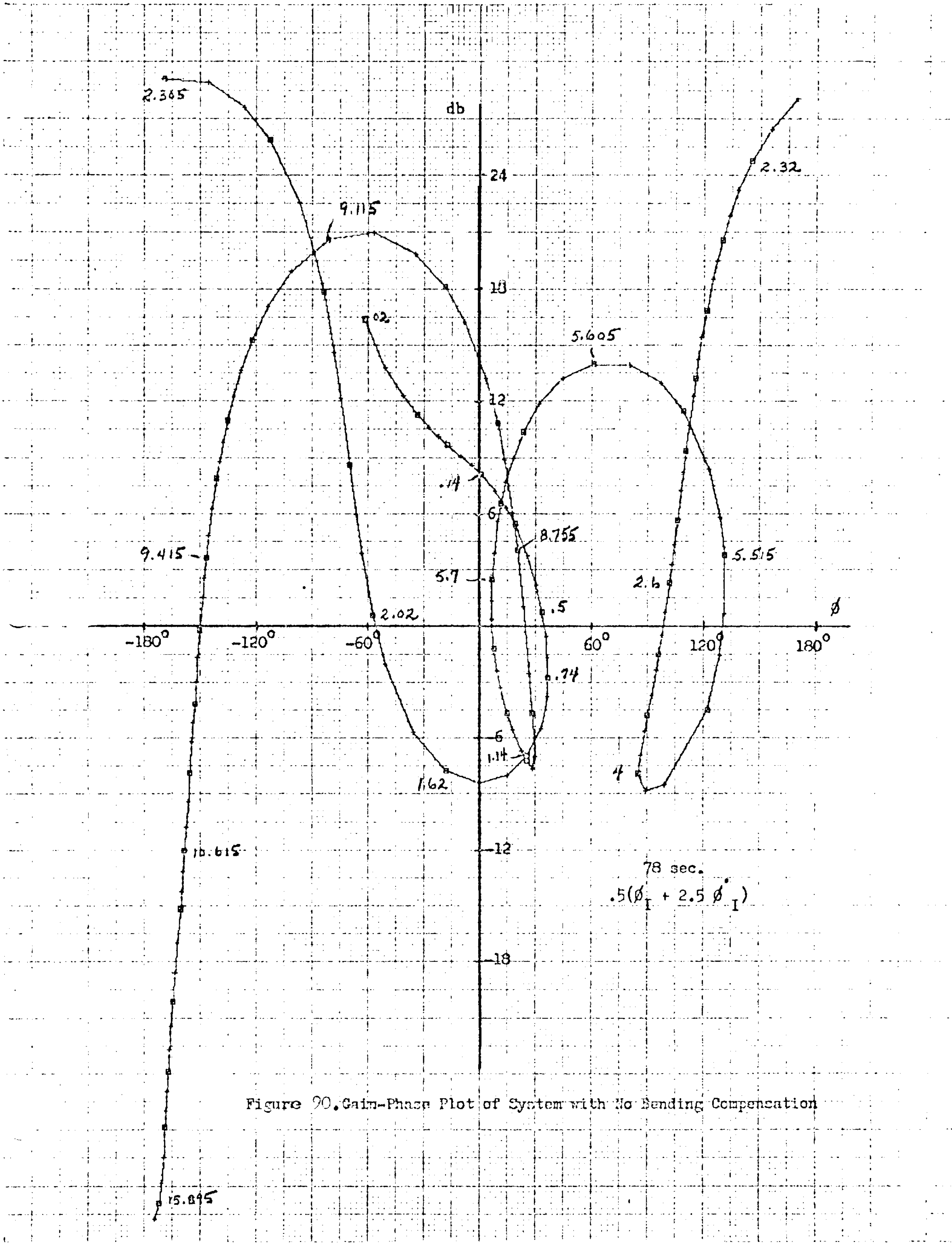

Figure 90. Gain-Phase Plot of System with No Bending Compensation

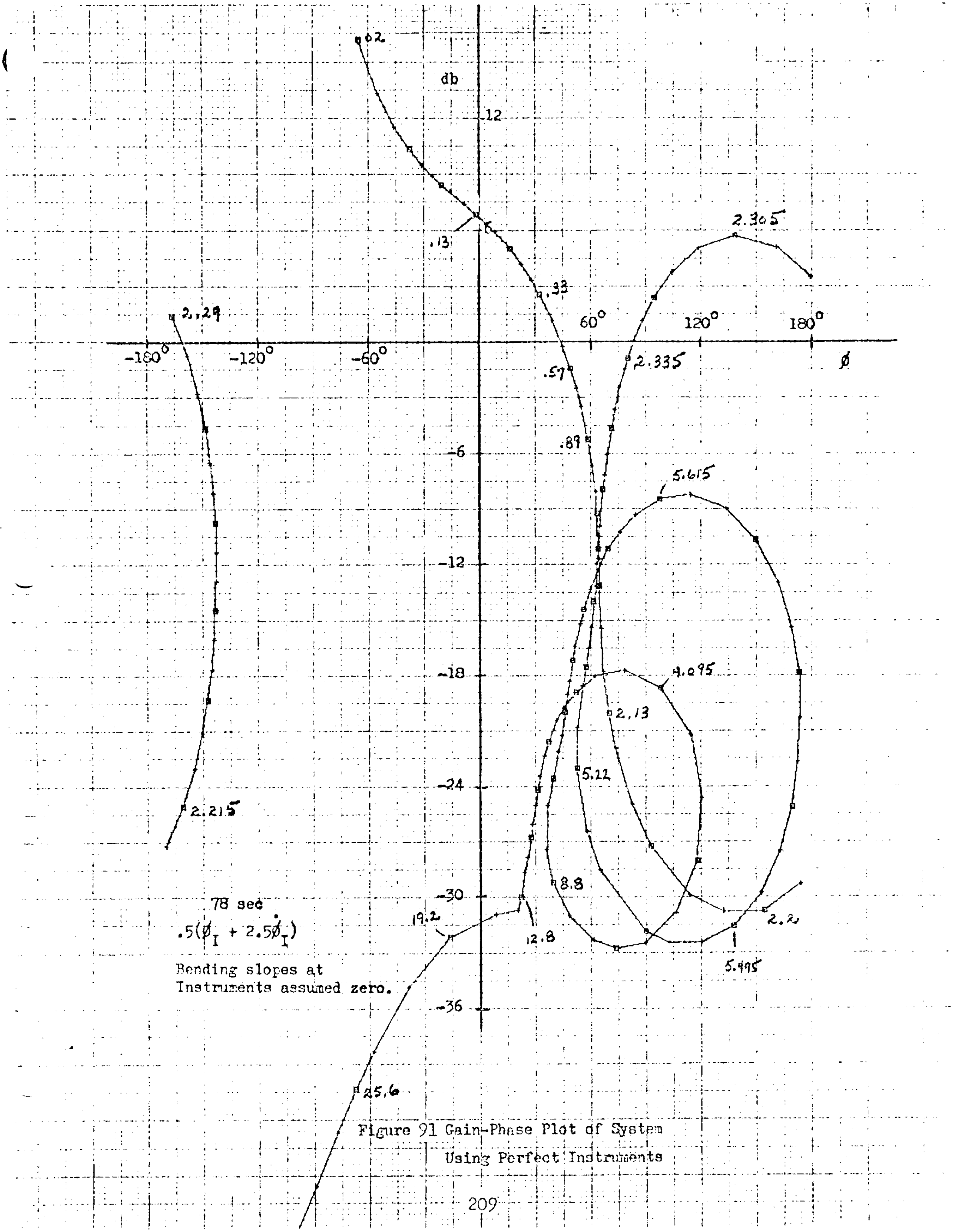

Figure 91 Gain-Phase Plot of System
Using Perfect Instruments

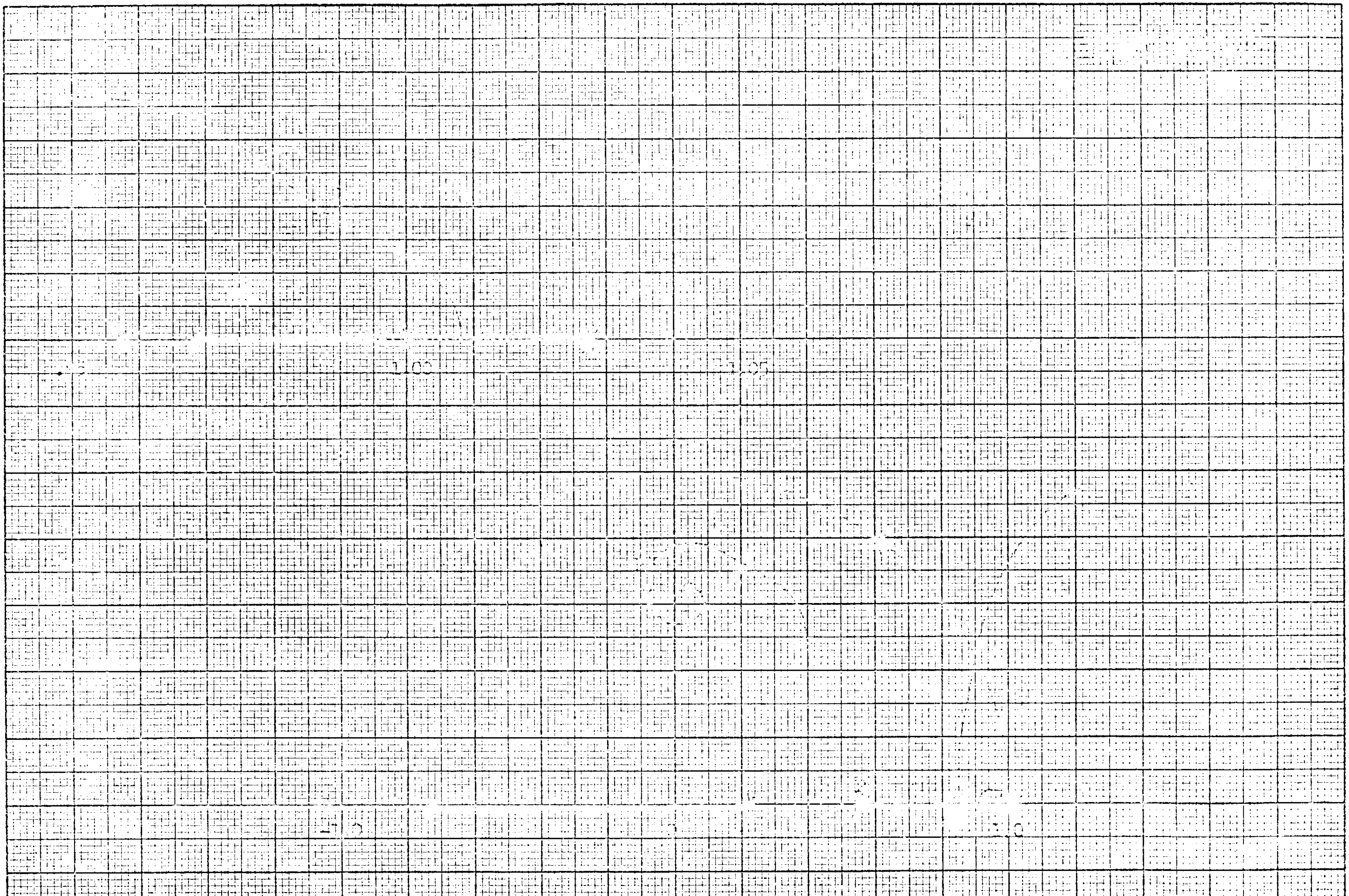

Figure 92 Root Locus of System with Perfect Bending Cancellation

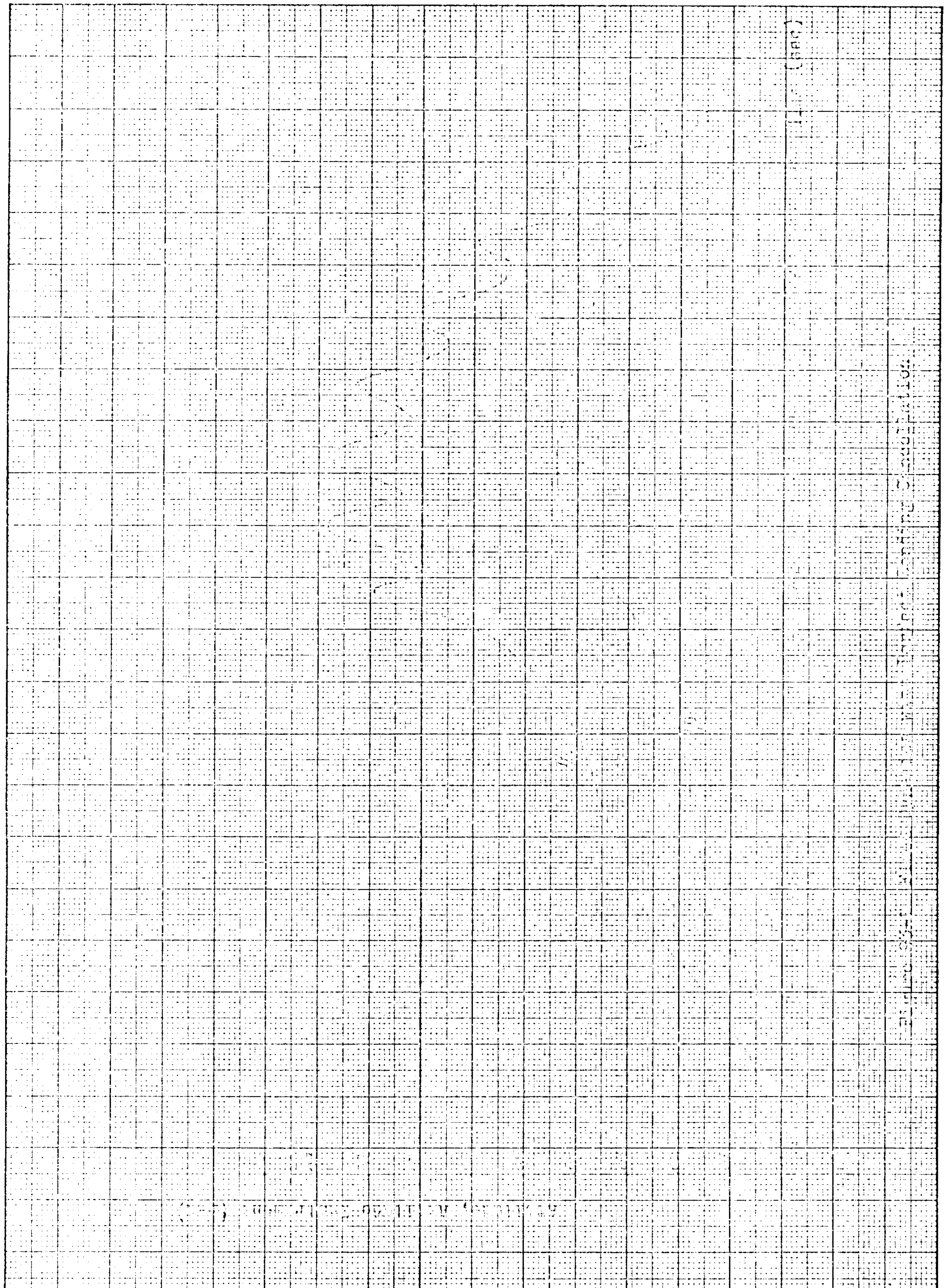

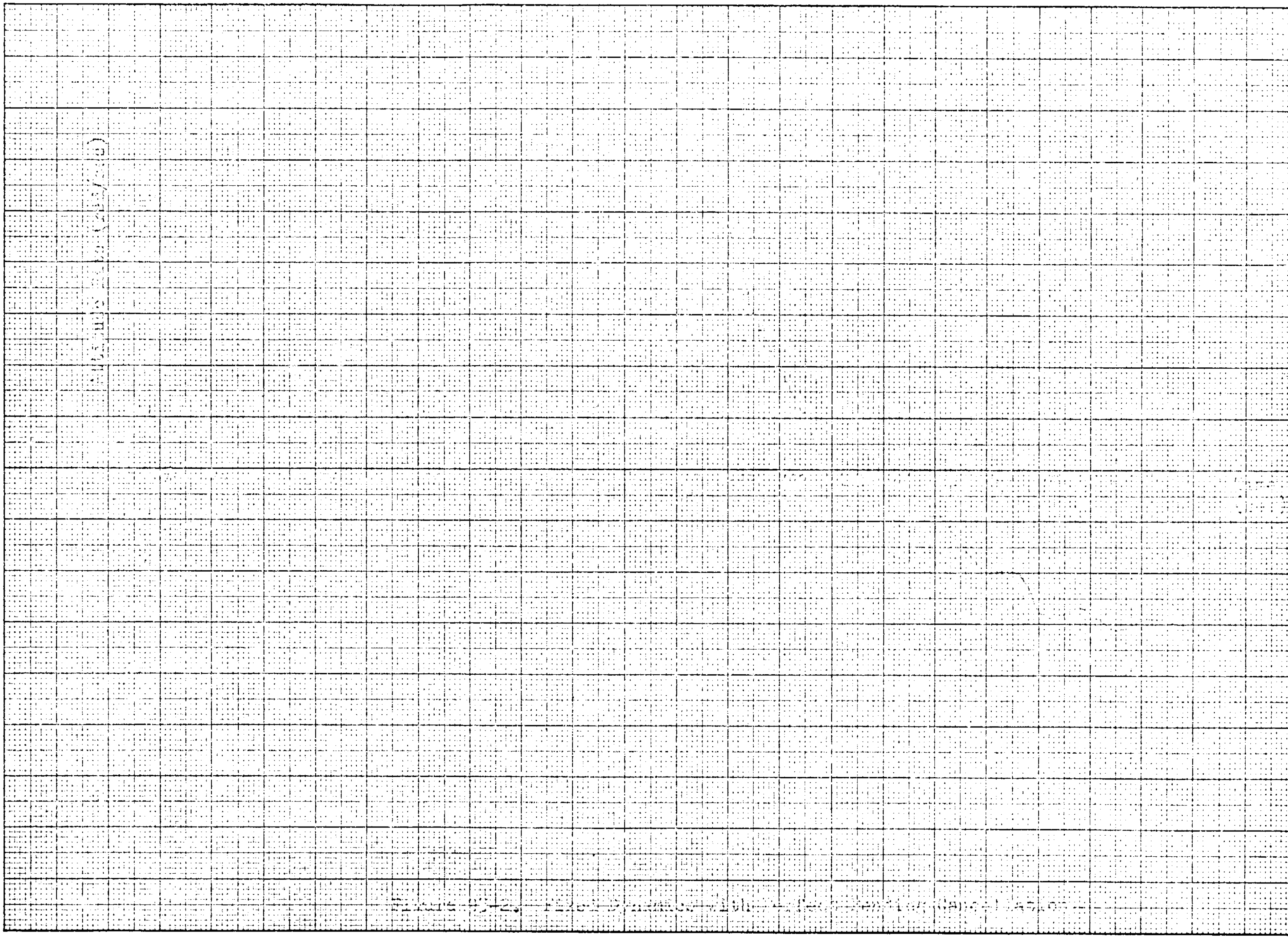

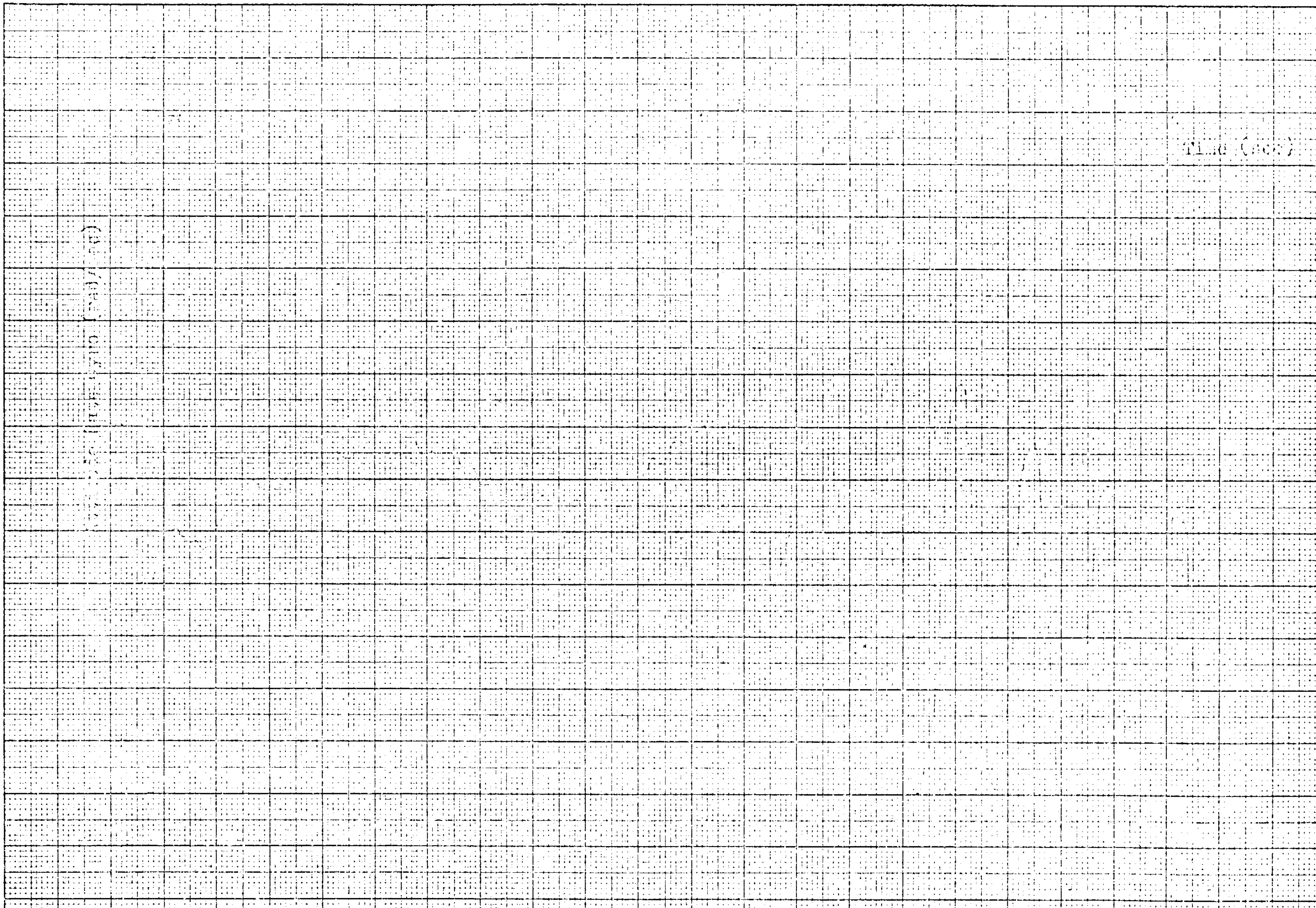

Figure 5-3. Fixed Dynamics with Perfect Rolling Cancellation

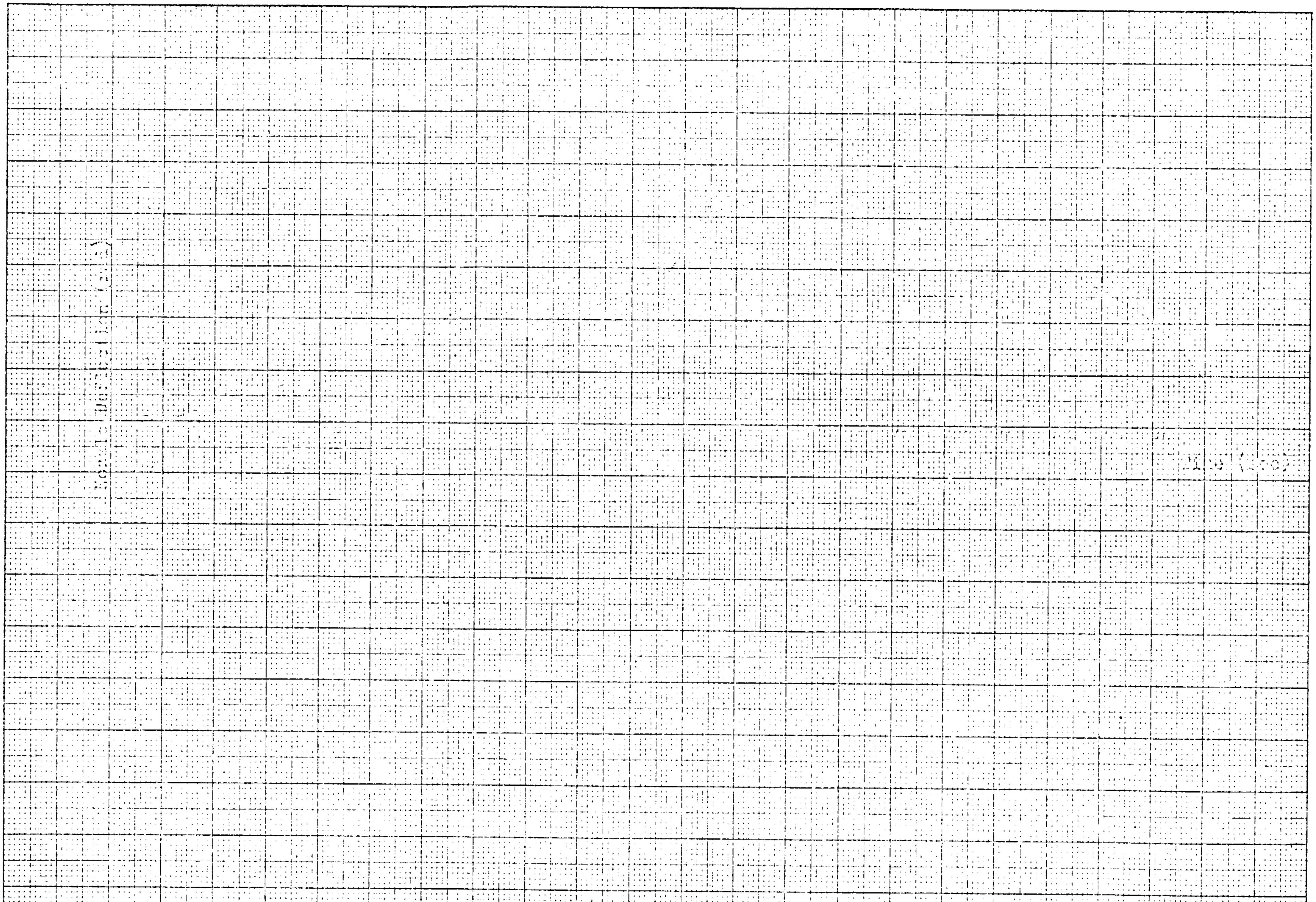

FIGURE 10-5, Pitch Dynamics with Perfect Bending Cancellation

10 X 10 TO THE CENTIMETER 46 1517
10 X 25 CM. • ALBANENE®
KEUFFEL & ESSER CO.
MADE IN U.S.A.

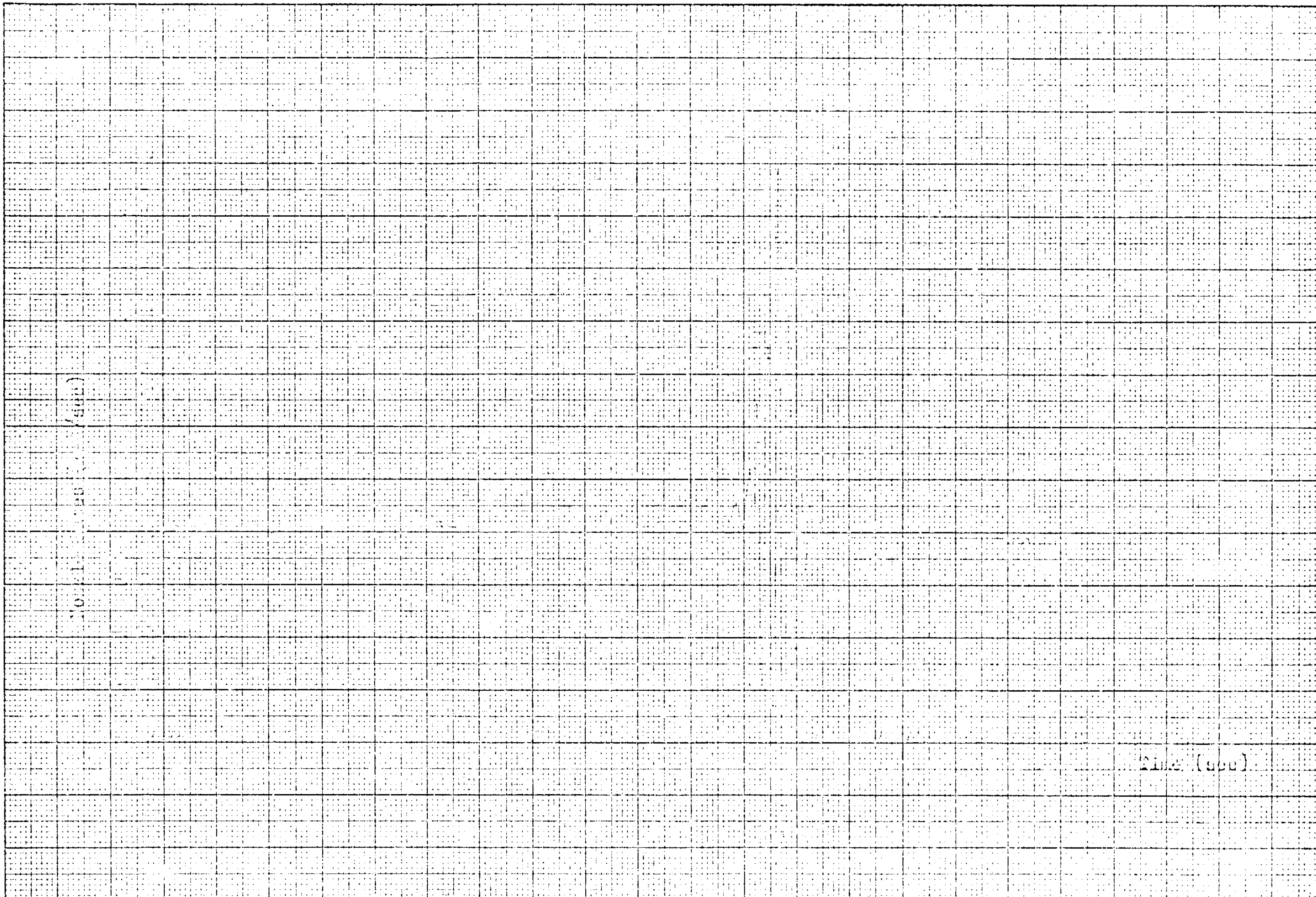

Figure [illegible]. [illegible] Dynamics with Perfect Bending Cancellation

Angle of Attack (rad)

Time (sec)

Figure D2-5. Fixed Dynamics with Perfect Bending Cancellation

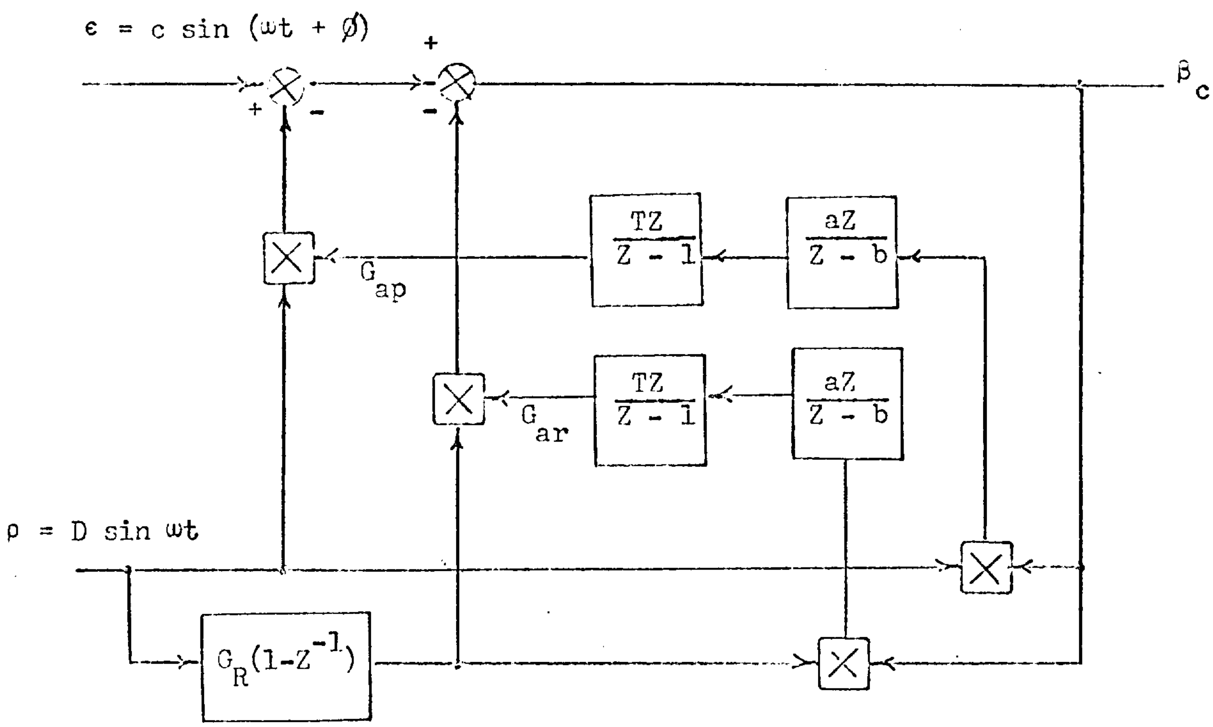

Figure 94. Adaptive Bending Suppression System

Figure 95. β_c' Response vs. Time

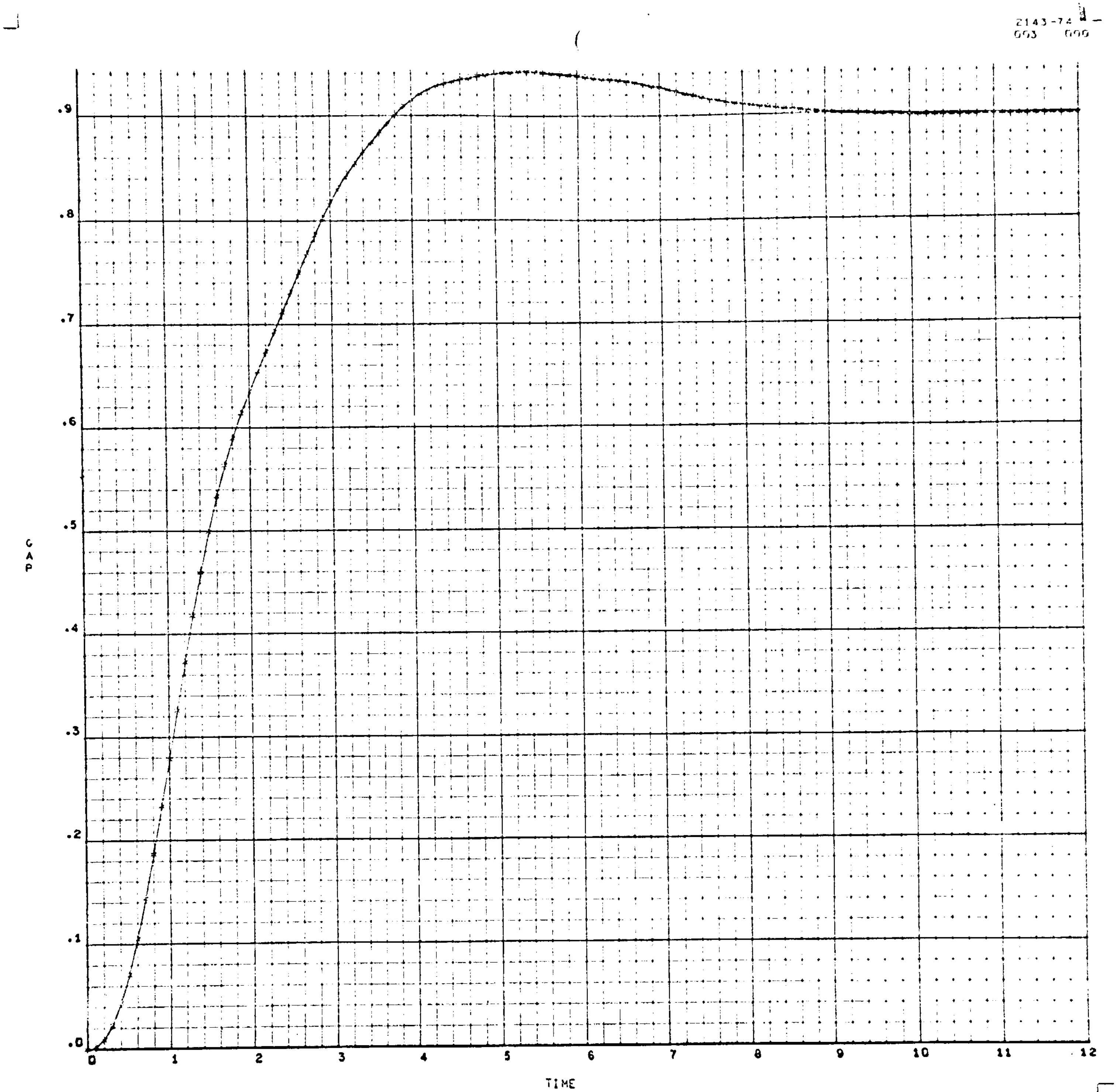

Figure 96. Adaptive Gain G_{aP} vs. Time

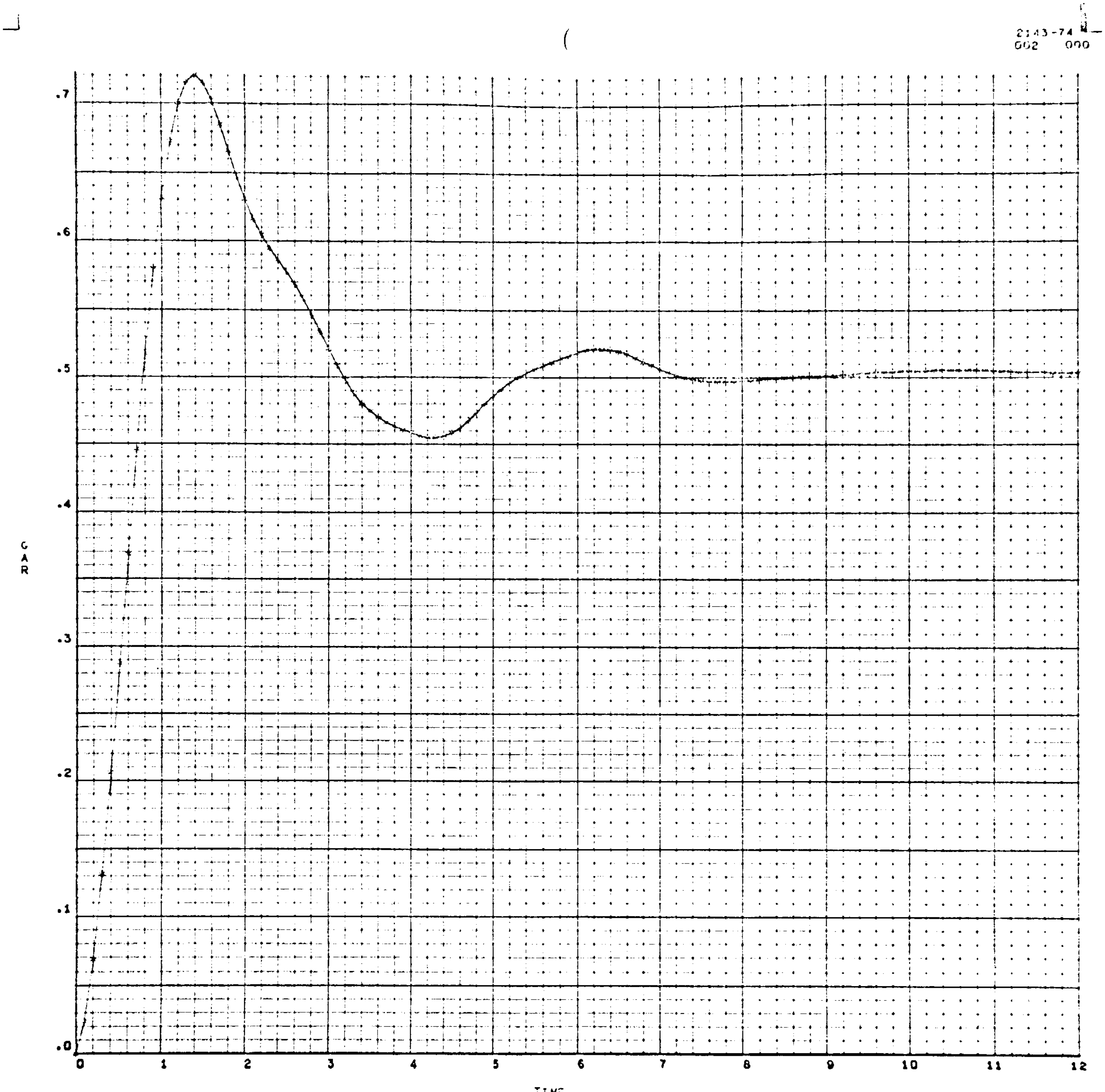

Figure 97. Adaptive Gain G_{aR} vs. Time

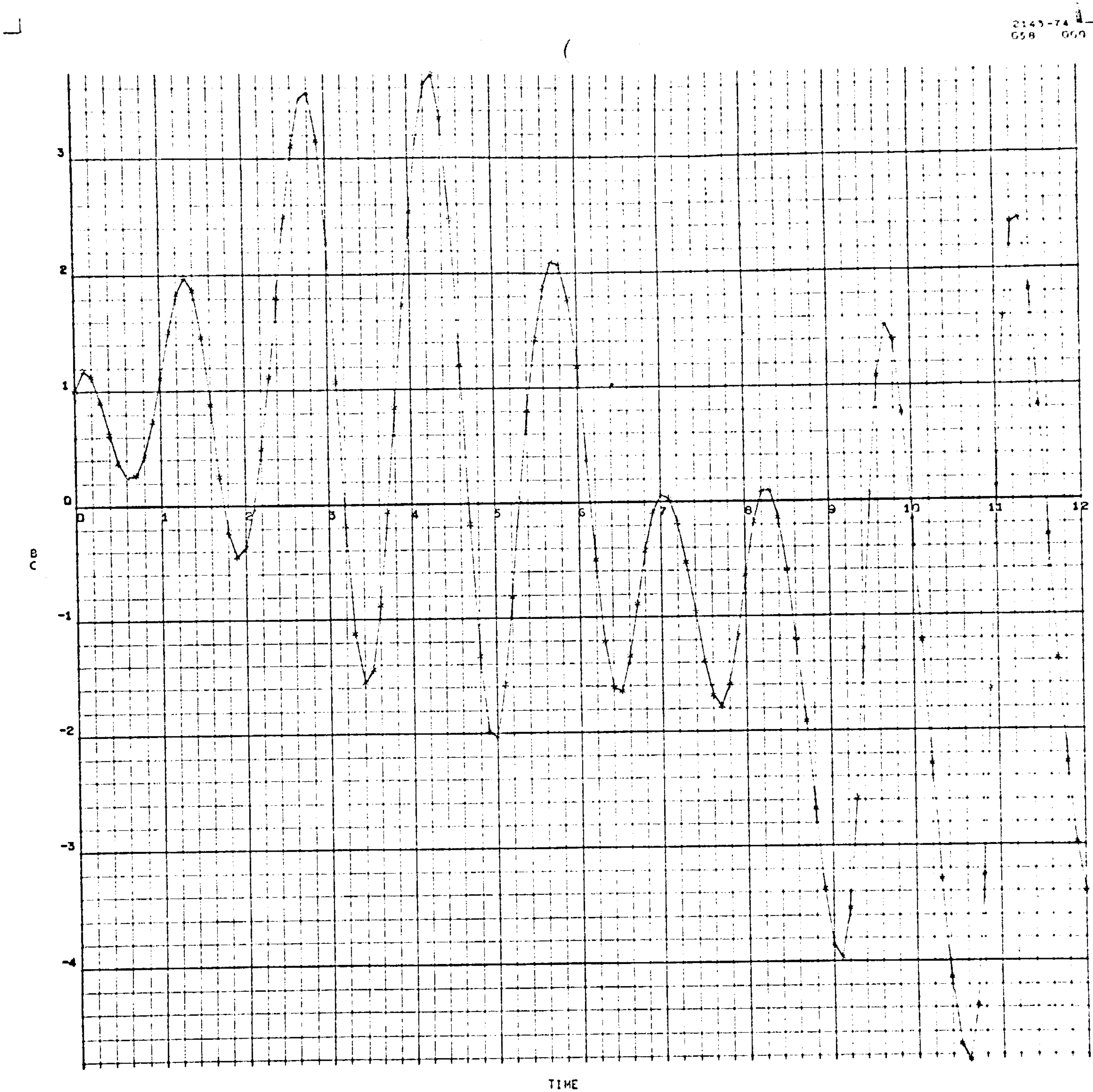

Figure 98. β_c Response for Twice the Input Amplitude on ρ

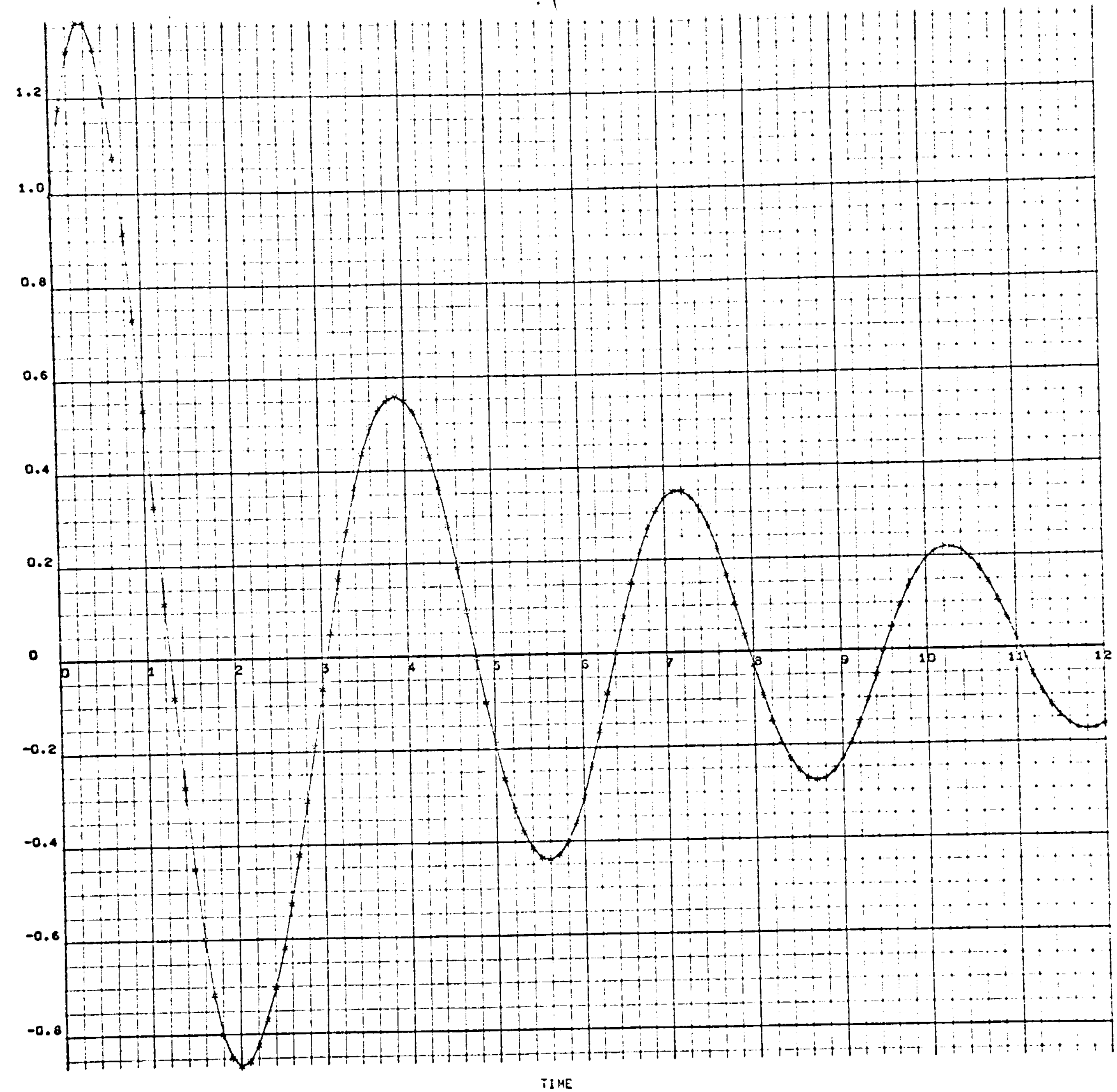

Figure 99. ρ_c Response for Half the Input Amplitude on ρ

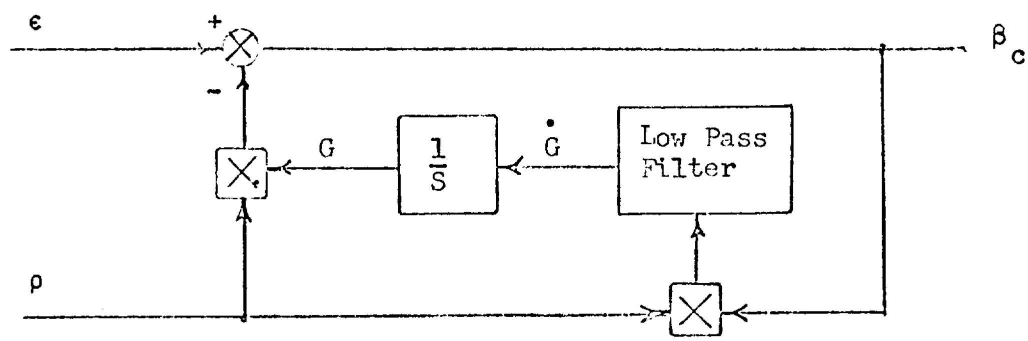

Figure 100. Simplified Adaptive Loop for Half of the Adaptive Bending Suppression System

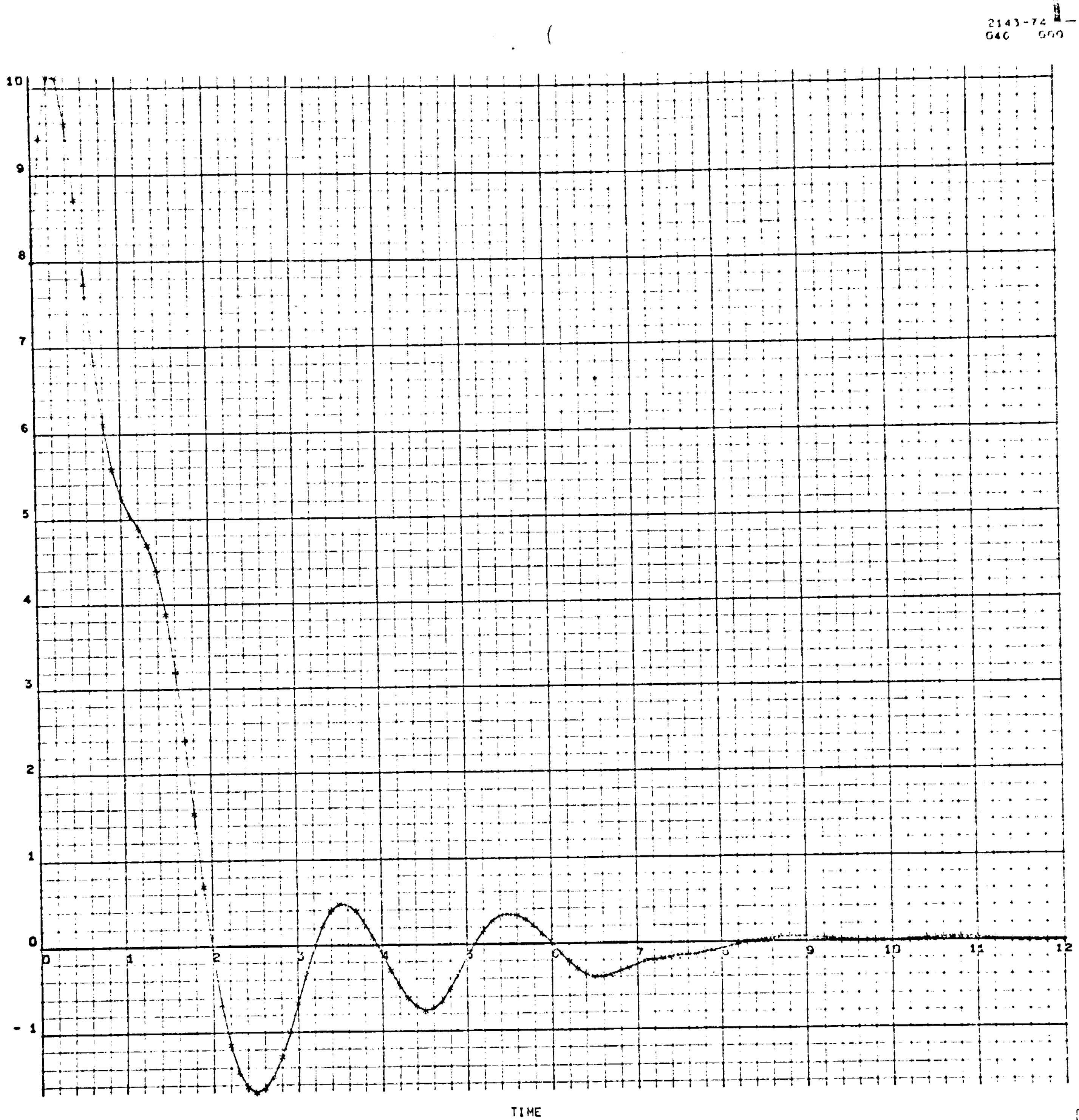

Figure 101 β_c Response with $\mathcal{E}$ Amplitude Increased by 8

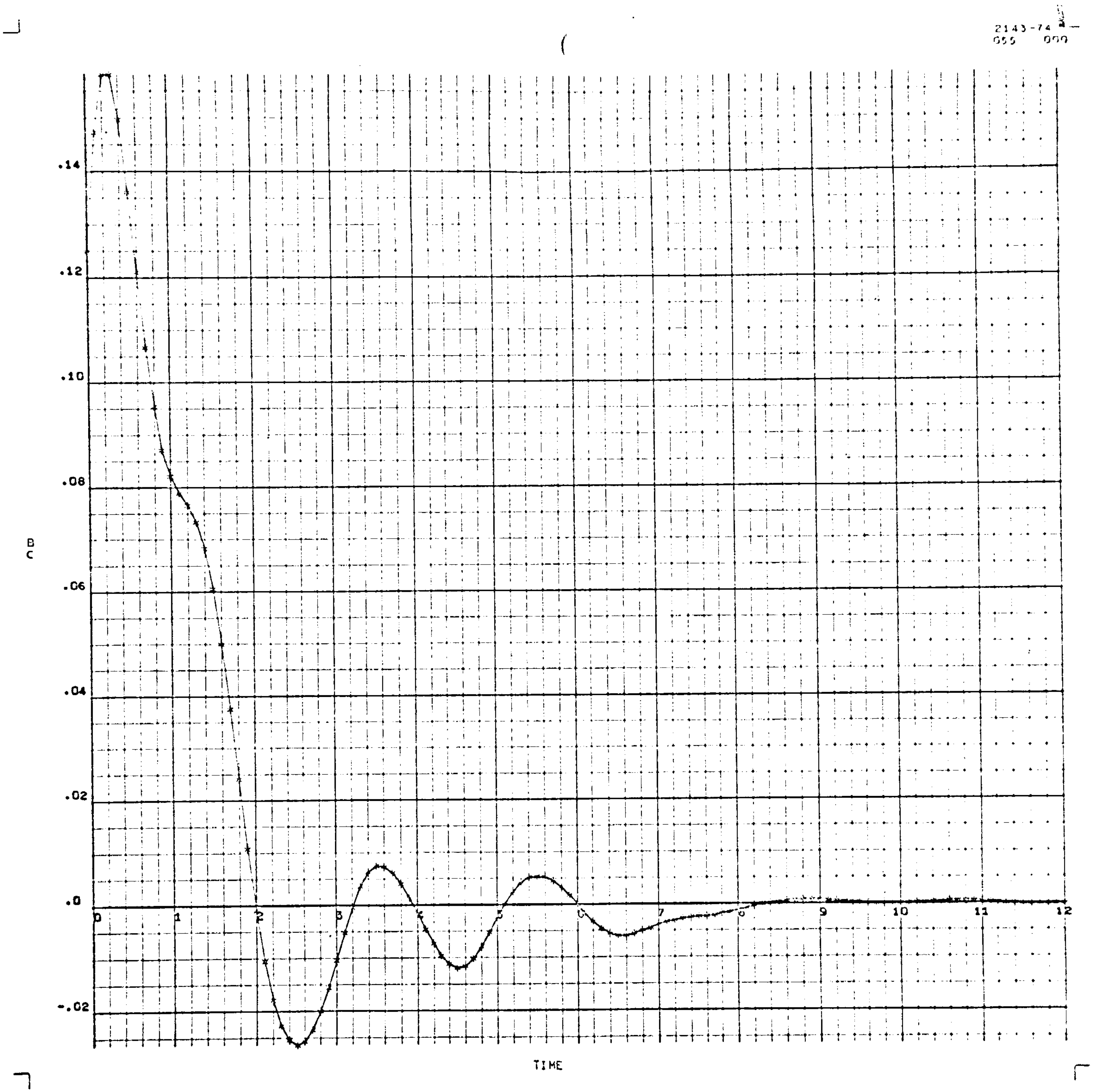

Figure 102 β_c Response with $\hat{\varepsilon}$ Amplitude Decreased by 8

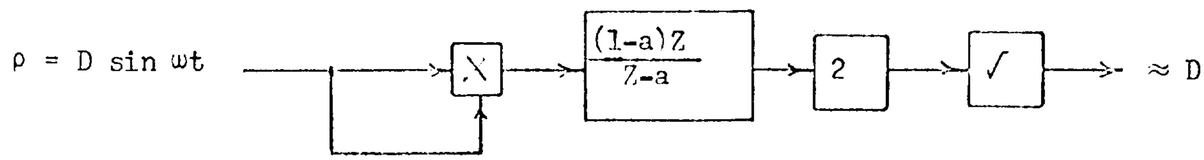

Figure 103. Mechanization to Measure D

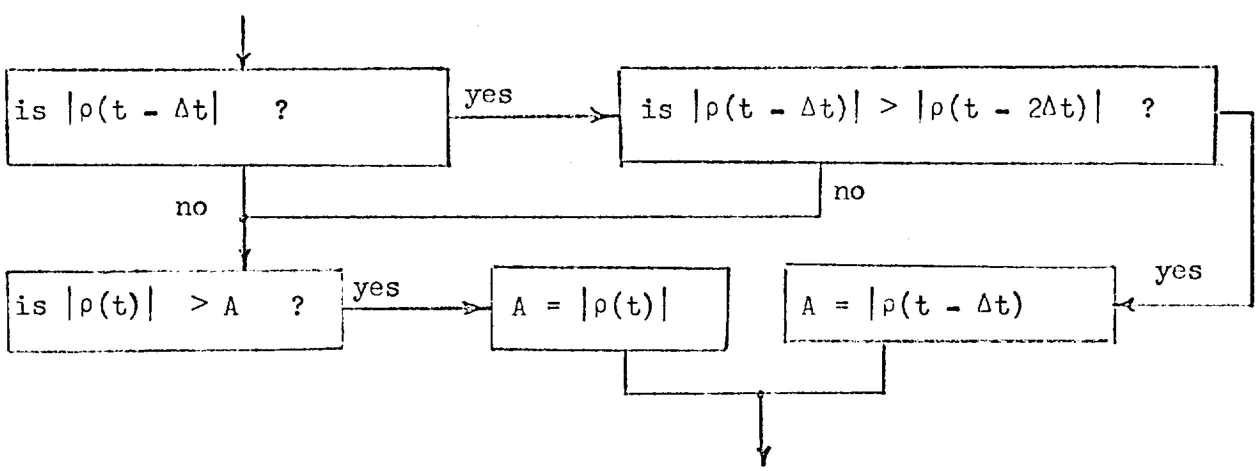

Figure 104. Amplitude Peak Detector

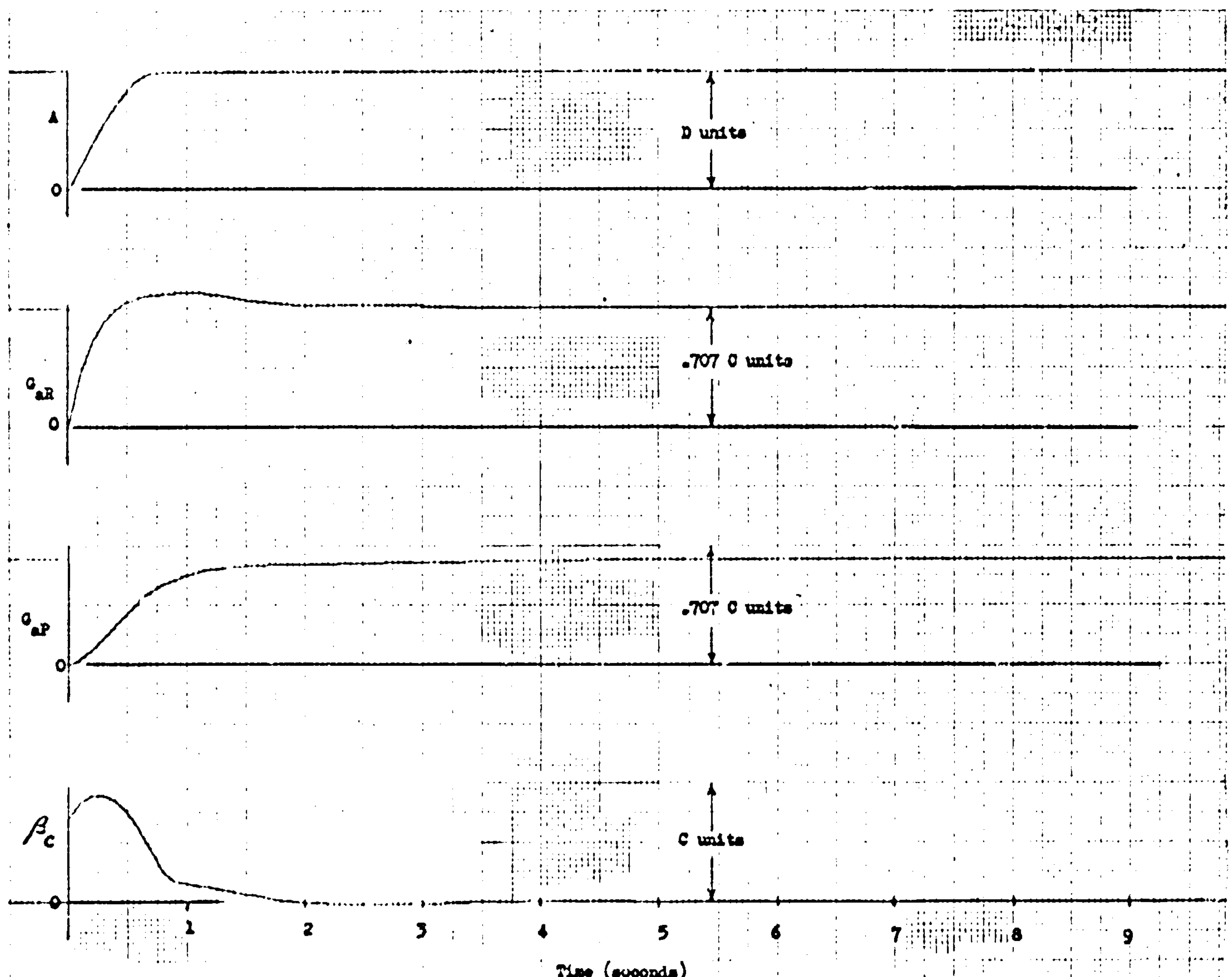

Figure 105. Bending Suppression System Response with a Pure Sine Wave Input and Amplitude Peak Detection System

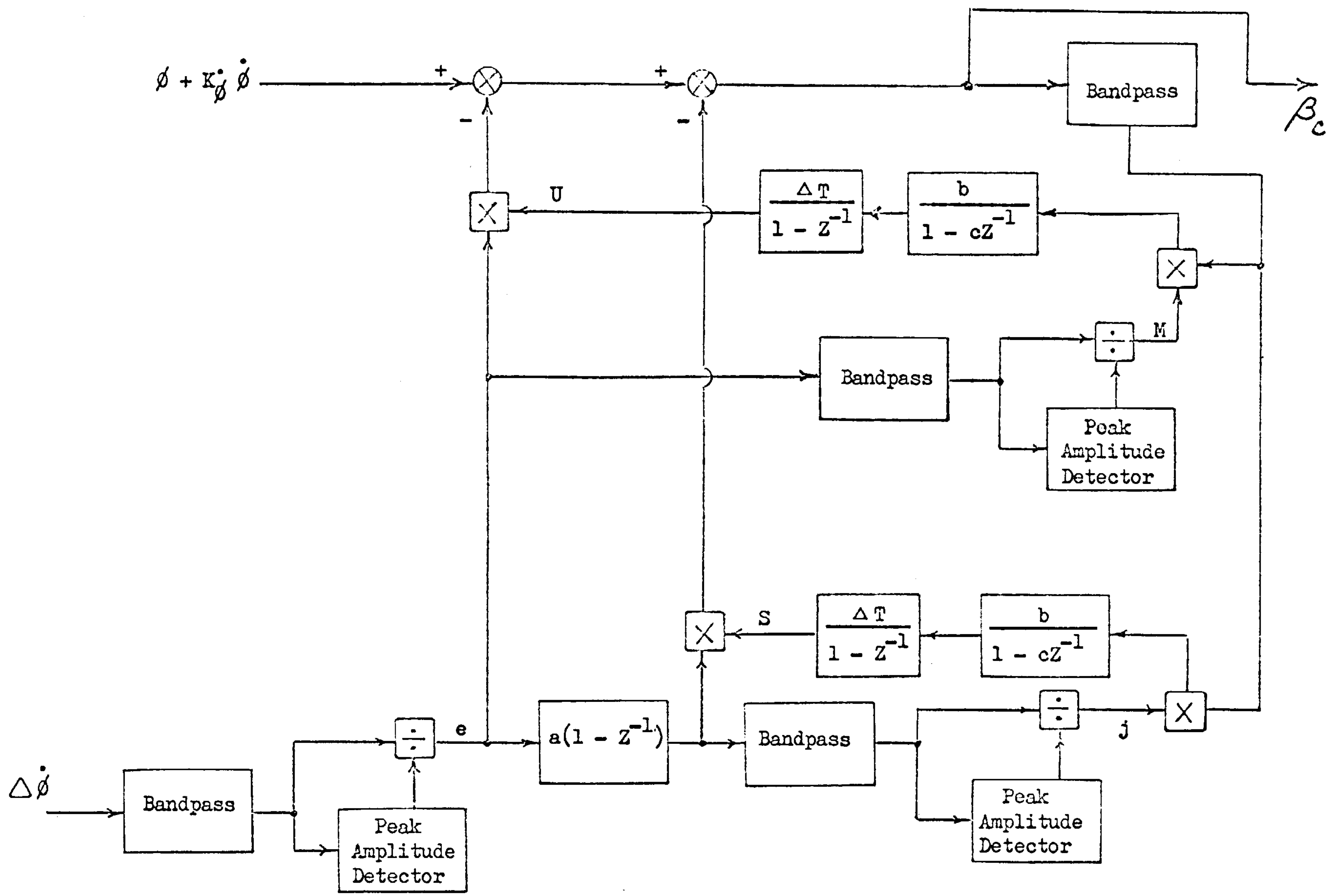

Figure 106. Adaptive Bending Suppression System for One Bending Mode with Bandpass Filtering

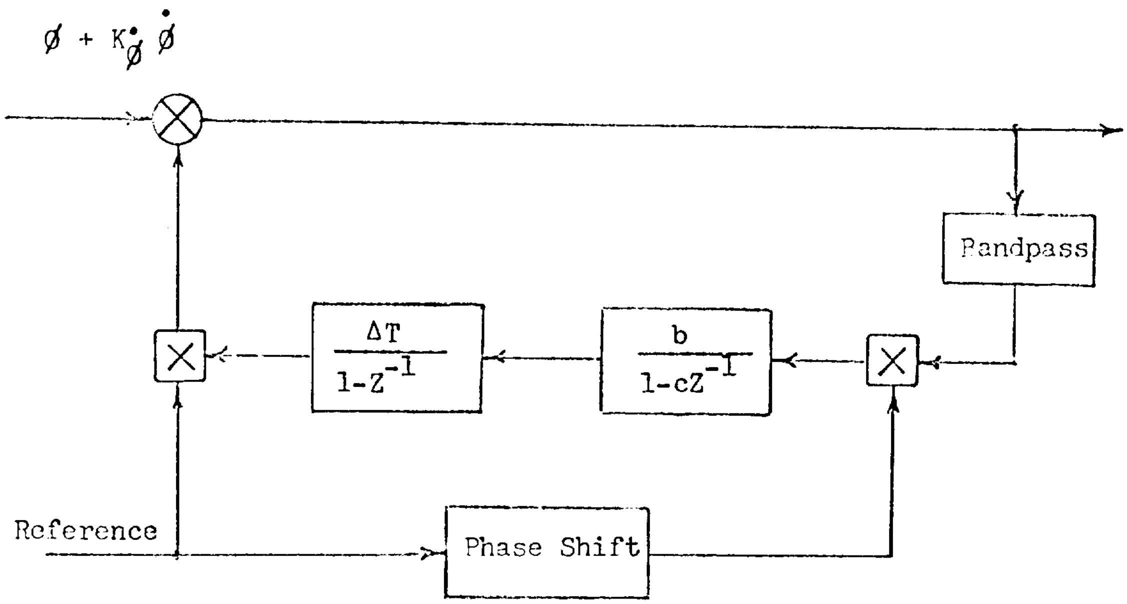

Figure 107. Equivalent Adaptive Loop

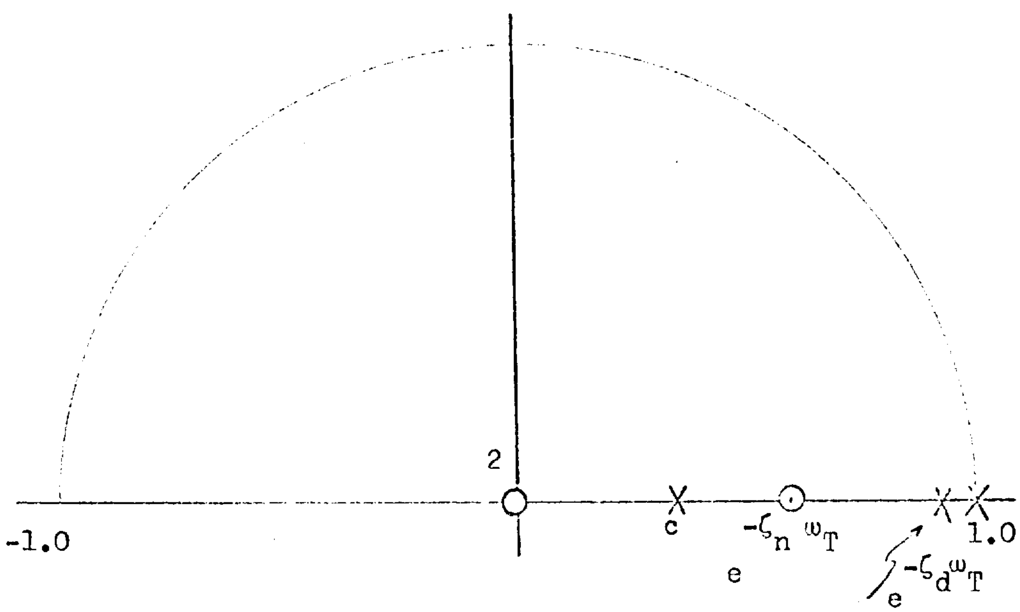

Figure 108. Open Loop Pole Zero Configuration of Servo System

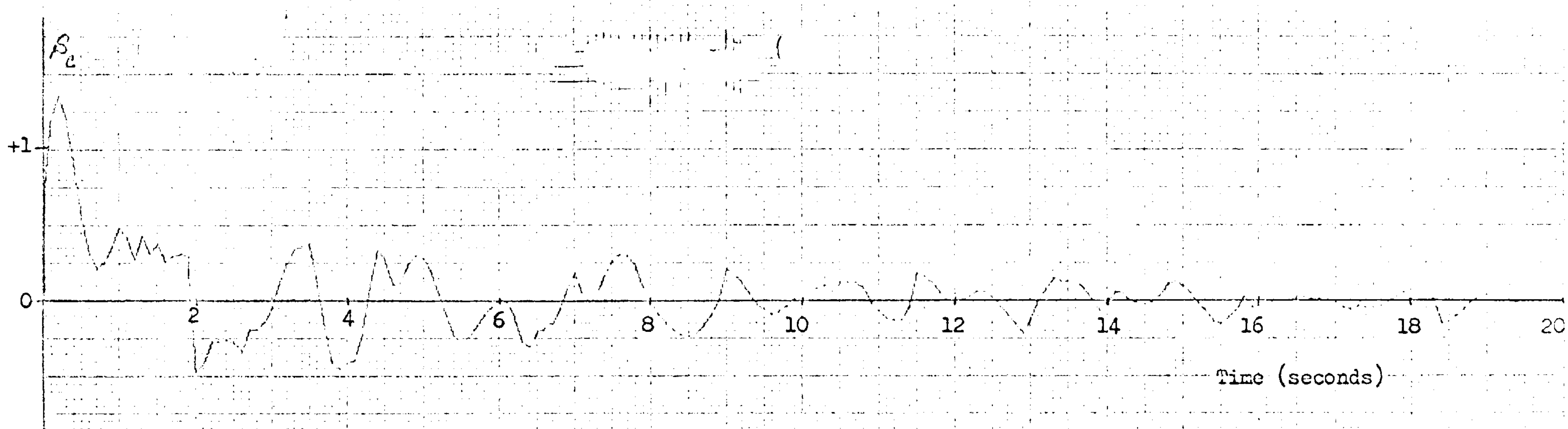

Figure 109-1 β_c vs Time

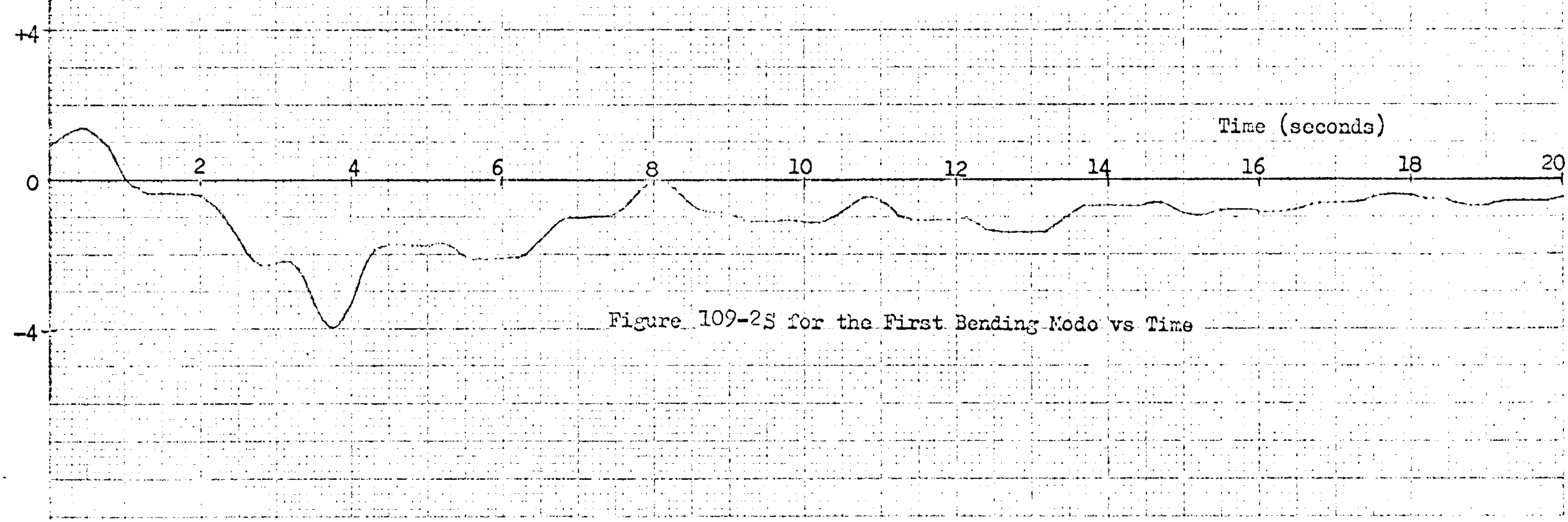

Figure 109-2S for the First Bending Mode vs Time

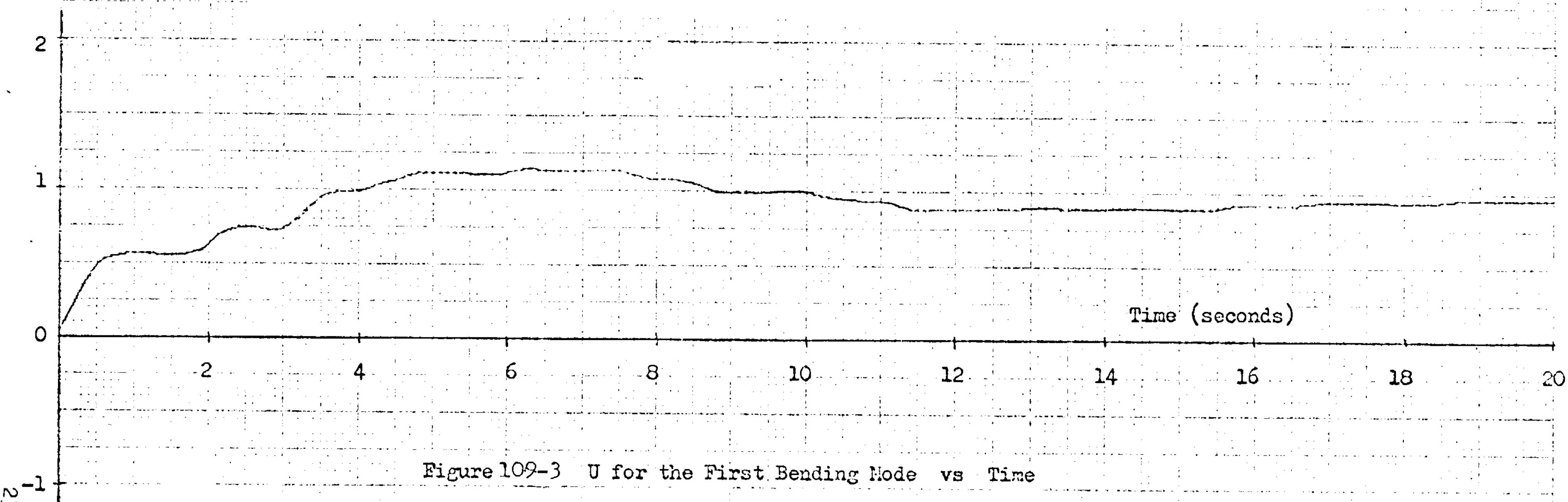

Figure 109-3 U for the First Bending Mode vs Time

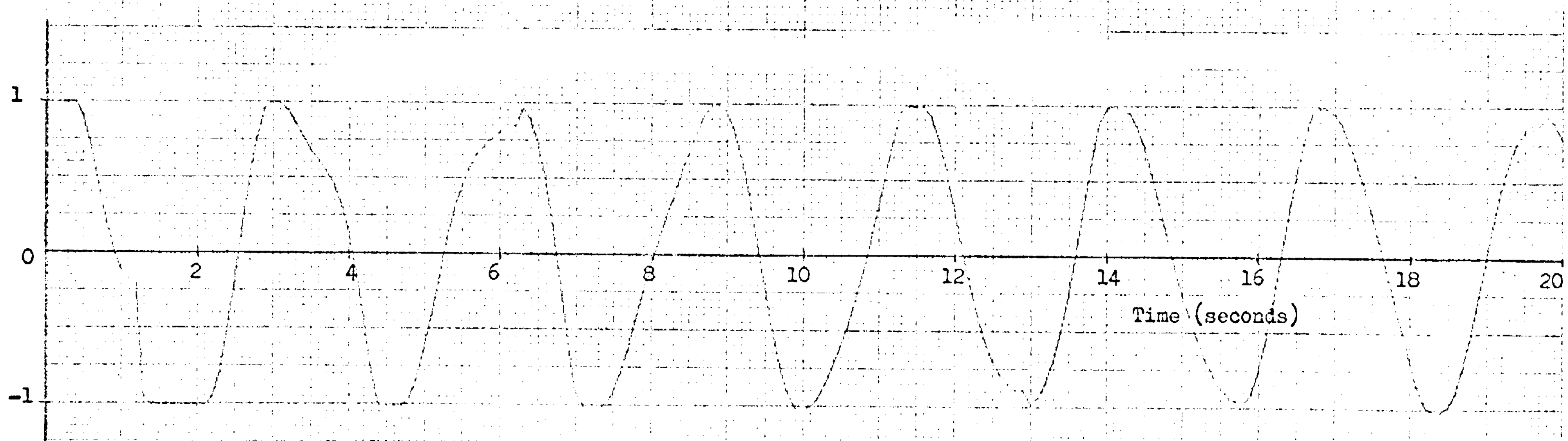

Figure 109-4 e for the First Bending Mode vs Time

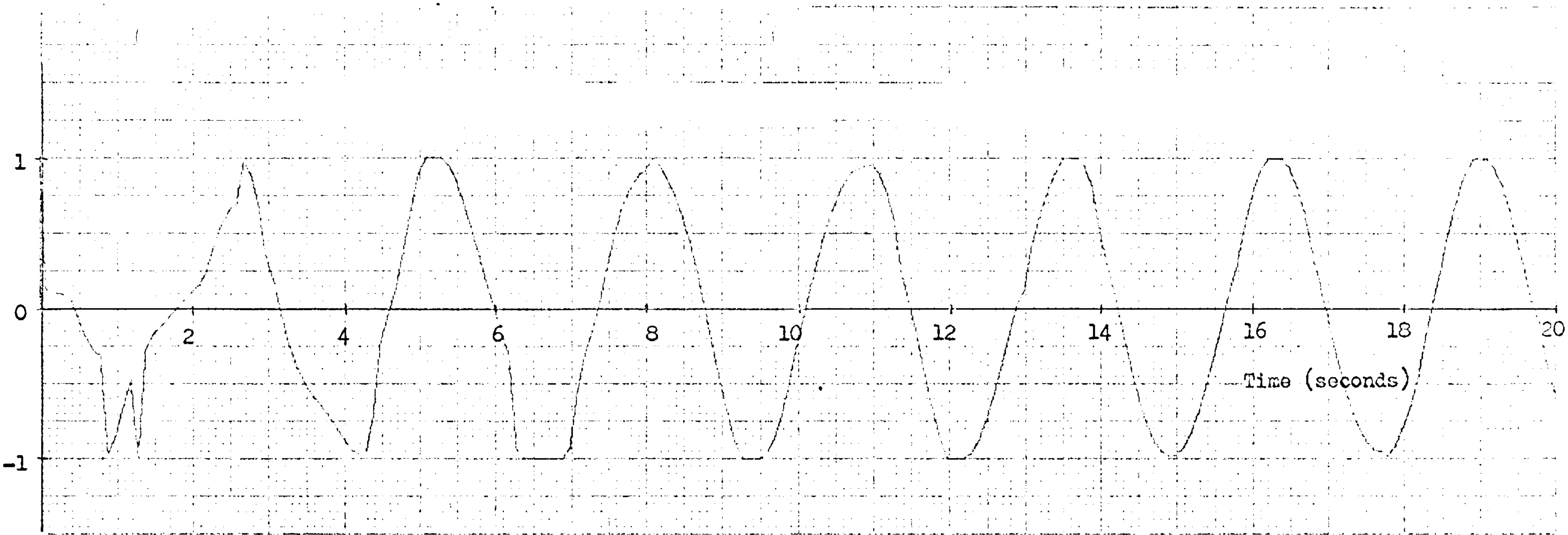

Figure 109-5 j for the First Bending Mode vs Time

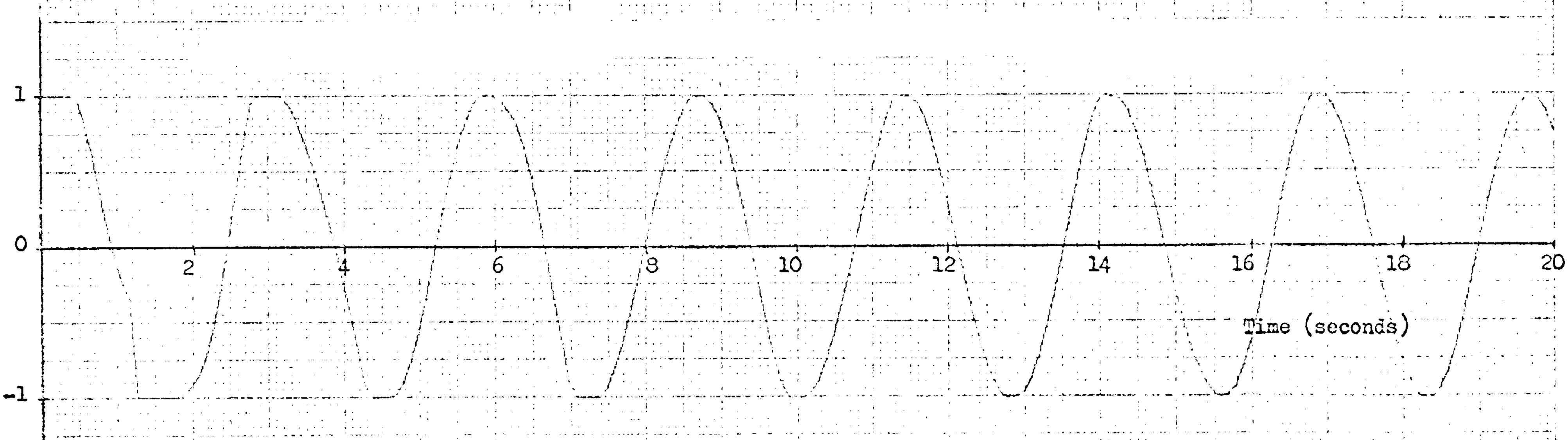

Figure 109-6 M for the First Bending Mode vs Time

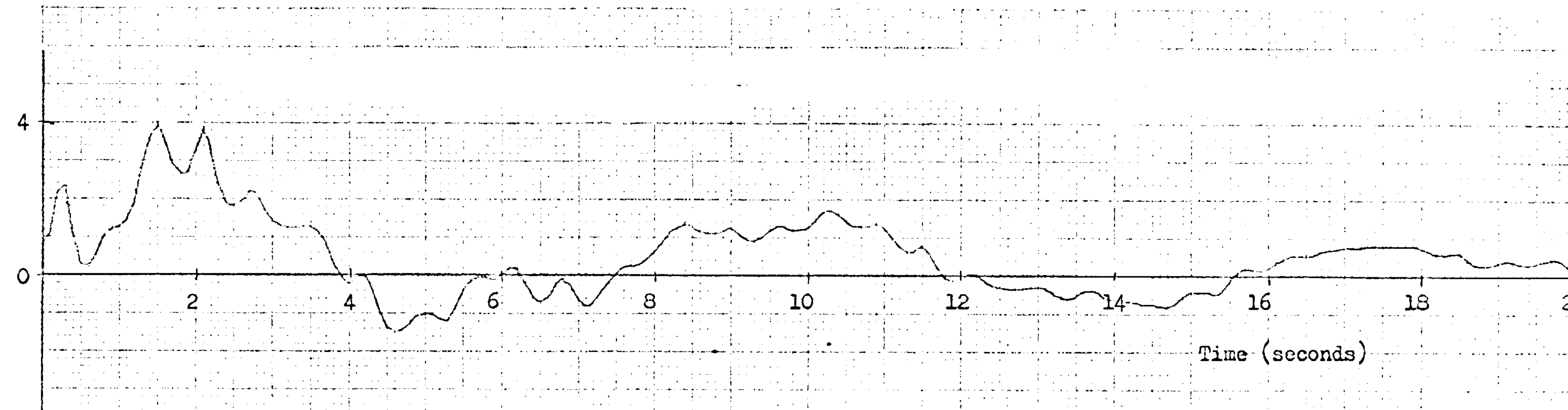

Figure 109-7 S for the Second Bending Mode vs Time

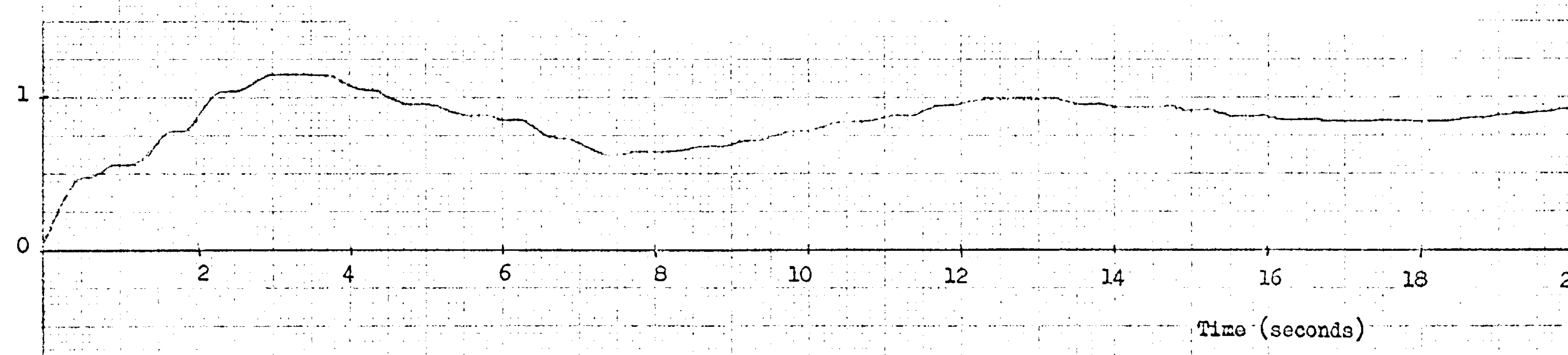

Figure 109-8 U for the Second Bending Mode vs Time

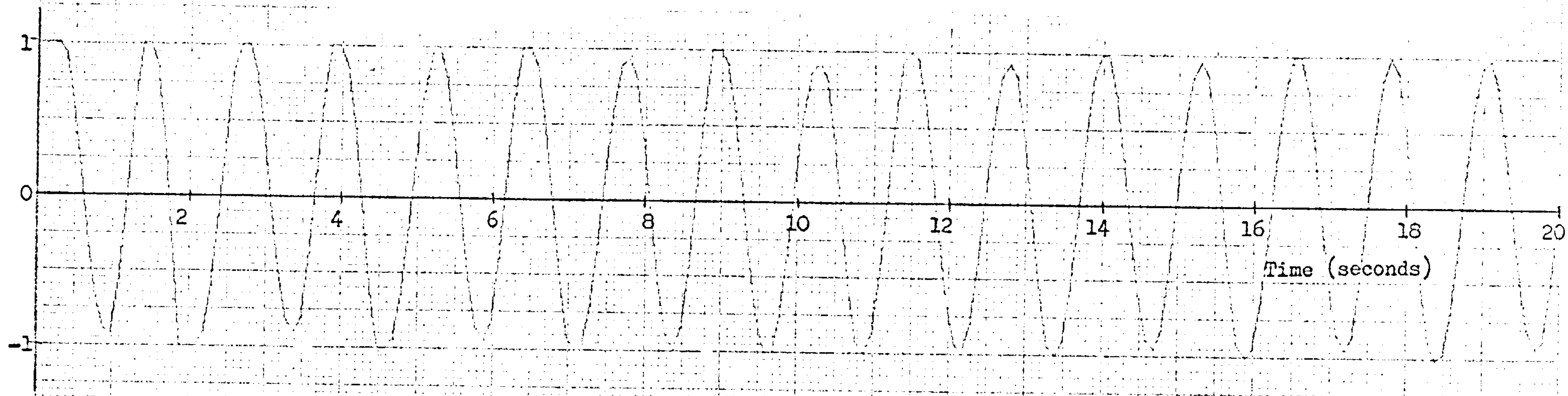

Figure 109-9 e for the Second Bending Mode vs Time

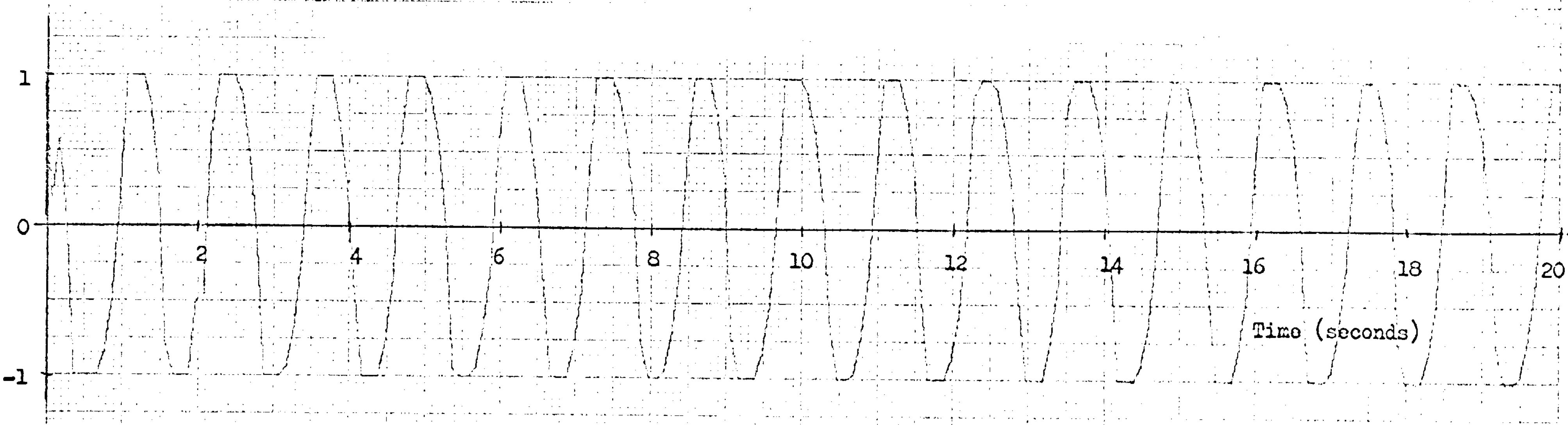

Figure 109-10 j for the Second Bending Mode Vs Time

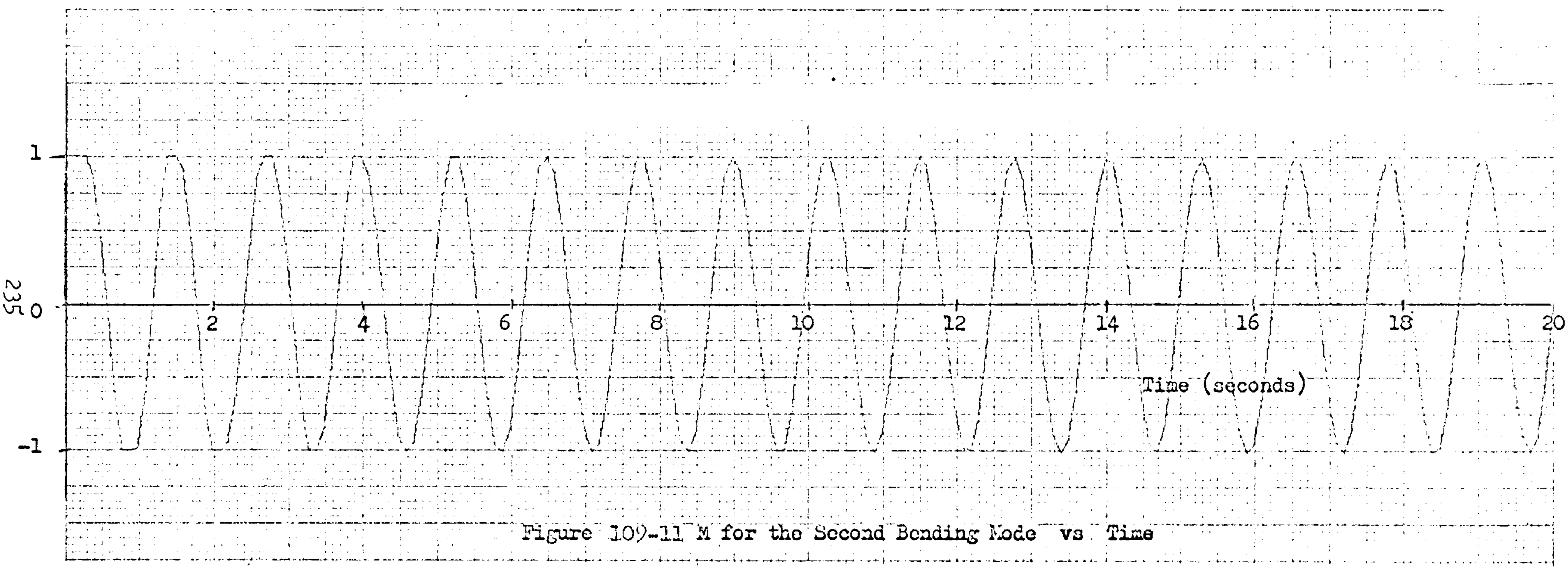

Figure 109-11 M for the Second Bending Mode vs Time

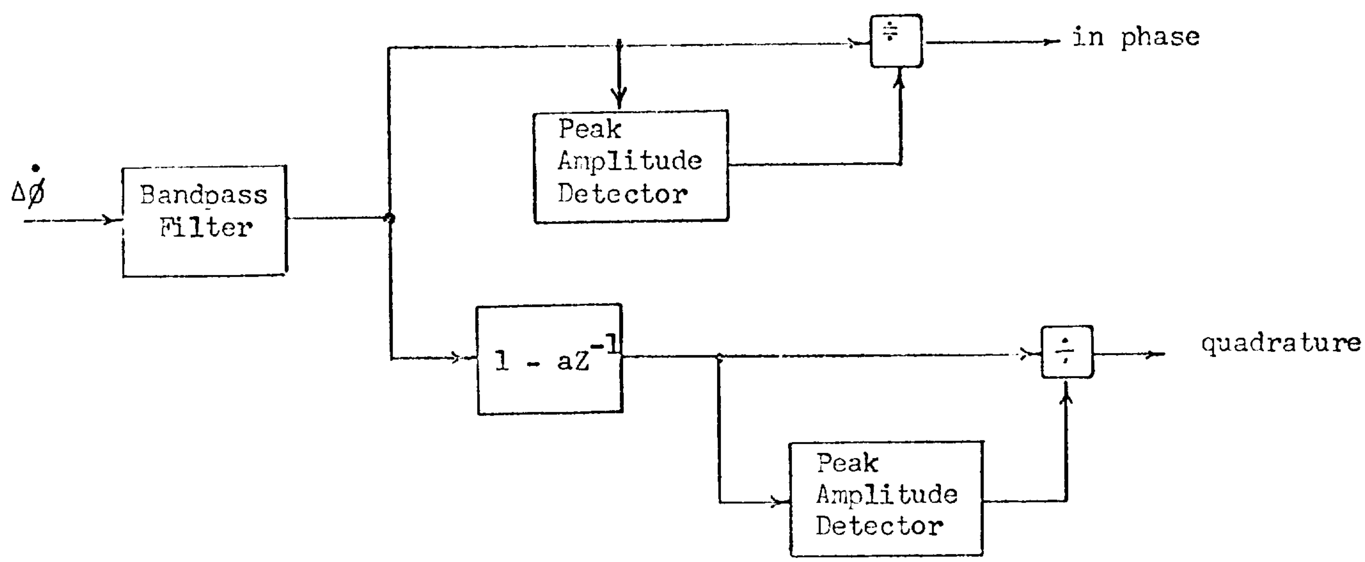

Figure 110. Circuit for Generating In-Phase and Quadrature Reference

APPENDIX

SECTION 6.0

APPENDIX

6.1 SPECTRAL IDENTIFICATION SYSTEM

A periodic function of time, f(t), of periodicity ℓ seconds can be written as a Fourier Series sum of sine and cosine functions[1] by the formula

$$f(t) = \sum_{n=0}^{\infty} A_n \sin\left(\frac{\pi n t}{\ell}\right) + \sum_{n=0}^{\infty} B_n \cos\left(\frac{\pi n t}{\ell}\right) \qquad \text{A-1}$$

where

$$A_n = \frac{2}{\ell}\int_0^{\ell} f(t) \sin\left(\frac{n\pi t}{\ell}\right) dt \qquad \text{A-2}$$

$$B_n = \frac{2}{\ell}\int_0^{\ell} f(t) \cos\left(\frac{n\pi t}{\ell}\right) dt \qquad \text{A-3}$$

If the function f(t) is non-periodic then it cannot be represented by a summation of periodic frequencies but contains components at all frequencies. A_n and B_n are the sine and cosine discrete frequency amplitudes for the periodic case and become continuous functions of frequency, ω, for the non-periodic case. These functions are

$$A(\omega) = \frac{2}{\pi}\int_0^{\infty} \sin(\omega t)\, f(t)\, dt \qquad \text{A-4}$$

$$B(\omega) = \frac{2}{\pi}\int_0^{\infty} \cos(\omega t)\, f(t)\, dt \qquad \text{A-5}$$

The function f(t) can then be expressed as

1. Morse, Philip M., and Feshback, Herman: "Methods of Theoretical Physics", Vol. 1, pp. 454-455, McGraw-Hill, New York, 1953.

$$f(t) = \int_0^\infty A(\omega) \sin(\omega t)\, d\omega + \int_0^\infty B(\omega) \cos(\omega t)\, d\omega \qquad \text{A-6}$$

$A(\omega)$ and $B(\omega)$ thus represent the sine and cosine amplitudes of $f(t)$ at the frequency ω and the total squared amplitude at the frequency is $A^2(\omega) + B^2(\omega)$.

The theory behind the generation of the spectral filter output is to determine an approximate squared amplitude at a frequency, ω_o, for a time slice of a sensor output. A time slice of the sensor output is used because the purpose of the spectral filters is their use in a system to identify frequencies which change in time; therefore, a time slice is taken which is long enough to include several periods of ω_o but short enough so that the frequency to be determined does not change significantly. Figure A-1 shows a typical differential rate gyro output and the time slice used to generate a spectral filter output for ω_o. p is one-half period of ω_o. The dashed line represents the time slice of the input

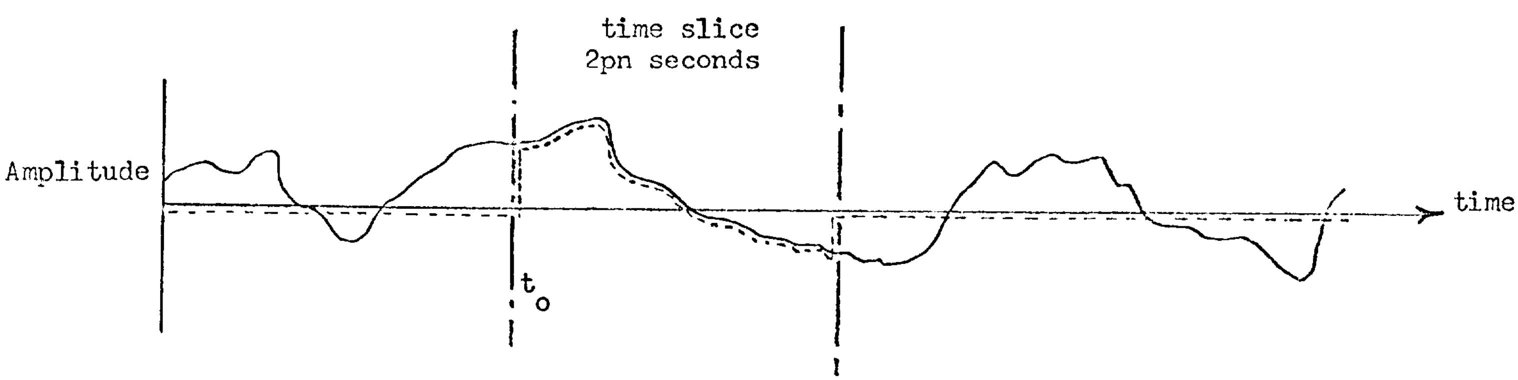

Figure A-1. Typical Spectral Filter Input Time Slice function which is defined as f(t). Thus f(t) has a value between t_o and $2pn + t_o$ and is zero everywhere else. Equations A-4 and A-5 then become

$$A(\omega) = \frac{2}{\pi} \int_{t_o}^{t_o + 2pn} \sin (\omega t)\ f(t)\ dt \qquad \text{A-7}$$

and

$$B(\omega) = \frac{2}{\pi} \int_{t_o}^{t_o + 2pn} \cos (\omega t)\ f(t)\ dt \qquad \text{A-8}$$

Since the spectral filter evaluates $A(\omega)$ and $B(\omega)$ at only the frequency point ω_o, ω_o can be substituted into Equations A-8 and A-9.

Solutions for $A(\omega_o)$ and $B(\omega_o)$ will be developed in a digital computer at a rapid sampling rate. The sin $(\omega_o t)$ and cos $(\omega_o t)$ are costly to form in a digital computer if they are required at a fast rate. In evaluating the sin $(\omega_o t)$ and cos $(\omega_o t)$ either the series expansion for sine and cosine must be evaluated or a difference equation solution must be used to propagate the functions. The fastest way is to use a difference equation solution since ω_o and the sampling rate is fixed for each spectral filter. To do this requires four multiplications and two additions to propagate the sine-cosine pair a single increment in time. The sampling rate required for Model Vehicle II at which the sine-cosine propagation would have to be conducted is .01 seconds. The total number of spectral filters required is 24. If a flight computer were used with computational speed capabilities equivalent to the IBM 7094, .002 seconds of computation time would be required to propagate the sine-cosine pairs for all 24 spectral filters. This amounts to 20% of the available computation time.

If instead of using a sine and cosine function a square wave function of the same frequency is used a fair approximation of Equation A-7 and A-8 is maintained at a significant reduction in computational complexity.

A square wave can be propagated by testing for the time when it changes from +1 to -1 and -1 to +1. Thus, the 4 multiplications and 2 additions are eliminated from the requirements. In addition to this if sine and cosine waves are used they must be multiplied by f(t) before the integration is made. With square waves of amplitude $\pm$ 1 a multiplication is not required, but only a change in sign of the integration as the square wave changes sign. Thus, we will define two kernal functions

$$\text{sqs}\ (\omega t) = \frac{\sin \omega t}{|\sin \omega t|} \tag{A-9}$$

and

$$\text{sqc}\ (\omega t) = \frac{\cos \omega t}{|\cos \omega t|} \tag{A-10}$$

That is sqs (ωt) is a square wave in phase with the sin (ωt) and sqc (ωt) a square wave in phase with the cos (ωt). Using these kernal functions $A(\omega_o)$ and $B(\omega_o)$ became

$$A(\omega_o) = \frac{2}{\pi} \int_{t_o}^{t_o + 2pn} \text{sqs}\ (\omega_o t)\ f(t)\ dt \tag{A-11}$$

$$B(\omega_o) = \frac{2}{\pi} \int_{t_o}^{t_o + 2pn} \text{sqc}\ (\omega_o t)\ f(t)\ dt \tag{A-12}$$

The Fourier Series of sqs ($\omega_o t$) is

$$\text{sqs}\ (\omega_o t) = \frac{2}{\pi}\ (\sin \omega_o t - \frac{1}{3} \sin 3\ \omega_o t + \frac{1}{5} \sin 5\ \omega_o t + \ldots) \tag{A-13}$$

Comparing the values of $A(\omega_o)$ developed from Equation A-11 and $A(\omega_o)$ developed by Equation A-7 by substituting A-13 into A-11 we find

$$A(\omega_o)_{A-11} = \frac{2}{\pi} A(\omega_o)_{A-7} - \frac{2}{\pi} (\tfrac{1}{3}) A(3\omega_o)_{A-7} + \frac{2}{\pi} (\tfrac{1}{5}) A(5\omega_o)_{A-7} \ldots \tag{A-14}$$

This shows that when square wave kernals are used the amplitude of the frequency component at ω_o is found but distorted by the amplitude components at $3\omega_o$, $5\omega_o$, $7\omega_o$, etc. These higher frequency components are down by a factor of $\frac{1}{3}$, $\frac{1}{5}$, $\frac{1}{7}$, etc. Another way of viewing this is that Equation A-7 determines the magnitude of the sin $(\omega_o t)$ component in $f(t)$ while Equation A-11 determines the magnitude of the sqs $(\omega_o t)$ component in $f(t)$.

In the application of the spectral filters the time slice is so chosen so that t_o always occurs when the sqs $(\omega_o t)$ changes sign. In computing the frequency response of $A(\omega_o)$ and $B(\omega_o)$ a test input of $f(t) = \sin(\omega t + \emptyset)$ is used and in this development t_o can be set equal to zero with no loss in generality. If this is done then Equation A-11 can be rewritten as a sum of shorter integration times as

$$A(\omega_o) = \frac{2}{\pi}\left[\int_o^p f(t)dt - \int_p^{2p} f(t)dt + \int_{2p}^{3p} f(t)dt - \dots - \int_{(2n-1)p}^{2np} f(t)\,dt\right] \tag{A-15}$$

and Equation A-12 becomes

$$B(\omega_o) = \frac{2}{\pi}\left[\int_o^{p/2} f(t)dt - \int_{p/2}^{3p/2} f(t)dt + \int_{3p/2}^{5p/2} f(t)dt - \dots - \int_{(2n-\frac{1}{2})p}^{2np} f(t)dt\right] \tag{A-16}$$

If we define

$$X_i \triangleq \frac{2}{\pi}\int_{ip/2}^{(i+1)p/2} f(t)dt \tag{A-17}$$

then Equation A-15 becomes

$$A(\omega_o) = X_0 + X_1 - X_2 - X_3 + X_4 + X_5 - \dots - X_{4n-1} \tag{A-18}$$

and Equation A-16 becomes

$$B(\omega_o) = X_0 - X_1 - X_2 + X_3 + X_4 - \cdots + X_{4n-1} \qquad \text{A-19}$$

A frequency response is obtained by letting $f(t)$ equal $\sin(\omega t + \phi)$. Therefore, for a frequency response Equation A-17 becomes

$$X_i = \frac{2}{\pi} \int_{ip/2}^{(i+1)p/2} \sin(\omega t + \phi)\, dt \qquad \text{A-20}$$

Making the substitution

$$y + \omega t + \phi \qquad \text{A-21}$$

then

$$X_i = \frac{2}{\omega\pi} \int_{\frac{i\omega p}{2} + \phi}^{\frac{(1+i)p\omega}{2} + \phi} \sin y\, dy \qquad \text{A-22}$$

making the substitutions of

$$p = \frac{\pi}{\omega_o} \qquad \text{A-23}$$

and using the normalized frequency

$$r = \frac{\omega}{\omega_o} \qquad \text{A-24}$$

then

$$X_i = \frac{2}{\omega\pi} \int_{\frac{ir\pi}{2} + \phi}^{\frac{(i+1)\pi r}{2} + \phi} \sin y\, dy \qquad \text{A-25}$$

performing the integration yields

$$X_i = \frac{2}{\omega\pi} \left[\cos\left(\frac{ir\pi}{2} + \phi\right) - \cos\left(\frac{i\pi r}{2} + \frac{\pi r}{2} + \phi\right)\right] \qquad \text{A-26}$$

simplifying

$$X_i = \frac{4}{\omega\pi} \sin \frac{\pi r}{4} \sin \left(\frac{i\pi r}{2} + \frac{\pi r}{4} + \emptyset\right) \qquad \text{A-27}$$

The integration for sqs and sqc kernals, respectively, performed over 1/2 period with i = 0, 2, 4, 6, etc. is

$$S_i = (-1)^{i/2} \frac{4}{\omega\pi} \sin \frac{\pi r}{4} \left\{\sin \left[\left(i + \frac{1}{2}\right) \frac{\pi r}{2} + \emptyset\right] + \sin \left[\left(i + \frac{3}{2}\right) \frac{\pi r}{2} + \emptyset\right]\right\} \qquad \text{A-28}$$

and

$$C_i = (-1)^{i/2} \frac{4}{\omega\pi} \sin \frac{\pi r}{4} \left\{\sin \left[\left(i + \frac{1}{2}\right) \frac{\pi r}{2} + \emptyset\right] - \sin \left[\left(i + \frac{3}{2}\right) \frac{\pi r}{2} + \emptyset\right]\right\} \qquad \text{A-29}$$

simplifying by trig identities gives

$$S_i = (-1)^{i/2} \frac{4}{\omega\pi} \sin \frac{\pi r}{2} \sin \left[(i+1) \frac{\pi r}{2} + \emptyset\right] \qquad \text{A-30}$$

and

$$C_i = -(-1)^{i/2} \frac{8}{\omega\pi} \sin^2 \frac{\pi r}{4} \cos \left[(i+1) \frac{\pi r}{2} + \emptyset\right] \qquad \text{A-31}$$

The frequency response of a normal n^{th} order filter is then determined by

$$S_0 + S_2 + S_4 + \dots S_{4n-2} \text{ and } C_0 + C_2 + C_4 + \dots + C_{4n-2}$$

giving

$$S = \frac{4}{\omega\pi} \sin \frac{\pi r}{2} \sum_{i=0}^{2n-1} (-1)^i \sin \left[(2i+1) \frac{\pi r}{2} + \emptyset\right] \qquad \text{A-32}$$

and

$$C = -\frac{8}{\omega\pi} \sin^2 \frac{\pi t}{4} \sum_{i=0}^{2n-1} (-1)^i \cos \left[(2i+1) \frac{\pi r}{2} + \emptyset\right] \qquad \text{A-33}$$

Making the substitution

$$\phi' = \phi + \frac{\pi}{2} \qquad \text{A-34}$$

then Equation A-33 is

$$C = \frac{8}{\omega\pi} \sin^2 \frac{\pi r}{4} \sum_{i=0}^{2n-1} (-1)^i \sin\left[(2i+1)\frac{\pi r}{2} + \phi'\right] \qquad \text{A-35}$$

Thus, the problem is one of evaluating the series

$$V = \sin\left(\frac{\pi r}{2} + \phi\right) - \sin\left(\frac{3\pi r}{2} + \phi\right) + \sin\left(\frac{5\pi r}{2} + \phi\right) - \ldots - \sin\left[\frac{(4n-1)}{2}\pi r + \phi\right]$$

A-36

Regrouping the series

$$V = \left\{ \sin\left(\frac{\pi r}{2} + \phi\right) - \sin\left[\frac{(4n-1)}{2}\pi r + \phi\right]\right\} - \left\{\sin\left(\frac{3\pi r}{2} + \phi\right)\right.$$

$$\left. - \sin\left[\frac{4n-3}{2}\pi r + \phi\right]\right\} + \ldots - (-1)^n \left\{\sin\left[\frac{(2n-1)}{2}\pi r + \phi\right] - \sin\left[\frac{(2n+1)}{2}\pi r + \phi\right]\right\}$$

A-37

Evaluating each term in the brackets $\{\ \}$ by trig identities gives

$$V = -2\cos\left[n\pi r + \phi\right]\left\{\sin\left[\frac{2n-1}{2}\pi r\right] - \sin\left[\frac{2n-3}{2}\pi r\right] + \ldots + (-1)^n \sin\left[\frac{\pi r}{2}\right]\right\}$$

A-38

multiplying and dividing the series by $\cos\frac{\pi r}{2}$ and using the identity $2\sin x \cos y = \sin(x+y) + \sin(x-y)$ yields

$$V = \frac{-\cos\left[n\pi r + \phi\right]}{\cos\frac{\pi r}{2}}\left[\sin(n\pi r) + \sin(n-1)\pi r - \sin(n-1)\pi r - \sin(n-2)\pi r\right.$$

$$\left. + \ldots + (-1)^n \sin\pi r + (-1)^n \sin\right] \qquad \text{A-39}$$

simplifying

$$V = \frac{\cos [n\pi r + \phi] \sin (n\pi r)}{\cos \frac{\pi r}{2}} \qquad \text{A-40}$$

therefore

$$S = \frac{-4}{\omega\pi} \frac{\sin \frac{\pi r}{2} \sin (n\pi r) \cos (n\pi r + \phi)}{\cos \frac{\pi r}{2}} \qquad \text{A-41}$$

$$C = \frac{8}{\omega\pi} \frac{\sin^2 \frac{\pi r}{2} \sin (n\pi r) \cos (n\pi r + \phi')}{\cos \frac{\pi r}{2}}$$

$$= \frac{8}{\omega\pi} \frac{\sin^2 \frac{\pi r}{2} \sin (n\pi r) \sin (n\pi r + \phi)}{\cos \frac{\pi r}{2}} \qquad \text{A-42}$$

The output amplitude is computed by $S^2 + C^2$ which can be represented by

$$D = F_1(r) \cos^2 (n\pi r + \phi) + F_2(r) \sin^2 (n\pi r + \phi) \qquad \text{A-43}$$

where $F_1(r)$ and $F_2(r)$ can be determined from inspection of Equations A-41 and A-42. To determine the bounds on the amplitude response maximum and minimum values of Equation A-43 must be found with respect to ϕ. This occurs when

$$\frac{\partial D}{\partial \phi} = 2 [F_2(r) - F_1(r)] \sin (n\pi r + \phi) \cos (n\pi r + \phi) = 0 \qquad \text{A-44}$$

Solving A-44 for ϕ yields

$$\phi = -n\pi r \text{ or } \frac{\pi}{2} - n\pi r \qquad \text{A-45}$$

This shows that maximum and minimum amplitude response curves are determined by squaring A-41 and A-42 with $\phi = -n\pi r$ and $\frac{\pi}{2} - n\pi r$, respectively. To normalize A-41 and A-42 to an amplitude of 1 at r=1 (i.e., the tuned frequency) equation A-41 must be multiplied by $\frac{\omega_o \pi}{8 n}$ and equation A-42 by $\frac{\pi\omega_o}{16n}$ generating boundary equations for frequency response amplitudes of

$$D = \frac{\sin^2 \frac{\pi r}{2} \sin^2 (n\pi r)}{4n^2 r^2 \cos^2 \frac{\pi r}{2}} \qquad \text{A-46}$$

and

$$D = \frac{\sin^4 \frac{\pi r}{2} \sin^2 (n\pi r)}{4n^2 r^2 \cos^2 \frac{\pi r}{2}} \qquad \text{A-47}$$

Equations A-46 and A-47 describe what has been named a standard spectral filter. A plot of the value of D in db vs. normalized frequency, r, is shown in Figure A-2 for n = 5. The filter peaks at the tuned frequency (r=1). There are also peaks at the odd harmonic frequencies (r=3, 5, 7, etc). This is caused by the square wave kernal which is composed of these same harmonics.

It was discovered that the spectral filter amplitude response was improved if S and C were formed by

$$S = S_0 + 2\,(S_2 + S_4 + \ldots + S_{4n-4}) + S_{4n-2} \qquad \text{A-48}$$

$$C = C_0 + 2\,(C_2 + C_4 + \ldots + C_{4n-4}) + C_{4n-2} \qquad \text{A-49}$$

The equations representing the maximum and minimum limits on D can be developed for this system in the same manner as was done for the standard filter.

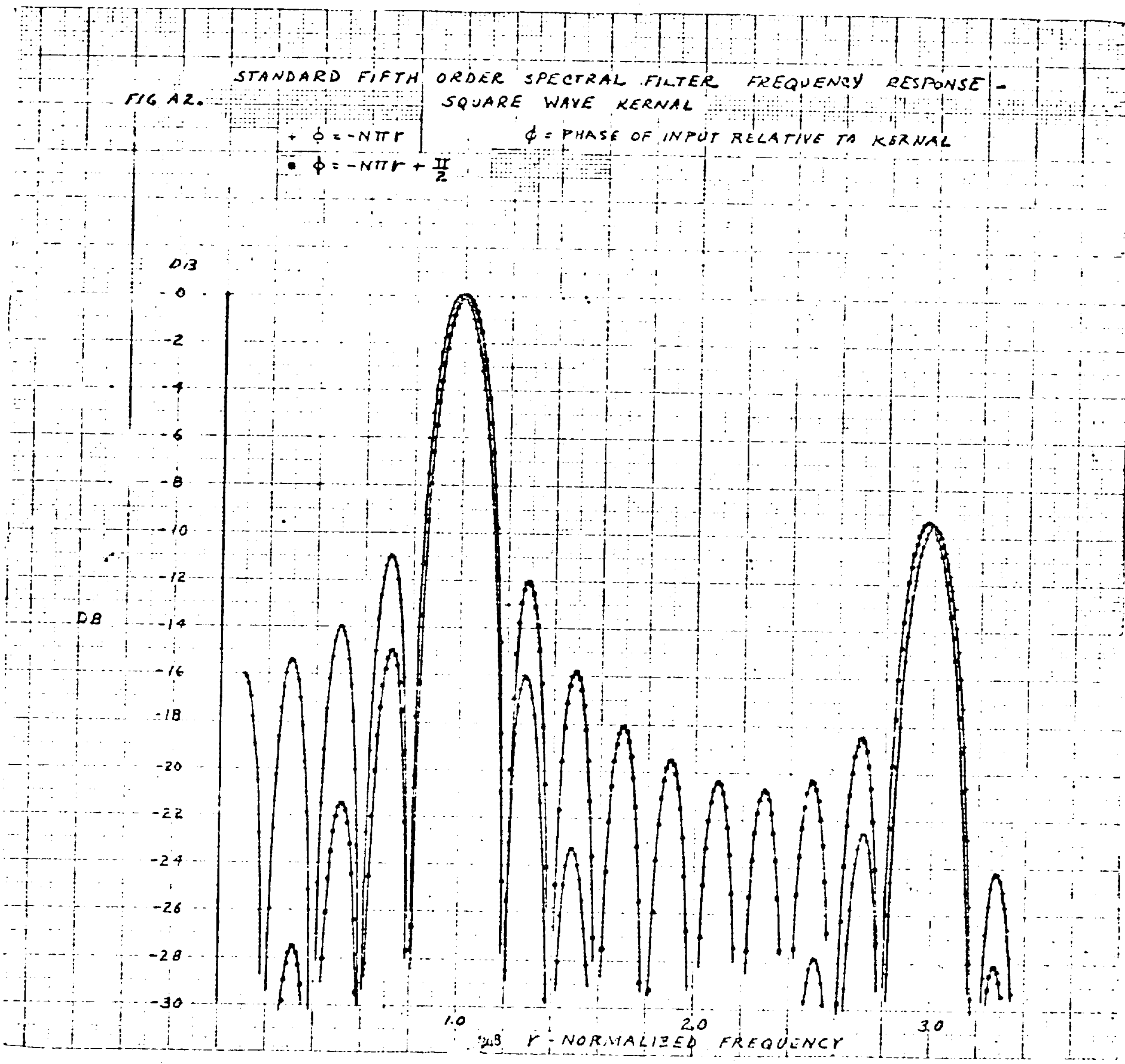
FIG A2.
STANDARD FIFTH ORDER SPECTRAL FILTER FREQUENCY RESPONSE - SQUARE WAVE KERNAL
+ φ = -Nπr
• φ = -Nπr + π/2
φ = PHASE OF INPUT RELATIVE TA KERNAL
DB
0
-2
-4
-6
-8
-10
-12
-14
-16
-18
-20
-22
-24
-26
-28
-30
1.0
2.0
3.0
r - NORMALIZED FREQUENCY

The result being:

$$D = \frac{\sin^4 \frac{\pi r}{2} \cos^2 (2n-1) \frac{\pi r}{2}}{(2n-1)^2 r^2 \cos^2 \frac{\pi r}{2}} \qquad \text{A-50}$$

and

$$D = \frac{\sin^2 \frac{\pi r}{2} (1 - \cos \frac{\pi r}{2})^2 \cos^2 (2n-1) \frac{\pi r}{2}}{(2n-1)^2 r^2 \cos^2 \frac{\pi r}{2}} \qquad \text{A-51}$$

The value of D computed from A-50 and A-51 is given in Figure 1 for n=5. In comparing this with Figure A-1 it can be seen that the major peaks are unchanged, however with the modified filter the minor peaks between the odd harmonics and below the tuned frequency are improved.

The difference in mechanization within a digital computer is insignificant between the standard and modified filter form. It is possible in either form to obtain a spectral filter output at any desired time interval. The speed with which spectral filter outputs are desired is most dependent upon the starting process. If initially the bending mode frequencies are unknown by a large percentage, the control system will cause unstable bending at launch time. The identification must be rapid enough that bending amplitudes do not diverge far enough while initially unstable to exceed vehicle loads. When the filters are initially started, at least $\frac{1}{2}$ period of the kernal wave form must elapse before any useful information is generated by the filters.

For this reason it was decided that an output for each spectral filter would be generated every $\frac{1}{2}$ period of kernal frequency. Each spectral filter output was generated by a program with a block diagram as shown in Figure A-3. M_n is the number of sampling times in $\frac{1}{2}$ period. X and Y contain the partial integration values for the spectral filters. They are

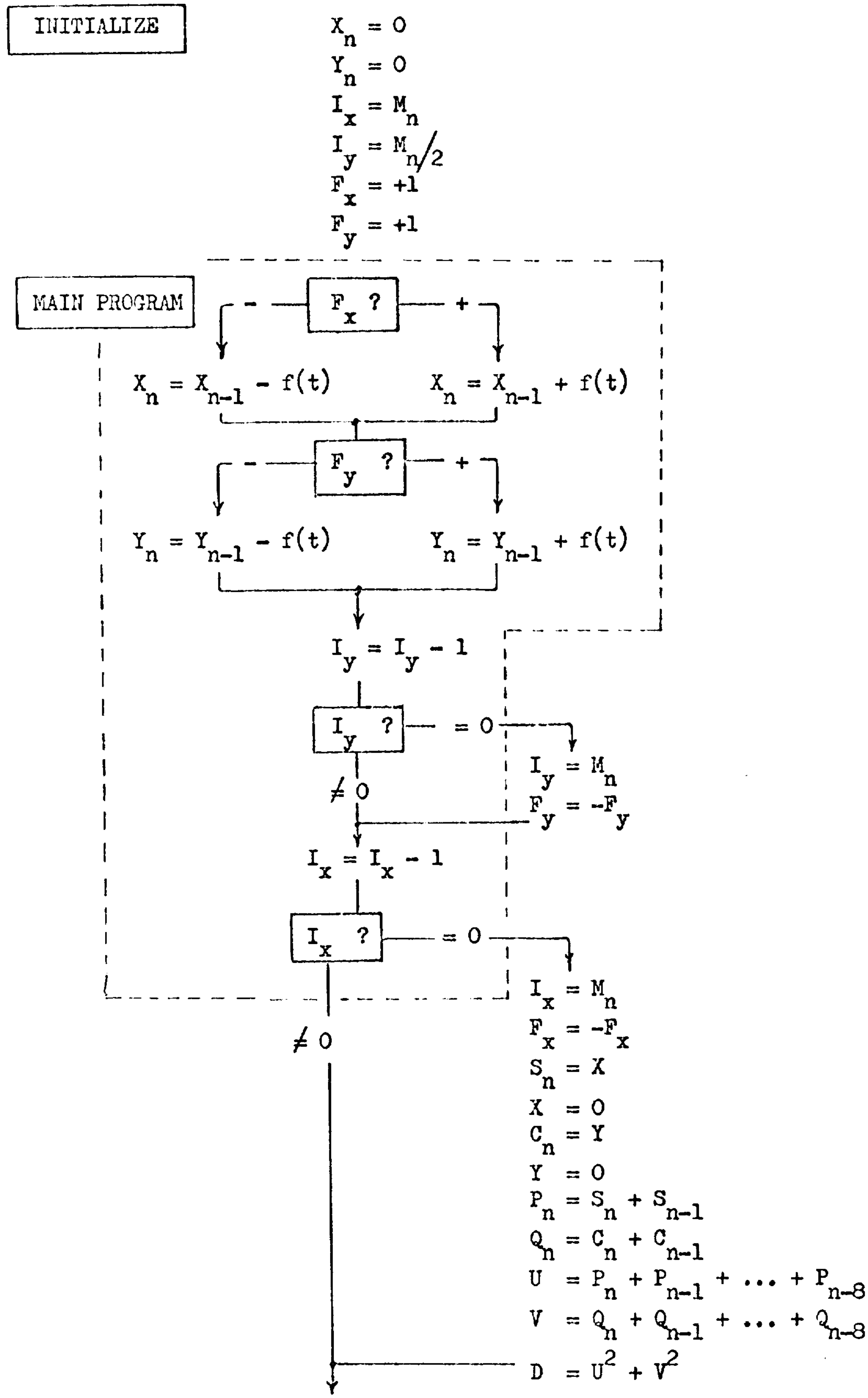

Figure A-3. Spectral Filter Program Block Diagram allowed to integrate for 1/2 period and then reset to zero. F_x and F_y specify the instantaneous sign of the sine and cosine kernals respectively and I_x and I_y are counter values used to determine when the kernal changes sign. When a full half period has been processed the value of X and Y are stored away. A full period value for each kernal integrator is generated in P and Q by summing the present and past half period integrator outputs then stored in S and C. U and V are the outputs of the modified 5^{th} order sine and cosine integrators and are formed by summing the present and past values of P and Q. The total spectral filter output, D, is obtained by forming $U^2 + V^2$. Before D is used, it is multiplied by a normalizing constant. The value of the normalizing constant changes during the starting operation reaching a constant value of $(\frac{1}{18M_n})^2$ for each spectral filter during the major portion of the flight. With each half period of the kernal the normalizing constant has a new value. These values are given in terms of M_n for each half period of the kernal in Tablė A-1.

Half Period	Normalizing Factor
1	$(1/M_n)^2$
2	$(1/4\ M_n)^2$
3	$(1/6\ M_n)^2$
4	$(1/8\ M_n)^2$
5	$(1/10\ M_n)^2$
6	$(1/12\ M_n)^2$
7	$(1/14\ M_n)^2$
8	$(1/16\ M_n)^2$
9 or more	$(1/18\ M_n)^2$

Table A-1. Values of the Normalizing Factor at each Half Period

M_n must be an even integer when determining thetuned frequency of each spectral filter. This requirement exists because each computer computation occurs at a sampling time and the sqc kernal changes sign at $M_n/2$ sampling times after the sqs kernal changes sign, $M_n/2$ must be a whole value integer. If M_n is odd the sqc and sqs kernals will not have a $\frac{\pi}{2}$ rad phase shift between them. The effect will be greater at high frequencies with the error from $\frac{\pi}{2}$ radians being $\pi/2M_n$ radians.

The range of bending frequencies for the nominal vehicle is 2.15 radians/sec (the first bending mode at t=0 sec) to 11.7 radians/sec (the third bending mode at t=157 sec). The spectral filters were placed over the band of frequencies ranging from 1.51 radians/sec to 14.28 radians/sec. This band can easily be extended by adding more spectral filters. A separation between spectral filters of approximately 10% was maintained. This does not mean however, that identification of bending frequencies is limited to 10%. Further processing on the spectral filter output improves this accuracy to within 1 or 2% if the mode is at all excited.

The integration required by the spectral filters is performed in the computer using rectangular integration. If it is desirable to perform the integration of

$$y(\tau) = \int_0^{\tau} f(t)\ dt \qquad \text{A-52}$$

within a digital computer by means of rectangular integration then the algorithm

$$y(\tau) = T \sum_{i=0}^{\tau/T} f(iT) \qquad \text{A-53}$$

is solved where T is the sampling rate. f(iT) has values only at the sampling times. It is possible to determine a function g(t) such that

$$\int_0^{\tau} g(t)\ dt = T \sum_{i=0}^{\tau/T} f(iT) \qquad \text{A-54}$$

Figure A-4 shows f(t) a sine wave and the resultant g(t). The difference between g(t) and f(t) is an indication of the quality obtained using rectangular integration. The difference is less for higher sampling rates. Trajectory runs indicated that the third bending mode was not as accurately identified as the first and second modes. This was interpreted as being partially due to the sampling effects. A method exists for eliminating the effects of sampling. In order to explain this method the reasons for the choice of input to the spectral filters must be considered.

The input to the spectral filters was obtained by mounting two rate gyros--one at the instrument unit and one at the first-second interstage region. The outputs of these two rate gyros were subtracted to obtain the spectral filter input signal. The output of a rate gyro at a body station X_1 is given by

$$\dot{\phi}_I = \dot{\phi} - Y_1'(X_1)\,\dot{\eta}_1 - Y_2'(X_1)\,\dot{\eta}_2 - Y_3'(X_1)\,\dot{\eta}_3 \qquad \text{A-55}$$

where $\dot{\phi}$ is the rigid body pitch rate, $\dot{\eta}_1$, $\dot{\eta}_2$ and $\dot{\eta}_3$ the time rate of charge of the normalized deflections for the 1^{st}, 2^{nd}, and 3^{rd} bending modes respectively, and $Y_1'(X_1)$, $Y_2'(X_1)$ and $Y_3'(X_1)$ the local bending slopes for the 1^{st}, 2^{nd}, and 3^{rd} bending modes, resepctively. By subtracting the outputs of two rate gyros at different locations the rigid body $\dot{\phi}$ term is removed and a signal is obtained which contains only bending information. This signal was chosen as an input to the spectral filters because it contains no rigid body information to distort the identification accuracy. Rate gyros were chosen not to obtain a signal composed of $\dot{\eta}$ rather than $\ddot{\eta}$ and/or η but because they are standard instruments throughout the industry and a simple inexpensive instrument.

This signal will be called $\Delta\dot{\phi}(t)$ and is a function of $\dot{\eta}_1$, $\dot{\eta}_2$ and $\dot{\eta}_3$ with an output defined by

$$\Delta\dot{\phi}(t) = Y_1'(\Delta\phi)\,\dot{\eta}_1 + Y_2'(\Delta\phi)\,\dot{\eta}_2 + Y_3'(\Delta\phi)\,\dot{\eta}_3 \qquad \text{A-56}$$

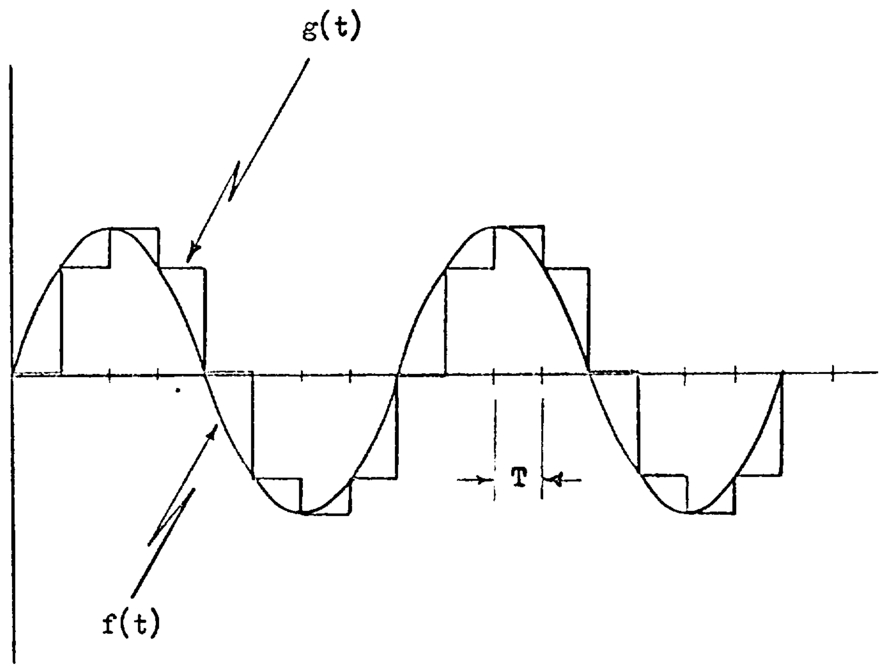

Figure A 4. The Effects of Sampling a Sine Wave

There is no reason to believe that equivalent operation would not be achieved if angular accelerometers mounted at the same location rather than rate gyros were used. If this were done the spectral filter input signal would be $\frac{d\Delta\dot{\phi}(t)}{dt}$. An integration without sampling effects over one period of an sqs kernal as required by the spectral filters would then be

$$S = \int_{o}^{2p} \text{sqs}\ (\omega_o t)\ \frac{d\Delta\dot{\phi}(t)}{dt} \qquad \text{A-57}$$

The integral can be broken up into two parts by evaluating sqs $(\omega_o t)$ and becomes

$$S = \int_{o}^{p} \frac{d\Delta\dot{\phi}(t)}{dt}\ dt - \int_{p}^{2p} \frac{d\Delta\dot{\phi}(t)}{dt} \qquad \text{A-58}$$

Performing the indicated integrations yields

$$S = -\Delta\dot{\phi}(0) + 2\Delta\dot{\phi}(p) - \Delta\dot{\phi}(2p) \qquad \text{A-59}$$

If the process is repeated for C then

$$C = -\Delta\dot{\phi}(0) + 2\Delta\dot{\phi}\ (\tfrac{p}{2}) - 2\Delta\dot{\phi}\ (\tfrac{3p}{2}) + \Delta\dot{\phi}(2p) \qquad \text{A-60}$$

is obtained. S and C could be formed by sampling $\Delta\dot{\phi}(t)$ at t=0, p/2, p, 3p/2, and 2p and performing the calculations indicated by A-59 and A-60. $\Delta\dot{\phi}(t)$ is the output of the difference in two rate gyros therefore a spectral filter output using perfect integrators and an input formed from the difference in two angular accelerometer signals can be obtained without integration by using the difference in two rate gyros.

The actual mechanization of this method was not done because its discovery was made late in the study and at the time adequate identification was being achieved using the rectangular integration algorithm. Using this method should increase identification accuracy or under the same accuracy requirements a reduction in the number of spectral filters required could be made.

Table A-2 are spectral filter parameters used in the study plus a typical spectral filter output set. "n" is an integer associated with each spectral filter. M_n the number of sampling times at the .01 second iteration rate in half a period of the tuned frequency for each spectral filter. ω_n is the spectral filter tuned frequency which can be computed from

$$\omega_n = \pi/.01\ M_n. \qquad \text{A-61}$$

D is a typical set of spectral filter output values. R are the resolution values for each spectral filter. Peaks will be rejected if they have a magnitude less than the resolution value. Figure A-5 is a plot of D (the spectral filter output amplitudes) vs. n (the integer associated with each filter). The resolution values are plotted with dashed lines. In this case all of the peaks are above the resolution level thus none are rejected for this reason. At first glance there appear to be 6 peaks located at values of n of 2, 7, 12, 16, 20 and 22. Of these the peak at n = 22 is not legitimate because there are not two values on each side of it less than the peak value. The peak at n = 2 is legitimate since it is handled as a special case. The three largest peaks are located at n values of 7, 12, and 20. It is these three peaks which are identified as defining the three bending frequencies. The spectral filter output in Figure A-5 were generated in an actual trajectory simulation and were taken from a point 59 seconds into the trajectory. The actual open loop bending frequencies at this time are 2.3, 5.4375 and 8.91875 radians per second for the 1^{st}, 2^{nd} and 3^{rd} bending modes, respectively. From Table A-2 the frequencies associated with n values of 20, 12, and 7 are 2.28, 5.24 and 8.73 radians/second. The identified frequency is not taken directly as the frequency associated with the peak but is computed by the formula

$$\omega_{F_I} = \frac{A_{n-1}\,\omega_{n-1} + A_n\,\omega_n + A_{n+1}\,\omega_{n+1}}{A_{n-1} + A_n + A_{n+1}} \qquad \text{A-62}$$

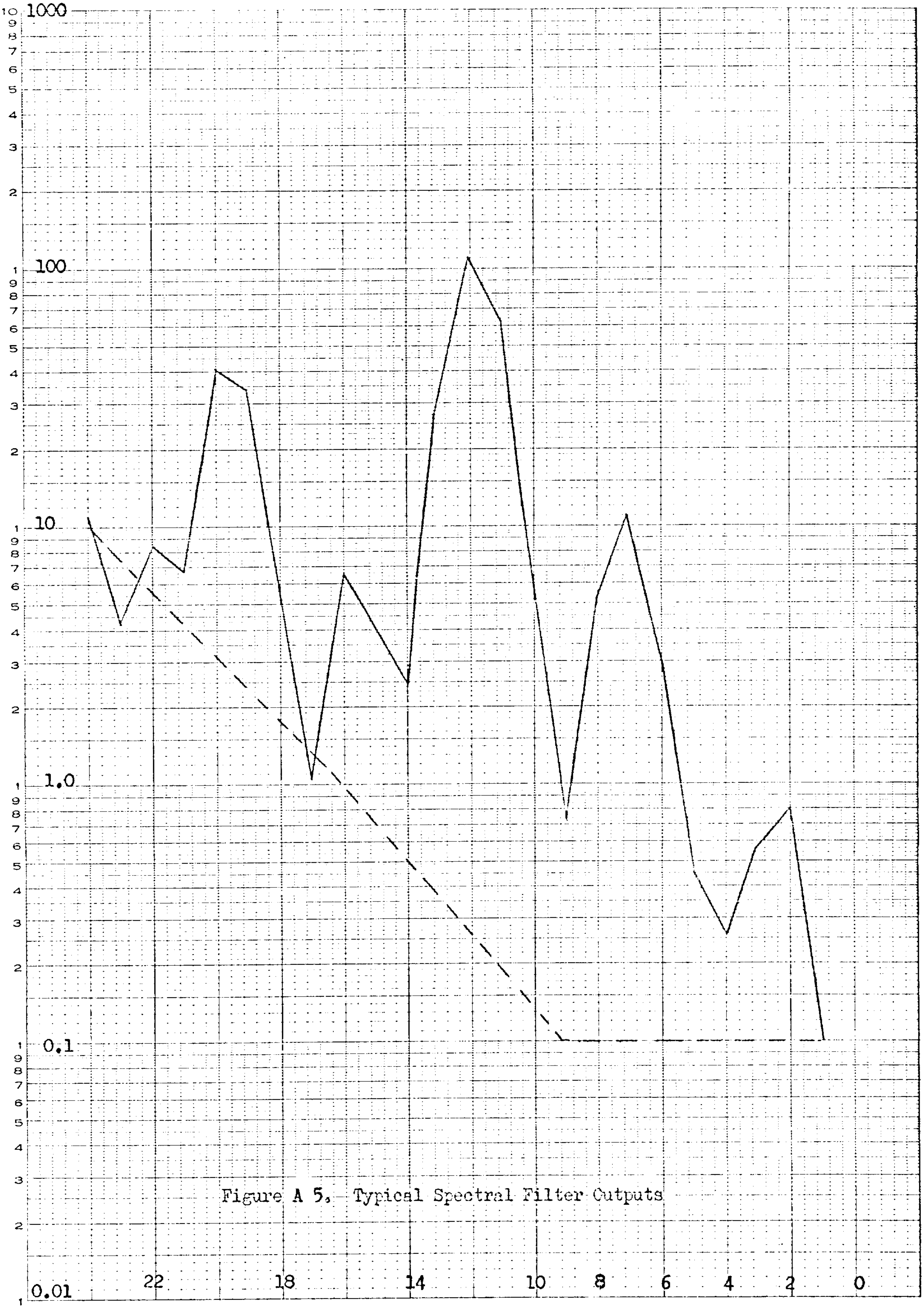

Figure A 5. Typical Spectral Filter Outputs

n	m_n	ω_n	D x 10^9	R x 10^9
1	22	14.28	.10	.1
2	24	13.09	.81	.1
3	26	12.083	.59	.1
4	28	11.22	.26	.1
5	30	10.472	.45	.1
6	32	9.81	2.99	.1
7	36	8.73	11.13	.1
8	40	7.85	5.26	.1
9	44	7.14	.73	.1
10	48	6.54	5.07	.136
11	54	5.82	64.47	.18
12	60	5.24	111.02	.28
13	66	4.76	32.61	.36
14	74	4.25	2.46	.52
15	82	3.83	3.79	.7
16	92	3.41	6.79	1.0
17	100	3.14	1.04	1.3
18	112	2.8	4.78	1.74
19	124	2.53	34.64	2.3
20	138	2.28	41.69	3.1
21	154	2.04	6.92	4.2
22	170	1.85	8.24	5.6
23	188	1.67	4.35	7.6
24	208	1.51	11.02	10.

Table A-2. Spectral Filter Parameters

for the second bending mode with n = 12 this becomes

$$\omega_{F_2} = \frac{A_{11}\,\omega_{11} + A_{12}\,\omega_{12} + A_{13}\,\omega_{13}}{A_{11} + A_{12} + A_{13}} \qquad \text{A-63}$$

which from Table A-2 is

$$\omega_{F_2} = \frac{64.47 \times 5.82 + 111.02 \times 5.24 + 32.61 \times 4.76}{64.47 + 111.02 + 32.61} = 5.342 \qquad \text{A-64}$$

Equivalent calculations for the first and third bending modes yield $\omega_{F_1} = 2.364$ and $\omega_{F_3} = 8.658$. The identification accuracy for this one point in time is 2.8%, 1.75% and 2.93% for the 1st, 2nd, and 3rd bending mode, respectively.

The identified frequencies are then filtered so that large temporary transients in the identified frequency are reduced. There are many factors which contribute to the identification accuracy. The two major factors are the excitation of the bending modes and the existence of external noise inputs to the system which contain a large amount of some frequency which could be identified as bending. Because the bending modes are more accurately identified when they are highly excited and poorly identified when the excitation is low a well operating system will exhibit poor identifications since a well operating system will have the bending modes well damped.

6.2 BASIC DISCUSSION OF DIGITAL CONTROL SYSTEMS

A single axis booster control system for Model Vehicle II consists of a set of control sensors, a computer and a nozzle control servo. In most designs the sensors will consist of an attitude sensor (either a gyro or gimbal angles read off of the stable platform) and an attitude rate gyro. In a "standard" control system the computer will consist of active and passive analog circuits. The computations performed by the analog system can also be accomplished by a digital computer. In a complex system a digital computer offers advantages in weight, power, reliability, flexibility and self checking capabilities. In designing a digital control system certain basic properties of a digital computer must be considered.

A digital computer does arithmetical computations in a step by step procedure. In adding three numbers A, B and C the computer does not miraculously produce the sum of the three numbers but, methodically using an arithmetical register called the accumulator, will go through a sequence of steps called commands which for the example would be

Put A in the accumulator

Add B to the accumulator

Add C to the accumulator

At this time the sum would be in the accumulator. Each step takes a finite amount of time to execute which is determined by the type of hardware and the way it is interconnected in constructing the computer.

The computer will have a memory which in the example above will contain the numbers A, B and C called data words plus codes for the Commands of "Put A in the accumulator, Add B to the accumulator, and Add C to the accumulator." In most computers a command occupies the same amount of memory as a data word, which is designated a unit of memory called a "word". In general, any word in memory can contain either data or command at the option of the programmer. The computer has no way in designating between data and commands but is told to pick up its first command at a particular spot in memory and then processes commands in sequence from that point.

A digital computer is most effective when it can process repetitively the same set of commands. When used as a flight control computer this repetitive operation is always used. As an example the simplest possible control system will be considered which has a control equation of

$$\beta_c = K_1 \phi_I + K_2 \dot{\phi}_I \qquad \text{B-1}$$

The command sequence within the computer would be

Put the present value of ϕ_I in the accumulator
Multiply the contents of the accumulator by K_1
Store the contents of the accumulator in D
Put the present value of $\dot{\phi}_I$ in the accumulator
Multiply the contents of the accumulator by K_2
Add D to the accumulator
Output the accumulator as a voltage to the nozzle servo
Take the next command from the start of the sequence

With the computer control returned to the start of the sequence the sequence will be repeated until the computer is stopped from external source. The total sequence will take a time T seconds to execute and for a digital control system this is defined as the sampling time. The voltage to the nozzle servos will be held at its commanded value until the computer executes another output command. Therefore β_c is a series of steps T seconds in duration.

The transfer function in Laplace operator notation of the vehicle dynamics from nozzle command (β_c) to instrument output can be written as

$$\frac{\phi_I\ (s)}{\beta_i\ (s)} = \frac{P\ (s)}{\prod_{i=1}^{n} s + a_i} \qquad \text{B-2}$$

where a_i can be real, complex or zero. This transfer function can be converted to partial fraction notation to have the form

$$\frac{\phi_I(s)}{\beta_c(s)} = \sum_{i=1}^{n} \frac{b_i}{s + a_i} \qquad \text{B-3}$$

where b_j is computed for non-multiple roots from

$$b_j = \lim_{s \to -a_j} \frac{(s+a_j)\,P(s)}{\prod_{i=1}^{n} s + a_i} \qquad \text{B-4}$$

Since Laplace transforms are commutative then $\phi_I(t)$ is determined by

$$\phi_I(t) = \sum_{i=1}^{n} \mathcal{L}^{-1} \frac{b_i\,\beta_c(s)}{s + a_i} \qquad \text{B-5}$$

If by definition we make

$$Y_i(t) \triangleq \mathcal{L}^{-1} \frac{b_i\,\beta_c(s)}{s + a_i} \qquad \text{B-6}$$

then

$$\phi_I(t) = \sum_{i=1}^{n} Y_i(t) \qquad \text{B-7}$$

The differential equation represented by Equation B-6 is

$$\frac{dY_i(t)}{dt} + a_i\,Y_i(t) = b_i\,\beta_c(t) \qquad \text{B-8}$$

$\beta_c(t)$ is a series of step inputs each of T seconds in duration. If at $t = 0$ one of these steps is initiated with a magnitude of β_c then the Laplace representation of Equation B-8 becomes

$$Y_i(s) = \frac{b_i\,\beta_c}{s(s + a_i)} + \frac{Y_i\,(0^+)}{s + a_i} \qquad \text{B-9}$$

The inverse Laplace transformation of Equation B-9 is then:

$$Y_i(t) = \frac{b_i\,\beta_c}{a_i}\,(1-e^{-a_i T}) + e^{-a_i T}\,Y_i(0^+) \qquad \text{B-10}$$

Equation B-10 can be evaluated at t=T which is the time the next β_c step is applied to the nozzle servo giving

$$Y_i(T) = \frac{b_i \beta_c}{a_i} (1-e^{-a_i T}) + e^{-a_i T} Y_i(0^+) \tag{B-11}$$

The only criteria used for selecting the time t = 0 was that a β_c step was initiated at this time, therefore a formula which is good at any time the step in β_c is being initiated (i.e., at the sampling times) is, from Equation B-11,

$$Y_i(t+T) = \frac{b_i}{a_i} (1-e^{-a_i T}) \beta_c (t+T) + e^{-a_i T} Y_i(t) \tag{B-12}$$

Making the definitions

$$c_i \triangleq e^{-a_i T} \tag{B-13}$$

and

$$d_i \triangleq \frac{b_i}{a_i} (1-e^{-a_i T}) \tag{B-14}$$

then Equation B-12 becomes

$$Y_i(t+T) = d_i \beta_c (t+T) + c_i Y_i(t) \tag{B-15}$$

The Laplace transform of Equation B-15 is

$$e^{sT} Y_i(s) = d_i e^{sT} \beta_c(s) + c_i Y_i(s) \tag{B-16}$$

Solving for the transfer function $Y_i(s)/\beta_c(s)$ yields

$$\frac{Y_i(s)}{\beta_c(s)} = \frac{d_i e^{sT}}{e^{sT} - c_i} \tag{B-17}$$

Making the substitution gives $z = e^{sT}$ B-18

$$\frac{Y_i(z)}{\beta_c(z)} = \frac{d_i z}{z - c_i} \tag{B-19}$$

From Equation B-7 then

$$\frac{\phi_I(z)}{\beta_c(z)} = \sum_{i=1}^{n} \frac{d_i z}{z - c_i} \qquad \text{B-20}$$

z is an operator in the same sense that s is an operator with the two inter-related by $z = e^{sT}$. It becomes more convenient in analyzing the stability of a digital control system to work in terms of z rather than s. Equation B-18 gives a one to one transformation for every value of s to a value of z. A standard stability analysis method is root locus. In this technique the system closed loop denomination roots are plotted in a plane determined by the real and imaginary part of s. This can also be done by plotting the real and imaginary part of z. In the first case using s, the plane in which the roots are plotted is called the s-plane and in the latter case the z-plane. Instead of transforming roots from the z-plane to the s-plane to determine if they are within the stable region the stability boundary of the s-plane is transposed to the z-plane so that stability can be interpreted in the z-plane. The stability boundary in the s-plane is $s = j\omega$, therefore, in the z-plane it is $z = e^{j\omega T}$ which is a circle with unit radius centered at the z-plane origin. The region inside the unit circle is the stable region and the region external to the unit circle the unstable region.

Another stability analysis method is to evaluate the open loop transfer function at the complex frequency $s = j\omega$. Thus, z is evaluated at $z = e^{j\omega T} = \cos \omega T + j \sin \omega T$.

Lead and lag compensation networks can be mechanized within the digital computer by considering the way in which an integrator and a differentiator would be approximated in a digital computer.

If in a digital computer there are stored values of x(t) at equal time intervals, i.e., X(0), X(T), X(2T), X(3T), etc., and the value of

$$y(\tau) = \int_0^{\tau} x(t)\, dt \qquad \text{B-21}$$

is desired, then $y(\tau)$ can be approximated by

$$y(\tau) = \sum_{i=0}^{\tau/T} x(iT) \cdot T \qquad \text{B-22}$$

Figure B-1 shows $x(t)$ plotted vs. time. Equation B-21 is the area under this curve from $t = 0$, to $t = \tau$. In Figure B-1 is also another curve generated from the $x(t)$ curve in a manner such that the second curve always has values of $x(iT)$ from $t = iT$ to $t = (i+1)T$. Equation B-22,

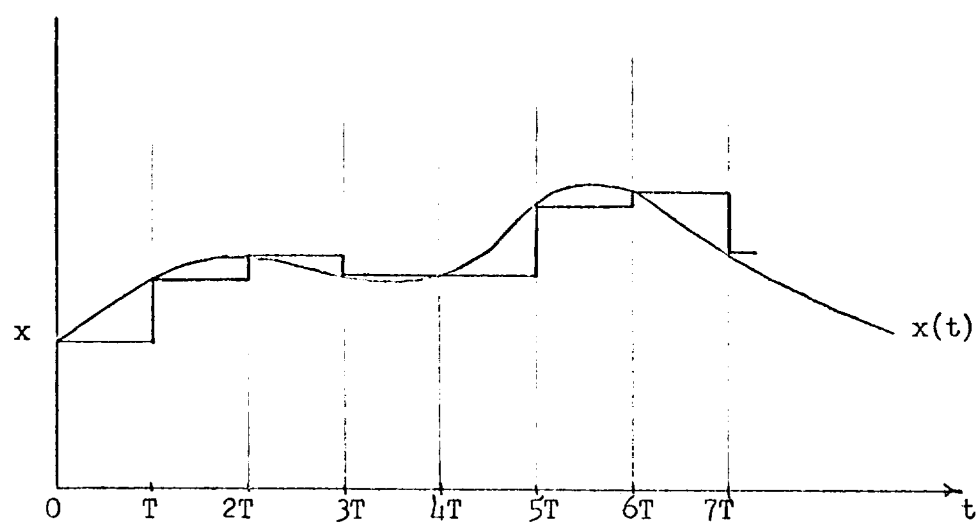

Figure B-1. Relationship Between Exact and Digital Integration the digital computer approximation of the integral, is the area under this second curve from $t = 0$ to $t = \tau$ if τ is evenly divisible by T. Obviously the shorter the time duration T is, the more closely the approximation between Equation B-22 and B-21. To propagate the integration from τ to $\tau + T$ the addition of $Tx(\tau+T)$ must be made to Equation B-22 thus,

$$y(\tau+T) = \sum_{i=0}^{\tau/T} x(iT) \cdot T + x(\tau+T) \cdot T \qquad \text{B-23}$$

Subtracting Equation B-22 yields

$$y(\tau+T) - y(\tau) = T\, x(\tau+T) \qquad \text{B-24}$$

Taking the Laplace transformation of Equation B-24 yields

$$(e^{sT}-1)\, y(s) = T\, e^{sT}\, x(s) \qquad \text{B-25}$$

Making the substitution $z = e^{sT}$ and solving for y/x yields

$$y(z)/x(z) = \frac{T\, z}{z-1} \qquad \text{B-26}$$

which is the z transform of an integrator (rectangular) mechanized on a digital computer. Equation B-24 can be rewritten

$$y(\tau+T) = y(\tau) + T\, x(\tau+T) \qquad \text{B-27}$$

which again is the formula for a digitally mechanized integrator. Equation B-19 is the z transform of $b_i/s+a_i$, a lag function. Equation B-19 in terms of an input function x and an output function y becomes

$$\frac{y(z)}{x(z)} = \frac{d_i z}{z-C_i} \qquad \text{B-28}$$

Making the substitution $e^{sT} = z$ to transform Equation B-28 to the s-plane yields

$$y(s)\ (e^{sT} - c_i) = d_i\ x(s)\ e^{sT} \qquad \text{B-29}$$

Rearranging and taking the inverse Laplace transformation yields

$$y(\tau+T) = c_i\ y(\tau) + d_i\ x\ (\tau+T) \qquad \text{B-30}$$

This is the form of a digital mechanized lag compensation. Comparing this with Equation B-27 shows the difference between a digital integrator and lag to be only in the value of the coefficients of $y(\tau)$ and $x\ (\tau+T)$.

Differentiation is the process of generating the slope of a function. This is easily seen to be

$$y(\tau+T) = [x(\tau+T) - x\ (\tau)]/T \qquad \text{B-31}$$

which has a z transform of

$$y/x = \frac{z-1}{T\ z}. \qquad \text{B-32}$$

which as would be expected is the inverse of the integration formula. In like manner a lead compensation network is the inverse of a lag network and thus should have time domain equations of

$$y(\tau+T) = \frac{1}{d_i}\ x(\tau+T) - \frac{c_i}{d_i}\ x(\tau) \qquad \text{B-33}$$

and a z transform of

$$y/x = \frac{z-c_i}{d_i\ z} \qquad \text{B-34}$$

A further transformation which is convenient to use is $z = \frac{1+W}{1-W}$. The W-plane stability boundary is identical to the s-plane stability boundary, i.e., the left half plane is the stable region. In the W plane all frequencies are ficticious in that the s plane frequency ω is transformed to the W plane frequency $\bar{\omega}$ by $\bar{\omega} = \tan \frac{\omega T}{2}$. This plane is convenient because compensation networks designed in the W plane using the ficticious frequency $\bar{\omega}$ using conventional s plane expressions will have fairly similar characteristics at the true frequency ω as would be expected by the s plane formulas.

The W-plane compensation networks can then be easily transformed to the z plane by $W = \frac{Z-1}{Z+1}$.

As an example of this a notch filter in the s-plane could be designed by

$$G(s) = \frac{\omega_d^2}{\omega_n^2} \frac{s^2 + 2\,\zeta_n\,\omega_n\,s + \omega_n^2}{s^2 + 2\,\zeta_d\,\omega_d\,s + \omega_d^2} \qquad \text{B-35}$$

This will be a notch filter at the frequency ω_n if $\zeta_n \ll \zeta_d$ or ω_n is much different than ω_d. The notch filter has a dc gain of 1. Equivalently a notch filter in the W plane will have the transformation

$$G(W) = \frac{\bar{\omega}_d^2}{\bar{\omega}_n^2} \frac{W^2 + 2\,\zeta_n\,\bar{\omega}_n\,W + \bar{\omega}_n^2}{W^2 + 2\,\zeta_d\,\bar{\omega}_d\,W + \bar{\omega}_d^2} \qquad \text{B-36}$$

If $\zeta_n \ll \zeta_d$ or $\bar{\omega}_n$ is much different than $\bar{\omega}_d$ Equation B-36 will be a notch filter at the frequency ω_n such that $\bar{\omega}_n = \tan \frac{\omega_n T}{2}$. Transforming Equation B-36 to the z plane yields

$$D(z) = \frac{\bar{\omega}_d^2}{\bar{\omega}_n^2} \frac{z^2\,(1+2\,\zeta_n\bar{\omega}_n + \bar{\omega}_n^2) + 2\,z\,(\bar{\omega}_n^2 - 1) + (1-2\,\zeta_n\bar{\omega}_n + \bar{\omega}_n^2)}{z^2\,(1+2\,\zeta_n\bar{\omega}_d + \bar{\omega}_d^2) + 2\,z\,(\bar{\omega}_d^2 - 1) + (1-2\,\zeta_d\bar{\omega}_d + \bar{\omega}_d^2)} \qquad \text{B-37}$$

At times it would be desirable to generate a notch zero without having to also include a pair of poles. This is, however, impossible. A notch zero without poles would have a z transfer function of

$$Y/X = z^2 + a\,z + b \qquad \text{B-38}$$

which in the time domain is

$$Y(t) = x(t+2T) + a\,x\,(t+T) = b\,x(t) \qquad \text{B-39}$$

In order to generate the output Y values of the input x must be known which occur in the future which is obviously impossible. If a pair of poles are added giving the z transfer function of

$$Y/X = \frac{z^2 + a\,z + b}{z^2 + c\,z + d} \tag{B-40}$$

then the conversion to the time domain yields

$$y(t) = X(t) + a\,x(t-T) + bx\,(t-2T) - c\,Y\,(t-T) - dY\,(t-2T) \tag{B-41}$$

and the most advanced value of x required occurs at the same time the output is generated.

6.3 EQUATIONS OF MOTION AND VEHICLE DATA

This section includes the basic equations of motion and pertinent vehicle data used in the study.

EQUATIONS OF MOTION

Moment Equation

$$
\begin{aligned}
\ddot{\phi} = {} & \frac{-C_{z_\alpha} q A (X_{cg} - C_{cp})\alpha}{I_{xx}} - \frac{F(X_{cg} - X_\beta)}{2 I_{xx}} \beta \\
& + \frac{F(X_{cg} - X_E)}{I_{xx}} \sum_i Y_i' (X_\beta) \eta_i - \frac{F}{I_{xx}} \sum_i Y_i (X_\beta) n_i \\
& + \sum_j \frac{\ell_{s_j} m_{s_j}}{I_{xx}} \ddot{Z}_{s_j} + \sum_j \frac{F - X}{m I_{xx}} m_{s_j} Z_{s_j} \\
& - \left[\frac{(X_{cg} - X_\beta) S_E}{I_{xx}} + \frac{I_E}{I_{xx}} \right] \ddot{\beta} - \frac{(F - X) S_{E_\beta}}{m I_{xx}}
\end{aligned} \qquad \text{C-1}
$$

Forces Normal to Velocity

$$
\begin{aligned}
\dot{\alpha} = {} & - \frac{(F - X)\alpha}{m V_o} - \frac{F}{2 m V_o} \beta - \frac{C_{z_\alpha}}{m V_o} q A\alpha \\
& + \frac{F}{m V_o} \sum_i Y_i' (X_\beta) \eta_i = \sum_j \frac{m_{s_j} \ddot{Z}_{s_j}}{m V_o} + \dot{\phi} - \frac{g \sin (\phi - \alpha)}{V_o}
\end{aligned} \qquad \text{C-2}
$$

Bending Equation

$$
\begin{aligned}
\ddot{\eta}_i + 2 \zeta_i W_i \eta_i + W_i^2 \eta_i = {} & \frac{F Y_i (X_\beta)}{2 m_i} \beta + \frac{S_E Y_i (X_\beta) + I_E Y_i (X_\beta)}{m_i} \ddot{\beta} \\
& - \sum \frac{m_{s_j}}{m_i} \left[Y_i (X_{s_j}) \ddot{Z}_{s_j} + \frac{F-X}{m} + Y_i' (X_{s_j}) Z_{s_j} \right] \\
& + \left[\int^x \frac{\partial C_{z_\alpha}}{\partial X} Y_i(X) dX \right] \frac{q A}{m_i} \alpha
\end{aligned} \qquad \text{C-3}
$$

Slosh Equation

$$\ddot{Z}_{s_j} + 2\zeta_{s_j} W_{s_j} \dot{Z}_{s_j} + W_{s_j}^{2} Z_{s_j} = \ell_{s_j} \ddot{\phi} - \frac{F}{2m} \beta - \frac{C_{z_\alpha} q A}{m} \alpha$$

$$+ \Sigma \frac{F}{m} Y_i' (X_\beta) \eta_i + \sum_j \frac{m_{s_j}}{m} \ddot{Z}_{s_j} \qquad \text{C-4}$$

$$- \sum_i Y_i (X_{s_j}) \ddot{\eta}_i + \frac{F-X}{m} Y_i' (X_{s_j}) \eta_i$$

Sensor Equations

$$\phi_I = \phi - \sum_i Y_i' (X_{\phi_I}) \eta_i \qquad \text{C-5}$$

$$\dot{\phi}_I = \dot{\phi} - \sum_i Y_i' (X_{\dot{\phi}_I}) \dot{\eta}_i \qquad \text{C-6}$$

$$N_z = \frac{F}{2m} \beta + \frac{C_{z_\alpha} q A}{m} \alpha - (X_{c_g} - X_{N_z}) \ddot{\phi} + \sum_i Y_i (X_{N_z}) \ddot{\eta}_i \qquad \text{C-7}$$

$$- \sum_i \frac{F}{m} Y_i' (X_\beta) \eta_i - \sum_i \frac{m_{s_j}}{m} \ddot{Z}_{s_j}$$

Control Equation

$$\beta_c = K_\phi (-\phi_c + \phi_I + K_{\dot{\phi}} \dot{\phi}_I + K_{N_z} N_z) \qquad \text{C-8}$$

Figure C-1, C-2, C-3 and C-4 show the bending slopes at the rate gyro location, bending slopes at attitude gyro location, differential slopes for instruments located at 120.54 and 46.54 meters and bending frequencies as a function of time respectively.

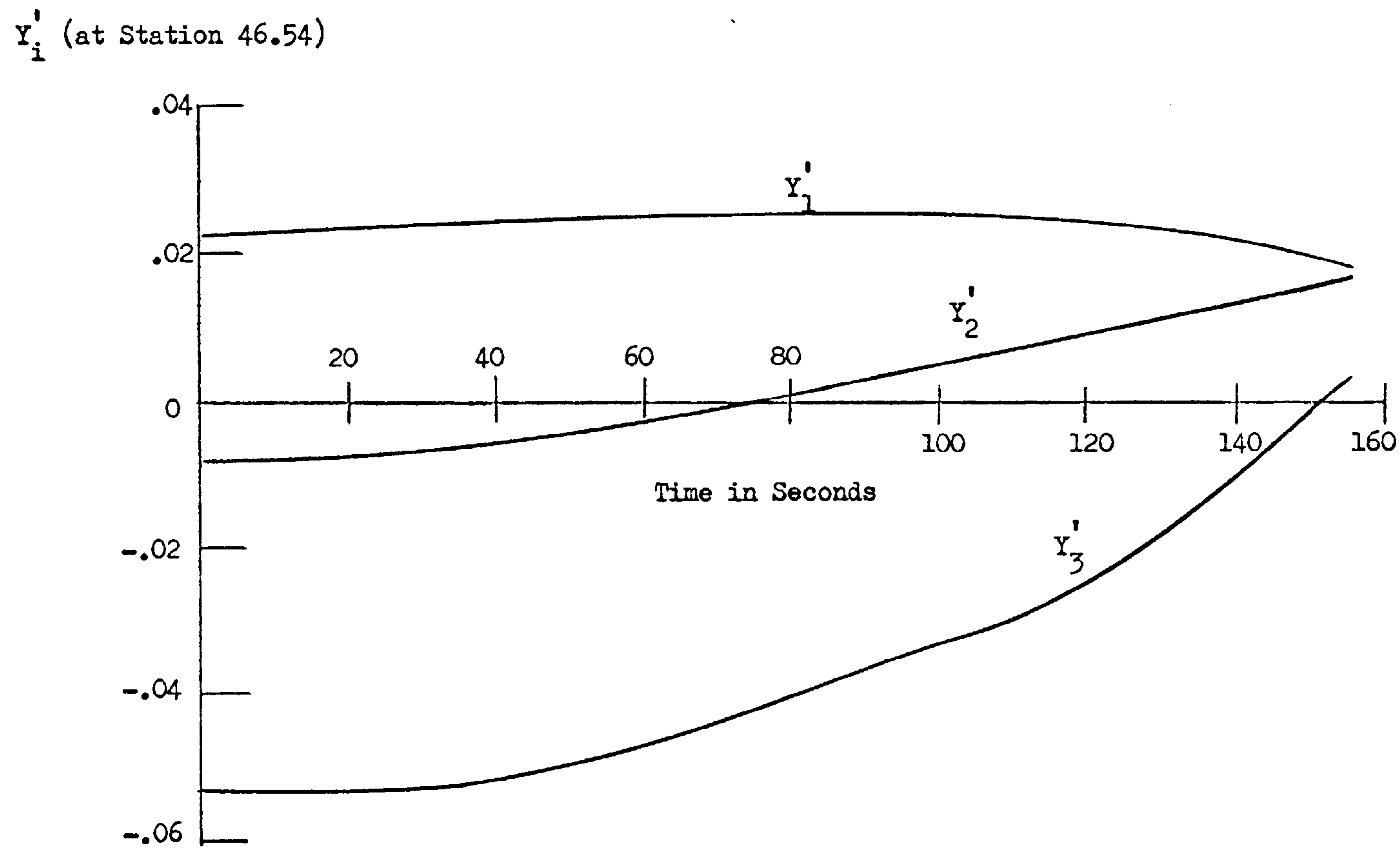

Figure C1. Bending Slopes at Rate Gyro Location

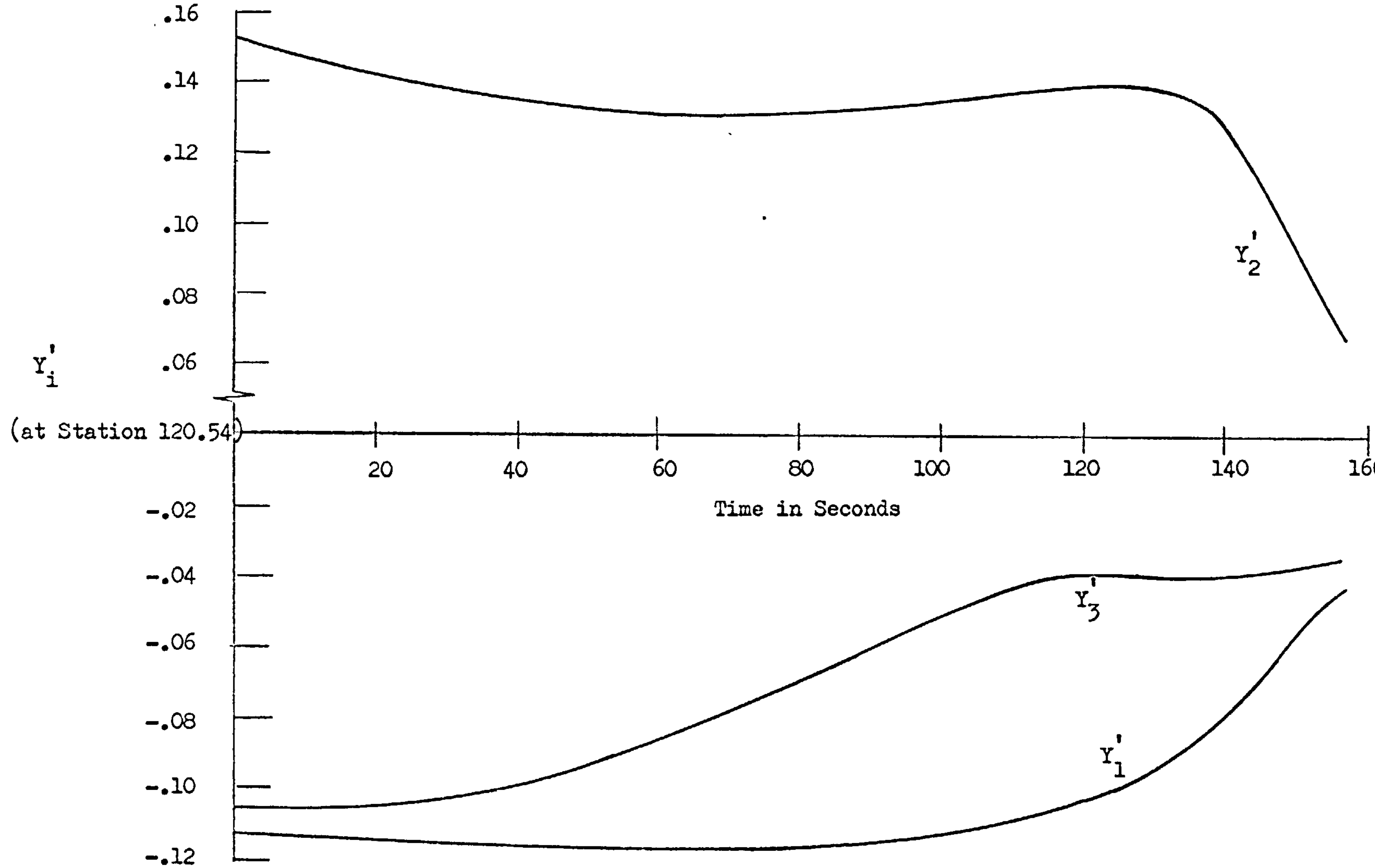

Figure C2. Bending Slopes at Attitude Gyro Location

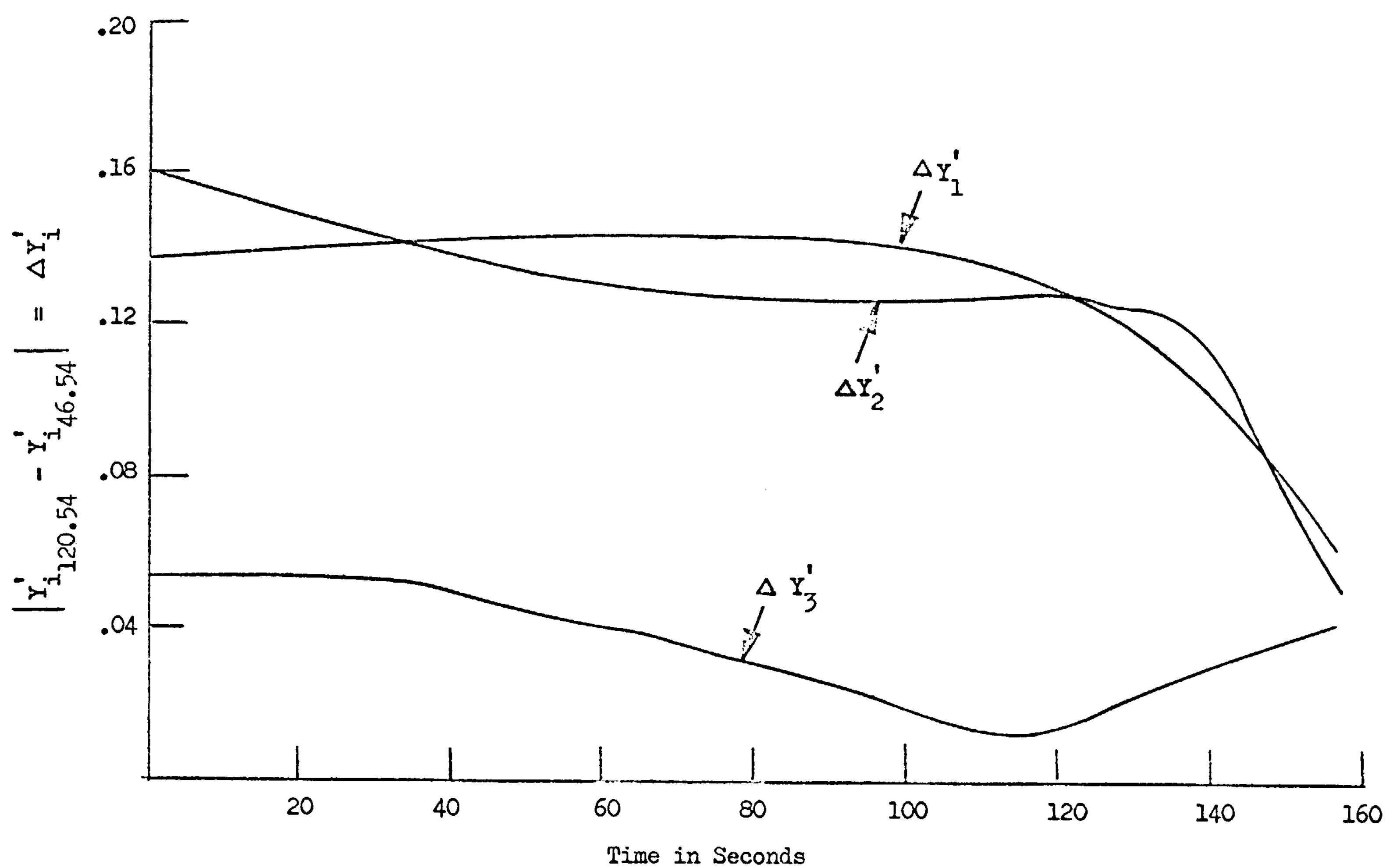

Figure C3. Magnitude of Defferential Slopes for 120.54 and 46.54 Meters

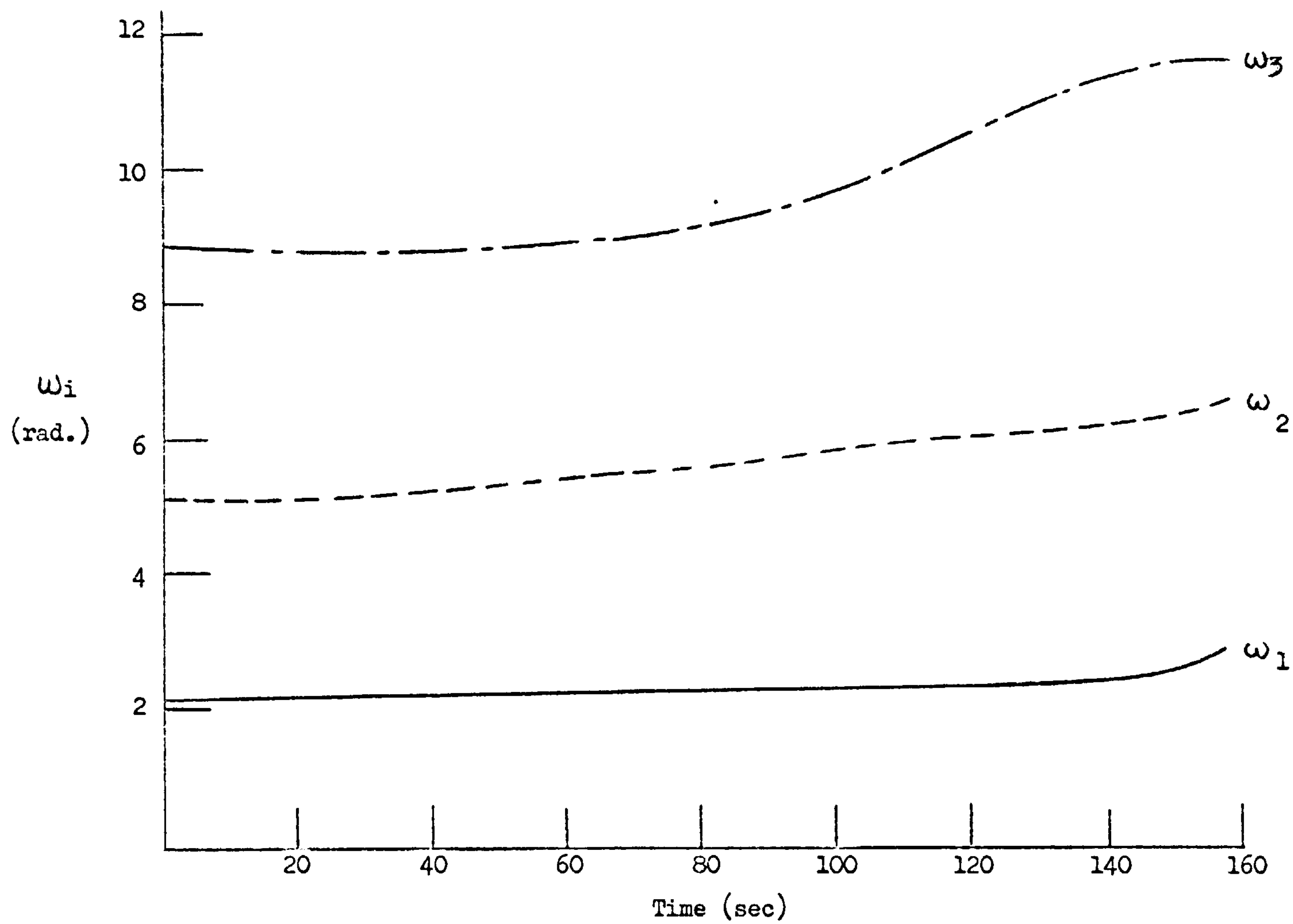

Figure C4. ω_i vs Time

Symbols	Definition	Computer Symbols
I_{xx}	pitch moment of inertia	IXX
C_{z_α}	normal force coefficient	CZA
X_{c_g}	location of vehicle Cg	XCG
X_{c_p}	location of vehicle Cp	XCP
X_β	location of vehicle gimbal point	XB
q	dynamic pressure	Q
A	cross sectional reference area	A
F	total thrust	F
X_E	location of nozzle cg	XE
$Y_i'(X_\beta)$	normalized bending slope at X_β	YP1, YP2, YP3
$Y_i(X_\beta)$	normalized bending displacement at X_β	
ℓ_{s_j}	distance from vehicle cg to slosh mass cg	
m_{s_j}	slosh mass	
X	drag force	X
S_E	first moment of swivel about gimbal point	SE
I_E	engine moment of inertia about gimbal point	IE
m	vehicle mass	M
V_o	vehicle velocity	VO
δ_i	bending damping	Z
W_i	bending frequency	W1, W2, W3
$Y_i(X_{s_j})$	bending displacement at slosh mass cg	
$Y_i'(X_{s_j})$	bending slope at slosh mass cg	
$\int^x \frac{\alpha C_{z_x}}{\alpha x} Y_i(X)dX$	normalized generalized force function	ICZY1, ICZY2, ICZY3

Symbols	Definition	Computer Symbols
m_i	bending model mass	M1, M2, M3
δ_{s_j}	slosh damping	
W_{s_j}	slosh frequency	
$Y_i'(X_{\phi_I})$	bending slope at gyro location	GYRO SLOPES
$Y_i'(X_{\dot{\phi}_I})$	bending slope at rate gyro location	RATE GYRO
$Y_i'(X_{N_z})$	bending slope at normal accelerometer location	
$Y_i(X_{N_z})$	bending displacement at normal accelerometer location	
X_{N_z}	location of N_z instrument	

A list of the vehicle parameter values for each time point along the trajectory is given in the numerical listing that follows. The values are defined by the computer symbol list. BR is the nozzle servo real root location and BC is the nozzle servo complex root location. The matrix coefficients are directly related to the moment, normal force and bending equations. It will be noted that the coefficients are arranged in a matrix having 6 columns and 5 major rows with each major row having three values. The first value in each row is the s^2 Laplace operator coefficient, the second the s Laplace operator coefficient, and the third the constant Laplace operator coefficient. The columns define coefficients of ϕ, α, η_1, η_2, η_3 and $-\beta$. The major rows define coefficients derived from the moment equation, the normal force equation, the first bending mode equation, the second bending mode equation and the third bending mode equation.

```
SYSTEM CONSTANTS
A        0.794602D 02
XB      -0.000000D-38
XE      -0.133858D 01
SE       0.444560D 04
IE       0.138255D 05
Z        0.500000D-02
BR       0.146423D 02
BC       0.453887D 01    0.458847D 02
DT       0.100000D-01
```

```
TIME POINT VARIABLES
W1     0.215000D 01  M1     0.193000D 06  W2     0.505000D 01  M2     0.165500D 06  W3     0.875000D 01
M3     0.162000D 06  XCG    0.376000D 02  XCP    0.467700D 02  CZA    0.455000D 01  Q      0.100000D 01
IXX    0.284000D 09  F      0.519323D 07  X      0.100000D 01  M      0.423565D 06  VO     0.100000D 01
ICZY1 0.429868D 01  ICZY2 0.274495D 01  ICZY3 0.486281D 01  YP1    0.345000D-01  YP2    0.440000D-01
YP3    0.520000D-01  TIME   0.000000D-38
GYRO SLOPES    -0.114080D 00    0.151630D 00   -0.105920D 00
RATE GYRO       0.230000D-01   -0.833000D-02   -0.526000D-01
SPECTRAL       -0.137000D 00    0.159960D 00   -0.533200D-01

THE MATRIX COEFICIENTS
 0.1000000000D 01  0.0000000000D-38  0.0000000000D-38  0.0000000000D-38  0.0000000000D-38 -0.6372538028D-
 0.0000000000D-38  0.0000000000D-38  0.0000000000D-38  0.0000000000D-38  0.0000000000D-38  0.0000000000D-
 0.0000000000D-38 -0.1167379456D-04 -0.6279076031D-02 -0.1304338106D-01 -0.1873963792D-01 -0.3439693200D

 0.0000000000D-38  0.0000000000D-38  0.0000000000D-38  0.0000000000D-38  0.0000000000D-38  0.0000000000D-3
-0.1000000000D 01  0.1000000000D 01  0.0000000000D-38  0.0000000000D-38  0.0000000000D-38  0.0000000000D-
 0.0000000000D-38  0.1226162111D 02 -0.4229965613D 00 -0.5394738753D 00 -0.6375600345D 00 -0.6130384947D 0

 0.0000000000D-38  0.0000000000D-38  0.1000000000D 01  0.0000000000D-38  0.0000000000D-38  0.2550559813D-01
 0.0000000000D-38  0.0000000000D-38  0.2150000000D-01  0.0000000000D-38  0.0000000000D-38  0.0000000000D-38
 0.0000000000D-38 -0.1769813329D-02  0.4622500000D 01  0.0000000000D-38  0.0000000000D-38  0.1345397150D 0

 0.0000000000D-38  0.0000000000D-38  0.0000000000D-38  0.1000000000D 01  0.0000000000D-38  0.3053729837D-01
 0.0000000000D-38  0.0000000000D-38  0.0000000000D-38  0.5050000000D-01  0.0000000000D-38  0.0000000000D-38
 0.0000000000D-38 -0.1317911033D-02  0.0000000000D-38  0.2550250000D 02  0.0000000000D-38  0.1568952568D 02

 0.0000000000D-38  0.0000000000D-38  0.0000000000D-38  0.0000000000D-38  0.1000000000D 01  0.3187979654D-01
 0.0000000000D-38  0.0000000000D-38  0.0000000000D-38  0.0000000000D-38  0.8750000000D-01  0.0000000000D-38
 0.0000000000D-38 -0.2385184291D-02  0.0000000000D-38  0.0000000000D-38  0.7656250000D 02  0.1602849691D 02
```

```
TIME POINT VARIABLES
W1     0.220000D 01  M1     0.190500D 06  W2     0.510000D 01  M2     0.158000D 06  W3     0.875000D 01
M3     0.165000D 06  XCG    0.376000D 02  XCP    0.469700D 02  CZA    0.455000D 01  Q      0.310000D 02
IXX    0.282000D 09  F      0.521300D 07  X      0.285500D 04  M      0.407814D 06  VO     0.207000D 02
ICZY1  0.424805D 01  ICZY2  0.271898D 01  ICZY3  0.483746D 01  YP1    0.350000D-01  YP2    0.440000D-01
YP3    0.535000D-01  TIME   0.800000D 01
GYRO SLOPES    -0.115000D 00   0.147000D 00  -0.107000D 00
RATE GYRO       0.235000D-01  -0.800000D-02  -0.530000D-01
SPECTRAL       -0.138500D 00   0.155000D 00  -0.540000D-01

THE MATRIX COEFICIENTS
 0.1000000000D 01  0.0000000000D-38  0.0000000000D-38  0.0000000000D-38  0.0000000000D-38 -0.6417733333D-0
 0.0000000000D-38  0.0000000000D-38  0.0000000000D-38  0.0000000000D-38  0.0000000000D-38  0.0000000000D-3
 0.0000000000D-38 -0.3724030480D-03 -0.6707583737D-02 -0.1318588642D-01 -0.2002409482D-01 -0.3477347377D 0

 0.0000000000D-38  0.0000000000D-38  0.0000000000D-38  0.0000000000D-38  0.0000000000D-38  0.0000000000D-38
-0.1000000000D 01  0.1000000000D 01  0.0000000000D-38  0.0000000000D-38  0.0000000000D-38  0.0000000000D-38
 0.0000000000D-38  0.6185154719D 00 -0.2161341005D-01 -0.2717114407D-01 -0.3303764108D-01 -0.3087630008D 00

 0.0000000000D-38  0.0000000000D-38  0.1000000000D 01  0.0000000000D-38  0.0000000000D-38  0.2587660472D-01
 0.0000000000D-38  0.0000000000D-38  0.2200000000D-01  0.0000000000D-38  0.0000000000D-38  0.0000000000D-38
 0.0000000000D-38 -0.5492954321D-01  0.4840000000D 01  0.0000000000D-38  0.0000000000D-38  0.1368241470D 02

 0.0000000000D-38  0.0000000000D-38  0.0000000000D-38  0.1000000000D 01  0.0000000000D-38  0.3198685367D-01
 0.0000000000D-38  0.0000000000D-38  0.0000000000D-38  0.5100000000D-01  0.0000000000D-38  0.0000000000D-38
 0.0000000000D-38 -0.4238969324D-01  0.0000000000D-38  0.2601000000D 02  0.0000000000D-38  0.1649683544D 02

 0.0000000000D-38  0.0000000000D-38  0.0000000000D-38  0.0000000000D-38  0.1000000000D 01  0.3142585042D-01
 0.0000000000D-38  0.0000000000D-38  0.0000000000D-38  0.0000000000D-38  0.8750000000D-01  0.0000000000D-38
 0.0000000000D-38 -0.7221788916D-01  0.0000000000D-38  0.0000000000D-38  0.7656250000D 02  0.1579696970D 02
```

```
TIME PCINT VARIABLES
W1     0.2200000D 01  M1     0.1885000D 06  W2     0.5150000D 01  M2     0.1510000D 06  W3     0.8800000D 01
M3     0.1660000D 06  XCG    0.3760000D 02  XCP    0.4727000D 02  CZA    0.4540000D 01  Q      0.1420000D 03
IXX    0.2780000D 09  F      0.5248000D 07  X      0.1194900D 05  M      0.3920620D 06  VO     0.4650000D 02
ICZY1  0.4222590D 01  ICZY2  0.2693060D 01  ICZY3  0.4812310D 01  YP1    0.3500000D-01  YP2    0.4450000D-01
YP3    0.5450000D-01  TIME   0.1600000D 02
GYRO SLOPES   -0.1160000D 00   0.1440000D 00  -0.1070000D 00
RATE GYRO      0.2400000D-01  -0.7500000D-02  -0.5300000D-01
SPECTRAL      -0.1400000D 00   0.1515000D 00  -0.5400000D-01

THE MATRIX COEFFICIENTS
 0.1000000000D 01  0.0000000000D-38  0.0000000000D-38  0.0000000000D-38  0.0000000000D-38 -0.6510074820D-03
 0.0000000000D-38  0.0000000000D-38  0.0000000000D-38  0.0000000000D-38  0.0000000000D-38  0.0000000000D-38
 0.0000000000D-38 -0.1781868003D-02 -0.6849778325D-02 -0.1383295043D-01 -0.2118365790D-01 -0.3551142867D 00

 0.0000000000D-38  0.0000000000D-38  0.0000000000D-38  0.0000000000D-38  0.0000000000D-38  0.0000000000D-38
-0.1000000000D 01  0.1000000000D 01  0.0000000000D-38  0.0000000000D-38  0.0000000000D-38  0.0000000000D-38
 0.0000000000D-38  0.2900176257D 00 -0.1007521139D-01 -0.1280991162D-01 -0.1568854345D-01 -0.1439315912D 00

 0.0000000000D-38  0.0000000000D-38  0.1000000000D 01  0.0000000000D-38  0.0000000000D-38  0.2615115756D-01
 0.0000000000D-38  0.0000000000D-38  0.2200000000D-01  0.0000000000D-38  0.0000000000D-38  0.0000000000D-38
 0.0000000000D-38 -0.2527583773D 00 -0.4840000000D 01  0.0000000000D-38  0.0000000000D-38  0.1392042440D 02

 0.0000000000D-38  0.0000000000D-38  0.0000000000D-38  0.1000000000D 01  0.0000000000D-38  0.3351546781D-01
 0.0000000000D-38  0.0000000000D-38  0.0000000000D-38  0.5150000000D-01  0.0000000000D-38  0.0000000000D-38
 0.0000000000D-38 -0.2012366506D 00  0.0000000000D-38  0.2652250000D 02  0.0000000000D-38  0.1737748344D 02

 0.0000000000D-38  0.0000000000D-38  0.0000000000D-38  0.0000000000D-38  0.1000000000D 01  0.3131982434D-01
 0.0000000000D-38  0.0000000000D-38  0.0000000000D-38  0.0000000000D-38  0.8800000000D-01  0.0000000000D-38
 0.0000000000D-38 -0.3271022310D 00  0.0000000000D-38  0.0000000000D-38  0.7744000000D 02  0.1580722892D 02
```

```
TIME POINT VARIABLES
W1     0.220000D 01  M1     0.186500D 06  W2     0.520000D 01  M2     0.144000D 06  W3     0.880000D 01
M3     0.164000D 06  XCG    0.380000D 02  XCP    0.477800D 02  CZA    0.455000D 01  Q      0.353000D 03
IXX    0.276000D 09  F      0.529500D 07  X      0.264840D 05  M      0.376311D 06  VO     0.771000D 02
ICZY1 0.414668D 01  ICZY2 0.266715D 01  ICZY3 0.476170D 01  YP1    0.355000D-01  YP2    0.450000D-01
YP3    0.545000D-01  TIME   0.240000D 02
GYRO SLOPES   -0.116000D 00   0.140000D 00  -0.106000D 00
RATE GYRO       0.241000D-01  -0.700000D-02  -0.530000D-01
SPECTRAL      -0.140100D 00   0.147000D 00  -0.530000D-01

THE MATRIX COEFFICIENTS
 0.1000000000D 01  0.0000000000D-38  0.0000000000D-38  0.0000000000D-38  0.0000000000D-38 -0.6621678261D-03
 0.0000000000D-38  0.0000000000D-38  0.0000000000D-38  0.0000000000D-38  0.0000000000D-38  0.0000000000D-38
 0.0000000000D-38 -0.4522364139D-02 -0.7607142134D-02 -0.1477681214D-01 -0.2194648214D-01 -0.3647363779D 00

 0.0000000000D-38  0.0000000000D-38  0.0000000000D-38  0.0000000000D-38  0.0000000000D-38  0.0000000000D-38
-0.1000000000D 01  0.1000000000D 01  0.0000000000D-38  0.0000000000D-38  0.0000000000D-38  0.0000000000D-38
 0.0000000000D-38  0.1859867467D 00 -0.6478776914D-02 -0.8212534117D-02 -0.9946291319D-02 -0.9125037908D-01

 0.0000000000D-38  0.0000000000D-38  0.1000000000D 01  0.0000000000D-38  0.0000000000D-38  0.2646866466D-01
 0.0000000000D-38  0.0000000000D-38  0.2200000000D-01  0.0000000000D-38  0.0000000000D-38  0.0000000000D-38
 0.0000000000D-38 -0.6236573502D 00  0.4840000000D 01  0.0000000000D-38  0.0000000000D-38  0.1419571046D 02

 0.0000000000D-38  0.0000000000D-38  0.0000000000D-38  0.1000000000D 01  0.0000000000D-38  0.3519269722D-01
 0.0000000000D-38  0.0000000000D-38  0.0000000000D-38  0.5200000000D-01  0.0000000000D-38  0.0000000000D-38
 0.0000000000D-38 -0.5195284178D 00  0.0000000000D-38  0.2704000000D 02  0.0000000000D-38  0.1838541667D 02

 0.0000000000D-38  0.0000000000D-38  0.0000000000D-38  0.0000000000D-38  0.1000000000D 01  0.3170177341D-01
 0.0000000000D-38  0.0000000000D-38  0.0000000000D-38  0.0000000000D-38  0.8800000000D-01  0.0000000000D-38
 0.0000000000D-38 -0.8144089568D 00  0.0000000000D-38  0.0000000000D-38  0.7744000000D 02  0.1614329268D 02
```

```
TIME POINT VARIABLES
W1     0.220000D 01  M1     0.185000D 06  W2     0.525000D 01  M2     0.137500D 06  W3     0.880000D 01
M3     0.158500D 06  XCG    0.380000D 02  XCP    0.479800D 02  CZA    0.457000D 01  Q      0.701000D 03
IXX    0.274000D 09  F      0.534700D 07  X      0.455230D 05  M      0.360560D 06  VO     0.113100D 03
ICZY1 0.409637D 01  ICZY2 0.261623D 01  ICZY3 0.471139D 01  YP1    0.355000D-01  YP2    0.450000D-01
YP3    0.500000D-01  TIME   0.320000D 02
GYRO SLOPES    -0.116000D 00    0.136000D 00   -0.104000D 00
RATE GYRO       0.245000D-01   -0.650000D-02   -0.520000D-01
SPECTRAL       -0.140500D 00    0.142500D 00   -0.520000D-01

THE MATRIX COEFICIENTS
 0.1000000000D 01  0.0000000000D-38  0.0000000000D-38  0.0000000000D-38  0.0000000000D-38 -0.6670011679D-03
 0.0000000000D-38  0.0000000000D-38  0.0000000000D-38  0.0000000000D-38  0.0000000000D-38  0.0000000000D-38
 0.0000000000D-38 -0.9271795631D-02 -0.7737920612D-02 -0.1503084827D-01 -0.1886923125D-01 -0.3710159331D 00

 0.0000000000D-38  0.0000000000D-38  0.0000000000D-38  0.0000000000D-38  0.0000000000D-38  0.0000000000D-38
-0.1000000000D 01  0.1000000000D 01  0.0000000000D-38  0.0000000000D-38  0.0000000000D-38  0.0000000000D-38
 0.0000000000D-38  0.1362462918D 00 -0.4654771721D-02 -0.5900414857D-02 -0.6556016508D-02 -0.6556016508D-01

 0.0000000000D-38  0.0000000000D-38  0.1000000000D 01  0.0000000000D-38  0.0000000000D-38  0.2668327546D-01
 0.0000000000D-38  0.0000000000D-38  0.2200000000D-01  0.0000000000D-38  0.0000000000D-38  0.0000000000D-38
 0.0000000000D-38 -0.1233374941D 01  0.4840000000D 01  0.0000000000D-38  0.0000000000D-38  0.1445135135D 02

 0.0000000000D-38  0.0000000000D-38  0.0000000000D-38  0.1000000000D 01  0.0000000000D-38  0.3685635200D-01
 0.0000000000D-38  0.0000000000D-38  0.0000000000D-38  0.5250000000D-01  0.0000000000D-38  0.0000000000D-38
 0.0000000000D-38 -0.1059841436D 01  0.0000000000D-38  0.2756250000D 02  0.0000000000D-38  0.1944363636D 02

 0.0000000000D-38  0.0000000000D-38  0.0000000000D-38  0.0000000000D-38  0.1000000000D 01  0.3240931230D-01
 0.0000000000D-38  0.0000000000D-38  0.0000000000D-38  0.0000000000D-38  0.8800000000D-01  0.0000000000D-38
 0.0000000000D-38 -0.1655722159D 01  0.0000000000D-38  0.0000000000D-38  0.7744000000D 02  0.1686750789D 02
```

```
TIME POINT VARIABLES
W1     0.2250000D 01  M1     0.1835000D 06  W2     0.5300000D 01  M2     0.1320000D 06  W3     0.8850000D 01
M3     0.1525000D 06  XCG    0.3840000D 02  XCP    0.4768000D 02  CZA    0.4650000D 01  Q      0.1192000D 04
IXX    0.2720000D 09  F      0.5399160D 07  X      0.6340300D 05  M      0.3448080D 06  VO     0.1560000D 03
ICZY1 0.4040700D 01  ICZY2 0.2565080D 01  ICZY3 0.4660580D 01  YP1    0.3575000D-01  YP2    0.4550000D-01
YP3    0.5000000D-01  TIME   0.4000000D 02
GYRO SLOPES   -0.1171700D 00   0.1340900D 00  -0.1002400D 00
RATE GYRO      0.2456000D-01  -0.4950000D-02  -0.5099000D-01
SPECTRAL      -0.1417300D 00   0.1390400D 00  -0.4925000D-01

THE MATRIX COEFICIENTS
 0.1000000000D 01   0.0000000000D-38   0.0000000000D-38   0.0000000000D-38   0.0000000000D-38  -0.6784432353D-3
 0.0000000000D-38   0.0000000000D-38   0.0000000000D-38   0.0000000000D-38   0.0000000000D-38   0.0000000000D-3
 0.0000000000D-38  -0.1502650341D-01  -0.8349918518D-02  -0.1604076127D-01  -0.1959038100D-01  -0.3813698122D

 0.0000000000D-38   0.0000000000D-38   0.0000000000D-38   0.0000000000D-38   0.0000000000D-38   0.0000000000D-3
-0.1000000000D 01   0.1000000000D 01   0.0000000000D-38   0.0000000000D-38   0.0000000000D-38   0.0000000000D-3
 0.0000000000D-38   0.1073838974D 00  -0.3588392912D-02  -0.4567045525D-02  -0.5018731346D-02  -0.5018731346D-01

 0.0000000000D-38   0.0000000000D-38   0.1000000000D 01   0.0000000000D-38   0.0000000000D-38   0.2692023074D-01
 0.0000000000D-38   0.0000000000D-38   0.2250000000D-01   0.0000000000D-38   0.0000000000D-38   0.0000000000D-38
 0.0000000000D-38  -0.2085674101D 01   0.5062500000D 01   0.0000000000D-38   0.0000000000D-38   0.1471159673D 02

 0.0000000000D-38   0.0000000000D-38   0.0000000000D-38   0.1000000000D 01   0.0000000000D-38   0.3844440273D-01
 0.0000000000D-38   0.0000000000D-38   0.0000000000D-38   0.5300000000D-01   0.0000000000D-38   0.0000000000D-38
 0.0000000000D-38  -0.1840572346D 01   0.0000000000D-38   0.2809000000D 02   0.0000000000D-38   0.2045134848D 02

 0.0000000000D-38   0.0000000000D-38   0.0000000000D-38   0.0000000000D-38   0.1000000000D 01   0.3368443279D-01
 0.0000000000D-38   0.0000000000D-38   0.0000000000D-38   0.0000000000D-38   0.8850000000D-01   0.0000000000D-38
 0.0000000000D-38  -0.2894649821D 01   0.0000000000D-38   0.0000000000D-38   0.7832250000D 02   0.1770215082D 02
```

```
TIME POINT VARIABLES
W1     0.225000D 01  M1     0.182000D 06  W2     0.535000D 01  M2     0.126500D 06  W3     0.885000D 01
M3     0.144000D 06  XCG    0.388000D 02  XCP    0.462700D 02  CZA    0.485000D 01  Q      0.188900D 04
IXX    0.268000D 09  F      0.547300D 07  X      0.100778D 06  M      0.329057D 06  VO     0.207500D 03
ICZY1 0.399560D 01  ICZY2 0.253878D 01  ICZY3 0.458471D 01  YP1    0.360000D-01  YP2    0.455000D-01
YP3    0.500000D-01  TIME   0.480000D 02
GYRO SLOPES    -0.118000D 00    0.131000D 00   -0.960000D-01
RATE GYRO       0.250000D-01   -0.400000D-02   -0.500000D-01
SPECTRAL       -0.143000D 00    0.135000D 00   -0.460000D-01

THE MATRIX COEFICIENTS
 0.1000000000D 01  0.0000000000D-38  0.0000000000D-38  0.0000000000D-38  0.0000000000D-38 -0.6952044776D-
 0.0000000000D-38  0.0000000000D-38  0.0000000000D-38  0.0000000000D-38  0.0000000000D-38  0.0000000000D-
 0.0000000000D-38 -0.2029126666D-01 -0.9087403508D-02 -0.1687451268D-01 -0.2056314335D-01 -0.3964506693D

 0.0000000000D-38  0.0000000000D-38  0.0000000000D-38  0.0000000000D-38  0.0000000000D-38  0.0000000000D-
-0.1000000000D 01  0.1000000000D 01  0.0000000000D-38  0.0000000000D-38  0.0000000000D-38  0.0000000000D-
 0.0000000000D-38  0.8934195407D-01 -0.2885617173D-02 -0.3647099483D-02 -0.4007801629D-02 -0.4007801629D-0

 0.0000000000D-38  0.0000000000D-38  0.1000000000D 01  0.0000000000D-38  0.0000000000D-38  0.2716109187D-01
 0.0000000000D-38  0.0000000000D-38  0.2250000000D-01  0.0000000000D-38  0.0000000000D-38  0.0000000000D-38
 0.0000000000D-38 -0.3295279285D 01 -0.5062500000D 01  0.0000000000D-38  0.0000000000D-38  0.1503571429D 0

 0.0000000000D-38  0.0000000000D-38  0.0000000000D-38  0.1000000000D 01  0.0000000000D-38  0.4011589850D-01
 0.0000000000D-38  0.0000000000D-38  0.0000000000D-38  0.5350000000D-01  0.0000000000D-38  0.0000000000D-38
 0.0000000000D-38 -0.3012424386D 01  0.0000000000D-38  0.2862250000D 02  0.0000000000D-38  0.2163241107D 0

 0.0000000000D-38  0.0000000000D-38  0.0000000000D-38  0.0000000000D-38  0.1000000000D 01  0.3567275000D-01
 0.0000000000D-38  0.0000000000D-38  0.0000000000D-38  0.0000000000D-38  0.8850000000D-01  0.0000000000D-3
 0.0000000000D-38 -0.4778933528D 01  0.0000000000D-38  0.0000000000D-38  0.7832250000D 02  0.1900347222D 0
```

```
TIME POINT VARIABLES
W1     0.230000D 01   M1     0.180000D 06   W2     0.540000D 01   M2     0.122500D 06   W3     0.890000D 01
M3     0.133000D 06   XCG    0.392000D 02   XCP    0.402300D 02   CZA    0.540000D 01   Q      0.257600D 04
IXX    0.265000D 09   F      0.554800D 07   X      0.179354D 06   M      0.313305D 06   VO     0.268300D 03
ICZY1  0.392014D 01   ICZY2  0.246240D 01   ICZY3  0.450864D 01   YP1    0.360000D-01   YP2    0.460000D-01
YP3    0.550000D-01   TIME   0.560000D 02
GYRO SLOPES   -0.118000D 00    0.130000D 00   -0.900000D-01
RATE GYRO      0.250000D-01   -0.300000D-02   -0.480000D-01
SPECTRAL      -0.143000D 00    0.133000D 00   -0.420000D-01

THE MATRIX COEFICIENTS
 0.1000000000D 01   0.0000000000D-38   0.0000000000D-38   0.0000000000D-38   0.0000000000D-38  -0.7097850566D-03
 0.0000000000D-38   0.0000000000D-38   0.0000000000D-38   0.0000000000D-38   0.0000000000D-38   0.0000000000D-38
 0.0000000000D-38  -0.4296161740D-02  -0.9617696250D-02  -0.1810479217D-01  -0.2574317850D-01  -0.4106301045D 0

 0.0000000000D-38   0.0000000000D-38   0.0000000000D-38   0.0000000000D-38   0.0000000000D-38   0.0000000000D-38
-0.1000000000D 01   0.1000000000D 01   0.0000000000D-38   0.0000000000D-38   0.0000000000D-38   0.0000000000D-38
 0.0000000000D-38   0.7701629604D-01  -0.2376024720D-02  -0.3036031587D-02  -0.3630037767D-02  -0.3300343333D-01

 0.0000000000D-38   0.0000000000D-38   0.1000000000D 01   0.0000000000D-38   0.0000000000D-38   0.2746288178D-01
 0.0000000000D-38   0.0000000000D-38   0.2300000000D-01   0.0000000000D-38   0.0000000000D-38   0.0000000000D-38
 0.0000000000D-38  -0.4457841107D 01   0.5290000000D 01   0.0000000000D-38   0.0000000000D-38   0.1541111111D 02

 0.0000000000D-38   0.0000000000D-38  -0.0000000000D-38   0.1000000000D 01   0.0000000000D-38   0.4148223608D-01
 0.0000000000D-38   0.0000000000D-38   0.0000000000D-38   0.5400000000D-01   0.0000000000D-38   0.0000000000D-38
 0.0000000000D-38  -0.4114509092D 01   0.0000000000D-38   0.2916000000D 02   0.0000000000D-38   0.2264489796D 02

 0.0000000000D-38   0.0000000000D-38   0.0000000000D-38   0.0000000000D-38   0.1000000000D 01   0.3914288421D-01
 0.0000000000D-38   0.0000000000D-38   0.0000000000D-38   0.0000000000D-38   0.8900000000D-01   0.0000000000D-38
 0.0000000000D-38  -0.6938880868D 01   0.0000000000D-38   0.0000000000D-38   0.7921000000D 02   0.2085714286D 02
```

```
TIME POINT VARIABLES
W1     0.230000D 01  M1     0.177000D 06  W2     0.550000D 01  M2     0.119000D 06  W3     0.895000D 01
M3     0.118000D 06  XCG    0.396000D 02  XCP    0.387200D 02  CZA    0.570000D 01  Q      0.320500D 04
IXX    0.261000D 09  F      0.563000D 07  X      0.269712D 06  M      0.297554D 06  VO     0.338100D 03
ICZY1 0.384499D 01  ICZY2 0.238618D 01  ICZY3 0.438257D 01  YP1    0.360000D-01  YP2    0.465000D-01
YP3    0.550000D-01  TIME   0.640000D 02
GYRO SLOPES    -0.119000D 00   0.128000D 00  -0.840000D-01
RATE GYRO       0.250000D-01  -0.100000D-02  -0.440000D-01
SPECTRAL       -0.144000D 00   0.129000D 00  -0.400000D-01

THE MATRIX COEFFICIENTS
 0.1000000000D 01  0.0000000000D-38  0.0000000000D-38  0.0000000000D-38  0.0000000000D-38 -0.7274761686D-03
 0.0000000000D-38  0.0000000000D-38  0.0000000000D-38  0.0000000000D-38  0.0000000000D-38  0.0000000000D-38
 0.0000000000D-38  0.4894346452D-02 -0.1022004366D-01 -0.1949239675D-01 -0.2699858734D-01 -0.4274102884D 00

 0.0000000000D-38  0.0000000000D-38  0.0000000000D-38  0.0000000000D-38  0.0000000000D-38  0.0000000000D-38
-0.1000000000D 01 -0.1000000000D 01  0.0000000000D-38  0.0000000000D-38  0.0000000000D-38  0.0000000000D-38
 0.0000000000D-38  0.6771076571D-01 -0.2014651502D-02 -0.2602258191D-02 -0.3077939795D-02 -0.2798127087D-01

 0.0000000000D-38  0.0000000000D-38  0.1000000000D 01  0.0000000000D-38  0.0000000000D-38  0.2792835435D-01
 0.0000000000D-38  0.0000000000D-38  0.2300000000D-01  0.0000000000D-38  0.0000000000D-38  0.0000000000D-38
 0.0000000000D-38 -0.5532222466D 01  0.5290000000D 01  0.0000000000D-38  0.0000000000D-38  0.1590395480D 02

 0.0000000000D-38  0.0000000000D-38  0.0000000000D-38  0.1000000000D 01  0.0000000000D-38  0.4276039227D-01
 0.0000000000D-38  0.0000000000D-38  0.0000000000D-38  0.5500000000D-01  0.0000000000D-38  0.0000000000D-38
 0.0000000000D-38 -0.5106624536D 01  0.0000000000D-38  0.3025000000D 02  0.0000000000D-38  0.2365546218D 02

 0.0000000000D-38  0.0000000000D-38  0.0000000000D-38  0.0000000000D-38  0.1000000000D 01  0.4411867458D-01
 0.0000000000D-38  0.0000000000D-38  0.0000000000D-38  0.0000000000D-38  0.8950000000D-01  0.0000000000D-38
 0.0000000000D-38 -0.9458549520D 01  0.0000000000D-38  0.0000000000D-38  0.8010250000D 02  0.2385593220D 02
```

```
TIME POINT VARIABLES
W1     0.230000D 01  M1     0.174500D 06  W2     0.555000D 01  M2     0.117000D 06  W3     0.905000D 01
M3     0.115000D 06  XCG    0.404000D 02  XCP    0.452600D 02  CZA    0.510000D 01  Q      0.372100D 04
IXX    0.256000D 09  F      0.572000D 07  X      0.271777D 06  M      0.281802D 06  VO     0.421000D 03
ICZY1 0.374499D 01  ICZY2 0.173511D 01  ICZY3 0.425635D 01  YP1    0.360000D-01  YP2    0.470000D-01
YP3    0.560000D-01  TIME   0.720000D 02
GYRO SLOPES    -0.118000D 00    0.128000D 00   -0.770000D-01
RATE GYRO       0.260000D-01    0.500000D-03   -0.420000D-01
SPECTRAL       -0.144000D 00    0.123000D 00   -0.350000D-01

THE MATRIX COEFFICIENTS
 0.1000000000D 01  0.0000000000D-38  0.0000000000D-38  0.0000000000D-38  0.0000000000D-38 -0.7555771875D-03
 0.0000000000D-38  0.0000000000D-38  0.0000000000D-38  0.0000000000D-38  0.0000000000D-38  0.0000000000D-38
 0.0000000000D-38 -0.2862699775D-01 -0.1122972029D-01 -0.2148828065D-01 -0.2988164822D-01 -0.4516794886D 0?

 0.0000000000D-38  0.0000000000D-38  0.0000000000D-38  0.0000000000D-38  0.0000000000D-38  0.0000000000D-38
-0.1000000000D 01  0.1000000000D 01  0.0000000000D-38  0.0000000000D-38  0.0000000000D-38  0.0000000000D-38
 0.0000000000D-38  0.5863306461D-01 -0.1735690805D-02 -0.2266040773D-02 -0.2699963474D-02 -0.2410681673D-01

 0.0000000000D-38  0.0000000000D-38  0.1000000000D 01  0.0000000000D-38  0.0000000000D-38  0.2832847404D-01
 0.0000000000D-38  0.0000000000D-38  0.2300000000D-01  0.0000000000D-38  0.0000000000D-38  0.0000000000D-38
 0.0000000000D-38 -0.6345481100D 01  0.5290000000D 01  0.0000000000D-38  0.0000000000D-38  0.1638968481D 02

 0.0000000000D-38  0.0000000000D-38  0.0000000000D-38  0.1000000000D 01  0.0000000000D-38  0.4355042256D-01
 0.0000000000D-38  0.0000000000D-38  0.0000000000D-38  0.5550000000D-01  0.0000000000D-38  0.0000000000D-38
 0.0000000000D-38 -0.4384806924D 01  0.0000000000D-38  0.3080250000D 02  0.0000000000D-38  0.2444444444D 02

 0.0000000000D-38  0.0000000000D-38  0.0000000000D-38  0.0000000000D-38  0.1000000000D 01  0.4538981843D-01
 0.0000000000D-38  0.0000000000D-38  0.0000000000D-38  0.0000000000D-38  0.9050000000D-01  0.0000000000D-38
 0.0000000000D-38 -0.1094331288D 02  0.0000000000D-38  0.0000000000D-38  0.8190250000D 02  0.2486956522D 02
```

```
TIME POINT VARIABLES
W1     0.230000D 01  M1     0.172000D 06  W2     0.560000D 01  M2     0.115500D 06  W3     0.910000D 01
M3     0.101500D 06  XCG    0.412000D 02  XCP    0.523000D 02  CZA    0.485000D 01  Q      0.385600D 04
IXX    0.253000D 09  F      0.579300D 07  X      0.238780D 06  M      0.269989D 06  VO     0.506900D 03
ICZY1  0.362030D 01  ICZY2  0.138465D 01  ICZY3  0.415558D 01  YP1    0.357500D-01  YP2    0.475000D-01
YP3    0.560000D-01  TIME   0.780000D 02
GYRO SLOPES   -0.118000D 00   0.128000D 00  -0.720000D-01
RATE GYRO      0.255000D-01   0.250000D-02  -0.400000D-01
SPECTRAL      -0.143500D 00   0.125500D 00  -0.320000D-01

THE MATRIX COEFICIENTS
 0.1000000000D 01  0.0000000000D-38  0.0000000000D-38  0.0000000000D-38  0.0000000000D-38 -0.7785938340D-03
 0.0000000000D-38  0.0000000000D-38  0.0000000000D-38  0.0000000000D-38  0.0000000000D-38  0.0000000000D-39
 0.0000000000D-38 -0.6519748983D-01 -0.1192383116D-01 -0.2336851665D-01 -0.3164765083D-01 -0.4720444861D 00

 0.0000000000D-38  0.0000000000D-38  0.0000000000D-38  0.0000000000D-38  0.0000000000D-38  0.0000000000D-38
-0.1000000000D 01  0.1000000000D 01  0.0000000000D-38  0.0000000000D-38  0.0000000000D-38  0.0000000000D-38
 0.0000000000D-38  0.5144224307D-01 -0.1513251848D-02 -0.2010614344D-02 -0.2370408490D-02 -0.2116436152D-01

 0.0000000000D-38  0.0000000000D-38  0.1000000000D 01  0.0000000000D-38  0.0000000000D-38  0.2872012988D-01
 0.0000000000D-38  0.0000000000D-38  0.2300000000D-01  0.0000000000D-38  0.0000000000D-38  0.0000000000D-38
 0.0000000000D-38 -0.6449154666D 01  0.5290000000D 01  0.0000000000D-38  0.0000000000D-38  0.1684011628D 02

 0.0000000000D-38  0.0000000000D-38  0.0000000000D-38  0.1000000000D 01  0.0000000000D-38  0.4417586320D-01
 0.0000000000D-38  0.0000000000D-38  0.0000000000D-38  0.5600000000D-01  0.0000000000D-38  0.0000000000D-38
 0.0000000000D-38 -0.3673201093D 01  0.0000000000D-38  0.3136000000D 02  0.0000000000D-38  0.2507792208D 02

 0.0000000000D-38  0.0000000000D-38  0.0000000000D-38  0.0000000000D-38  0.1000000000D 01  0.5142688788D-01
 0.0000000000D-38  0.0000000000D-38  0.0000000000D-38  0.0000000000D-38  0.9100000000D-01  0.0000000000D-38
 0.0000000000D-38 -0.1254446905D 02  0.0000000000D-38  0.0000000000D-38  0.8281000000D 02  0.2853694581D 02
```

```
TIME POINT VARIABLES
W1     0.230000D 01  M1     0.171000D 06  W2     0.565000D 01  M2     0.115000D 06  W3     0.915000D 01
M3     0.985000D 05  XCG    0.413000D 02  XCP    0.530100D 02  CZA    0.485000D 01  Q      0.384100D 04
IXX    0.252000D 09  F      0.581980D 07  X      0.227178D 06  M      0.266051D 06  VO     0.519300D 03
ICZY1  0.333586D 01  ICZY2  0.108136D 01  ICZY3  0.388229D 01  YP1    0.355000D-01  YP2    0.475000D-01
YP3    0.565000D-01  TIME   0.800000D 02
GYRO SLOPES    -0.118180D 00    0.129270D 00   -0.701500D-01
RATE GYRO       0.259100D-01    0.111000D-02   -0.398000D-01
SPECTRAL       -0.144090D 00    0.128160D 00   -0.303200D-01

THE MATRIX COEFICIENTS
 0.1000000000D 01  0.0000000000D-38  0.0000000000D-38  0.0000000000D-38  0.0000000000D-38 -0.7834476190D-03
 0.0000000000D-38  0.0000000000D-38  0.0000000000D-38  0.0000000000D-38  0.0000000000D-38  0.0000000000D-38
 0.0000000000D-38 -0.6878473269D-01 -0.1186292400D-01 -0.2367950596D-01 -0.3254194242D-01 -0.4772715226D 00

 0.0000000000D-38  0.0000000000D-38  0.0000000000D-38  0.0000000000D-38  0.0000000000D-38  0.0000000000D-38
-0.1000000000D 01  0.1000000000D 01  0.0000000000D-38  0.0000000000D-38  0.0000000000D-38  0.0000000000D-38
 0.0000000000D-38  0.5119328744D-01 -0.1495386887D-02 -0.2000869779D-02 -0.2379981948D-02 -0.2106178715D-01

 0.0000000000D-38  0.0000000000D-38  0.1000000000D 01  0.0000000000D-38  0.0000000000D-38  0.2886787111D-01
 0.0000000000D-38  0.0000000000D-38  0.2300000000D-01  0.0000000000D-38  0.0000000000D-38  0.0000000000D-38
 0.0000000000D-38 -0.5953956624D 01  0.5290000000D 01  0.0000000000D-38  0.0000000000D-38  0.1701697368D 02

 0.0000000000D-38  0.0000000000D-38  0.0000000000D-38  0.1000000000D 01  0.0000000000D-38  0.4436793217D-01
 0.0000000000D-38  0.0000000000D-38  0.0000000000D-38  0.5650000000D-01  0.0000000000D-38  0.0000000000D-38
 0.0000000000D-38 -0.2869897735D 01  0.0000000000D-38  0.3192250000D 02  0.0000000000D-38  0.2530350000D 02

 0.0000000000D-38  0.0000000000D-38  0.0000000000D-38  0.0000000000D-38  0.1000000000D 01  0.5306336934D-01
 0.0000000000D-38  0.0000000000D-38  0.0000000000D-38  0.0000000000D-38  0.9150000000D-01  0.0000000000D-38
 0.0000000000D-38 -0.1202944813D 02  0.0000000000D-38  0.0000000000D-38  0.8372250000D 02  0.2954215736D 02
```

```
TIME POINT VARIABLES
W1     0.2350000D 01  M1     0.1660000D 06  W2     0.5750000D 01  M2     0.1150000D 06  W3     0.9300000D 01
M3     0.8700000D 05  XCG    0.4220000D 02  XCP    0.5713000D 02  CZA    0.4880000D 01  Q      0.3342000D 04
IXX    0.2460000D 09  F      0.5901000D 07  X      0.1687440D 06  M      0.2503000D 06  VO     0.6391000D 03
ICZY1  0.3261380D 01  ICZY2  0.1005380D 01  ICZY3  0.3755500D 01  YP1    0.3550000D-01  YP2    0.4750000D-01
YP3    0.5700000D-01  TIME   0.8800000D 02
GYRO SLOPES   -0.1170000D 00   0.1300000D 00  -0.6300000D-01
RATE GYRO      0.2600000D-01   0.4000000D-02  -0.3600000D-01
SPECTRAL      -0.1430000D 00   0.1260000D 00  -0.2700000D-01

THE MATRIX COEFFICIENTS
 0.1000000000D 01   0.0000000000D-38   0.0000000000D-38   0.0000000000D-38   0.0000000000D-38  -0.8188204878D-03
 0.0000000000D-38   0.0000000000D-38   0.0000000000D-38   0.0000000000D-38   0.0000000000D-38   0.0000000000D-38
 0.0000000000D-38  -0.7865034319D-01  -0.1308821626D-01  -0.2562095580D-01  -0.3554270794D-01  -0.5065565492D 00

 0.0000000000D-38   0.0000000000D-38   0.0000000000D-38   0.0000000000D-38   0.0000000000D-38   0.0000000000D-38
-0.1000000000D 01   0.1000000000D 01   0.0000000000D-38   0.0000000000D-38   0.0000000000D-38   0.0000000000D-38
 0.0000000000D-38   0.4393519342D-01  -0.1309556681D-02  -0.1752223728D-02  -0.2102668474D-02  -0.1844446029D-01

 0.0000000000D-38   0.0000000000D-38   0.1000000000D 01   0.0000000000D-38   0.0000000000D-38   0.2973738530D-01
 0.0000000000D-38   0.0000000000D-38   0.2350000000D-01   0.0000000000D-38   0.0000000000D-38   0.0000000000D-38
 0.0000000000D-38  -0.5217343310D 01   0.5522500000D 01   0.0000000000D-38   0.0000000000D-38   0.1777409639D 02

 0.0000000000D-38   0.0000000000D-38   0.0000000000D-38   0.1000000000D 01   0.0000000000D-38   0.4436793217D-01
 0.0000000000D-38   0.0000000000D-38   0.0000000000D-38   0.5750000000D-01   0.0000000000D-38   0.0000000000D-38
 0.0000000000D-38  -0.2321605910D 01   0.0000000000D-38   0.3306250000D 02   0.0000000000D-38   0.2565652174D 02

 0.0000000000D-38   0.0000000000D-38   0.0000000000D-38   0.0000000000D-38   0.1000000000D 01   0.6015694989D-01
 0.0000000000D-38   0.0000000000D-38   0.0000000000D-38   0.0000000000D-38   0.9300000000D-01   0.0000000000D-38
 0.0000000000D-38  -0.1146316683D 02   0.0000000000D-38   0.0000000000D-38   0.8649000000D 02   0.3391379310D 02
```

```
TIME POINT VARIABLES
W1     0.237500D 01  M1     0.159500D 06  W2     0.580000D 01  M2     0.116000D 06  W3     0.955000D 01
M3     0.770000D 05  XCG    0.436000D 02  XCP    0.590400D 02  CZA    0.481000D 01  Q      0.253600D 04
IXX    0.240000D 09  F      0.597600D 07  X      0.112746D 06  M      0.234548D 06  VO     0.779500D 03
ICZY1 0.323762D 01  ICZY2 0.930125D 00  ICZY3 0.365388D 01  YP1    0.350000D-01  YP2    0.480000D-01
YP3    0.580000D-01  TIME   0.960000D 02
GYRO SLOPES    -0.116000D 00   0.132000D 00  -0.560000D-01
RATE GYRO       0.260000D-01   0.500000D-02  -0.340000D-01
SPECTRAL       -0.142000D 00   0.127000D 00  -0.220000D-01

THE MATRIX COEFICIENTS
 0.1000000000D 01  0.0000000000D-38  0.0000000000D-38  0.0000000000D-38  0.0000000000D-38 -0.8652236667D-03
 0.0000000000D-38  0.0000000000D-38  0.0000000000D-38  0.0000000000D-38  0.0000000000D-38  0.0000000000D-38
 0.0000000000D-38 -0.6235625634D-01 -0.1426397247D-01 -0.2881059082D-01 -0.4000029724D-01 -0.5432830481D 00

 0.0000000000D-38  0.0000000000D-38  0.0000000000D-38  0.0000000000D-38  0.0000000000D-38  0.0000000000D-38
-0.1000000000D 01 -0.1000000000D 01  0.0000000000D-38  0.0000000000D-38  0.0000000000D-38  0.0000000000D-38
 0.0000000000D-38  0.3737086928D-01 -0.1144012526D-02 -0.1568931464D-02 -0.1895792186D-02 -0.1634303608D-01

 0.0000000000D-38  0.0000000000D-38  0.1000000000D 01  0.0000000000D-38  0.0000000000D-38  0.3090591348D-01
 0.0000000000D-38  0.0000000000D-38  0.2375000000D-01  0.0000000000D-38  0.0000000000D-38  0.0000000000D-38
 0.0000000000D-38 -0.4090384084D 01  0.5640625000D 01  0.0000000000D-38  0.0000000000D-38  0.1873354232D 02

 0.0000000000D-38  0.0000000000D-38  0.0000000000D-38  0.1000000000D 01  0.0000000000D-38  0.4404504276D-01
 0.0000000000D-38  0.0000000000D-38  0.0000000000D-38  0.5800000000D-01  0.0000000000D-38  0.0000000000D-38
 0.0000000000D-38 -0.1615780012D 01  0.0000000000D-38  0.3364000000D 02  0.0000000000D-38  0.2575862069D 02

 0.0000000000D-38  0.0000000000D-38  0.0000000000D-38  0.0000000000D-38  0.1000000000D 01  0.6814909299D-01
 0.0000000000D-38  0.0000000000D-38  0.0000000000D-38  0.0000000000D-38  0.9550000000D-01  0.0000000000D-38
 0.0000000000D-38 -0.9562302055D 01  0.0000000000D-38  0.0000000000D-38  0.9120250000D 02  0.3880519481D 02
```

```
TIME POINT VARIABLES
W1     0.240000D 01  M1     0.150000D 06  W2     0.590000D 01  M2     0.117000D 06  W3     0.985000D 01
M3     0.690000D 05  XCG    0.448000D 02  XCP    0.600500D 02  CZA    0.465000D 01  Q      0.182900D 04
IXX    0.232000D 09  F      0.603800D 07  X      0.723120D 05  M      0.218797D 06  VO     0.940700D 04
ICZY1 0.321412D 01  ICZY2 0.830625D 00  ICZY3 0.360188D 01  YP1    0.345000D-01  YP2    0.480000D-01
YP3    0.585000D-01  TIME   0.104000D 03
GYRO SLOPES    -0.113000D 00    0.134000D 00   -0.490000D-01
RATE GYRO       0.260000D-01    0.600000D-02   -0.320000D-01
SPECTRAL       -0.139000D 00    0.128000D 00   -0.170000D-01

THE MATRIX COEFICIENTS
 0.1000000000D 01  0.0000000000D-38  0.0000000000D-38  0.0000000000D-38  0.0000000000D-38 -0.9180534483D-03
 0.0000000000D-38  0.0000000000D-38  0.0000000000D-38  0.0000000000D-38  0.0000000000D-38  0.0000000000D-38
 0.0000000000D-38 -0.4442200647D-01 -0.1540161094D-01 -0.3161236125D-01 -0.4422072260D-01 -0.5835017806D 00

 0.0000000000D-38  0.0000000000D-38  0.0000000000D-38  0.0000000000D-38  0.0000000000D-38  0.0000000000D-38
-0.1000000000D 01 -0.1000000000D 01  0.0000000000D-38  0.0000000000D-38  0.0000000000D-38  0.0000000000D-38
 0.0000000000D-38  0.3226804802D-02 -0.1012091312D-03 -0.1408127043D-03 -0.1716154833D-03 -0.1466799003D-02

 0.0000000000D-38  0.0000000000D-38  0.1000000000D 01  0.0000000000D-38  0.0000000000D-38  0.3281720293D-01
 0.0000000000D-38  0.0000000000D-38  0.2400000000D-01  0.0000000000D-38  0.0000000000D-38  0.0000000000D-38
 0.0000000000D-38 -0.3114111709D 01  0.5760000000D 01  0.0000000000D-38  0.0000000000D-38  0.2012666667D 02

 0.0000000000D-38  0.0000000000D-38  0.0000000000D-38  0.1000000000D 01  0.0000000000D-38  0.4366858940D-01
 0.0000000000D-38  0.0000000000D-38  0.0000000000D-38  0.5900000000D-01  0.0000000000D-38  0.0000000000D-38
 0.0000000000D-38 -0.1031769049D 01  0.0000000000D-38  0.3481000000D 02  0.0000000000D-38  0.2580341880D 02

 0.0000000000D-38  0.0000000000D-38  0.0000000000D-38  0.0000000000D-38  0.1000000000D 01  0.7615062203D-01
 0.0000000000D-38  0.0000000000D-38  0.0000000000D-38  0.0000000000D-38  0.9850000000D-01  0.0000000000D-38
 0.0000000000D-38 -0.7586535744D 01  0.0000000000D-38  0.0000000000D-38  0.9702250000D 02  0.4375362319D 02
```

```
TIME POINT VARIABLES
W1     0.240000D 01  M1     0.138500D 06  W2     0.595000D 01  M2     0.118000D 06  W3     0.102000D 02
M3     0.630000D 05  XCG    0.464000D 02  XCP    0.607500D 02  CZA    0.443000D 01  Q      0.121200D 04
IXX    0.222000D 09  F      0.608500D 07  X      0.429150D 05  M      0.203046D 06  VO     0.112470D 04
ICZY1 0.311625D 01  ICZY2 0.756250D 00  ICZY3 0.359975D 01  YP1    0.330000D-01  YP2    0.475000D-01
YP3    0.595000D-01  TIME   0.112000D 03
GYRO SLOPES    -0.109000D 00    0.136000D 00   -0.430000D-01
RATE GYRO       0.260000D-01    0.800000D-02   -0.290000D-01
SPECTRAL       -0.135000D 00    0.128000D 00   -0.140000D-01

THE MATRIX COEFFICIENTS
 0.1000000000D 01  0.0000000000D-38  0.0000000000D-38  0.0000000000D-38  0.0000000000D-38 -0.9914475676D-03
 0.0000000000D-38  0.0000000000D-38  0.0000000000D-38  0.0000000000D-38  0.0000000000D-38  0.0000000000D-38
 0.0000000000D-38 -0.2757750211D-01 -0.1577092593D-01 -0.3474432350D-01 -0.5044644562D-01 -0.6365058050D 00

 0.0000000000D-38  0.0000000000D-38  0.0000000000D-38  0.0000000000D-38  0.0000000000D-38  0.0000000000D-38
-0.1000000000D 01  0.1000000000D 01  0.0000000000D-38  0.0000000000D-38  0.0000000000D-38  0.0000000000D-38
 0.0000000000D-38  0.2832612634D-01 -0.8793127875D-03 -0.1265677497D-02 -0.1585427602D-02 -0.1332292102D-01

 0.0000000000D-38  0.0000000000D-38  0.1000000000D 01  0.0000000000D-38  0.0000000000D-38  0.3539236217D-01
 0.0000000000D-38  0.0000000000D-38  0.2400000000D-01  0.0000000000D-38  0.0000000000D-38  0.0000000000D-38
 0.0000000000D-38 -0.2166879654D 01  0.5760000000D 01  0.0000000000D-38  0.0000000000D-38  0.2196750903D 02

 0.0000000000D-38  0.0000000000D-38  0.0000000000D-38  0.1000000000D 01  0.0000000000D-38  0.4323993390D-01
 0.0000000000D-38  0.0000000000D-38  0.0000000000D-38  0.5950000000D-01  0.0000000000D-38  0.0000000000D-38
 0.0000000000D-38 -0.6172138374D 00  0.0000000000D-38  0.3540250000D 02  0.0000000000D-38  0.2578389831D 02

 0.0000000000D-38  0.0000000000D-38  0.0000000000D-38  0.0000000000D-38  0.1000000000D 01  0.8362251492D-01
 0.0000000000D-38  0.0000000000D-38  0.0000000000D-38  0.0000000000D-38  0.1020000000D 00  0.0000000000D-38
 0.0000000000D-38 -0.5502804257D 01  0.0000000000D-38  0.0000000000D-38  0.1040400000D 03  0.4829365079D 02
```

```
TIME POINT VARIABLES
W1     0.240000D 01  M1     0.123000D 06  W2     0.605000D 01  M2     0.119000D 06  W3     0.106000D 02
M3     0.635000D 05  XCG    0.486000D 02  XCP    0.611600D 02  CZA    0.414000D 01  Q      0.781000D 03
IXX    0.210000D 09  F      0.612283D 07  X      0.248020D 05  M      0.187299D 06  VO     0.133320D 04
ICZY1 0.304385D 01  ICZY2 0.682390D 00  ICZY3 0.369834D 01  YP1    0.325000D-01  YP2    0.470000D-01
YP3    0.600000D-01  TIME   0.120000D 03
GYRO SLOPES    -0.103920D 00    0.138000D 00   -0.401300D-01
RATE GYRO       0.251000D-01    0.100600D-01   -0.249600D-01
SPECTRAL       -0.129020D 00    0.128320D 00   -0.151700D-01

THE MATRIX COEFICIENTS
 0.1000000000D 01  0.0000000000D-38  0.0000000000D-38  0.0000000000D-38  0.0000000000D-38 -0.1094674667D-02
 0.0000000000D-38  0.0000000000D-38  0.0000000000D-38  0.0000000000D-38  0.0000000000D-38  0.0000000000D-38
 0.0000000000D-38 -0.1536637309D-01 -0.1816450792D-01 -0.3927688325D-01 -0.5820521975D-01 -0.7091881314D 00

 0.0000000000D-38  0.0000000000D-38  0.0000000000D-38  0.0000000000D-38  0.0000000000D-38  0.0000000000D-38
-0.1000000000D 01  0.1000000000D 01  0.0000000000D-38  0.0000000000D-38  0.0000000000D-38  0.0000000000D-38
 0.0000000000D-38  0.2544962360D-01 -0.7969017835D-03 -0.1152442579D-02 -0.1471203293D-02 -0.1226002744D-01

 0.0000000000D-38  0.0000000000D-38  0.1000000000D 01  0.0000000000D-38  0.0000000000D-38  0.3979617398D-01
 0.0000000000D-38  0.0000000000D-38  0.2400000000D-01  0.0000000000D-38  0.0000000000D-38  0.0000000000D-38
 0.0000000000D-38 -0.1535743985D 01  0.5760000000D 01  0.0000000000D-38  0.0000000000D-38  0.2488955285D 02

 0.0000000000D-38  0.0000000000D-38  0.0000000000D-38  0.1000000000D 01  0.0000000000D-38  0.4281848269D-01
 0.0000000000D-38  0.0000000000D-38  0.0000000000D-38  0.6050000000D-01  0.0000000000D-38  0.0000000000D-38
 0.0000000000D-38 -0.3558659045D 00  0.0000000000D-38  0.3660250000D 02  0.0000000000D-38  0.2572617647D 02

 0.0000000000D-38  0.0000000000D-38  0.0000000000D-38  0.0000000000D-38  0.1000000000D 01  0.8307293228D-01
 0.0000000000D-38  0.0000000000D-38  0.0000000000D-38  0.0000000000D-38  0.1060000000D 00  0.0000000000D-38
 0.0000000000D-38 -0.3614379889D 01  0.0000000000D-38  0.0000000000D-38  0.1123600000D 03  0.4821125984D 02
```

```
TIME POINT VARIABLES
W1     0.2450000D 01  M1     0.1055000D 06  W2     0.6100000D 01  M2     0.1155000D 06  W3     0.1100000D 02
M3     0.7600000D 05  XCG    0.5120000D 02  XCP    0.6126000D 02  CZA    0.3900000D 01  Q      0.4990000D 03
IXX    0.1940000D 09  F      0.6145000D 07  X      0.1418300D 05  M      0.1715420D 06  VO     0.1568500D 04
ICZY1  0.2922120D 01  ICZY2  0.6340000D 00  ICZY3  0.4146880D 01  YP1    0.3100000D-01  YP2    0.4600000D-01
YP3    0.6050000D-01  TIME   0.1280000D 03
GYRO SLOPES    -0.9700000D-01   0.1380000D 00  -0.4100000D-01
RATE GYRO       0.2400000D-01   0.1150000D-01  -0.2000000D-01
SPECTRAL       -0.1210000D 00   0.1265000D 00  -0.2100000D-01

THE MATRIX COEFICIENTS
 0.1000000000D 01  0.0000000000D-38  0.0000000000D-38  0.0000000000D-38  0.0000000000D-38 -0.1244537320D-02
 0.0000000000D-38  0.0000000000D-38  0.0000000000D-38  0.0000000000D-38  0.0000000000D-38  0.0000000000D-38
 0.0000000000D-38 -0.8018830938D-02 -0.1991410720D-01 -0.4487670314D-01 -0.6900721254D-01 -0.8117055841D 00

 0.0000000000D-38  0.0000000000D-38  0.0000000000D-38  0.0000000000D-38  0.0000000000D-38  0.0000000000D-38
-0.1000000000D 01  0.1000000000D 01  0.0000000000D-38  0.0000000000D-38  0.0000000000D-38  0.0000000000D-38
 0.0000000000D-38  0.2336047635D-01 -0.7079923887D-03 -0.1050569351D-02 -0.1381727081D-02 -0.1141923208D-01

 0.0000000000D-38  0.0000000000D-38  0.1000000000D 01  0.0000000000D-38  0.0000000000D-38  0.4620086370D-01
 0.0000000000D-38  0.0000000000D-38  0.2450000000D-01  0.0000000000D-38  0.0000000000D-38  0.0000000000D-38
 0.0000000000D-38 -0.1098236280D 01  0.6002500000D 01  0.0000000000D-38  0.0000000000D-38  0.2912322275D 02

 0.0000000000D-38  0.0000000000D-38  0.0000000000D-38  0.1000000000D 01  0.0000000000D-38  0.4399631100D-01
 0.0000000000D-38  0.0000000000D-38  0.0000000000D-38  0.6100000000D-01  0.0000000000D-38  0.0000000000D-38
 0.0000000000D-38 -0.2176493994D 00  0.0000000000D-38  0.3721000000D 02  0.0000000000D-38  0.2660173160D 02

 0.0000000000D-38  0.0000000000D-38  0.0000000000D-38  0.0000000000D-38  0.1000000000D 01  0.6950057842D-01
 0.0000000000D-38  0.0000000000D-38  0.0000000000D-38  0.0000000000D-38  0.1100000000D 00  0.0000000000D-38
 0.0000000000D-38 -0.2163505858D 01  0.0000000000D-38  0.0000000000D-38  0.1210000000D 03  0.4042763158D 02
```

```
TIME POINT VARIABLES
W1     0.247500D 01  M1     0.850000D 05  W2     0.620000D 01  M2     0.108000D 06  W3     0.113000D 02
M3     0.111500D 06  XCG    0.548000D 02  XCP    0.613600D 02  CZA    0.374000D 01  Q      0.275000D 03
IXX    0.176000D 09  F      0.615300D 07  X      0.698600D 04  M      0.155791D 06  VO     0.183500D 04
ICZY1  0.280225D 01  ICZY2  0.638375D 00  ICZY3  0.464638D 01  YP1    0.290000D-01  YP2    0.440000D-01
YP3    0.605000D-01  TIME   0.136000D 03
GYRO SLOPES   -0.880000D-01   0.134000D 00  -0.420000D-01
RATE GYRO      0.230000D-01   0.130000D-01  -0.140000D-01
SPECTRAL      -0.111000D 00   0.121000D 00  -0.280000D-01

THE MATRIX COEFICIENTS
 0.1000000000D 01  0.0000000000D-38  0.0000000000D-38  0.0000000000D-38  0.0000000000D-38 -0.1462752273D-02
 0.0000000000D-38  0.0000000000D-38  0.0000000000D-38  0.0000000000D-38  0.0000000000D-38  0.0000000000D-38
 0.0000000000D-38 -0.3046106767D-02 -0.2195568068D-01 -0.5139494341D-01 -0.8377813242D-01 -0.9589067080D 00

 0.0000000000D-38  0.0000000000D-38  0.0000000000D-38  0.0000000000D-38  0.0000000000D-38  0.0000000000D-38
-0.1000000000D 01  0.1000000000D 01  0.0000000000D-38  0.0000000000D-38  0.0000000000D-38  0.0000000000D-38
 0.0000000000D-38  0.2178471872D-01 -0.6241751573D-03 -0.9470243766D-03 -0.1302158518D-02 -0.1076164064D-01

 0.0000000000D-38  0.0000000000D-38  0.1000000000D 01  0.0000000000D-38  0.0000000000D-38  0.5701811859D-01
 0.0000000000D-38  0.0000000000D-38  0.2475000000D-01  0.0000000000D-38  0.0000000000D-38  0.0000000000D-38
 0.0000000000D-38 -0.7203943529D 00  0.6125625000D 01  0.0000000000D-38  0.0000000000D-38  0.3619411765D 02

 0.0000000000D-38  0.0000000000D-38  0.0000000000D-38  0.1000000000D 01  0.0000000000D-38  0.4679558222D-01
 0.0000000000D-38  0.0000000000D-38  0.0000000000D-38  0.6200000000D-01  0.0000000000D-38  0.0000000000D-38
 0.0000000000D-38 -0.1291619113D 00  0.0000000000D-38  0.3844000000D 02  0.0000000000D-38  0.2848611111D 02

 0.0000000000D-38  0.0000000000D-38  0.0000000000D-38  0.0000000000D-38  0.1000000000D 01  0.4737259157D-01
 0.0000000000D-38  0.0000000000D-38  0.0000000000D-38  0.0000000000D-38  0.1130000000D 00  0.0000000000D-38
 0.0000000000D-38 -0.9105885930D 00  0.0000000000D-38  0.0000000000D-38  0.1276900000D 03  0.2759192825D 02
```

```
TIME POINT VARIABLES
W1     0.2550000D 01  M1     0.5850000D 05  W2     0.6300000D 01  M2     0.8600000D 05  W3     0.1155000D 02
M3     0.1510000D 06  XCG    0.5920000D 02  XCP    0.6156000D 02  CZA    0.3500000D 01  Q      0.1710000D 03
IXX    0.1480000D 09  F      0.6152000D 07  X      0.3842000D 04  M      0.1400390D 06  VO     0.2138200D 04
ICZY1  0.2633880D 01  ICZY2  0.7493800D 00  ICZY3  0.5005000D 01  YP1    0.2650000D-01  YP2    0.4000000D-01
YP3    0.5650000D-01  TIME   0.1440000D 03
GYRO SLOPES    -0.7300000D-01   0.1140000D 00  -0.4000000D-01
RATE GYRO       0.2200000D-01   0.1500000D-01  -0.8000000D-02
SPECTRAL       -0.9500000D-01   0.9900000D-01  -0.3200000D-01

THE MATRIX COEFICIENTS
 0.1000000000D 01  0.0000000000D-38  0.0000000000D-38  0.0000000000D-38  0.0000000000D-38 -0.1871655676D-02
 0.0000000000D-38  0.0000000000D-38  0.0000000000D-38  0.0000000000D-38  0.0000000000D-38  0.0000000000D-38
 0.0000000000D-38 -0.7583402304D-03 -0.2511813257D-01 -0.5909009302D-01 -0.1006113780D 00 -0.1231718757D 01

 0.0000000000D-38  0.0000000000D-38  0.0000000000D-38  0.0000000000D-38  0.0000000000D-38  0.0000000000D-38
-0.1000000000D 01  0.1000000000D 01  0.0000000000D-38  0.0000000000D-38  0.0000000000D-38  0.0000000000D-38
 0.0000000000D-38  0.2069160128D-01 -0.5444586157D-03 -0.8218243256D-03 -0.1160826860D-02 -0.1027280407D-01

 0.0000000000D-38  0.0000000000D-38  0.1000000000D 01  0.0000000000D-38  0.0000000000D-38  0.8225600479D-01
 0.0000000000D-38  0.0000000000D-38  0.2550000000D-01  0.0000000000D-38  0.0000000000D-38  0.0000000000D-38
 0.0000000000D-38 -0.6117667692D 00  0.6502500000D 01  0.0000000000D-38  0.0000000000D-38  0.5258119658D 02

 0.0000000000D-38  0.0000000000D-38  0.0000000000D-38  0.1000000000D 01  0.0000000000D-38  0.5812349767D-01
 0.0000000000D-38  0.0000000000D-38  0.0000000000D-38  0.6300000000D-01  0.0000000000D-38  0.0000000000D-38
 0.0000000000D-38 -0.1183993753D 00  0.0000000000D-38  0.3969000000D 02  0.0000000000D-38  0.3576744186D 02

 0.0000000000D-38  0.0000000000D-38  0.0000000000D-38  0.0000000000D-38  0.1000000000D 01  0.3461418464D-01
 0.0000000000D-38  0.0000000000D-38  0.0000000000D-38  0.0000000000D-38  0.1155000000D 00  0.0000000000D-38
 0.0000000000D-38 -0.4503735727D 00  0.0000000000D-38  0.0000000000D-38  0.1334025000D 03  0.2037086093D 02
```

```
TIME POINT VARIABLES
W1     0.260000D 01  M1     0.390000D 05  W2     0.640000D 01  M2     0.600000D 05  W3     0.116500D 02
M3     0.169000D 06  XCG    0.630000D 02  XCP    0.618600D 02  CZA    0.333000D 01  Q      0.122000D 03
IXX    0.130000D 09  F      0.615042D 07  X      0.255700D 04  M      0.130194D 06  VO     0.237610D 04
ICZY1 0.251375D 01  ICZY2 0.858130D 00  ICZY3 0.521338D 01  YP1    0.245000D-01  YP2    0.360000D-01
YP3    0.540000D-01  TIME   0.149000D 03
GYRO SLOPES   -0.610000D-01   0.960000D-01  -0.390000D-01
RATE GYRO      0.200000D-01   0.160000D-01  -0.200000D-02
SPECTRAL      -0.810000D-01   0.800000D-01  -0.370000D-01

THE MATRIX COEFICIENTS
 0.1000000000D 01  0.0000000000D-38  0.0000000000D-38  0.0000000000D-38  0.0000000000D-38 -0.2260756308D-02
 0.0000000000D-38  0.0000000000D-38  0.0000000000D-38  0.0000000000D-38  0.0000000000D-38  0.0000000000D-38
 0.0000000000D-38  0.2830839305D-03 -0.2726505835D-01 -0.6227011086D-01 -0.1170606278D 00 -0.1491908883D 01

 0.0000000000D-38  0.0000000000D-38  0.0000000000D-38  0.0000000000D-38  0.0000000000D-38  0.0000000000D-38
-0.1000000000D 01  0.1000000000D 01  0.0000000000D-38  0.0000000000D-38  0.0000000000D-38  0.0000000000D-38
 0.0000000000D-38  0.1997758307D-01 -0.4870966848D-03 -0.7157339042D-03 -0.1073600856D-02 -0.9940748669D-02

 0.0000000000D-38  0.0000000000D-38  0.1000000000D 01  0.0000000000D-38  0.0000000000D-38  0.1226750062D 00
 0.0000000000D-38  0.0000000000D-38  0.2600000000D-01  0.0000000000D-38  0.0000000000D-38  0.0000000000D-38
 0.0000000000D-38 -0.6248373201D 00  0.6760000000D 01  0.0000000000D-38  0.0000000000D-38  0.7885153846D 02

 0.0000000000D-38  0.0000000000D-38  0.0000000000D-38  0.1000000000D 01  0.0000000000D-38  0.8238864533D-01
 0.0000000000D-38  0.0000000000D-38  0.0000000000D-38  0.6400000000D-01  0.0000000000D-38  0.0000000000D-38
 0.0000000000D-38 -0.1386472689D 00  0.0000000000D-38  0.4096000000D 02  0.0000000000D-38  0.5125350000D 02

 0.0000000000D-38  0.0000000000D-38  0.0000000000D-38  0.0000000000D-38  0.1000000000D 01  0.3072294722D-01
 0.0000000000D-38  0.0000000000D-38  0.0000000000D-38  0.0000000000D-38  0.1165000000D 00  0.0000000000D-38
 0.0000000000D-38 -0.2990488671D 00  0.0000000000D-38  0.0000000000D-38  0.1357225000D 03  0.1819650888D 02
```

```
TIME POINT VARIABLES
W1     0.2800000D 01  M1     0.2250000D 05  W2     0.6500000D 01  M2     0.3700000D 05  W3     0.1170000D 02
M3     0.1710000D 06  XCG    0.6600000D 02  XCP    0.6196000D 02  CZA    0.3300000D 01  Q      0.1010000D 03
IXX    0.1060000D 09  F      0.6134000D 07  X      0.1980000D 04  M      0.1203500D 06  VO     0.2462300D 04
ICZY1  0.2394120D 01  ICZY2  0.1041750D 01  ICZY3  0.5270250D 01  YP1    0.2250000D-01  YP2    0.3300000D-01
YP3    0.5100000D-01  TIME   0.1540000D 03
GYRO SLOPES   -0.4900000D-01   0.7800000D-01  -0.3700000D-01
RATE GYRO      0.1900000D-01   0.1650000D-01   0.3000000D-02
SPECTRAL      -0.6800000D-01   0.6150000D-01  -0.4000000D-01

THE MATRIX COEFICIENTS
 0.1000000000D 01   0.0000000000D-38   0.0000000000D-38   0.0000000000D-38   0.0000000000D-38  -0.2898444528D-02
 0.0000000000D-38   0.0000000000D-38   0.0000000000D-38   0.0000000000D-38   0.0000000000D-38   0.0000000000D-38
 0.0000000000D-38   0.1009393415D-02  -0.2980881244D-01  -0.7072462303D-01  -0.1408660126D 00  -0.1911778399D 01

 0.0000000000D-38   0.0000000000D-38   0.0000000000D-38   0.0000000000D-38   0.0000000000D-38   0.0000000000D-38
-0.1000000000D 01  -0.1000000000D 01   0.0000000000D-38   0.0000000000D-38   0.0000000000D-38   0.0000000000D-38
 0.0000000000D-38   0.2078203989D-01  -0.4657353793D-03  -0.6830785562D-03  -0.1055666860D-02  -0.1034967509D-01

 0.0000000000D-38   0.0000000000D-38   0.1000000000D 01   0.0000000000D-38   0.0000000000D-38   0.2114077422D 00
 0.0000000000D-38   0.0000000000D-38   0.2800000000D-01   0.0000000000D-38   0.0000000000D-38   0.0000000000D-38
 0.0000000000D-38  -0.8539538958D 00   0.7840000000D 01   0.0000000000D-38   0.0000000000D-38   0.1363111111D 03

 0.0000000000D-38   0.0000000000D-38   0.0000000000D-38   0.1000000000D 01   0.0000000000D-38   0.1324822205D 00
 0.0000000000D-38   0.0000000000D-38   0.0000000000D-38   0.6500000000D-01   0.0000000000D-38   0.0000000000D-38
 0.0000000000D-38  -0.2259606486D 00   0.0000000000D-38   0.4225000000D 02   0.0000000000D-38   0.8289189189D 02

 0.0000000000D-38   0.0000000000D-38   0.0000000000D-38   0.0000000000D-38   0.1000000000D 01   0.3012106152D-01
 0.0000000000D-38   0.0000000000D-38   0.0000000000D-38   0.0000000000D-38   0.1170000000D 00   0.0000000000D-38
 0.0000000000D-38  -0.2473467077D 00   0.0000000000D-38   0.0000000000D-38   0.1368900000D 03   0.1793567251D 02
```

```
TIME POINT VARIABLES
W1     0.2[illegible]D 01  M1     0.1650000D 05  W2     0.6600000D 01  M2     0.2900000D 05  W3     0.1170000D 02
M3     0.1690000D 06  XCG    0.6800000D 02  XCP    0.6216000D 02  CZA    0.3250000D 01  Q      0.9300000D 02
IXX    0.9920000D 08  F      0.6125000D 07  X      0.1735000D 04  M      0.1164120D 06  VO     0.2520500D 04
ICZY1  0.2322630D 01  ICZY2  0.1172100D 01  ICZY3  0.5224710D 01  YP1    0.2100000D-01  YP2    0.3100000D-01
YP3    0.4[illegible]D-01  TIME   0.1570000D 03
GYRO SLOPES   -0.4482000D-01    0.6600000D-01   -0.3549000D-01
RATE GYRO      0.1776000D-01    0.1554000D-01    0.4890000D-02
SPECTRAL      -0.6150000D-01    0.5046000D-01   -0.4038000D-01

THE MATRIX COEFICIENTS
 0.1000000000D 01  0.0000000000D-38  0.0000000000D-38  0.0000000000D-38  0.0000000000D-38 -0.3186757258D-02
 0.0000000000D-38  0.0000000000D-38  0.0000000000D-38  0.0000000000D-38  0.0000000000D-38  0.0000000000D-38
 0.0000000000D-38  0.1413894934D-02 -0.2816204488D-01 -0.7097442417D-01 -0.1480367069D 00 -0.2101651596D 01

 0.0000000000D-38  0.0000000000D-38  0.0000000000D-38  0.0000000000D-38  0.0000000000D-38  0.0000000000D-38
-0.1000000000D 01  0.1000000000D 01  0.0000000000D-38  0.0000000000D-38  0.0000000000D-38  0.0000000000D-38
 0.0000000000D-38  0.2095070651D-01 -0.4383701110D-03 -0.6471177829D-03 -0.1022863592D-02 -0.1043738360D-01

 0.0000000000D-38  0.0000000000D-38  0.1000000000D 01  0.0000000000D-38  0.0000000000D-38  0.2870264194D 00
 0.0000000000D-38  0.0000000000D-38  0.2900000000D-01  0.0000000000D-38  0.0000000000D-38  0.0000000000D-38
 0.0000000000D-38 -0.1040228359D 01  0.8410000000D 01  0.0000000000D-38  0.0000000000D-38  0.1856060606D 03

 0.0000000000D-38  0.0000000000D-38  0.0000000000D-38  0.1000000000D 01  0.0000000000D-38  0.1680755559D 00
 0.0000000000D-38  0.0000000000D-38  0.0000000000D-38  0.6600000000D-01  0.0000000000D-38  0.0000000000D-38
 0.0000000000D-38 -0.2986752738D 00  0.0000000000D-38  0.4356000000D 02  0.0000000000D-38  0.1056034483D 03

 0.0000000000D-38  0.0000000000D-38  0.0000000000D-38  0.0000000000D-38  0.1000000000D 01  0.3031390817D-01
 0.0000000000D-38  0.0000000000D-38  0.0000000000D-38  0.0000000000D-38  0.1170000000D 00  0.0000000000D-38
 0.0000000000D-38 -0.2284589032D 00  0.0000000000D-38  0.0000000000D-38  0.1368900000D 03  0.1812130178D 02
```